The physics of magnetic particle inspection

Westwood, Stephen Mark

The Physics of Magnetic Particle Inspection

Stephen Mark Westwood B.Sc.
(St Aidans College)

This thesis submitted to the University of Durham in
Candidature for the Degree of Doctor of Philosophy,
September 1993

To my Parents a small reward

Declaration

The work contained in this thesis was carried out by the author between 1990 and 1993 while a postgraduate student in the Physics Department at the University of Durham. Work carried out in collaboration with other parties is clearly acknowledged at the appropriate point. None of the work contained in this thesis has been submitted in candidature for any other degree.

Abstract

This thesis describes the results of an investigation into the Physics of Magnetic Particle Inspection. This is a non destructive technique used to detect the presence of surface breaking cracks in ferrous metals. On applying a magnetic ink to the surface of the part being magnetised, particles will be attracted towards any regions of flux discontinuity. This allows the defect to be visible to the eye. The main areas of study were the magnetic properties of the inks used, a computer simulation of the indication process and work of a more practical nature concerning MPI.

From the magnetic measurements it was found that field induced agglomeration of the particles imparts the ink with a coercivity and remanence which varies with concentration. Low field time decay measurements show the existence of two reversal mechanisms within the magnetic ink, i.e. Brownian and Néel. The effect interparticle interactions have on a single aggregate has been studied by the use of remanence curves and this was found to lower the aggregates' magnetisation. This therefore lowers the magnetic force on a particle during the inspection process. The spin reversal mechanism has also been determined.

The computer simulation of the indication mechanism originally written by McCoy has been improved to accommodate time varying waveforms. Results from this investigation indicate that the rms of the waveform is the important parameter when specifying field values for magnetisation levels for low remanence steels. This is contrary to the British Standard BS 6072 but in agreement with the draft European Standard. It was also found that increasing the paint layer thickness decreased the number of particles at a crack. This variation was found to be similar to the variation of the magnetic leakage field from the crack with increasing paint thickness. From a study of the effects of viscosity and radii on the number of particles arriving at a crack, we find that for particles whose radius is greater than 10 microns no change is observed as the viscosity is altered.

Thyristor controlled power supplies are increasingly being used to magnetise inspection pieces and for this reason the relationship between the mean and rms of the waveform has been determined. It was found that the relationship between the two is non linear. This has implications if the user wishes to remain within BS 6072. Experimental

verification of the simulation results is also presented. An offshoot of this is a possible method of determining the crack width using MPI, this is also presented. Finally it was noted that upon increasing the applied magnetic field, particles present at the crack rotated through 180 degrees. This also occurred upon decreasing the magnetic field. Investigation of this unusual effect are reported as well as a possible mechanism for it.

Acknowledgements

Firstly, I would like to thank Professor A.D.Martin and Professor D.Bloor for making the facility of the Department of Physics available to me. A number of people have helped and cajoled me during my three years of research at Durham University. I would like to take this opportunity to thank those people. Professor Brian Tanner who has been my supervisor throughout these three years has been a source of knowledge, who has inspired me. Dr Tony Wagg who has been my industrial supervisor, thanks for the encouragement you gave. Special mention must be made to Dr. R.Gerber who inspired me to persist with the computer simulation work presented in this thesis while attending a Nato Advanced Summer School in Applied Magnetism. Nuclear Electric and the Science and Engineering Research Council for their financial assistance.

The staff on the Teaching Workshop under the supervision of Phil Armstrong deserve thanks for doing so many small technical jobs that were beyond my ability. On the electronics and computer side Chris Mullaney and Dave Stockdale have saved me from many hours of frustration and despair. Thanks also to Mike Lee, Vicky Greener and Pauline Russell to whom I am indebted to for help in producing diagrams in this thesis.

While being at Durham I have been fortunate to have shared a office and a beer with the following, Chris Gregory, Chris Friend, John Hudson, Paul Foley, Harry Rambsbottom, Rob Lubscombe, Li Charong, Paul Barker and Mr Ali. Thanks for all your help. Outside of the Department I wish to express my gratitude to Paul Richardon, Fiona Carter, West Bromwich Albion and Monday nights at the Strawberry.

List of Publications

Westwood, S.M.,"Waveform Characteristics of Thyristor Controlled Power Supplies as used in Magnetic Particle Inspection", *The British Journal of Non Destructive Testing*, **34**, 333-334 (1992)

Westwood, S.M., Lewis, V.J., O'Grady, K., and Tanner, B.K., "Measurements of Inter-particle Interactions in a Single Magnetic Ink Aggregate", *Journal of Magnetism and Magnetic Materials*, **125**, L247-250, (1993)

Blazina, Z., and Westwood, S.M., "On The Structural and Magnetic Properties of the $CePt_{5-x}Al_x$ System", *To be published in The Journal of Alloys and Compounds*

Westwood, S.M., Blazina, Z., and Drasner, A., "Magnetic Characterisation of Some Hypersoichmetric $ZrCr_2$ based Alloys and Their Hydrides", *Submitted to the Journal of Material Science Letters*

Westwood, S.M., Blazina, Z., and Drasner, A., "Magnetic Characterisation of $Zr(Cr_{1-x}Cu_x)^2$ and Hydrides", *Submitted to the Journal of Material Science Letters*

Symbols Used

B	Magnetic Flux Intensity
H	Magnetic Field
μ_o	Permeability of Free Space
M	Magnetisation per Unit Volume
χ	Volume Susceptibility
σ	Mass Magnetisation
χ_{mass}	Mass Susceptibility
μ	Permeability of a Material
μ_r	Relative Permeability
m	Magnetic Moment
θ	Angle
k	Boltzmann Constant
T	Temperature
L	Langevin Function
N	Number of Atoms per Unit Volume
C	Curie Constant
C	Contrast in Chapter 6
Φ	Waveform Position
ϕ	Waveform Spin
J_{12}	Exchange Constant
S_1,S_2	Spin Vectors
D	Demagnetising Factor
K_1	Anisotropy Constant
V	Volume
f_o	Larmor Processional Frequency
τ	Time
δ	Skin Depth
f	Frequency
Ω	Conductivity
σ_s	Surface Polarity
b	Depth of a Defect
a	Half Width of a Defect
x,y	Displacement
n	Aspect Ratio
M_d	Demagnetising Remanence
M_r	Isothermal Remanence
W_r	Rotational Hysteresis
M_s	Saturation Magnetisation
p	Distribution Function
V_o	Velocity
r	Radius

ρ_p	Density of Particulate Media
ρ_w	Density of Carrier Fluid
h	Small Step in Time
P	Indication Power

Contents

Chapter 1 : Introduction to Magnetism

Chapter 2 : Introduction to Magnetic Particle Inspection

Chapter 3 : Experimental Methods

Chapter 4 : Magnetic Measurements

Chapter 5 : Computer Simulation of the Indication Mechanism in Magnetic Particle Inspection

Chapter 6 : Practical MPI

Chapter 7 : Conclusion and Suggestions for Further Work

Appendices

Chapter 1

Introduction to Magnetism

1.0 Introduction

Magnetism is important from a technological and scientific viewpoint. The areas of interest range from the magnetic recording industries to probing the nature of matter. In this section a brief review of magnetism will be given with particular regard to those properties which are of interest to Magnetic Particle Inspection. This is mainly the magnetic properties of single domain particles and the information available from magnetic measurement on arrays of single domain particles.

1.1 Units and definitions in Magnetism

The magnetic field H measured in A/m and the magnetic flux density B in Tesla are related in free space by:

$$B = \mu_o H \qquad 1.1$$

where μ_0 is the permeability of free space and has a value of $4\pi.10^{-7}$ H/m. However if a material is placed in a magnetic field then there will be a change in the magnetic flux density B by an amount proportional to the magnetisation per unit volume of the material M also measured in A/m. Under these circumstances 1.1 becomes:

$$B = \mu_0 (M + H) \qquad 1.2$$

Physicists often like to characterise a material response to a magnetic field; this is the volume susceptibility χ defined as:

$$\chi = \frac{M}{H} \qquad 1.3$$

were χ is dimensionless. Materials with a negative value of χ are called diamagnetic, materials with a small positive value of χ are paramagnetic. As it is easier to measure the mass of a material than its volume, the magnetisation per unit mass σ measured in Am^2/kg is often used. The volume magnetisation M is related to its mass magnetisation σ via the material's density ρ by the relation:

$$\sigma = \frac{M}{\rho} \qquad 1.4$$

The mass susceptibility χ_{mass} is therefore defined by:

$$\chi_{mass} = \frac{\sigma}{H} \qquad 1.5$$

χ_{mass} has units of m^3/kg. Engineers often wish to know the magnetic flux density in a material for a certain magnetic field. This aspect of a material's response to a magnetic field is called the permeability and is defined as:

$$\mu = \frac{B}{H} = \frac{\mu_o(M+H)}{H} = \mu_0(\chi+1) \qquad 1.6$$

the permeability has units of H/m. The relative permeability μ_r is defined by:

$$\mu_r = \frac{\mu}{\mu_o} \qquad 1.7$$

and is dimensionless.

1.2 Origin of the Magnetic Moments of atoms

In the discussion above, the magnetisation of a body was described but no attempt was made to attribute this magnetisation to any physical effect. The magnetic moment of an atom has three principal components[1]; the spin of the electron, the angular momentum of the electron about the nucleus and the change in orbital momentum induced by a magnetic field. The first two effects lead to a positive component of the susceptibility and the last has a negative effect on the susceptibility. These two effects are

responsible for a wide range of magnetic states, some of the simpler ones being shown in Fig.1.1a-d. Fig.1.1a shows the alignment of magnetic moments in a paramagnet in which the magnetic moments are disordered by thermal motion therefore there is no overall magnetisation. Fig.1.1b shows how the magnetic moments are aligned in a ferromagnet at 0 K, giving rise to a spontaneous magnetisation. Fig.1.1c shows the alignment of moments in a antiferromagnet indicating that the magnetic moments on different atoms are the same size but opposite direction also at 0 K, giving no overall magnetisation. Fig.1.1d shows a special case of antiferromagnetism at 0 K in which the magnetic moments on different atoms have opposite directions but do not cancel out and therefore there is a spontaneous magnetisation. This arrangement of magnetic moments is called ferrimagnetism.

1.2.1 Diamagnetism

The theory of diamagnetism was first worked out by Langevin[2]. An electron orbiting round a nucleus can be considered similar to a current flowing in a loop. Consequently there will be a magnetic moment associated with the orbital motion. For any molecules or atoms with a closed electron shell in the absence of a magnetic field these moments will cancel each other out.

On application of a magnetic field there will be a change in flux through the electrons orbit. This change in flux will induce a emf according to Faradays law. This induced emf acts in such a way as to oppose the change in flux and is a consequence of Lenz's law. To oppose the change in flux there is a decrease in the magnetic moment of the electrons whose orbits are in the direction of the magnetic field and an increase in the magnetic moment of those electrons whose orbits are in the opposite direction to that of the magnetic field. This leads to an induced magnetic moment in the opposite direction to the magnetic field. All materials exhibit diamagnetism but this is often masked by other magnetic states.

1.2.2 Paramagnetism without interactions

Langevin in his paper on diamagnetism also derived the classical theory of paramagnetism, brief details of which are given here. Suppose each atom of a material with unpaired electrons has a net magnetic moment m and the individual moments of the atoms do not interact. Then a moment m making an angle β with the magnetic field H has an energy:

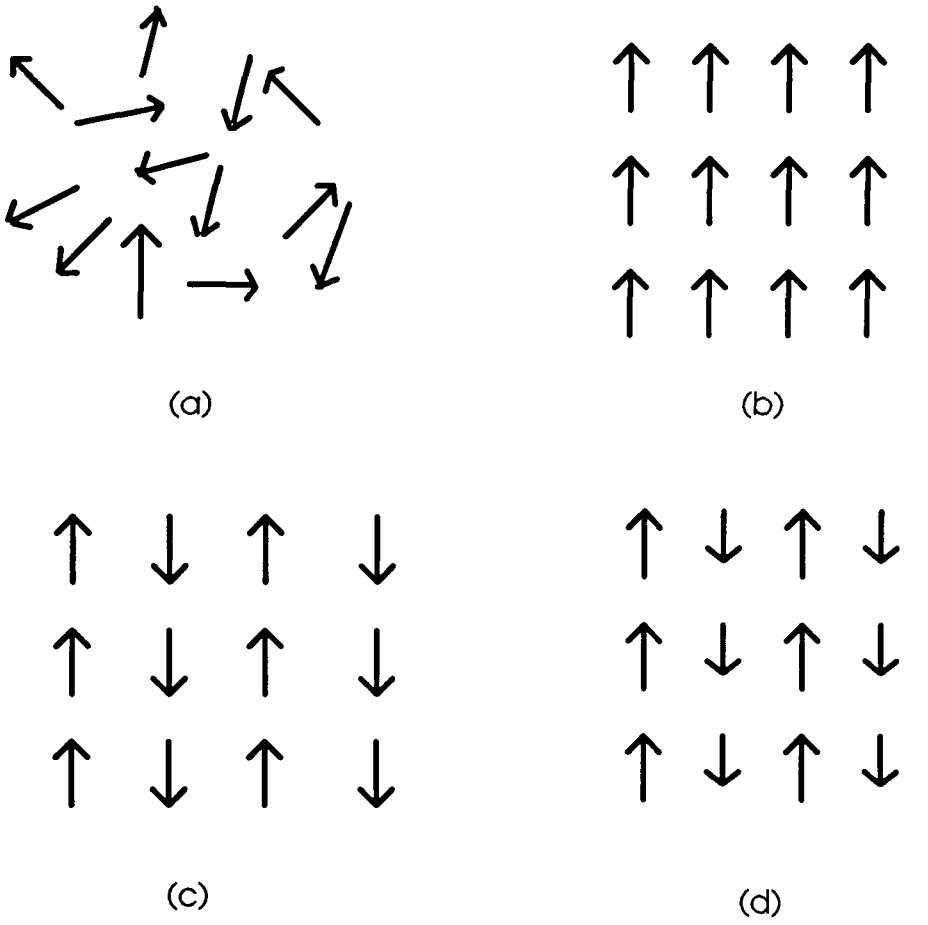

Fig.1.1a-d (a) Alignment of magnetic moments in a paramagnet. (b) Alignment of magnetic moments in a ferromagnet below its Curie temperature. (c) Alignment of magnetic moments in a antiferromagnetic below its Néel temperature. (d) Alignment of magnetic moments in a ferrimagnet below its Curie temperature.

$$E = -\mu_0 m.H\cos\theta \qquad 1.8$$

The tendency for the magnetic moments to align themselves with the magnetic field are resisted by the effect of the thermal energy that tends to randomise the direction of moments. Langevin showed that the magnetisation M of an array of N atoms per unit volume with a magnetic moment m at a temperature T is:

$$M = Nm\left[\coth\left(\frac{\mu_o mH}{kT}\right) - \frac{kT}{\mu_o mH}\right] = M_s L\left(\frac{\mu_o mH}{kT}\right) \qquad 1.9$$

M_S is the saturation magnetisation of the array and is the magnetisation if all the moments were aligned in the same direction, i.e. $M_S=Nm$. k is the Boltzmann constant and L is the Langevin function. The Langevin function can be approximated by an infinite power series. In most cases of interest, i.e. at high temperatures and low magnetic fields, $\frac{\mu_o mH}{k_b T} \langle\langle 1$. Therefore equation 1.9 can then be expressed by the first term in the infinite power series expansion of the Langevin series and so the magnetisation M is given by:

$$M = \frac{N\mu_o m^2 H}{3kT} \qquad 1.10$$

The susceptibility is therefore given by

$$\chi = \frac{M}{H} = \frac{N\mu_o m^2}{3kT} = \frac{C}{T} \qquad 1.11$$

where C is called the Curie Constant. Therefore the paramagnetic susceptibility based on the Langevin model leads to a susceptibility which is inversely proportional to the temperature. Curie[3] reported measurements on a wide range of materials which verify this model and therefore equation 1.11 is known as the Curie law. Equation 1.11 was derived using classical mechanics in that the value of θ in equation 1.8 was assumed to be a continuous variable whereas in a quantum mechanical derivation it can only take

certain values. However the equations derived for the temperature dependence of the susceptibility using quantum mechanics[4] are effectively identical to equation 1.11.

1.2.3 Paramagnetism with interactions

Not all paramagnetic materials obey the Curie law. Weiss [5] found the temperature dependence of the susceptibility for some materials obeyed the following law:

$$\chi = \frac{C}{T - \beta} \qquad 1.12$$

where β is the transition temperature and can have positive, negative or zero value. A zero value corresponds to the Curie law mentioned earlier. A positive value indicates a material that undergoes a transition from the paramagnetic state to a ferromagnetic state. In this case β corresponds to the Curie temperature. A negative value of β corresponds to a material that undergoes a transition from a paramagnetic state to a antiferromagnetic state. However the value of β does not correspond to the temperature of the transition which is known as the Néel temperature. Equation 1.12 is valid at temperatures above the transition temperature.

Weiss[6] postulated that the deviations from Curie behaviour were due to the magnetic moments of individual atoms interacting with one another. He expressed the nature of the interactions in terms of a molecular field H_m. This molecular field was assumed to be dependent upon the magnetisation of the surrounding material.

$$H_m = \alpha M \qquad 1.13$$

The total magnetic field acting on the material becomes:

$$H_{tot} = H_m + H \qquad 1.14$$

With this molecular field acting Weiss showed that the temperature dependence of the susceptibility follows equation 1.12. In the last two sections we assumed that the electrons responsible for the magnetic moments are localised and this leads to Curie or Curie Weiss paramagnetism. However if the electrons are not localised this leads to Pauli paramagnetism [7] which is temperature independent.

1.2.4 Ferromagnetism

In the previous section the fact that the magnetic moments interacted with one another led to a transition from a disordered magnetic state (paramagnetism) to an ordered magnetic state such as ferromagnetism. In a ferromagnetic material below its Curie temperature the magnetic moments are aligned even in the absence of a magnetic field. However its magnetisation can still be zero. In the next few sections we discuss the properties of ordered magnetic systems and in particular the formation of domains, anisotropy energy, single domain particles and superparamagnetism.

Weiss postulated that the observed properties of ferromagnets (i.e. spontaneous ordering of the moments in zero field but yet having zero magnetisation) could be explained by the presence of a molecular field and the formation of domains. The molecular field which causes deviations from the Curie law above the Curie temperature of a ferromagnet is due to magnetic moments interacting. Below the Curie temperature this molecular field causes the moments to order spontaneously. Domains are areas in which the magnetisation has a value equal to the saturation value but the direction of the magnetisation is different for each domain. In the demagnetised state the magnetisation of the domains cancel each other out and this lead to zero magnetisation overall. However upon application of a magnetic field the domains can grow and reorientate themselves, the material thereby acquires an overall magnetisation.

It was said earlier that the molecular field causes the spins to align in a ferromagnet. However the origin of this molecular field was not initially clear. The simplest theory is that developed by Heisenberg[8] who assumed that the electrons responsible for the magnetic moments are localised on the atoms. Heisenberg considered a hydrogen molecule, which consists of two electrons and two protons. For this molecule there are various electrostatic forces present which depend on the locations of the electrons and protons. The waveform for the two electron system has two components which describe the electrons' position $\Phi(1,2)$ the other is the electrons' spin $\phi(1,2)$. On exchanging the two electrons $1 \leftrightarrow 2$ the total waveform must be antisymmetric as a consequence of the Pauli exclusion principle. Therefore if the position part of the waveform Φ is symmetric then the spin part ϕ must be antisymmetric and vice a versa.

Therefore if the spin of one electron is changed then the electrons' position must change and therefore the electrostatic energy of the system is altered. This effect is as if there was an interaction energy between the electron spins, proportional to their scalar product. When the Schrodinger equation is written out there is a Heisenberg contribution to the total Hamiltonian:

$$H_{heiss} = -2J_{12}S_1.S_2 \qquad 1.15$$

where S_1 and S_2 are the spin vectors for the electrons and J_{12} is the exchange constant. If J_{12} is positive then the spins are parallel to each other and the system is ferromagnetic. If J_{12} is negative then the spins are anti-parallel and the system is antiferromagnetic or ferrimagnetic. When extending this model to solids it is necessary to sum this exchange energy over all pairs of electrons which can contribute in which case equation 1.15 becomes:

$$\langle H_{heiss} \rangle = -2\sum\sum J_{ij}S_i.S_j$$

This increases the complexity of the model. This model of ferromagnetism has its limitations in that it assumes that the magnetic moments are localised which is not the case for nickel, iron and cobalt as the 3d and 4s electrons responsible for the magnetic moments are relatively free to move throughout the solid. The Band theory of ferromagnetism[9] accommodates the problem that electrons responsible for the magnetic moments are not localised, which is the case for all the room temperature ferromagnets. Band theory also predicts the temperature independent susceptibility associated with Pauli paramagnetism. The limitations with Band theory are that it is extremely difficult to make fundamental calculations based upon it.

It is worthwhile considering how the magnetisation of a ferromagnet changes with magnetic field, Fig.1.2 show a typical hysteresis loop for a ferromagnet material. Starting from the demagnetised state the magnetisation increases slowly and reversibly. It then changes irreversibly to the value of the saturation magnetisation M_S. This part of the hysteresis curve is called the virgin curve. If the magnetic filed is decreased then the value of the magnetisation in zero magnetic field after being saturated is called the remanent magnetisation M_r. By applying a negative magnetic field, zero magnetisation can be obtained. The magnetic field needed to achieve this zero magnetisation state is known as the coercivity H_C. Increasing the strength of the negative magnetic field the material becomes saturated in the opposite direction. Decreasing the magnetic field to

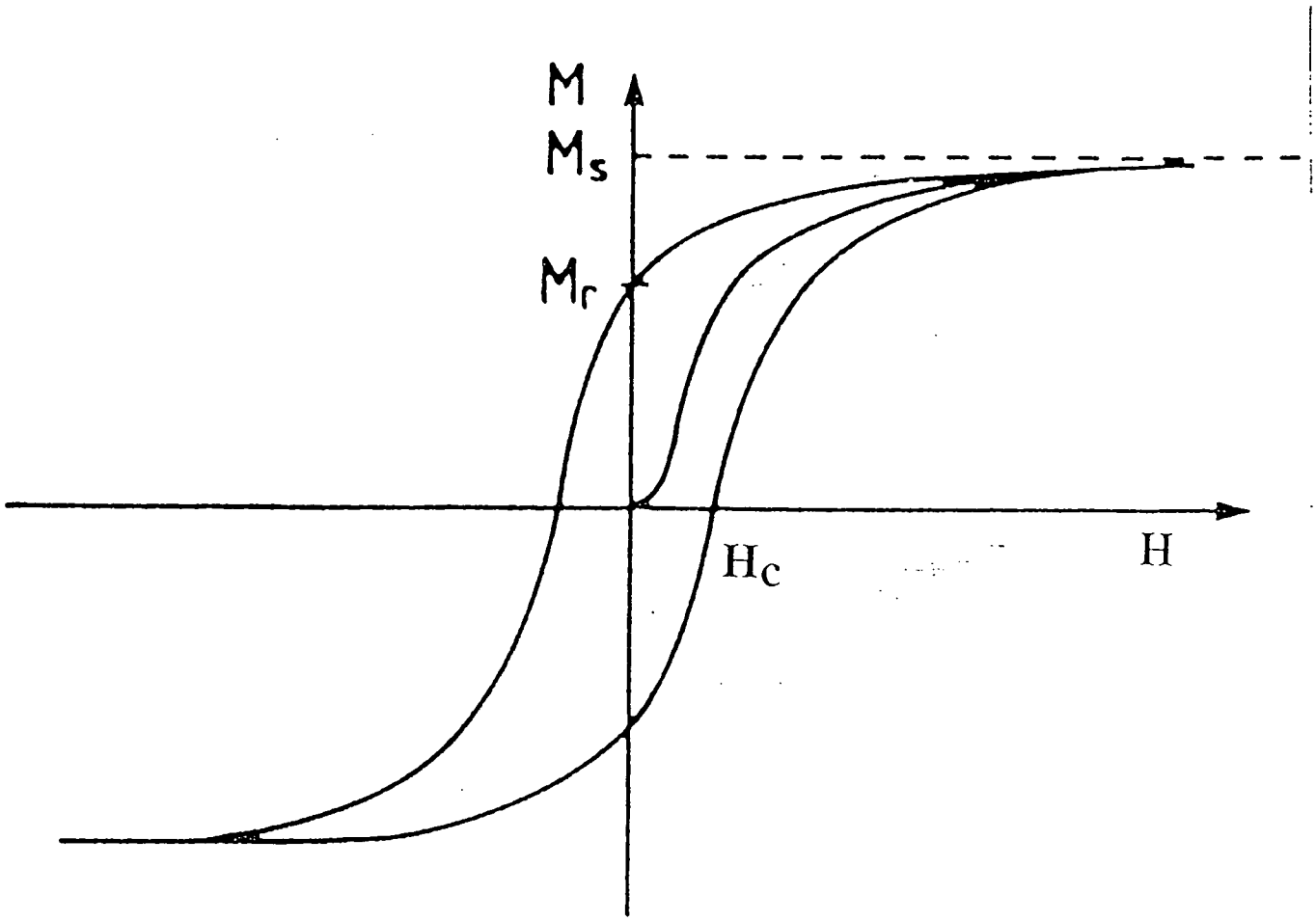

Fig.1.2 Hysteresis loop for a Ferro or ferrimagnetic material. Indicating the virgin curve and hysteresis also shown is the coercivity H_c and remanence M_r.

zero, the value of the magnetisation becomes equal to the remanent magnetisation but in the opposite direction. Increasing the magnetic field causes the material to become saturated in the positive direction again. This is known as the major hysteresis loop.

1.2.5 Antiferromagnetism

The existence of antiferromagnetism as an ordered state of magnet moments was postulated by Néel [10] in 1932. In antiferromagnets the exchange integral J_{12} is negative and neighbouring spins are therefore anti-parallel to one another. Over the material as a whole there is no overall magnetisation. The phenomenon of antiferromagnetism is directly observable only by neutron scattering.

1.2.6 Ferrimagnetism

Ferrimagnetism is a special case of antiferromagnetism as J_{12} is negative. However in a ferrimagnet the magnetic moments of neighbouring atoms do not cancel out and therefore there is a spontaneous magnetisation. These classes of material are of technological importance as γ Fe_2O_3, which is used extensively in the magnetic recording media, is a ferrimagnet. As with ferromagnetic materials, ferrimagnets exhibit hysteresis and domain effects.

It is worthwhile discussing the magnetic properties of magnetite Fe_3O_4 as this ferrite is used in magnetic particle inspection. Magnetite is a ferrimagnet and has the structural formula $Fe^{3+}O[Fe^{2+}Fe^{3+}]O_3$. The spins associated with the Fe^{3+} ions and the $Fe^{2+}Fe^{3+}$ ions are antiparralel, and its spontaneous magnetisation is the result of the net difference between these spins[11] . The mass magnetisation of magnetite at room temperature depends on the state of the magnetite. In a bulk form it has a mass magnetisation of 92 Am^2/kg whereas in a powder form it has a mass magnetisation of 84 Am^2/kg [12].

1.3 Properties of Ferro and Ferri-Magnetic Materials

The magnetisation of a ferromagnet can take many values ranging from zero to M_S, the saturation magnetisation but what factors influence its response to a magnetic field. In this section we discuss the parameters which affect its magnetisation.

1.3.1 Demagnetising Fields

When a specimen is magnetised, free poles are induced on the surface of the specimen. These free poles create an internal field which opposes the direction of the magnetisation. The strength of this internal field is dependent upon the shape of the specimen and the specimen magnetisation and is given by:

$$H_d = -DM$$

where M is the specimen magnetisation and D is called the demagnetisation factor and is dependent upon the specimen geometry. The demagnetisation factor has been calculated by Stoner[13] and Osborne[14] for various ellipsoids. Other shapes such as rods and disc can usually be approximated by an ellipsoid.

Therefore measurements of the applied magnetic field need to be corrected for the effect of this demagnetising field if the true hysteresis properties of the material are needed. The correction is given by:

$$H = H_{appl} - DM \qquad 1.16$$

Where H_{appl} is the applied magnetic field and H is the true magnetic field experienced by the specimen.

1.3.2 Magnetic Domains

Weiss postulated that the magnetisation of a ferromagnet can be zero due to the formation of domains in which the magnetisation of each domain was M_S the saturation magnetisation of the material, but $\sum M_s = 0$. Application of a magnetic field causes movement of the domain boundaries or "walls" such that those oriented towards the field direction increase in size at the expense of the other domains.

The existence of domains was explained by Landau and Lifshitz [15] as a direct result of energy minimisation of the magnetic system. The domain walls have an energy associated with them which is proportional to their thickness and area. This energy arises from the fact that the magnetisation changes its direction at the interface between the domains. This energy is lowered if the transition is spread out however the fact that the magnetisation prefers to lie along certain directions prevent the domain

wall spreading too far. The gain in energy by the formation of a domain wall is balanced against the energy associated with the surface poles mentioned in the last section. Fig.1.3 shows the division of a rectangular ferromagnetic block into parallel domains. The splitting of the block into two domains lowers the demagnetising energy at the cost of a gain in the domain wall energy.

1.3.3 Magnetic Anisotropy

When a sample is magnetised from the demagnetised state to saturation along a particular direction an amount of energy is expended in the process. The amount of energy expended depends upon the direction of the magnetisation. The magnetisation prefers to lie along certain directions called the easy axis as the free energy of the crystal contains a term which is dependent on the magnetisation direction with respect to this easy axis. This easy axis can be due to shape, crystal or stress anisotropy or a combination of all three.

Crystal Anisotropy[16]: The magnetisation prefers to lie along certain crystallographic directions. This is illustrated in Fig.1.4 which shows the magnetisation curves along certain crystallographic axes for iron. Indicating it is easier to magnetise the sample along certain directions. For a uniaxial crystal the energy associated with the anisotropy is often expressed as:

$$E = K_1 \sin^2 \theta \qquad 1.17$$

where θ is the angle between the magnetisation and the easy axis and K_1 is the anisotropy constant.

Shape Anisotropy: This is due to demagnetising fields, as the magnetisation prefers to lie along the direction with the lowest demagnetisation factor

Stress Anisotropy: If a material is stressed in one direction it can become easier or hardier to magnetise it, depending on the material along that particular direction

The anisotropy forces that bind the magnetisation to a particular direction can be expressed as a fictitious anisotropy field H_{ok}. This anisotropy field is parallel to the easy axis and exerts the same torque on the magnetisation for small angular deviations of the magnetisation from the easy direction as the anisotropy itself.

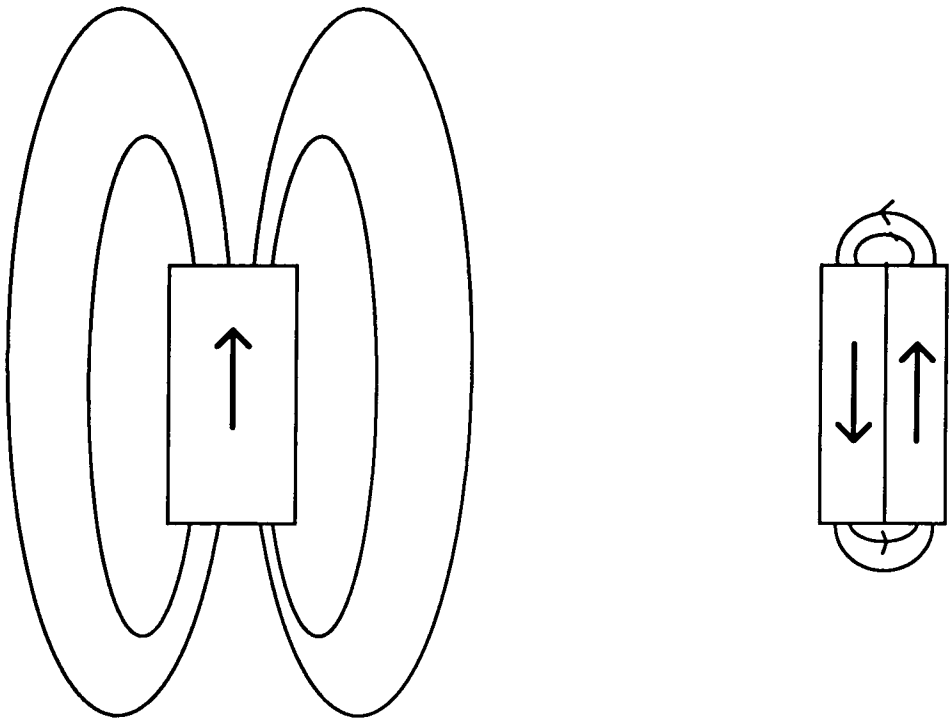

Fig.1.3 Diagram showing the formation of domains and the lowering of the demagnetising energy due to domain formation

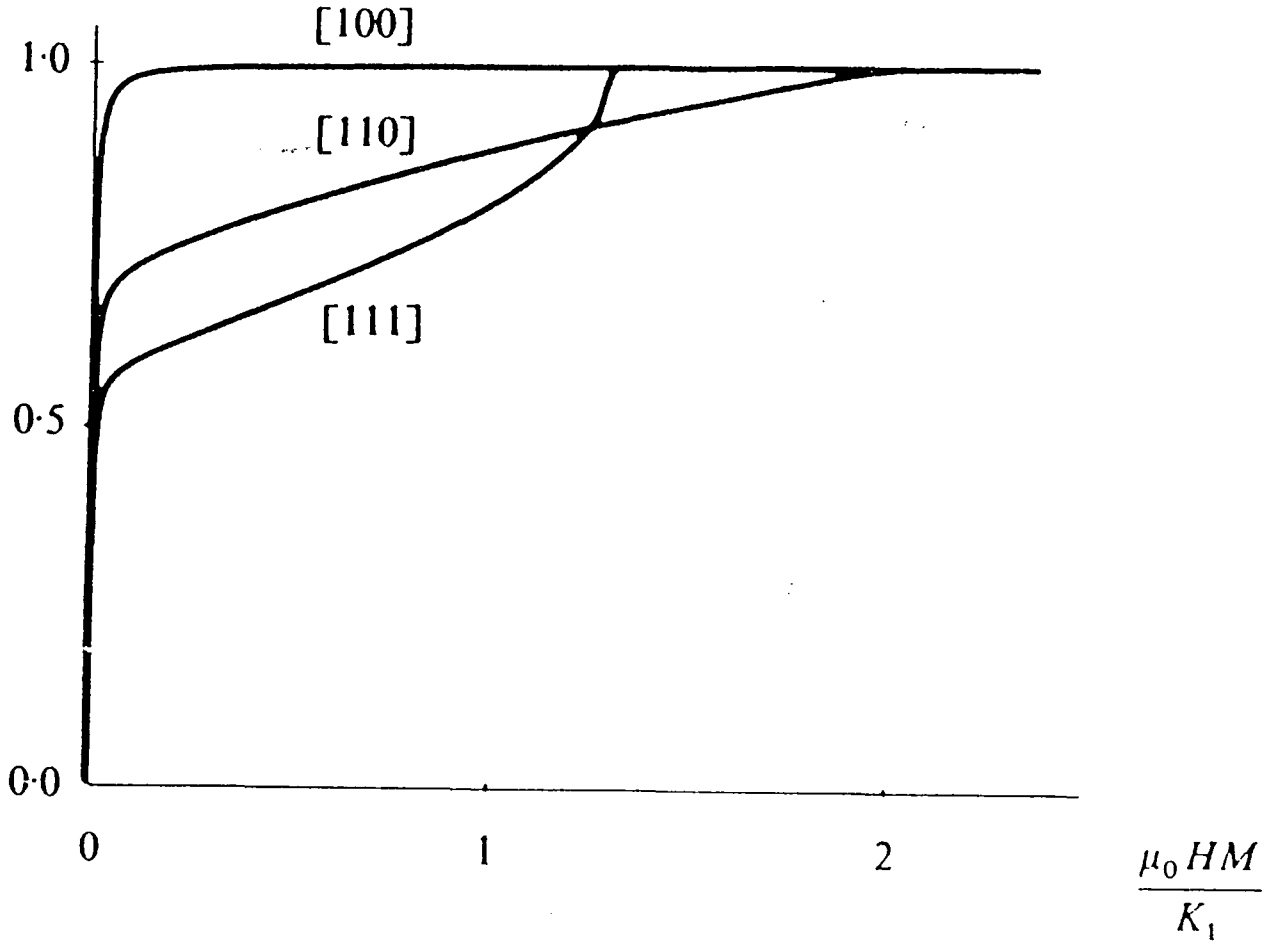

Fig.1.4 Magnetisation Curves for iron in various crystallographic orientations. Indicating that it is easier to magnetise iron along the [100] direction.

1.4 Single Domain Particles

Single domain particles occur in very many practical materials of scientific and technological interest. These include ferrofluids, magnetic recording media, permanent magnets and spin glasses. A good review article on the various properties of single domain particles is given by Wohlfarth[17]. The reason why single domain particles are formed will be briefly discussed. This then leads to a discussion on superparamagnetism and the effect of magnetic viscosity on magnetic measurements.

1.4.1 Formation of Single Domain Particles

Single domain particles are formed as the size of the ferromagnetic particles decreases. At a certain size it becomes energetically unfavourable to form a domain wall. Once this size is reached the particle is then said to be single domain. In a single domain particle all the spins are aligned in the same direction. The existence of single domain particles was suggested by Frenkel and Dorfman[18]. Calculations of the size at which single domain particles become energetically favourable were made by Kittel[19] and Néel[20]. The critical size for the multi-domain to single domain transition of Fe_3O_4 has been calculated at between ~0.08 to ~0.4 μm[21,22].

1.4.2 Superparamagnetism

As the size of a single domain particle decreases the thermal energy kT can become comparable to the anisotropy energy KV where K is the anisotropy constant and V is the volume of the particle. In which case thermal fluctuations can overcome the anisotropy barriers and spontaneously reverse the direction of the magnetisation from one easy direction to another in the absence of an applied field. Magnetisation of an array of particle whose moments can thermally reverse direction within the measurement time is given by:

$$M = M_s L\left(\frac{M_s V H \mu_0}{kT}\right) \qquad 1.18$$

This is identical to the magnetisation of an array of paramagnetic moments. However the magnetic moment associated with it is greater than the paramagnetic case by an

order of 10^5 and therefore the term superparamagnetic is used. Bean and Livingston[23] defined the critical size V_C below which superparamagnetism occurs as:

$$V_c = 25\frac{kT}{K} \qquad 1.19$$

For particles having a volume $V<V_C$ the Néel [24] relaxation time τ_n is less than the measurement time assumed in deriving equation 1.19 which Bean and Livingston took to be 100 seconds. For particles whose volume $V>V_C$ the magnetisation is stable and is said to be blocked. The relationship between particle volume and τ_n is given by:

$$\tau_n = f_o^{-1}\exp\left(\frac{KV}{kT}\right) \qquad 1.20$$

where f_O is approximately the Larmor precessional frequency of the magnetisation vector and is of the order $10^9 s^{-1}$. However in a magnetic ink at room temperature another reversal mechanism is also present, this is Brownian[25] reversal of the moment. In Brownian reversal the particle physically rotates. The dominant reversal mechanism is the one with the shortest relaxation time. In a magnetic field H equation 1.20 is modified to become:

$$\tau_n = f_o^{-1}\exp\left(\frac{KV}{kT}\left(1-\frac{H}{H_{ok}}\right)^2\right) \qquad 1.21$$

where H_{Ok} is the anisotropy field.

1.5 Magnetic Viscosity in Single Domain Particles

From equation 1.21 the fact that the Néel relaxation depends critically on the particle's volume gives rise to three measurement situations. These are

$V < V_C$ Particle is single domain and superparamagnetic. The magnetisation thermally relaxes on a time scale less than 100 seconds.

$V \sim V_C$ Particle is single domain but the magnetisation can thermally relax on a time scale greater than 100 seconds.

$V \gg V_C$ Particle is single domain and the magnetisation is stable over a geological time scale.

Consequently if the magnetisation of an array of single domain particles with constant anisotropy barriers is measured as a function of time τ the magnetisation decay as [26]:

$$M = M_0 \exp\left(-\frac{\tau}{\tau_n}\right) \qquad 1.22$$

where M_O is the magnetisation when the measurement was started and τ_n is the Néel relaxation time for the particles. However if a distribution of anisotropy barriers are present then equation 1.22 is modified. Street and Woolley [27] showed that the exact form of the distribution affects how the magnetisation decays and under certain conditions equation 1.22 can become:

$$M = M_0 - S\ln(\tau) \qquad 1.23$$

This ln(time) dependence has frequently been observed in a wide range of magnetic systems [28,29,30]. It was found by O'Grady[31] that S is dependent on temperature. Also a peak is observed as a function of magnetic field [32,33], this peak occurring at the coercivity of the particles. Chantrell et al [34] have observed departures from ln(time) behaviour for a system of frozen Co fine particles.

1.6 Reversal Mechanism in Single Domain Particles

In a single domain particle all the spins are aligned in the direction of the magnetisation. Upon application of a magnetic field in the opposite direction to that of magnetisation, the magnetic moments will reverse direction at the coercive field. This spin reversal can occur coherently, in which the spins rotate in a parallel manner or incoherently in which the spins rotate in a non-parallel manner so as to minimise the total energy.

1.6.3 Coherent and Incoherent Rotation

Stoner and Wohlfarth[35] calculated the hysteresis loops of single domain particles in which the moments rotate parallel to one another during the reversal mechanism. They found that the coercivity of a random assembly of non-interacting unaxial single domain particles was given by:

$$H_c = 0.48 H_{ok} \qquad 1.24$$

where H_{Ok} is the anisotropy field of the particle. The source of the anisotropy field can be due to crystal, shape or stress anisotropy. However measurements on dilute compacts of thin elongated iron particles found that the measured value of coercivity could not be explained. This was because the coercivity was too high for crystal anisotropy and to low for shape anisotropy. For a review of these measurements see Luborsky[36]. Theoreticians then began to formulate models in which the moments reversed incoherently. Jacobs et al [37] and Frei, Shtrikman and Treves [38] have proposed the reversal mechanisms shown in Fig.1.5. These are coherent rotation, rotation by fanning, rotation by curling and finally by spin reversal by buckling.

Reversal by fanning was suggested by the shape of the electrodeposited elongated iron particles which had periodic bulges rather than smooth sides. This suggests that the shape of the particles was similar to a chain of particles. In this reversal mechanism shown in Fig.1.5b, in each of the particles the reversal mechanism is coherent but in alternate directions in successive spheres.

In spin reversal by curling, shown in Fig.1.5c, the spins that are originally aligned in the z axis of a prolate spheroid experience a field in the negative z direction. This causes each spin to rotate about the radius, parallel to the xy plane on which it is located.

The final reversal mechanism is spin reversal by buckling shown in Fig.1.5d, in which the magnitude of the spins follows a sinusoidal variation along the original direction of the magnetisation upon application of a reverse magnetic field.

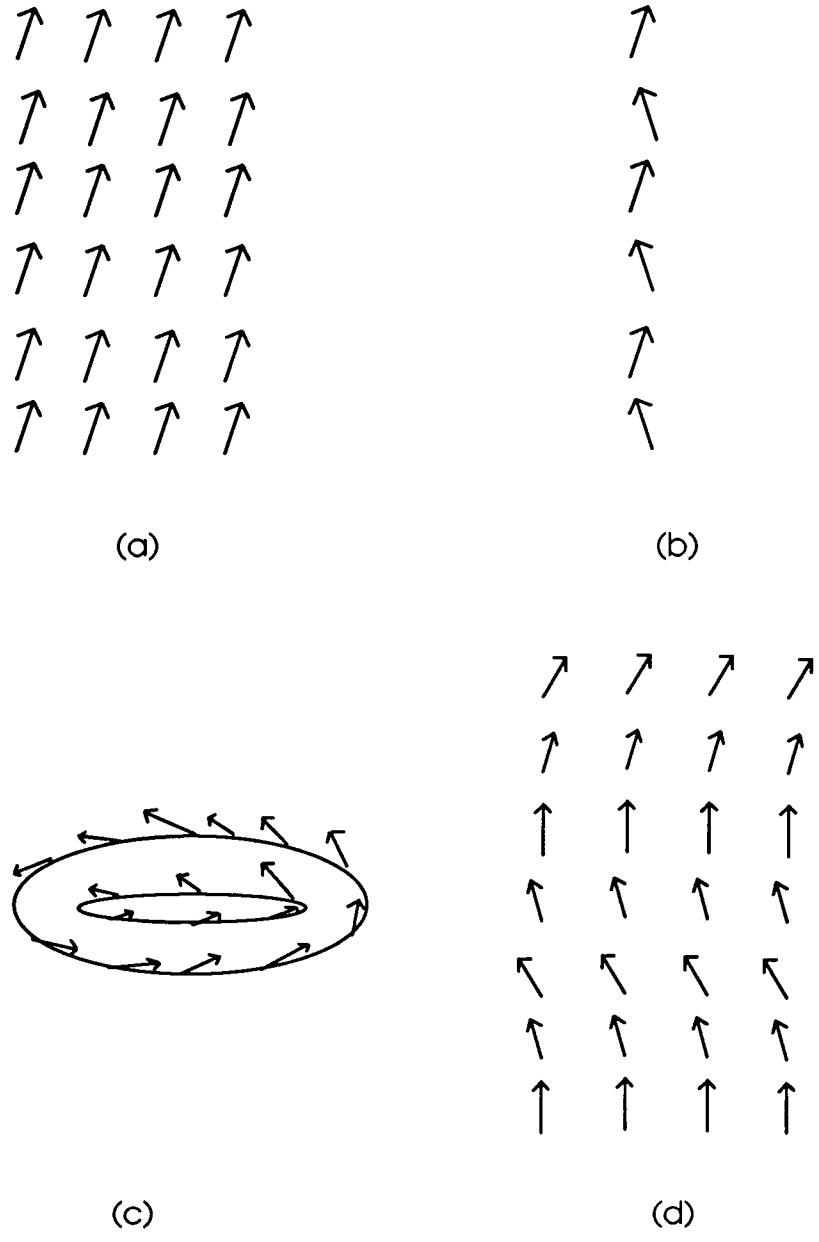

Fig.1.5 Diagram showing possible reversal mechanisms. (a) Coherent rotation of moments. (b) Incoherent reversal by fanning. (c) Incoherent rotation by curling. (d) Incoherent rotation by buckling.

1.7 Summary

The origin of the magnetic moments was discussed and how this lead to ordered magnetic states such as ferri and ferromagnetism. This then leads to a discussion of the properties of ferromagnets and the existence of domains. It was shown that as the size of the particles decreases then single domain particles can exist and how this lead to superparamagnetism and magnetic viscosity.

References Chapter 1

[1] Kittel, C., "Introduction to Solid State Physics", *John Wiley and Sons Inc.*, New York (1986)

[2] Langevin, P., *Annales de Chem. et Phys.*, **5**, 70 (1905)

[3] Curie, P., "Propriétés Magnétiques Des Corps a Diverses Températures", *Ann. Chem. Phys.*, **5**, 289 (1895)

[4] Ashcroft, N.W., and Mermin, N.D., "Solid State Physics", *Holt-Saunders International Editions*, 653-657 (1976)

[5] Weiss, P., "La variation du ferromagnetism avec la température", *Compt. Rend.*, **143**, 1136-1139 (1906)

[6] Weiss, P., "L'Hypothèse du Champ Moléculaire et la Propriété Ferromagnétique", *J. de Phys.*, **6**, 661 (1907)

[7] Pauli, W., "Über Gasentartung und Paramagnetismus", *Z.Phys.*, **41**, 81 (1926)

[8] Heisenberg, W., *Z.Phys.*, **49**, 619 (1928)

[9] Crangle, J., "Solid State magnetism", *Edward Arnold*, 45-49 (1991)

[10] Néel, L., "Influence of fluctuations in the molecular field on the properties of magnetic bodies", from "Selected Works of Louis Néel", Kurti, N., *Gordon and Breach*, 3-25 (1988)

[11] Tebble, R.S., and Craik, D.J., "Magnetic Materials", *Wiley-Interscience*, 252-259, (1969)

[12] Wohlfarth, E.P., "Ferromagnetic Materials", Vol 2, *North Holland Publishing Company*, 430-431 (1980)

[13] Stoner, E.C., "The demagnetizing factors for ellipsoids", *Phil. Mag.*, **36**, 803-821, (1945)

[14] Osborn, J.A., "Demagnetizing factors of the general ellipsoid", *Phys. Rev.*, **67**,351-357 (1945)

[15] Landau, L., and Lifshitz, E., "Theory of the Dispersion of Magnetic Permeability in Ferromagnetic Bodies", *Phys. Zeits. d. Sowjetunion*, **8.2**, 153-169 (1935)

[16] Cullity, B.D., "Introduction to Magnetic Materials", *Addisn-Wesley Publishing Company*, 207-247 (1972)

[17] Wohlfarth, E.P., "Magnetic properties of single domain ferromagnetic particles", *J. Magn. Magn. Mater.*, **39**, 39-44 (1983)

[18] Frenkel, J., and Dorfmann, J., "Spontaneous and induced magnetisation in ferromagnetic bodies", *Nature* , 274-275 (1930)

[19] Kittel, C., "Physical theory of ferromagnetic domains", *Rev. Mod. Phys.*, **21**, 541-582 (1949)

[20] Néel, l., "The properties of fine grained cubic ferromagnetic materials", from "Selected Works of Louis Néel", Kurti, N., *Gordon and Breach*, 206-207 (1988)

[21] Stacey, F.D., and Banerjee, S.K., "The Physical principles of rock magnetism", *Elsevier Scientific Publishing Company*, 58-59 (1974)

[22] Moskowitz, B.M., and Banerjee, S.K.,"Grain size limits for pseudosingle domain behavior in magnetite: Implications for paleomagnetism", *IEEE Trans. Magn.*, **Mag-15**, 1241-1246 (1979)

[23] Bean, C.P., and Livingston, J.D., "Superparamagnetism", *Journal of Applied Physics*, **30**, 120S-129S (1959)

[24] Néel, L., "Some theoretical Aspects of Rock-Magnetism", *Adv. phys.*, **4**, 191-243 (1955)

[25] Shliomis, M.I., "Magnetic Fluids", *Sov. Phys.-Usp.*, **17**, 153-169 (1974)

[26] Street, R., and Woolley, J.C., "A study of magnetiic viscosity", *Proc. Phys. Soc. A.*, **62**, 562-572 (1949)

[27] Sreet, R., and Woolley, J.C., "A study of magnetic viscosity", *Proc. Phys. Soc. A.*, **62**, 562-572 (1949)

[28] Guy, C.N.,"Spin glasses in low dc fields: II. Magnetic Viscosity" , *J.Phys. F:Met. Phys.*, **8**, 1309 (1978)

[29] Cayless, A.T., Hoon, S.R., Tanner, B.K., Chantrell, R.W., and Kilner, M., "High sensitivity measurements of néel relaxation in fine particle ferromagnetic systems ", *J.Magn. Magn. Mater*, **30**, 303-311 (1983)

[30] Anderson, P.W., "Theory of flux creep in hard superconductors", *Phys. Rev. Letts.*, **9**, 309-311 (1962)

[31] O'Grady, K., and Chantrell, R.W., "The temperature variation of the coefficient of magnetic viscosity", *J. Magn. Magn. Mater.*, **54-57**, 755-756 (1986)

[32] O'Grady, K., Chantrell, R.W., Popplewell, J., and Charles, S.W., "Time dependent magnetisation of a system of fine cobalt particles", *IEEE Trans. Magn.*, **17**, 2943-2945 (1981)

[33] Kloepper, R.M., Finkelstein, B., and Braunstein, D.P., "Time decay of magnetisation in Particulate media", *IEEE Trans. Magn.*, **20**, 757-759 (1984)

[34] Chantrell, R.W., Hoon, S.R.and Tanner, B.K., "Time-dependent Magnetisation in fine-particle ferromagnetic systems", *J. Magn. Magn. Mater.*, **38**, 133-141 (1983)

[35] Stoner, E.C., and Wohlfarth, E.P., "A mechanism of magnetic hysteresis in heterogeneous alloys", *Phil. Trans. Roy. Soc.*, **A-240**, 599-642 (1948)

[36] Luborsky, F.E., "Development of Elongated particle magnets", *J.Appl. Phys.*, **32**, 171S-183S (1961)

[37] Jacobs, I.S., and Bean, C.P., " An approach to elongated fine-particle magnets", *Phys. Rev.*, **100**, 1060-1067 (1955)

[38] Frei, E.H., Shtrikman, S., and Treves, D., "Critical size and nucleation field of ideal ferromagnetic particles", *Phys. Rev.*, **106**, 446-455 (1957)

Chapter 2

Magnetic Particle Inspection

2.0 Introduction to Magnetic Particle Inspection

Magnetic Particle Inspection (MPI) is a non destructive technique used to establish the presence of surface breaking cracks and sub surface flaws in ferrous metals. The technique has not changed much since the technique was first discovered accidentally by Hoke in 1919. The pioneering work was done by DeForest and Doane who formed the Magnaflux Corporation to exploit the technique. On magnetising a ferrous metal the presence of surface breaking cracks will cause flux leakage around the crack. When a magnetic ink (typically a suspension of magnetic particles in kerosene) or a magnetic powder is applied, the magnetic particles will be attracted towards the crack. Agglomeration will occur round the crack and its position can be easily detected by the eye. In this chapter a brief guide to practical MPI will be given so that the motivation behind this research can be better understood.

2.1 Magnetisation Levels in MPI

For the technique to be successful flux leakage needs to occur at a sufficient level to attract enough magnetic particles to the crack for it to be visible. Flux leakage occurs when the magnetic induction in a medium comes across a change in permeability (i.e. air in the case of a crack or a non magnetic inclusion within the metal) not parallel to the direction of the induction. Fig.2.1 indicates the flux leakage which occurs for various combinations of the magnetic induction and crack orientation. In Fig.2.1a the steel specimen does not contain a flaw and the magnetic induction remains inside the test piece with a very small magnetic field in the air above. In Fig.2.1b the flaw lies parallel to the magnetisation direction and there is no detectable change in the magnetic leakage flux, assuming that the width of the crack is small compared to its length. However if the specimen contains a flaw at right angles to the direction of the magnetisation as in Fig.2.1c then substantial flux leakage will occur. This is because the flux lines have to cross the air gap. Within the air gap they repel each other and spread out but this is limited by the desire to stay within the ferromagnetic medium. The presence of this defect could be detected by the application of a magnetic ink. Fig.2.1d shows why an embedded flaw is

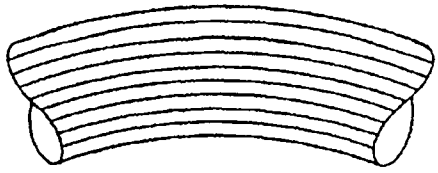

Fig.2.1 Diagram illustrating the flux leakage associated with a ferrous specimen with no flaw present.

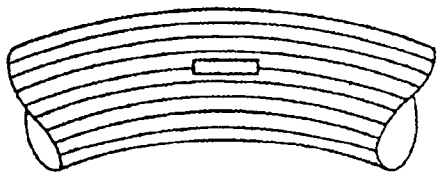

Fig.2.1b Diagram illustrating the flux leakage associated with a ferrous specimen with a flaw present but at parallel to the direction of magnetic induction.

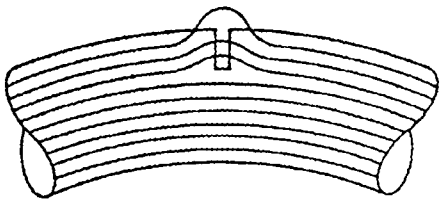

Fig.2.1c Diagram illustrating the flux leakage associated with a ferrous specimen with a flaw present at right angles to the direction of magnetic induction.

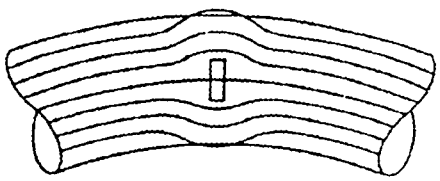

Fig.2.1d Diagram illustrating the flux leakage associated with a ferrous specimen with a embedded flaw present.

harder to detect with MPI than the equivalent surface breaking crack. This is because most of the flux which is distorted by the presence of the defect remains within the metal and very little flux leakage occurs. Therefore the attraction of the particles to the crack is less.

Obviously the degree of flux leakage depends on the physical dimensions of the crack as well as the level of magnetic flux density in the medium. To achieve reliable results over a wide range of magnetic materials the magnetic flux density in the test piece needs to be the same. With this in mind the British Standard [1] recommends a peak magnetic flux density of 0.72 Tesla. This is based on empirical results obtained over a wide range of constructional steels and cast irons. However as the magnetic flux density in a material is a difficult quantity to measure they go on to suggest a peak magnetic field at the surface of 2.4 kAm^{-1}. The justification for this is that most steels have a relative permeability greater than 240 and therefore the magnetic flux density will exceed 0.72 Tesla. The draft European Standard [2] however recommends a magnetic flux density of 1 Tesla in low carbon steels and states this should be exceeded in a magnetic field of 2 kAm^{-1}.

There is a disagreement between the required level of magnetic flux density and the magnetic field required to achieve this level of magnetic flux density for the two standards. This is due to the fact that each country within Europe has its own recommended level of magnetic flux density and magnetic field required to achieve this level of flux density and therefore the draft European Standard recommendation as such is a comprise. Within this research we are mainly concerned with the British Standard and how it compares with the draft European Standard, also which of the two Standards has the better physical basis.

2.1.1 Methods of Magnetisation

The generation of a peak magnetic field of 2.4 kAm^{-1} can be achieved in a variety of ways dependent upon the availability of equipment and the orientation of the cracks you wish to be detected. The main techniques are shown in Fig.2.2. An example of the current flow method is shown in Fig.2.2a, in which the test piece has a current passed through it via two points of contact. This technique favours the detection of cracks parallel to the current flow. By using 4 or more contacts and two ac power supplies with a phase shift of 90° between the two waveforms they produce, the magnetisation vector will then rotate through 360°. This rotation of the magnetic flux density allows cracks to be detected in any direction, this technique being called multi directional magnetisation. For more details see O'Bryan[3]. Fig.2.2b shows the magnetic flow methods in which the test specimen

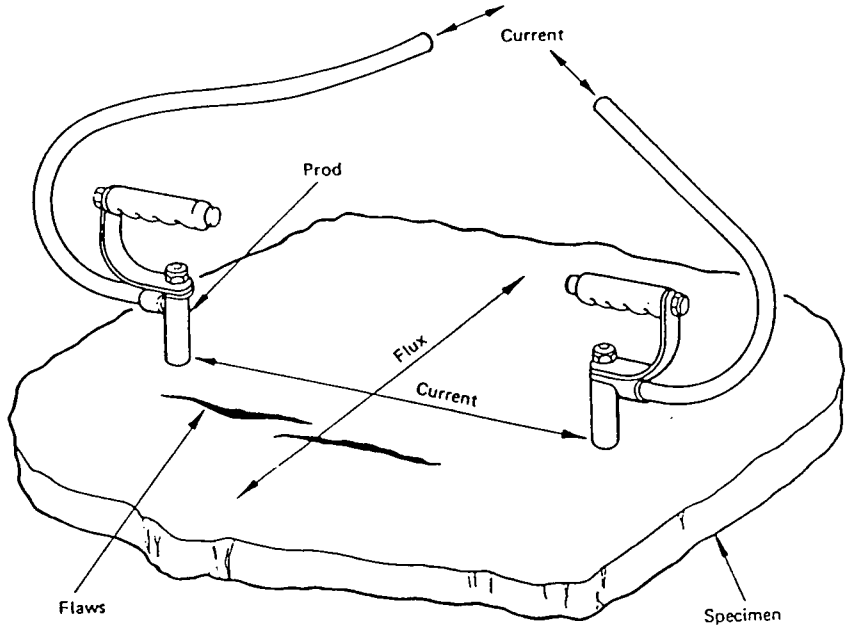

Current flow technique (prods)

Fig.2.2a Current flow method of magnetising an inspection piece.

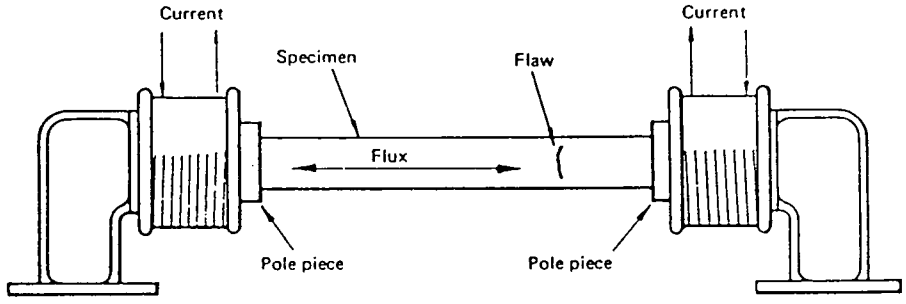

(a) Fixed bench with solenoid heads

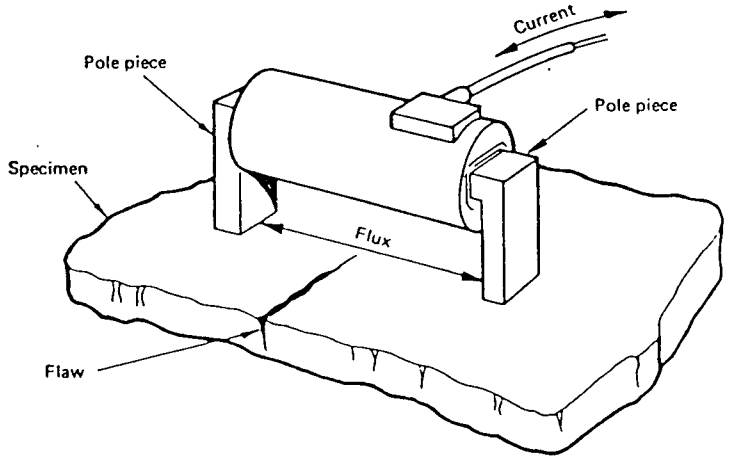

Yoke

Magnetic flow technique

Fig.2.2b Magnetic Flow methods of magnetising an inspection piece.

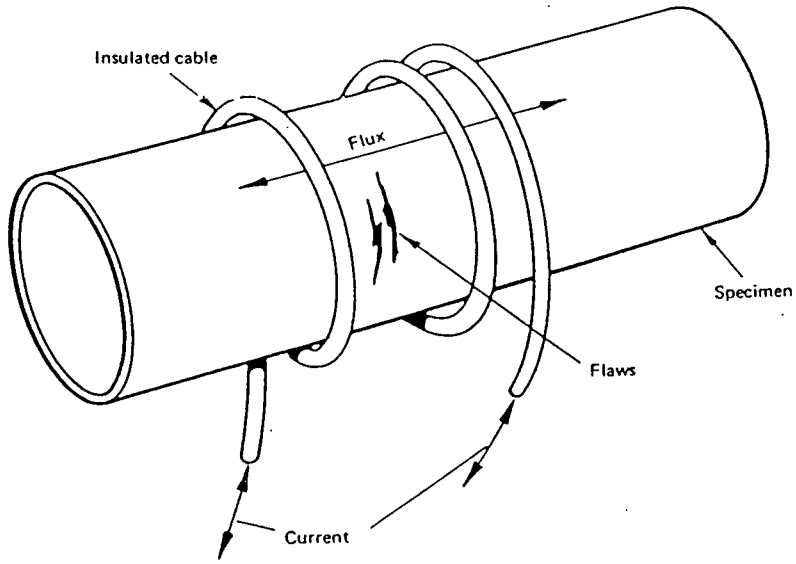

Flexible cable technique (using cable wound round the specimen)

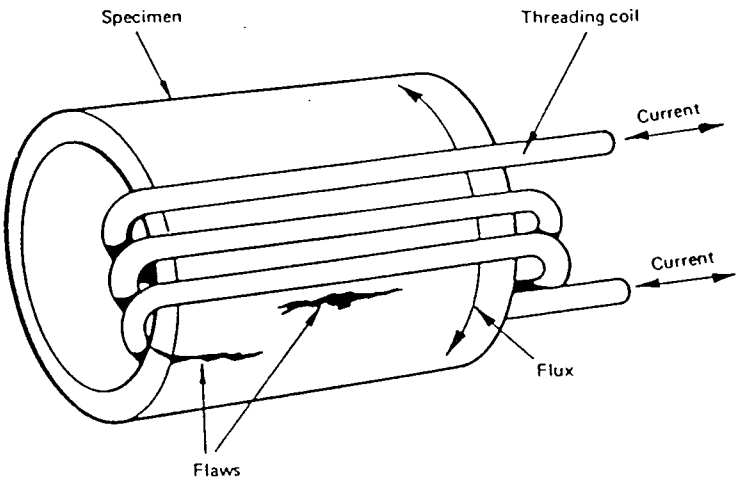

Flexible cable technique (using cable wound through the specimen)

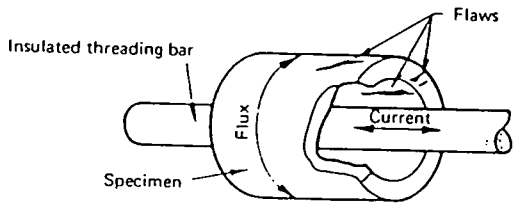

Threading bar or cable technique

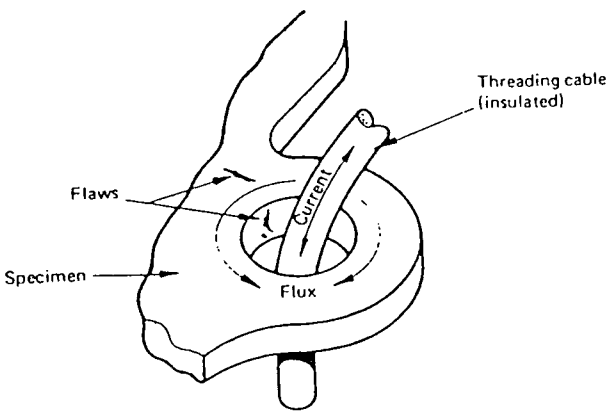

Flexible threading bar technique

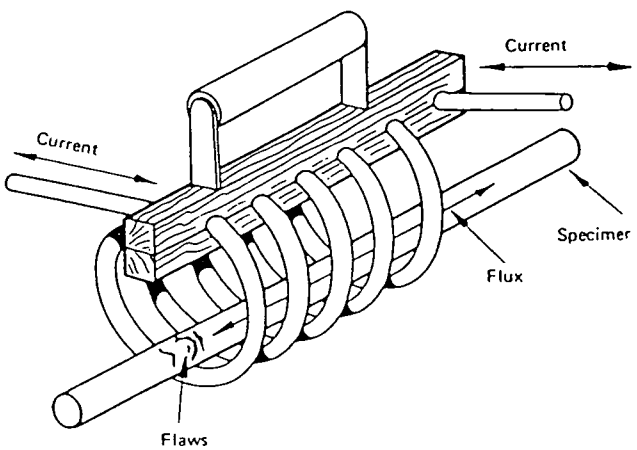

Coil technique

Fig.2.2c Other methods of magnetising an inspection piece.

becomes part of the magnetic circuit. Cracks will be detected in the transverse direction. In the other methods shown in Fig.2.2c a current is passed through either a cable or coil placed close to the specimen.

In all these techniques there are limits to the area in which the magnetic field at the surface exceeds 2.4 kAm^{-1}. This area is determined by factors such as prod or pole spacing and the current/field available to the operator. More details are given in the relevant standards.

The use of time varying power supplies to generate the necessary currents and magnetic fields is common. These time varying magnetic fields and currents obviously affects the level of magnetisation in the test piece due to the generation of eddy currents.

Magnetic fields which vary with time induce electric currents in a conducting medium. These electric currents have a magnetic field associated with them. These oppose the applied field and consequently the alternating magnetic field decreases in strength steadily into the medium. This decrease is characterised by the skin depth[4] of the medium δ

$$\delta = \frac{1}{\sqrt{\pi f \mu_r \mu_0 \Omega}} \qquad 2.1$$

where f is the frequency of the oscillation,Ω is the conductivity of the medium, μ_r is the relative permeability of the medium and μ_o is the absolute permeability. The skin depth in a typical steel is 1 mm, which means that 1 mm into the steel the strength of the applied field has decreased to 63% of the strength at the surface.

The effect of skin depth when using magnetic flow methods is to concentrate the magnetic flux within the surface[5]. Therefore when using field flow methods with time varying waveforms the magnetic field generated at the surface is greater than when a dc waveform is being used. However if current flow methods are being used then the fact that the current is alternating does not affect the field strength at the surface, only the distribution of the magnetic field within the material. The general effect of ac magnetisation is to increase the sensitivity of MPI to surface breaking cracks but to lessen its sensitivity to sub surface defects.

However time varying fields introduce a number of problems in understanding the physical processes in MPI. These additional problems are that hysteresis occurs in both the test piece and the magnetic particles in the magnetic ink. To get round these problems between different waveforms British Standard states *'Although there is no proof, the complicated effects associated with different waveforms are usually resolved by assuming that the peak value of the waveform is effective in Magnetic Particle flaw detection'*. It then goes onto list conversion factors so that the peak of the waveform can be found from its rms value. Most meters measure the rms value of a waveform. However Westwood [6] has recently reported that for thyristor waveforms there is not a linear relationship between the rms and peak values. The draft European Standard states *'That rms. should be used when specifying field values'* and Stadhaus[7] has presented experimental results on low remanence steels that back up this statement.

2.2 Aids to Increase the Visibility of a defect

The success of MPI relies on the operator being able to distinguish the indication associated with a crack from the background. If the test piece has a black finish to it then the black magnetic particles at an indication do not have a high contrast. To enhance the visibility of the indication a white paint layer is often applied to the surface. The black particles achieve a higher level of contrast against this white background. There is of course a trade off between the increased visibility of the defect and the decrease in the number of ink particles at the defect. This is because the leakage field the particle experiences depends on its distance from the crack. A paint layer increases this distance

The other way to increase the visibility of the defect is to use coloured or fluorescent inks. These inks give a better contrast against a black background than a black ink, although fluorescent inks need UV lamps to cause them to fluoresce. Their magnetic sensitivity is generally regarded as lower than a black ink but this is easily outweighed by their increased contrast.

2.3 Magnetic Inks and Powders

This section deals with the physical and magnetic properties of commercial magnetic inks and powders. In it we discuss the properties of a typical black magnetic ink, a typical fluorescent ink and a magnetic powder, before looking at the properties of ideal inks and powders.

2.3.1 Black Magnetic Ink

These consist of a suspension of iron oxide particles in a carrier fluid of either water or kerosene and are often applied with an aerosol. Most manufacturers quote a typical size of 10 μm in diameter for the particles; this varies with the task required of the ink. Smaller particles are used to reveal smaller defects. The structures of these ink particles have been investigated by Tanner et al[8]. The results of this study were that the basic building blocks of the inks were 20-200 nm single domain crystallites with no preferred axis of alignment. These crystallites are attracted to one another by their magnetic properties and form flux closure structures typical 1-3 μm in size. These then further aggregate to form the larger structures reported by the manufacturers

2.3.2 Fluorescent Inks

These consist of an iron or iron oxide core that is treated with a material with high fluorescence and then suspended in a carrier fluid. They are also often applied with an aerosol. From the manufacturers' data the mean diameter of these particles is 7 μm. However the structure of the particles is not known.

2.3.3 Magnetic Powders

Magnetic powders are used in MPI to detect the presence of gross surface defects in ferrous metals. The powder is applied to the surface via a powder blower. Magnetic powders consist of iron particles typically in the 60 micron range and can be coloured to give better contrast against black inspection pieces.

2.3.4 Ideal Properties of Magnetic Inks and Powders

In this section the ideal properties of magnetic inks and powders will be discussed. For a more detailed discussion the reader should consult Betz[9] and Lovejoy[10]. Parameters of importance are the magnetic characteristics of the particle, its density, the size and shape of the particle, the perceptibility of the particles and the viscosity of the carrier fluid used to suspend the particles. It will be seen that these parameters are interlinked and a material having good characteristic in any one of these parameters will not necessarily make a good material for a magnetic ink.

Magnetic properties of the ink particles are important as the magnetic force on a particle depends on its magnetisation. However it is not the saturation magnetisation values which are important but the initial magnetic response of the particles as the magnetic fields generated in MPI are small, being less than 4 kAm^{-1}. The higher is the particle's permeability, the higher the magnetic force will be, and therefore finer indications can be detected. Ideally the particles should have a low value of remanence and coercivity to stop the particles agglomerating in the storage containers used and to allow the particles to be easily removed from the inspection piece.

The size of the particles also affects the magnetic force on the particle. However if the size of the particles is too large then the particle will not be arrested by a small indication. On the other hand, if the particles are too small then they will be arrested by surface blemishes.

The density of the material is important because the time taken for the ink particles to fall through the liquid depends on its density. The longer the particles remain in the suspension, the better as they will experience a greater magnetic force if they remain in suspension.

The other parameters of the particles which affect the settling time are the size and shape of the particles. The larger the particle the quicker it will settle out of the suspension and therefore the leakage fields it experiences will be less than if it remained in suspension. The shape, as well as affecting the settling time, affects the magnetic properties of the particle as long thin needles like particles will have lower demagnetisation factors and therefore the magnetic force on the particle will increase. Thin needle like particles will also have a lower drag through the liquid. However the cost involved in producing needle like particles is generally considered not worth the increased sensitivity.

The viscosity of the carrier fluid also affects the settling time. If the viscosity is too high then the terminal velocity of the particles will be low and the time taken for an indication to form will be unacceptably long. If, on the other hand, the viscosity is low then the particles settling time will be low and the particles will not remain in suspension for long enough to be attracted to the crack.

The perceptibility of the particles is important because if the particles are present at the crack but can not be seen then there is no MPI indication. With this in mind, fluorescent and coloured inks are used on black surfaces. If black inks are used, a contrast layer is applied to the surface before the inspection is carried out.

2.4 The Calculation of the Magnetic Leakage Field

Up to now the flux leakage associated with a surface breaking crack has been discussed but we have not seen how parameters such as crack dimension, magnetising field and the permeability of the inspection piece affect the magnetic leakage field. For a general review on the calculation of the magnetic leakage field the reader should consult Dobmann and Höller[11]. The calculation of the magnetic leakage field is important in both modelling the indication mechanism in MPI and, with the advent of small Hall probes, the possibilities of sizing defects by measuring the leakage flux associated with a crack. Obviously the parameters which affect the leakage field are important and as such has received a lot of interest. Zatsepin and Shcherbinin[12] modelled the leakage field of a surface breaking flaw by considering it as an infinitely long strip of dipoles. The co-ordinate system used is shown in Fig.2.3. They found that the tangential magnetic leakage field H_x and the normal magnetic leakage field H_y were given by:

$$H_x = \frac{\sigma_s}{2\pi}\left(\tan^{-1}\frac{b(x+a)}{(x+a)^2+y(y+b)} - \tan^{-1}\frac{b(x-a)}{(x-a)^2+y(y+b)}\right) \qquad 2.2$$

$$H_y = \frac{\sigma_s}{4\pi}\ln\left[\frac{((x+a)^2+(y+b)^2)((x-a)^2+y^2)}{((x+a)^2+y^2)((x-a)^2+y(y+b)^2)}\right] \qquad 2.3$$

Here σ_S is the surface polarity of the rectangular slot. This work was extended to slots of finite length by Schcherbinin and Pashagin[13]. The main limitation with the work is that the expressions for the magnetic leakage fields do not contain a term which depends on the applied field. This is the main failure of the modelling work of Zatsepin, Schcherbinin and Pashagin, namely the inability to relate the magnetising field H_0 and the permeability of the inspection piece μ_r to the surface polarity σ_S.

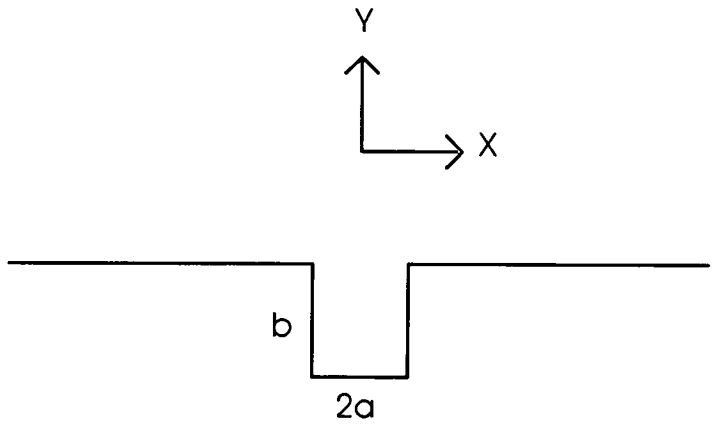

Fig.2.3 Diagram showing crack and axis geometry as used by Zatsepin and Shcherbinin and Edwards and Palmer. Zero of y axis is at the specimen surface and x axis zero is at centre of crack.

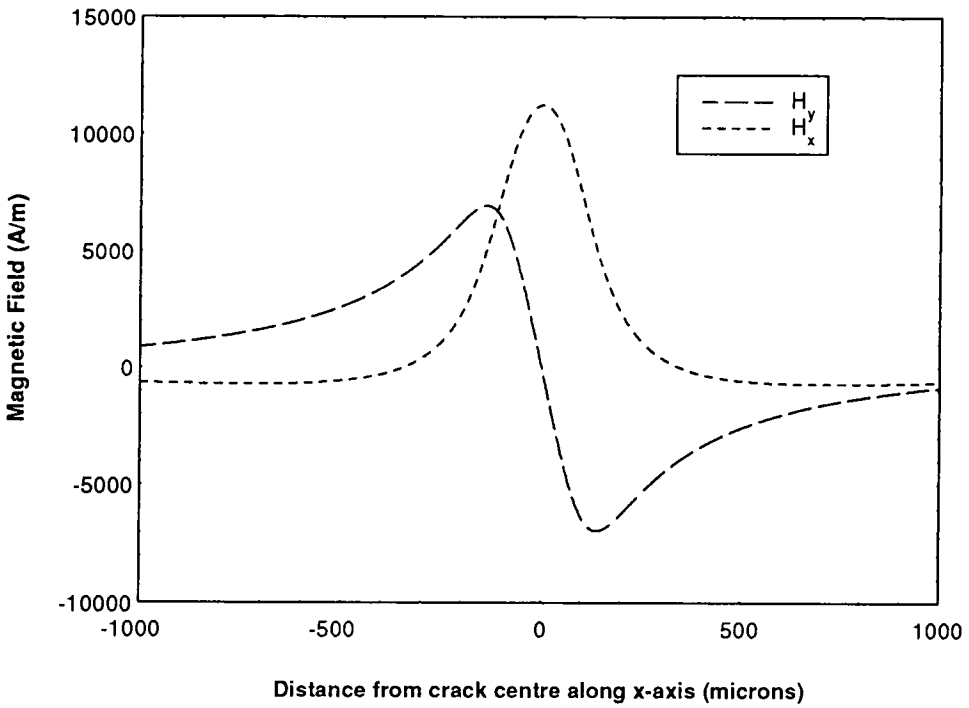

Fig.2.4 The variation of H_x and H_y as the distance along x-axis is varied according to the model of Edwards and Palmers. Parameters used are a=100 microns b=1mm H_o=2400 A/m μ_r=1400 and the distance above the surface is 100 microns.

These limitations were overcome by the work of Edwards and Palmer[14] who calculated the surface pole density for a semi elliptical surface breaking crack. A semi elliptical crack was used as the surface polarity of such a crack can be determined from a solution of Laplace equations. They used the functional dependence of the leakage field for a rectangular crack as calculated by Zatsepin and Schcherbinin and obtained the following expressions for the tangential and normal components of the field

$$H_x = \frac{H_o n(\mu_r - 1)}{2(n+\mu_r)\tan^{-1} n}\left(\tan^{-1}\frac{b(x+a)}{(x+a)^2 + y(y+b)} - \tan^{-1}\frac{b(x-a)}{(x-a)^2 + y(y+b)}\right)$$

2.4

$$H_y = \frac{H_0 n(\mu_r - 1)}{4(n+\mu_r)\tan^{-1} n}\ln\left[\frac{((x+a)^2 + (y+b)^2)((x-a)^2 + y^2)}{((x+a)^2 + y^2)((x-a)^2 + y(y+b)^2)}\right] \quad 2.5$$

$n(=b/a)$ is the aspect ratio of the crack. The functional dependence of H_y and H_x as x is varied from the crack centre is shown in Fig.2.4. The assumption used in deriving these equations were that an infinitely long rectangular cavity with a constant pole density could be approximated to an elliptical cavity whose pole density varied over its surface. Edwards and Palmer stated that this variation is slight except at the rim of the cavity.

Zhong[15] has recently proposed a new theory of magnetic particle inspection, in which he calculates the magnetic leakage field for point type holes and tiny cracks by assuming these can be approximated by a set of magnetic dipoles. However his expressions do not contain terms dependent on the magnetising field and as such are an extension of the much earlier work of Zatsepin and Schcherbinin.

The only way to calculate the leakage field if the permeability of the test piece varies as a function of magnetic field is to use finite element analysis. Hwang and Lord[16] have modelled the leakage field of a surface breaking crack in a medium of non constant permeability. However their method of analysis does not allow the functional dependence of the leakage field on parameters such as crack depth and width to be determined unless a large number of simulations are performed.

The other benefit of finite element analysis is in the determination of the magnetisation level and direction in structures with complex geometry. An example of this is in the automotive industry were it is essential that a piece such as the steering cam is checked for defects in all orientations. This is achieved by using multi-directional magnetisation. However it is a matter of skill and experience to ensure that in complex pieces the magnetisation is of the correct strength and direction. Recently commercial finite element packages such as those produced by Vector Fields[17] allow the magnetisation direction in complex structures to be determined thus reducing the risk of failure in safety critical parts.

2.5 Comparison of MPI with other NDT Techniques

There are a wide range of other non-destructive testing techniques for detecting the presence of surface breaking flaws in ferrous metals. These include ultrasonics, eddy current and alternating current potential drop (ACPD) methods. In this section we compare these techniques with Magnetic Particle Inspection.

2.5.1 Ultrasonics

Ultrasonics[18]: A piezoelectric transducer is used to generate a short pulse of high frequency waves (1-10 MHz) into the test specimen. When these waves impinge on a defect a fraction of the amplitude will be reflected back. Additionally waves which miss the defect will be reflected off the back surface of the specimen. These reflected waves are detected by a transducer which can be the one used to transmit the pulse. These waves are shown on a C.R.O and by measuring the distance between the start of the transmitted wave and the start of the reflected wave of the defect the distance to the defect can be calculated. By moving the transducers, various parameters of the crack can be deduced.

However the detection of surface breaking crack using this method requires highly trained personnel and is very time consuming. Whereas in MPI assuming that the test piece can be easily magnetised surface breaking flaws can be detected quickly and easily.

2.5.2 Eddy Currents

Eddy Current[19,20]: This inspection technique relies on the change in impedance of a search coil in the vicinity of the test specimen, caused by the generation of an electric current in

the test specimen when it is subject to a time varying field. Eddy currents can be used for the detection of cracks and other defects because the defect interrupts the flow of eddy currents generated in the material and this changes the inductance of the search coil. From the change in the inductance, crack parameters can be deduced with certain assumptions.

2.5.3 Alternating Current Potential Drop

Alternating Current Potential Drop[21]: This is used to measure the crack depth once the presence of the crack has been determined by another method. In this method the potential drop across two contacts, a known distance apart, is measured in a defect free area of the specimen at a high frequency. High frequency is used to confine the electric current to the surface due to the skin depth. Then the potential drop across the crack is measured. The presence of the defect changes the potential drop by an amount proportional to the crack depth assuming that the crack width is negligible. This is a technique used for crack measurement not detection.

The advantage of Magnetic Particle Inspection is that it is particularly sensitive to surface breaking crack. It is a lot simpler to use than eddy currents and ultrasonic methods. Although the crack length can be measured using MPI it can only be used on ferrous metals to detect surface breaking cracks and provides no information on crack depth or width. To conclude, MPI complements the other techniques available to the NDT technician.

2.6 Summary

The use of a Magnetic Particle Inspection as a Non Destructive Testing technique has been discussed. This includes the methods of magnetising the specimen to obtain the required level of magnetic flux leakage and the magnetic and physical properties of the inks and powders used to delineate a crack. Calculation of the leakage field due to a surface breaking crack has been discussed using both analytical and finite element methods. Finally MPI has been compared with some other NDT technique.

References Chapter 2

[1] British Standard BS 6072

[2] Draft European Standard, "General rules for Magnetic Particle Inspection"

[3] O'Bryan, L.J., "Multidirectional magnetisation of structural Welds", *Mater. Eval.*, **39**, 508-509 (1981)

[4] Grant, I.S., and Phillips, W.R., "Electromagnetism" ,*Wiley*, 381 (1986)

[5] Edwards, C., PhD thesis, University of Hull (1986)

[6] Westwood, S.M., "Waveform Characteristics of thyristor controlled Power supplies as used in magnetic particle inspection", *The British Journal of Non-Destructive Testing*, **30** , 333.-334 (1990)

[7] Stadthaus, M., Dichaut, E., and Prestel, W., "System performance in magnetic particle inspection", WCNDT, London (1987)

[8] Tanner, B.K., McCoy, J.M., Willcock, S.N.M., Hetherington, M.G., and Jakubovics, J.P., "The structure and behaviour of inks for magnetic particle inspection", *J. Mater. Sci Lett.*, **5**,296-298 (1986)

[9] Betz, C.E., "Principles of magnetic particle Testing", Magnaflux Corporation, Chicago,

(1967)

[10] Lovejoy, D.J., "The nature of magnetic inks and powders", *The British Journal of Non-Destructive Testing*, **23**, 242-245 (1980)

[11] Dobmann, G., and Höller, P., "Physical analysis of Magnetic flux leakage" in Research techniques in Nondestructive Testing Vol IV, *Academic Press*, New York (1980)

[12] Zatsepin, N.N, and Schcherbinin, V.E, "Calculation of the magnetostatic field of surface defects. I field topography of defect models", *Defektoskopiya*, **2**, 385-393 (1966)

[13] Scherbinn, V.E., and Pashagin, A.I., "Influence of the extension of a defect on the magnitude of its magnetic field", *Defektoskopiya*, **8**, 441-447 (1972)

[14] Edwards, C., and Palmer, S.B., "The magnetic leakage field of surface breaking cracks", *J. Phys. D: Appl. Phys.*, **19**, 657-673 (1986)

[15] Zhong, W.C., "Magnetic Particle Inspection - a new theory", *The British Journal of Non-Destructive Testing"*, **35**, 68-74 (1993)

[16] Hwang, J.H., and Lord, W.J., "Finite element modelling of magnetic field/defect interactions", *Test. and Eval.*, **3**, 21-25 (1975)

[17] Vector Fields, 24 Bankside, Kidlington, Oxford

[18] Blitz, J., "Fundamentals of Ultrasonics", *Butterworths*, London, 185-189, (1963)

[19] Libby, H.L., "Multiparameter Eddy Currents Concepts" in Research Techniques in Nondestructive Testing" *Academic Press,* London (1970)

[20] Libby, H.L., "Introduction to Electromagnetic Nondestructive Test Methods", *Wiley-Interscience* (1971)

[21] Frise, P.R., and Bell, R., "Improved probe array for ACPD crack measurements", *The British Journal of Non-Destructive Testing,* **34**, 15-19 (1992)

Chapter 3

Experimental Techniques

3.0.Introduction

The experimental apparatus used to obtain the results presented in the following chapters are discussed. There are two Vibrating Sample Magnetometers, one of which (a Low Field VSM) has been specially constructed for this work. In addition measurements have been made on an Alternating Gradient Force Magnetometer which is a 1000 times more sensitive than a conventional VSM (sensitivity 10^{-11} Am^2 [1]). These have been used to determine the magnetisation processes in Magnetic Inks both in liquid and powder states. A Torque Magnetometer has been used to study the spin reversal mechanism in the magnetic inks. The calibration of these devices is also discussed.

3.1 Vibrating Sample Magnetometer

The Vibrating Sample Magnetometer, relies on the fact that the sample magnetic dipole when subjected to periodic mechanical vibration causes an alternating voltage to be induced across a set of coils placed near the sample. This technique was first described by Foner[2]. The principal components of a VSM are shown in Fig.3.1. The sample is forced to vibrate perpendicular to an applied field at a fixed frequency and amplitude. The voltage induced is dependent upon the amplitude and frequency of the vibration as well as the coupling between the sample's magnetic moment and the detection coils. The variation of this voltage with applied field allows the magnetic moment of a material to be determined as a function of magnetic field.

To enhance the sensitivity of the method a phase sensitive lock-in amplifier is routinely used. This allows the signal due to the sample moment to be determined even if it is obscured by noise. Recently digital signal processing has been applied to Vibrating Sample Magnetometry[3], this is claimed to give an increase in sensitivity and speed of detection compared to an analogue lock-in amplifier. The calibration of the device is usually achieved with a high purity sample of nickel placed in a known saturating field.

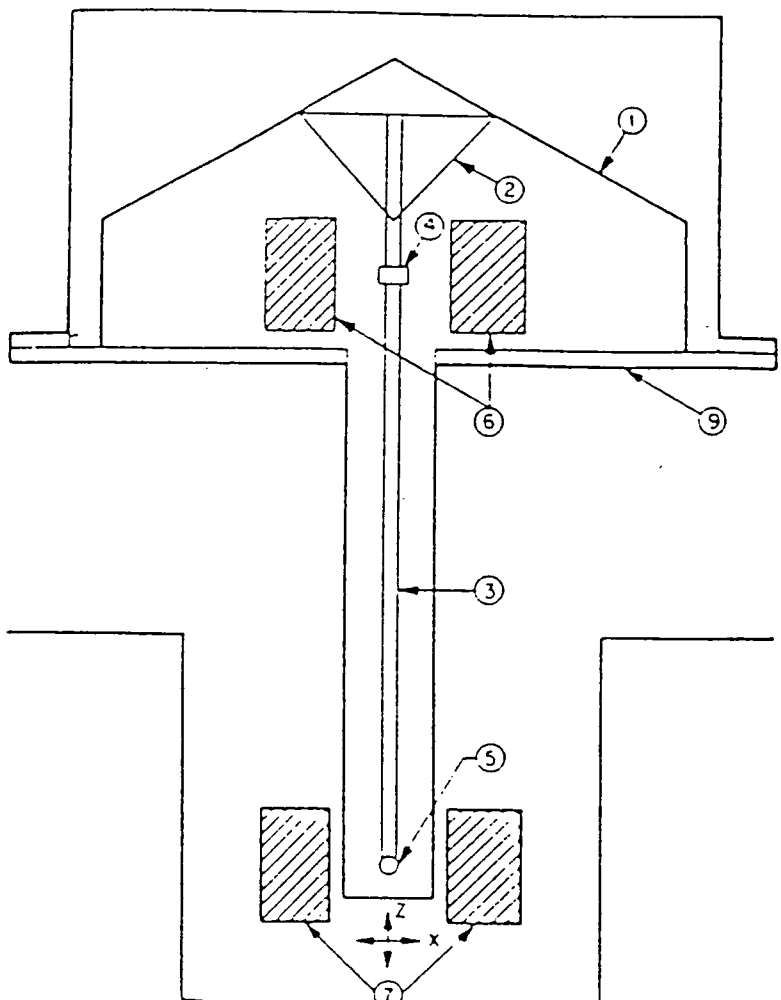

Fig.3.1. Foner's Vibrating Sample Magnetometer. 1) Loudspeaker transducer, 2) Conical paper cup support, 3) Drinking straw, 4) Reference Sample, 5) Sample, 6) Reference Coils, 7) Sample coils, 8) Magnet poles, 9) Metal container. From reference 2.

3.1.1 Durham 1.2 Tesla Vibrating Sample Magnetometer

This VSM was original built by Hoon and Wilcock[4] and has been described several times before, Thompson[5] and Gregory[6] . For this reason only a brief description of it will be given, outlining the improvements made by the author.

The outline of the Durham 1.2 Tesla Vibrating Sample Magnetometry is shown in Fig.3.2. The sample is vibrated within an Oxford Instruments CF 1200 cryostat. The detection coils used to obtain a signal due to the sample's magnetic moment are mounted on the pole pieces of the electromagnet. There are 4 coils, each of which has 16000 turns of 48 gauge wire and were balanced inductively to within 0.3 % by McCoy[7] . The coil geometry used is that described by Mallinson[8], this being shown schematically in Fig.3.3. The voltage obtained from one pair of coils V_a is the same magnitude but opposite sign as that developed across the other pair $V_b(=- V_a)$ assuming the sample is centred.

These voltages are fed into a Brookdeal 5206 lock-in amplifier operating on (A-B) mode so the signal obtained is $2V_a$. The reference signal needed for the lock-in amplifier is derived from the motor and cam assembly, which is used to vibrate the sample. A permanent magnet is placed on the shaft of the motor and rotated at the same frequency as the sample vibration this induces a voltage in a coil placed near it. This is then used as the reference signal for the lock-in amplifier.

The magnet is powered by an Amicrown amplifier. This is fed with a variable dc voltage which allows the magnetic field that the sample experiences to be varied.

The data collection process is controlled by a Personal Computer via the IEEE interface. The strength of the magnetic field is measured by a Bell 640 gaussmeter which then supplies a Digital Voltmeter with an analogue signal proportional to the magnetic field. This is read with the signal from the lock-in amplifier and recorded by the computer. The computer then changes the magnetic field by altering the dc voltage going into the Amicrown amplifier via a Bede Scientific[9] Digital to Analogue Converter. In this way full hysteresis loops may be obtained.

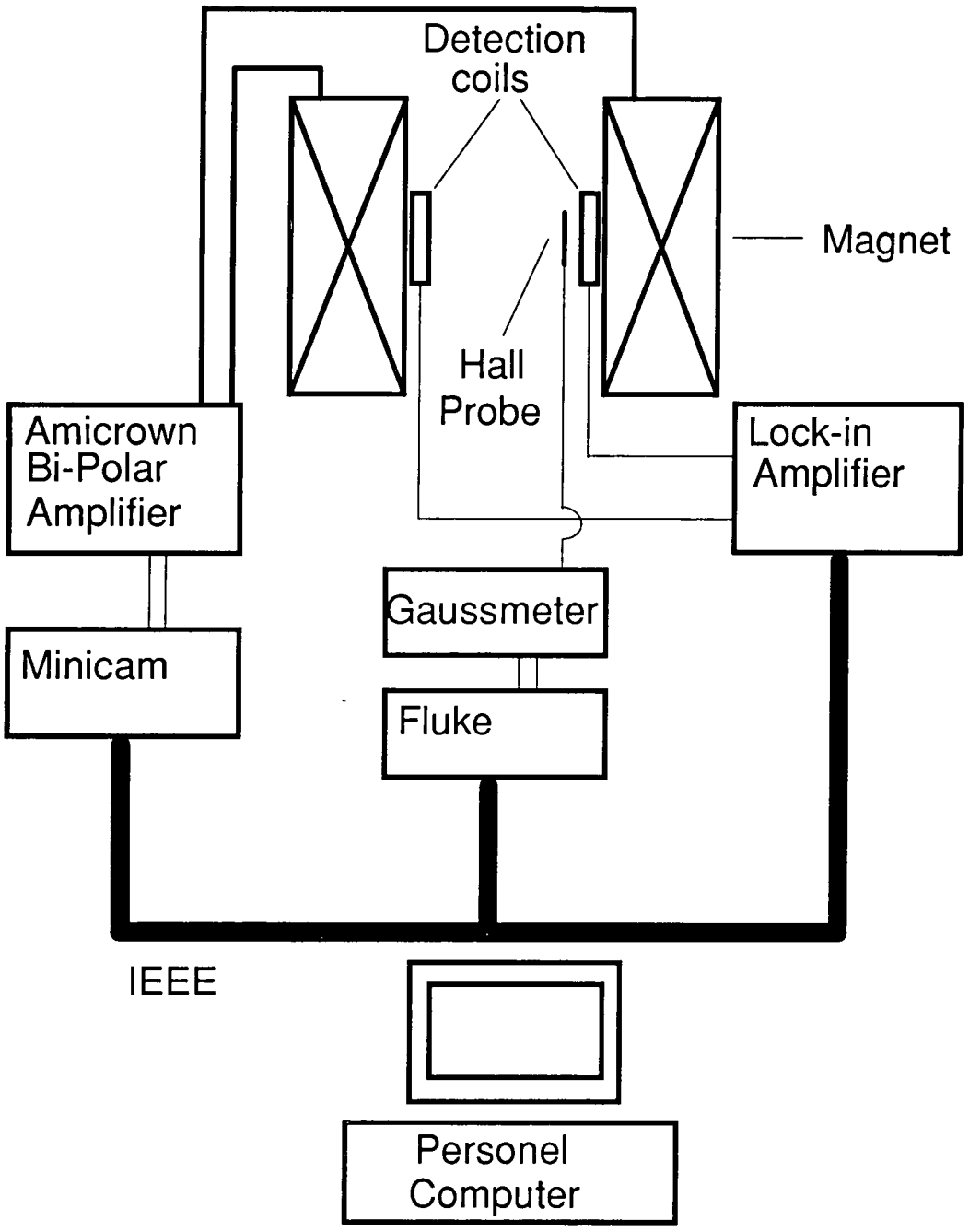

Fig.3.2 Outline of Durham 1.2 Tesla Vibrating Sample Magnetometer.

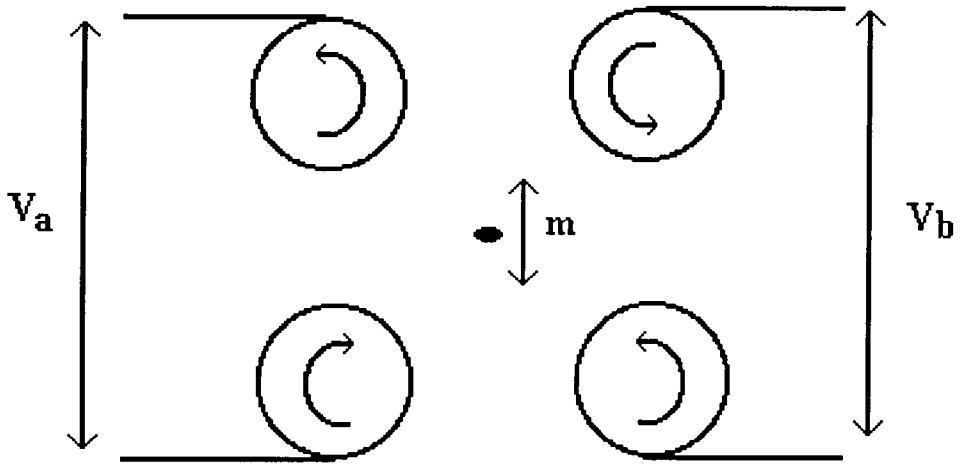

Fig.3.3 Diagram Illustrating the Mallinson geometry used in the Durham 1.2 Tesla VSM.

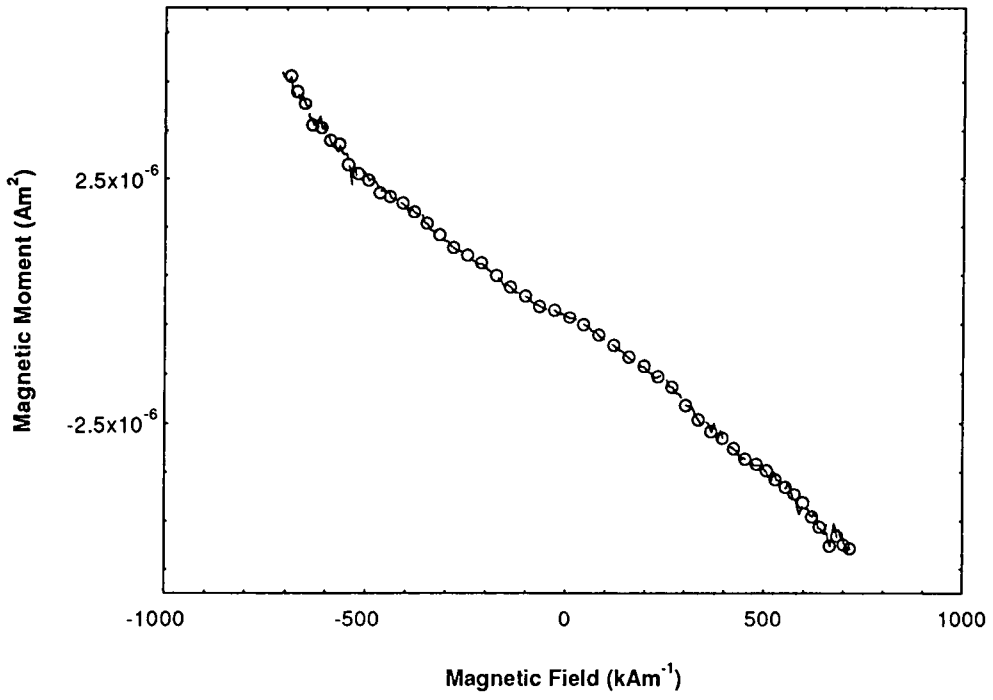

Fig.3.4 Typical residual curve from the VSM signal is due to the presence of PTFE tape,sample holder and glass rod.

3.1.2 Calibration and Residual Subtraction

To determine the calibration of the VSM an ellipsoidal sample of high purity nickel is used. The nickel sample has a mass of 0.0384g and the voltage produced is recorded in a magnetic field of 880 kA/m corresponding to an internal magnetic field of 800 kA/m. This author following the work of Lambrick[10] who surveyed the literature (e.g. Pauthenet[11] and Graham[12]) has used the following formula for the mass magnetisation of nickel with respect to temperature T.

$$\sigma(H = 800 \quad kA/m) = \sigma_0\left(1 - a_{32}T^{\frac{3}{2}} - a_{52}T^{\frac{5}{2}}\right) \qquad 3.1$$

$$\sigma_0 = 58.624 Am^2/kg$$

$$a_{32} = 6.64 \times 10^{-6}$$

$$a_{52} = 1.85 \times 10^{-8}$$

This calibration is carried out daily, a typical figure for this calibration being 0.242 Am^2/Volts.

The magnetic samples under investigation are mounted onto a sample holder and fixed onto a glass rod with PTFE tape. The sample holder, glass rod and the PTFE tape contribute to the induced signal. Therefore there is a need to subtract this contribution to the magnetisation from the induced signal. With this in mind a residual run is performed after each run without a sample in place. A typical residual run is shown in Fig.3.4. A linear fit is assumed and is subtracted from the raw data.

However for very weak samples this procedure is unsuitable due to the movement of the pole pieces. The pole pieces upon which the detection coils are mounted are attracted towards each other due to their magnetisation and at a certain field the pole pieces move slightly. The movement of the pole pieces produces a kink in the raw data shown in Fig.3.5 and occurs in both positive and negative quadrants. Lambrick [13] reported a similar problem however this occurred at a field of 480 kAm^{-1} whereas this kink occurs around 240 kAm^{-1}. However for stronger signals this kink in the raw data is obscured.

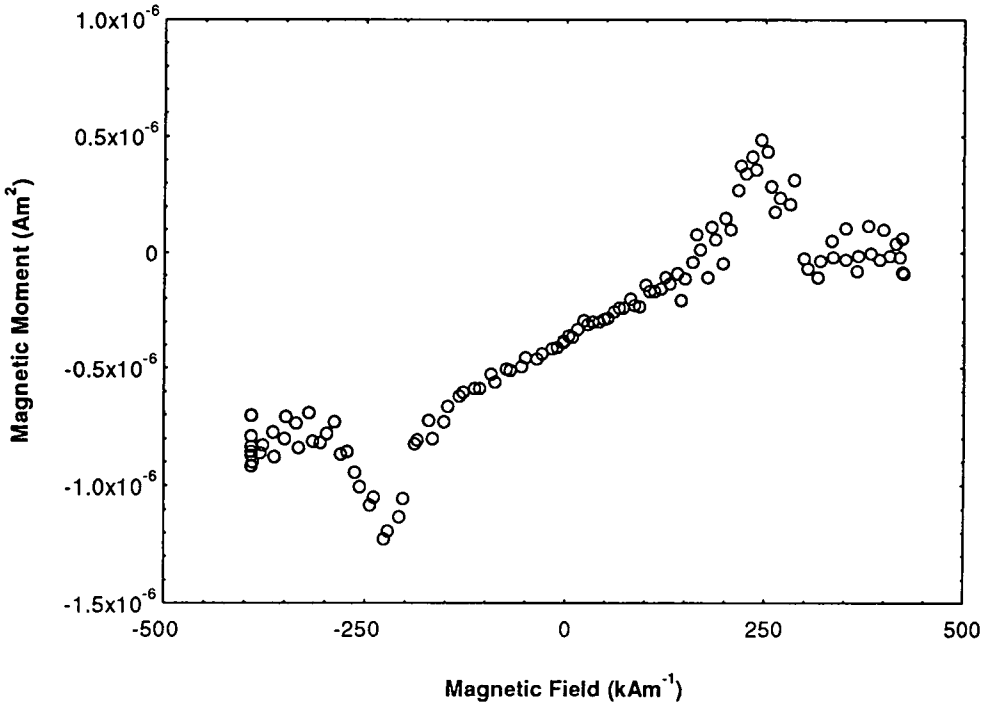

Fig.3.5 Showing the effect of magnet pole piece movement on the hysteresis curve of samples with a low magnetic moment.

3.1.3 Improvements to the Durham VSM

The power supply used to control the applied field is an Amicrown amplifier. This has replaced the Newport rotary generator previously used to control the VSM. The advantages of the Amicrown amplifier over the Newport rotary generator are that it is a bipolar device and therefore there is no need to reverse the current leads when a negative magnetic field is desired. The Amicrown is fed with a voltage from a Bede Scientific Digital to Analogue Converter (-5 Volts to +5 Volts) in steps of 0.0024 volt. This allows a field step of 0.8 kAm^{-1} in the remanent region of the magnet.

The Bede board has 4 DAC channels on it and we only use one of them. However by combining all four of them we can decrease the field step size by a factor of 4. This is achieved by using the circuit shown in Fig.3.6. Which splits the four outputs from the DAC into two pairs which are added together. Then one of the pair is inverted with respect to the other to give a negative section with the other pair giving a positive section. This allows a field step of 0.2 k Am^{-1}.

The use of the Amicrown Amplifier has greatly increased the reliability of the system. Programs have also been written by the author and Dr. C.I.Gregory which allow the magnetisation to be recorded as a function of temperature. These two factors have led to it being used routinely to investigate materials produced by other members of the Solid State Research Group at Durham University. These include Cerium based intermetallic compounds which are of interest because the 4f electrons can be localised or delocalised depending on their environment. Thus a whole array of electronic properties are observed in these systems. Other materials include alloys based on $ZrCr_2$. It is well known that these materials like many other intermetallic compounds react reversibly and absorb large quantities of hydrogen. While these systems are outside the research undertaken in this thesis, the improvements in the VSM have allowed these investigations to be undertaken and the results from it are included in Appendix A2.

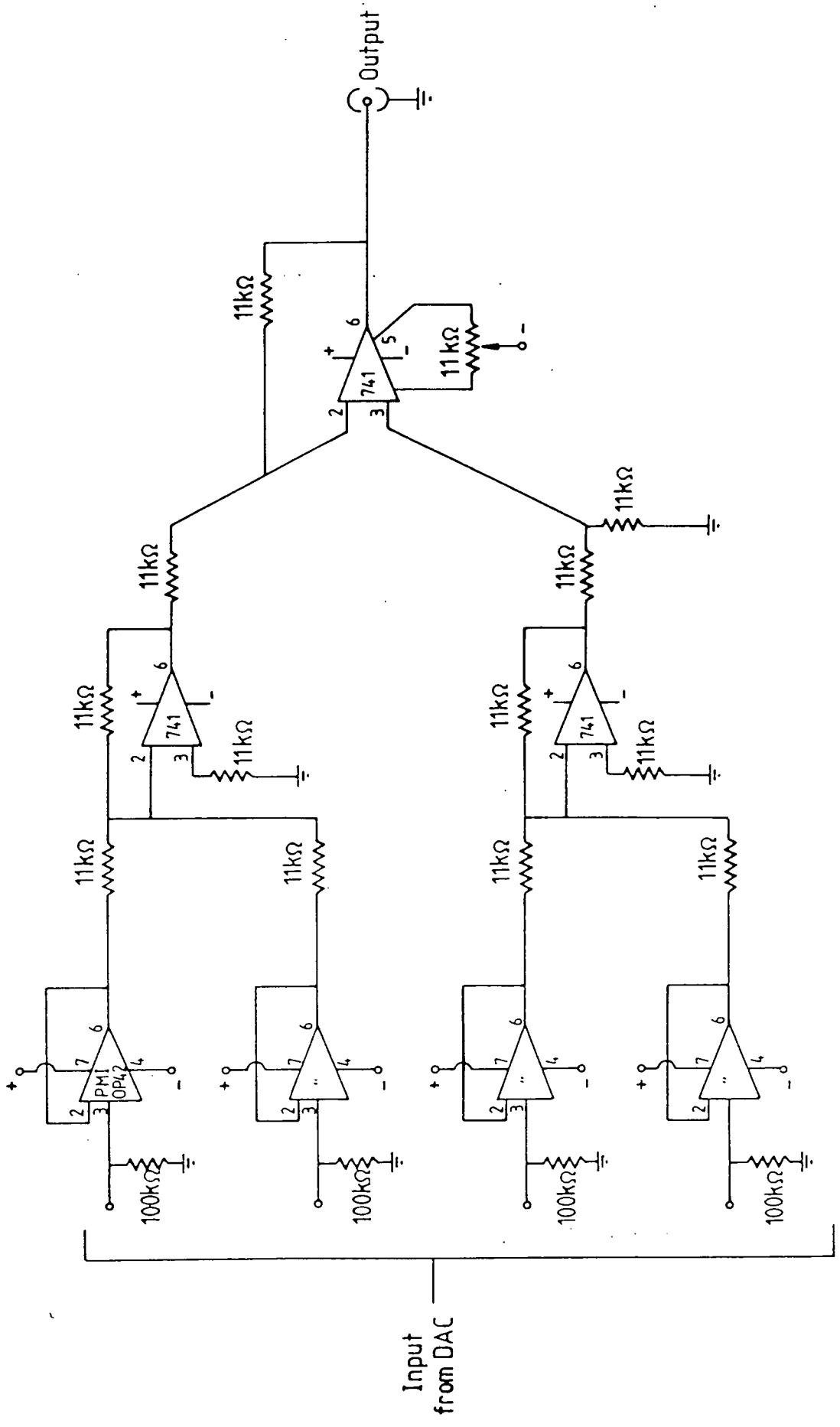

Fig.3.6. Diagram showing the circuit used to lower the step size by a factor of 4 by combining the four DAC chips on a Bede Scientific DAC board

3.2 Low Field Vibrating Sample Magnetometer

This section deals with the construction of a Low Field Vibrating Sample Magnetometer. This LFVSM is capable of a magnetic field of 4 kAm^{-1} with a step size of 2 Am^{-1} . The stability, sensitivity and the calibration of this device is discussed below.

3.2.1 Magnet

The magnetic field was generated by a set of Helmholtz coils. These were driven with a Kepco bipolar Amplifier via a Bede DAC board. The field uniformity in the x, y, z directions are shown in Fig.3.7. These indicate that the field is uniform to within 1% over a 25 mm sphere centred on the sample position. The magnetic field was found to be linear with the current supplied to it. However it was found that the gaussmeter drift with a LDJ gaussmeter on the 50 gauss scale was quite significant on the timescale of a hysteresis loop (30 minutes). For this reason a resistor was connected to the coils to provide a voltage proportional to the current. The variation of this voltage with the field measured on a gaussmeter is shown in Fig.3.8. This experiment was repeated on a number of occasions and was found to give the same calibration constant.

3.2.2 Detection Coils

These were of Mallinson geometry and were mounted as shown in Fig.3.9. The coils were wound with 48 swg wire (this was done by Aluminium Inductors Limited[14]) and were balanced inductively in situ to within 0.2% using a Wayne Kerr Bridge operating at 100 Hz.

The sensitivity of these coils to movement of the sample in the x, y, z plane is shown in Fig.3.10 and this indicates a wide saddle point. A 1% change in signal is achieved for sample displacements of $\Delta x=\pm 2.5$ mm, $\Delta y=\pm 1.5$ and $\Delta z=\pm 3$ mm.

3.2.3 Calibration

The use of nickel to calibrate the system is not possible because the fields generated by the magnet are not strong enough to saturate the magnetic moment of nickel. The use of a paramagnetic salt [15] was ruled out because the small magnetic moment induced by the

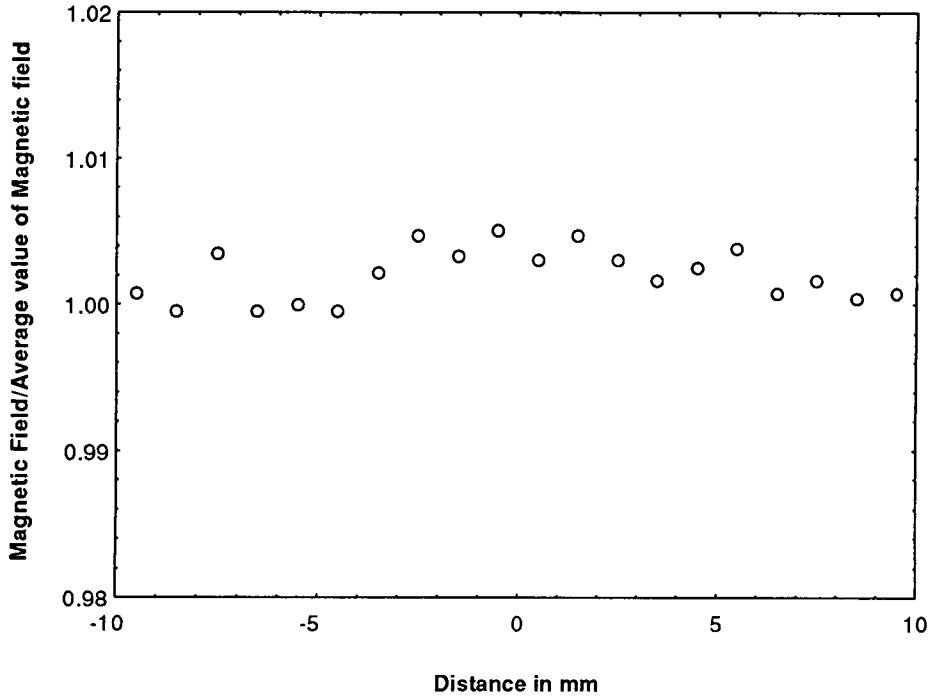

Fig.3.7a Variation of magnetic field with distance along x axis for the LFVSM.

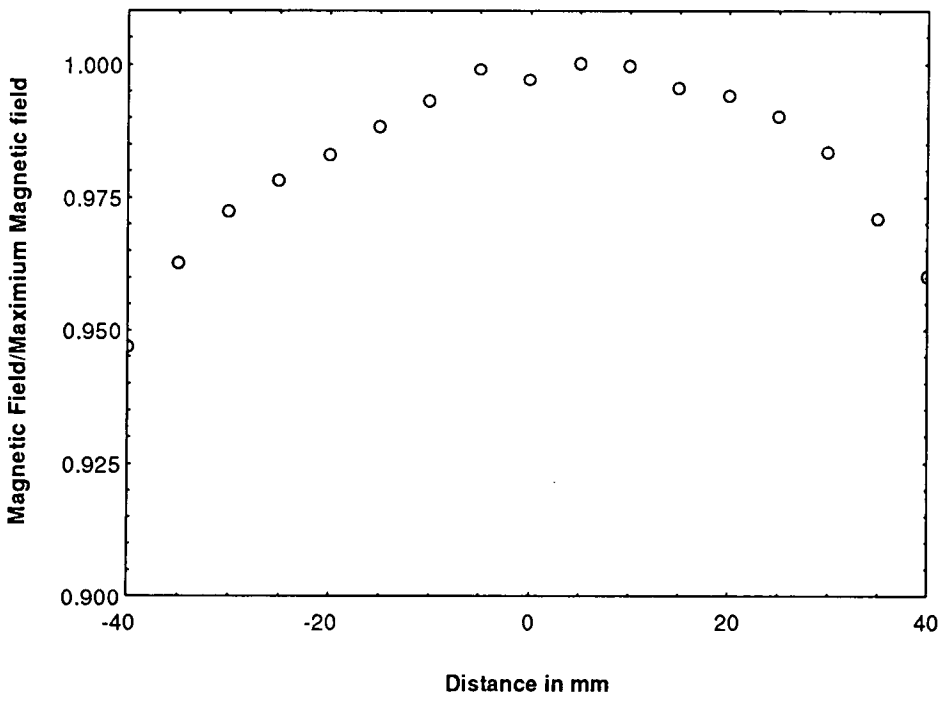

Fig.3.7b Variation of magnetic field with distance along the y axis for the LFVSM.

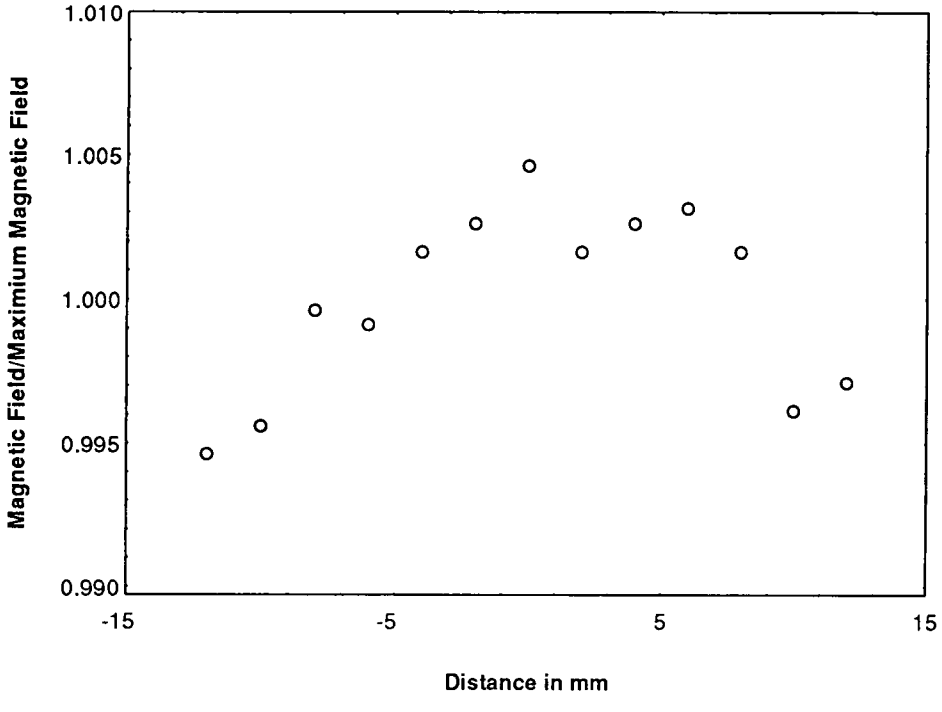

Fig.3.7c Variation of magnetic field with distance along the z axis for the LFVSM.

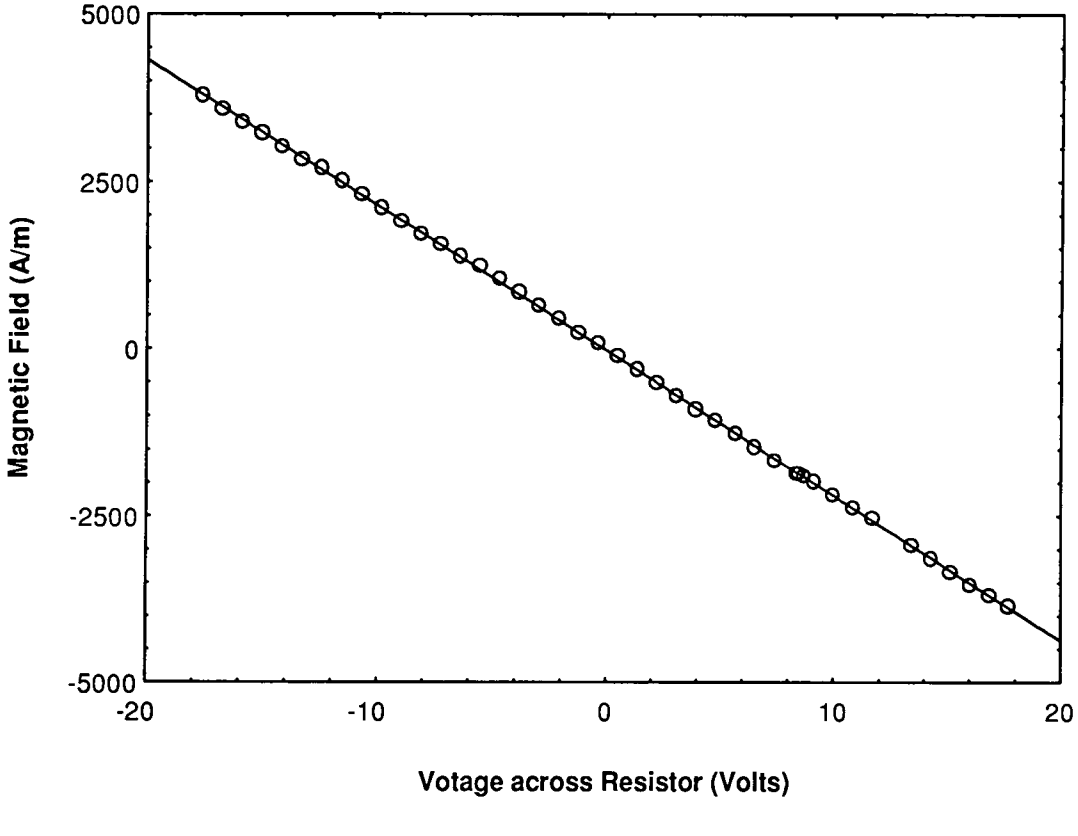

Fig.3.8 Variation of magnetic field with respect to voltage across the resistor used to calibrate the magnetic field on the low field Vibrating Sample Magnetometer. Line is a least squares fit to the data.

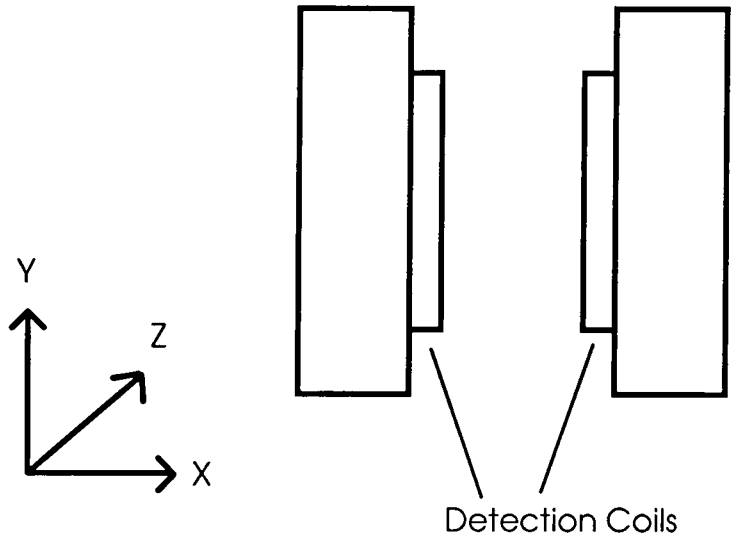

Fig.3.9 Diagram illustrating the coil geometry used for the Low field VSM.

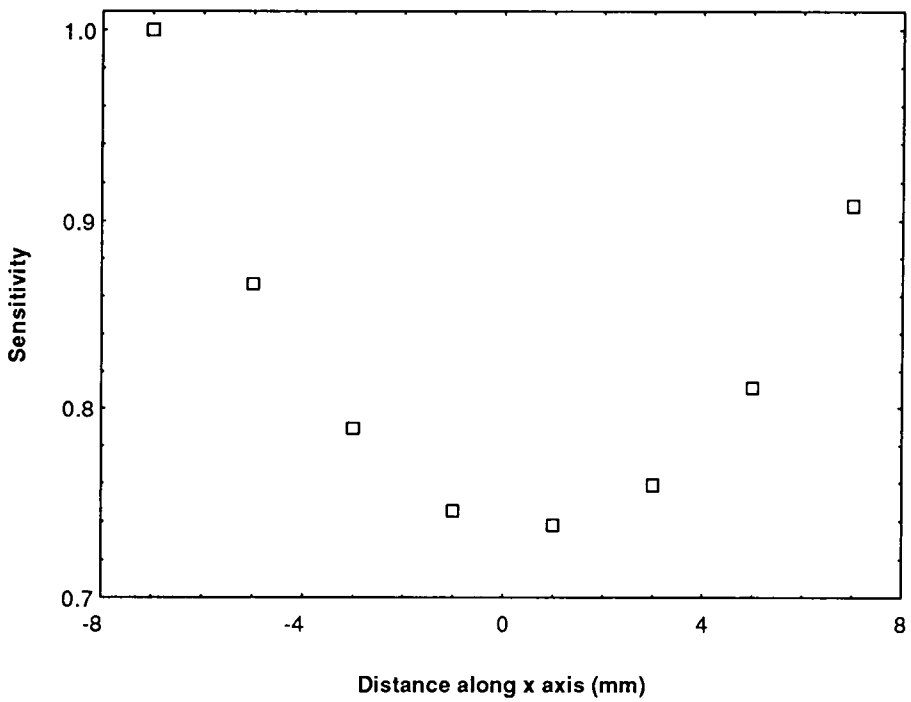

Fig.3.10a Sensitivity of the pickup coils used on the LFVSM to sample displacement in the x-axis.

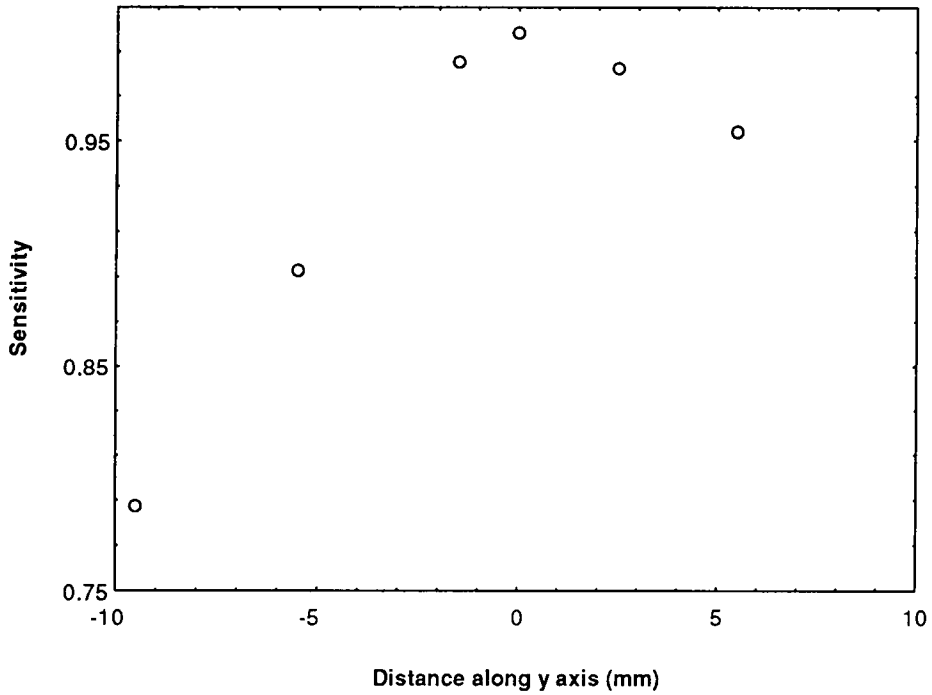

Fig.3.10b Sensitivity of the pickup coils of the LFVSM to sample displacement in the y axis.

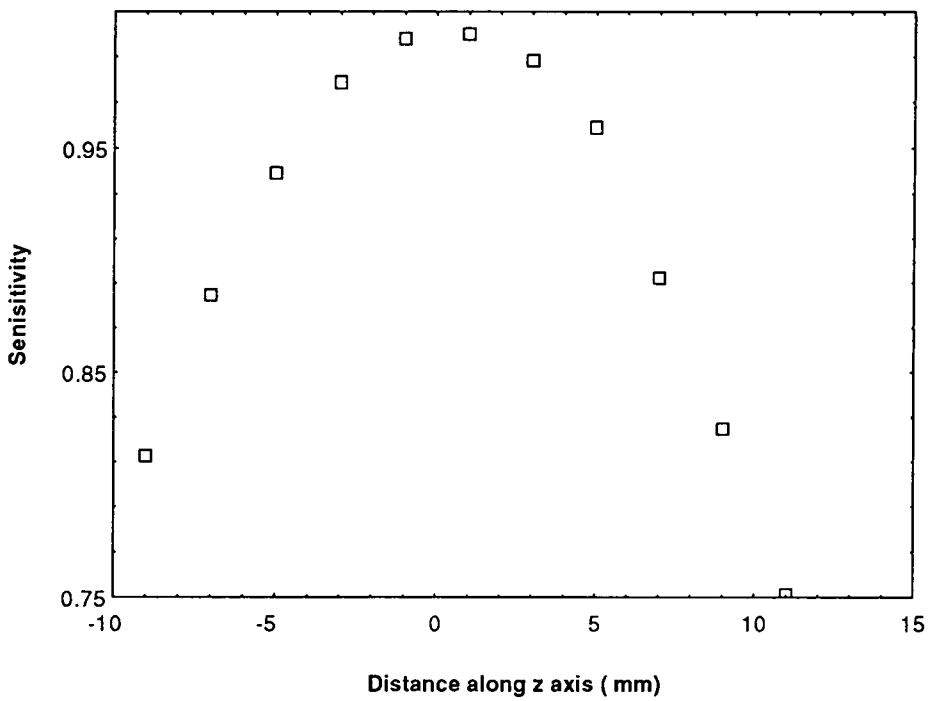

Fig.3.10c Sensitivity of the pickup coils of the LFVSM to sample displacement in the z axis.

applied field was not measurable. To calibrate the system a wire wound coil with a known area and number of turns was used. This was fed with a known current and from the variation of this current with induced voltage a calibration constant can be determined.

3.2.4 Residual Subtraction

The moment from the sample holder, glass rod and PTFE was measured after each run and was found to be diamagnetic. A straight line fit could be used to fit to this data and this is then subtracted from the raw data. The problem of movement of the pole pieces naturally did not occur for this VSM.

3.3 Bangor Alternating Gradient Force Magnetometer

This machine is a commercial Alternating Gradient Force Magnetometer built by Princeton Measurement Corporation. It has a sensitivity of $1x10^{-11}$ Am^2 and can reach fields of 1760 kAm^{-1}. The sensitivity, noise base and reproducibility of this instrument has been discussed by O'Grady[16]. In this section a brief description of the measurement technique will be described, and for more detail see Flanders[17,18] .

The sample is mounted on a glass rod, one end of which is connected to a piezoelectric crystal. As well as experiencing a dc field the sample is subjected to an ac field of a much smaller size. This ac field gradient causes the sample to vibrate due to the coupling of the ac field with the sample magnetic moment. If the frequency of the ac field is varied then a resonance condition can be achieved. This depends on the sample mass and the length of the rod. Once the resonance condition has been achieved then the voltage across the piezoelectric crystal is greatly amplified. By use of the resonance condition very small magnetic moments can be measured.

3.3.1 Calibration

Calibration is achieved by the use of a known mass of nickel and its saturation magnetisation or a known mass of palladium and its susceptibility. The quality of the resonance also needs to be measured for each run. However the software supplied with the AGFM carries out the calibration of the device automatically.

3.3.2 Residual

The magnetisation of the sample rod is recorded as a function of field and was found to be diamagnetic and this is subtracted from the magnetisation data.

3.3.3 Weak Signals

With samples which contain a very low mass of a ferromagnetic component, the substrate used to mount the sample will have a large relative moment (diamagnetic in the case of glass) and in large fields this diamagnetic moment will swamp the ferromagnetic component. This effect is shown in Fig.3.11 however in this case a straight line fit is performed to the data above 240 kAm^{-1} where it is assumed that the ferromagnetic component has saturated. This straight line fit is then subtracted from all the data. The corrected data is shown in Fig.11.b.

3.4 The Durham Torque Magnetometer

The Durham torque magnetometer allows the torque produced by a magnetic sample to be measured as the angle the magnetic field makes with the sample is changed. As the torque on the sample is simply the angular derivative of the anisotropy energy the anisotropy constants[19] can easily be determined assuming the material is saturated. For a useful review of experimental technique and instruments see Pearson[20] . The magnetic field experienced by the sample can also be varied and by performing torque curves at various field strengths the rotational hysteresis integral for the sample may be determined. With this information the spin reversal mechanism can be identified.

Fig.3.12 shows the torque magnetometer head. The inner transmitting coils are fed with a 5 Volt 6 KHz signal. This coil is connected to the sample via a tantalum wire and the sample rod. When the inner coil is rotated it will induce a voltage in the fixed detecting coils. The amplitude and phase of this signal are proportional to the amplitude and sense of the torque on the sample. Use of a lock-in amplifier permits the rejection of unwanted noise.

To vary the angle between the sample and the magnetic field, the magnet is rotated under computer control. Determination of the angle between the sample and the magnetic field is

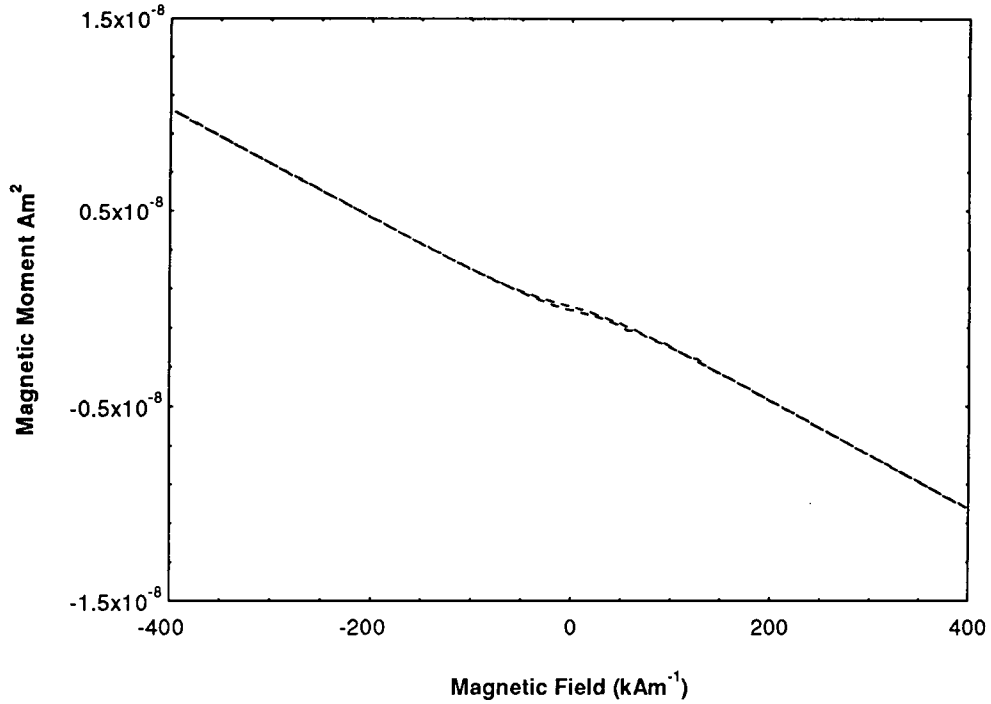

Fig.3.11a Hysteresis loop from the AGFM showing the effect of diamagnetic substrate on a weak ferromagnetic sample.

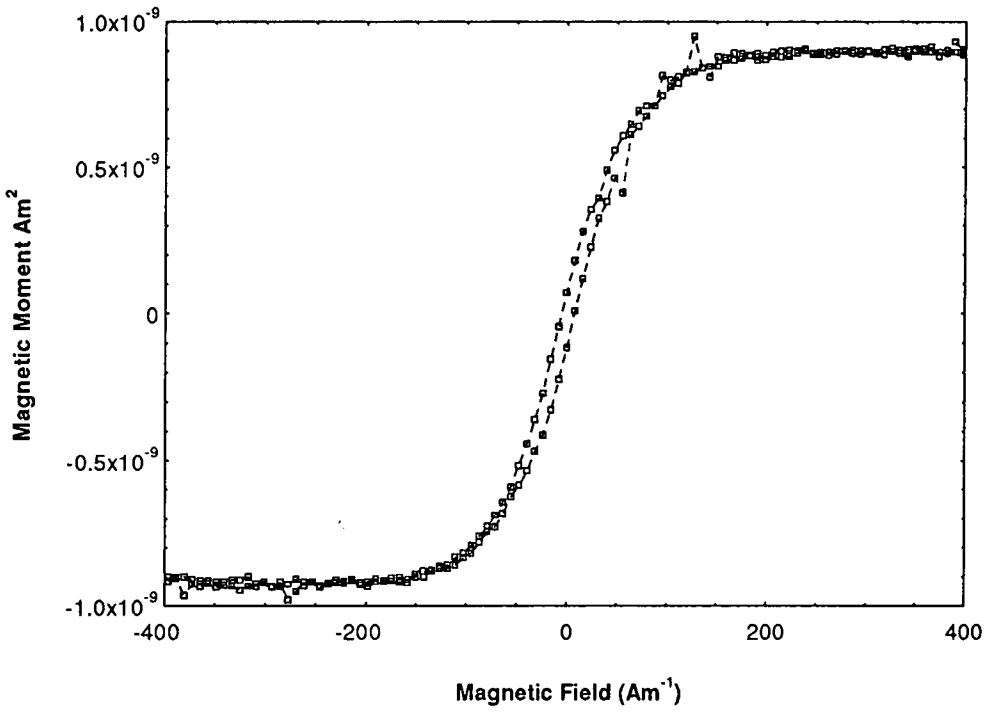

Fig.3.11b Hysteresis for the same sample as Fig.3.11a but with the diamagnetic substrate removed.

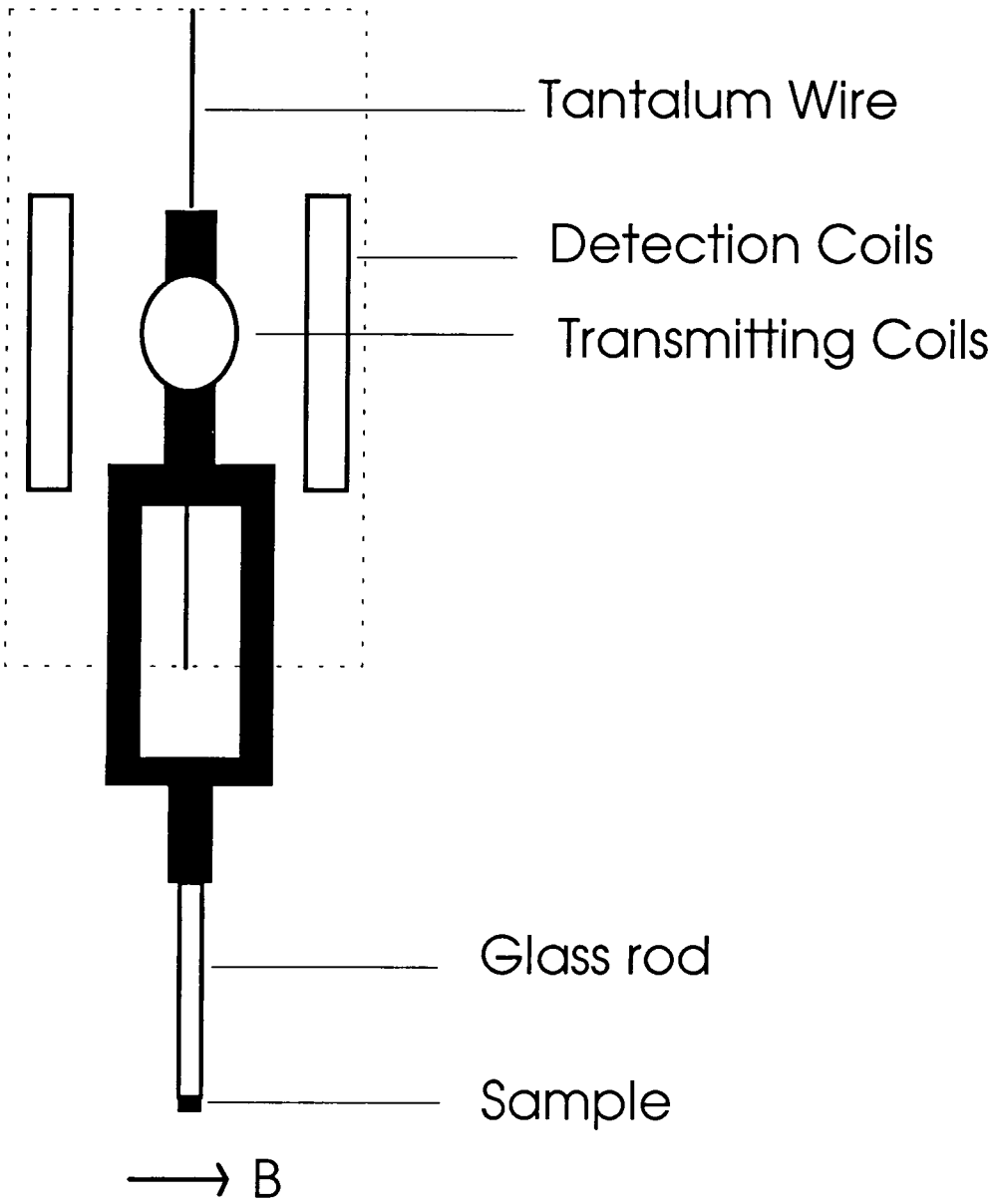

Fig.3.12 Diagram illustrating the Torque Magnetometer head.

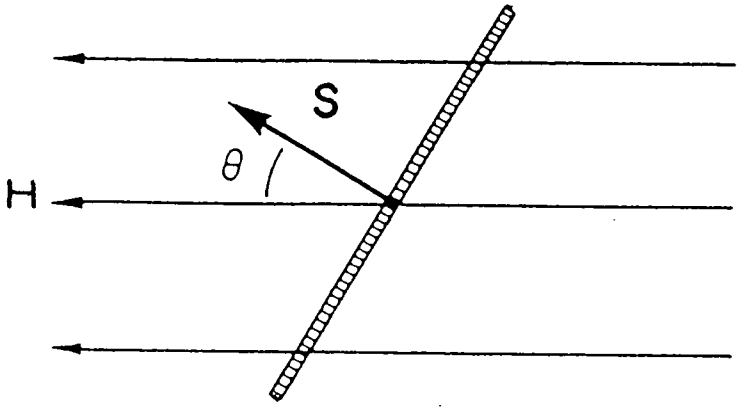

Fig.3.13 Diagram showing the coil and magnetic field geometry used to calibrate the Torque Magnetometer. The coil has N turns and an area S and makes an angle θ with the magnetic field H.

achieved with the measurement of the voltage across a potentiometer. This is connected to the rotating base of the magnet.

During a typical torque curve the computer records the angle of the applied field and the signal corresponding to the torque every 2° over a rotation of 180° with a 45° overshoot for rotational hysteresis measurements as this overshoot allows all the particles to undergo irreversible transition over a 180° [21] range. If rotational hysteresis measurements are being performed the applied field is changed and the measurement performed at the new field value.

3.4.1 Calibration

Calibration of the torque magnetometer is achieved by the use of a current carrying coil placed in a known field at the same position as the sample. This is shown in Fig.3.13. The torque produced by the coil is given by [22]

$$T = \mu_o HISP\cos\theta \qquad 3.2$$

Where T is the torque produced H is the applied field, S is the area of the coil and P is the number of turns on the coil, I is the current being supplied to the coil and θ is the angle between the coil axis and the magnetic field. The voltage this torque produces is recorded as the angle between the coil is varied. This avoids any errors in measuring θ. Then the current to the coil is changed to achieve a calibration over a wide torque range.

3.5 Summary

A brief review of the apparatus used to obtain the magnetic measurements in the next chapter has been given. This has outlined their use and calibration and any improvements made by the author. The high field VSM has proved to be reliable allowing the magnetic characterisation of a wide range of materials from 4.2K to 300K. These materials include $CePt_{5-x}Al_x$ and Zirconium based materials used for hydrogen storage. The Low Field Vibrating Sample Magnetometer has recently been used to measure the magnetic properties of magnetic multilayers as they have such a small coercivity.

Reference Chapter 3

[1] Princeton Measurement Corporation, Air Park Road, Princeton, NJ 08540

[2] Foner, S, "Versatile and Sensitive Vibrating-Sample Magnetometer", *The Review of Scientific Instruments*, **30**, 548-557 (1959)

[3] Josephs, M., Crompton, S., and Kraft S.,"Application of Digital Signal Processing to Vibrating Sample Magnetometry", *IEEE Transactions on Magnetics*, **23**, 241-244 (1987)

[4] Hoon, S. R., and Willcock, S.N.M., "The design and operation of an automated double crank vibrating sample magnetometer", *J. Phys. E: Sci. Instrum.*, **21**, 772-785 (1988)

[5] Thompson, S.M., PhD Thesis, University of Durham (1990)

[6] Gregory, C.I., PhD Thesis, University of Durham (1992)

[7] McCoy, J., PhD Thesis, University of Durham (1988)

[8] Mallinson, J., "Magnetometer Coils and Reciprocity", *J. Appl. Phys.*, **37** ,2514-2515 (1966)

[9] Bede Scientific, Lindsey Park, Bowburn, Durham DH6 5PF

[10] Lambrick, D.B., PhD Thesis University of Durham (1987)

[11] Pauthenet, R., "Experimental verification of spin wave theory in high fields", *J.Appl. Phys.*, **53**, 8187-8192 (1982)

[12] Graham, C.D., "Iron and Nickel as magnetization standards", *J.Appl. Phys.*, **53**, 2032-2034

[13] Lambrick, D.B., PhD Thesis University of Durham (1987)

[14] Aluminium Inductors Limited, 29 Lower Coombe St., Croydon, Surrey, CR 01 AA

[15] Figgis, B.N, and Nyholm, R.S., "A convient Solid for calibration of the Gouy Magnetic Susceptibility Apparatus", *J. Chem. Soc.*, 4190-4191 (1958)

[16] O'Grady, K, Lewis, V.G., and Dickson, D.P.E.,"Alternating Gradient Force Magnetometry: Applications and extension to Low temperatures", *J.Appl. Phys.*, **70**, 5608-5613 (1993)

[17] Flanders, J., "An alternating-gradient magnetometer",*J. Appl. Phys.*, **63**, 3940-3945 (1988)

[18] Flanders, J.,"A vertical force alternating-gradient magnetometer",*Rev. Sci. Instrum.*, **61**, 839-847, (1990)

[19] Cullity, B.D., "Introduction to Magnetic Materials", *Addison Wesley*, 215-224 (1972)

[20] Pearson, R.F.,"Experimental Magnetism",Vol 1, *Wiley*, 137-223 (1979)

[21] Paige, D.M., Hoon, S.R.,Tanner, B.K., and O'Grady,K., "High precision torque hysteresis measurements on fine particle systems", *IEEE Trans. on Magn.*, **20**, 1852-1854 (1984)

[22] Grant, I.S., and Phillips, W.R., "Electromagnetism.",*Wiley*,130-132 (1986)

Chapter 4.

Magnetic Measurements

4.0. Introduction

Results of an investigation into the magnetic properties of the powders used in MPI will be presented. These include Torque, VSM and AGFM measurements on samples in the liquid and bulk states as well as individual aggregates. From these measurements at both high and low magnetic fields we have gained a better understanding of the magnetisation processes in magnetic inks.

4.1. Sample Selection and Preparation

As a wide variety of samples were used it is important to detail their preparation and selection. The liquid samples used were placed in spherical glass bulbs. These bulbs had an inner diameter of 5.4 mm and an outer diameter of 8 mm, access being provided via a 2 mm circular hole. This was sealed with araldite once the liquid was in the bulb. Care was taken to ensure that no magnetic material was bonded to the araldite. As the particles agglomerate upon application of a large enough magnetic field then the demagnetising factor changes during the course of the experiment and therefore can not be calculated. Two magnetic inks were used, Magnaflux MHF7[1] a typical "black" magnetic ink and Meccana a fluorescent magnetic ink. The mass of magnetic powder in each sample was calculated from its saturation moment in comparison with the saturation moment of a known mass of the same material.

Bulk material was placed in a PTFE bucket of 2.6 mm diameter and 10.3 mm length; the magnetic field was applied perpendicular to the bucket's length. The powders were also mixed with araldite and made into pellets with a diameter 6.1 mm and thickness 2.3 mm. These pellets were used for torque magnetometry studies with the field being applied along the pellet's diameter.

Samples for the AGFM measurements of the magnetic properties of individual aggregates were selected from the bulk material by the use of 48 gauge copper wire and a microscope. Once an aggregate was selected it was placed on a section of a microscope cover slip and fixed into position with G.E varnish. Afterward it was checked under an optical microscope for the presence of smaller particles. The chance that particles smaller than the resolution of the microscope are affecting the

magnetisation of an aggregate can be discarded as the magnetic moment of a particle is proportional to its volume. The aggregates chosen were typically 100 microns in size and the resolution of the microscope is 1 micron. Thus there would need to be a million such particles to have a comparable moment.

4.2 High Field Studies of Commercial Magnetic Inks

A suspension of ferromagnetic material such as those used in MPI should not exhibit coercivity as the particles should align themselves with the new field direction. The time taken for this rotation has been calculated by Shliomis[2]. It is dependent upon the particle volume, particle magnetisation, viscosity of the carrier fluid and the strength of the applied field and is less than 1 second for the conditions found in the inks used in MPI (assuming a particle radius of 10 μm). As this relaxation time is less than the measurement time the sample should have zero coercivity. This is similar to a superparamagnetic particle in which the thermal relaxation time is less than the measurement time and therefore it has zero coercivity. However McCoy[3] has shown that commercial magnetic inks exhibit a coercivity 80±40 A/m. This was attributed to particle agglomeration inhibiting particle rotation.

Apart from McCoy's work very little research has been undertaken on the magnetic properties of commercial magnetic inks. However there are two active areas of research which are closely related to that of magnetic inks. These are ferrofluid[4] and magnetic tape dispersion[5] research. Ferrofluids consist of a suspension of superparamagnetic particles in a carrier fluid. A coating of a surfactant inhibits particle agglomeration. Magnetic tape dispersions consist of single domain particles of γFe_2O_3 in an organic binder.

4.2.1. Effect of Concentration on the Hysteresis Loop of Commercial Magnetic Inks

McCoy reported that coercivity of the magnetic ink suspension was due to particle agglomeration inhibiting particle rotation. Changing the concentration should therefore alter the coercivity of the sample. Samples of various concentrations were prepared and the coercivity and remanence was measured after exposure to a magnetic field of 800 kA/m.

The hysteresis loop for a freshly prepared magnetic ink sample is shown in Fig.4.1. The most striking feature is that the virgin curve is outside the main hysteresis curve. This occurred regardless of the concentration of magnetic ink present.

An explanation for the fact that the virgin curve was outside the main hysteresis loop is that upon magnetising the ink sample from the virgin state, particle agglomeration occurs. This agglomeration lowers the demagnetisation factor of the sample and when the hysteresis loop is measured the demagnetisation factor is lower than when the virgin curve was measured and therefore the virgin curve is outside the main hysteresis loop.

The hysteresis loops for all the samples investigated had in the coercive region a pinched shape as particle rotation becomes the main reversal mechanism. The effect of concentration on this area is shown in Fig.4.2a-e which shows the low field region up to a magnetic field of 4 kA/m as the concentration is increased. The offset in these graphs arises from sample and Hall probe asymmetry. The two curves shown on each graph are the forward and reverse sweeps of magnetic field. During these measurements the sweep rate was kept constant as Flanders[6] has shown the sweep rate affects the observed value of the coercivity. For all these samples it can be seen that the maximum hysteresis occurs above the coercive region as the two curves are diverging from one another whereas one would expect them to converge. Fig.4.3 and Fig.4.4 show the variation of coercivity and remanence as the concentration is varied. For both these parameters, as the concentration is increased the coercivity and remanence go through a minimum at a concentration of 7.1 ± 0.2 kg/m^3 and then increase again.

If particle agglomeration is prohibiting particle rotation we would expect the coercivity to increase with concentration as more particles are present to prevent particle rotation and therefore a larger magnetic field would be needed to reorientate the particles. The remanence however should not change with concentration. An explanation of the experimental results is that at low concentrations needle shaped aggregates are formed. These aggregate show a coercivity and remanence. However as the concentration is increased flux closed structures begin to form. These rotate with the applied field and therefore no coercivity can be measured. As they are flux closed they exhibit no remanence. On increasing the concentration needle shaped aggregates are formed again and have a definite coercivity and remanence. These needle shaped aggregates have been observed in the specimens under investigation.

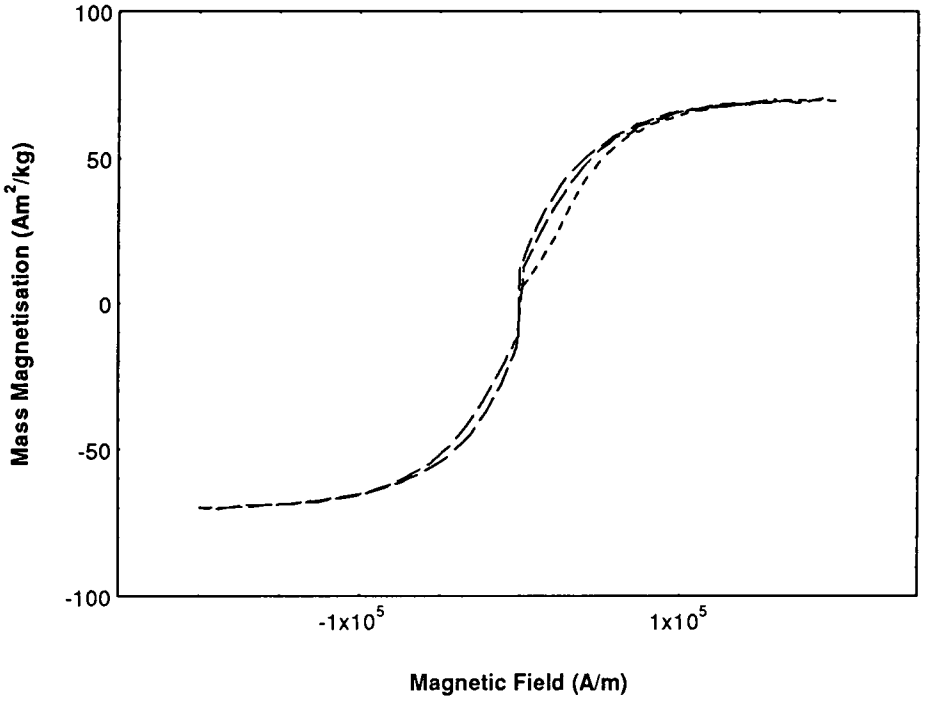

Fig.4.1 Hysteresis loop and virgin curve for a freshly prepared magnetic ink. The virgin curve is outside the main hysteresis curve this occurred regardless of concentration.

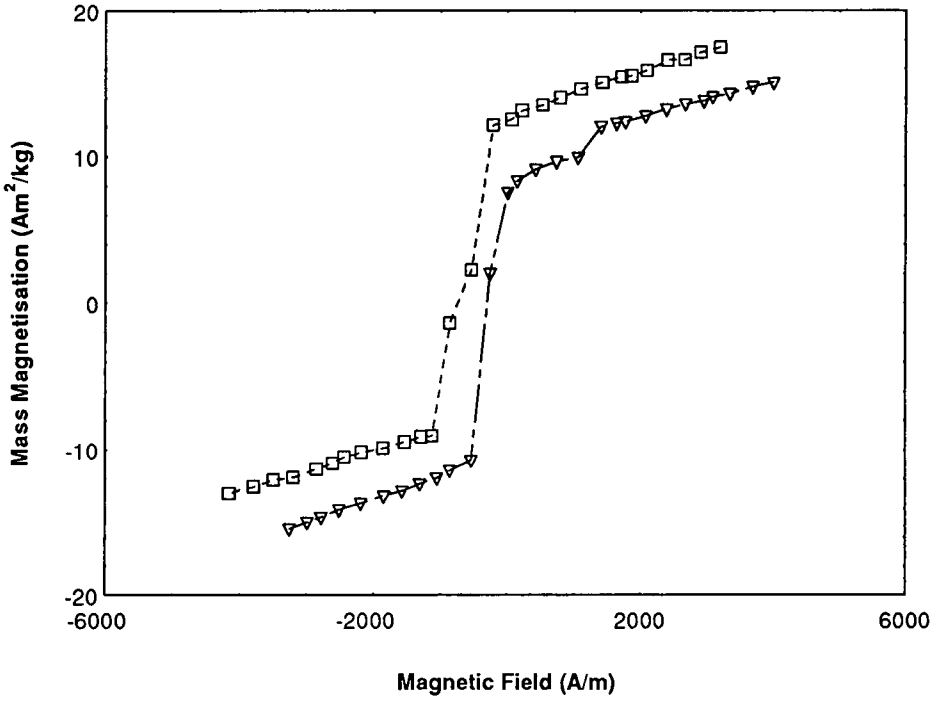

Fig.4.2a Low field region of a magnetic ink with a concentration of 0.9 kg/m^3

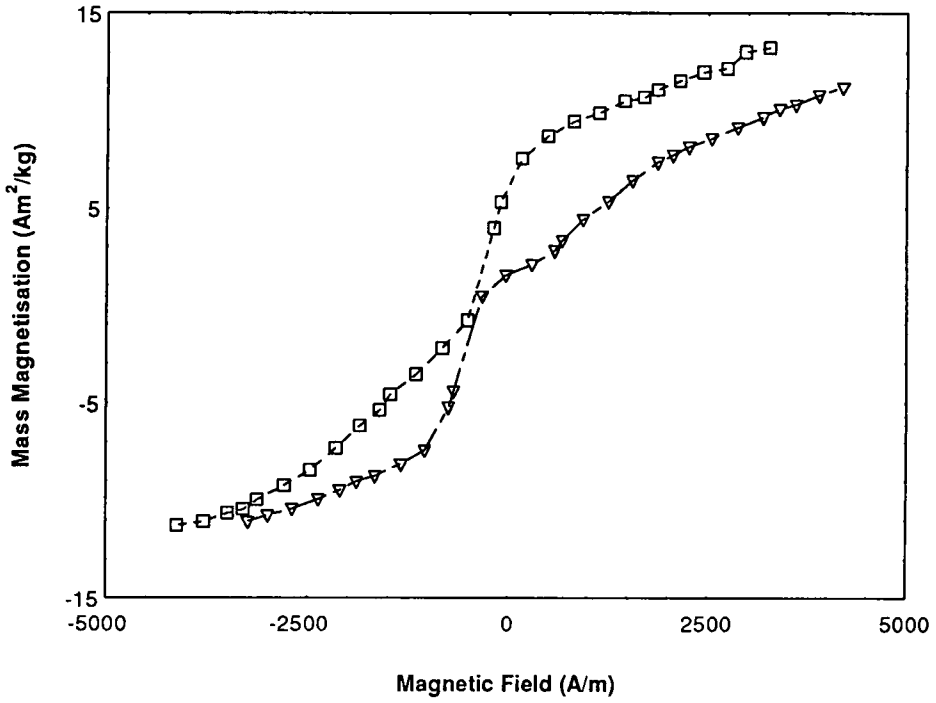

Fig.4.2b Low field region of a magnetic ink with a concentration of 4.7 kg/m^3.

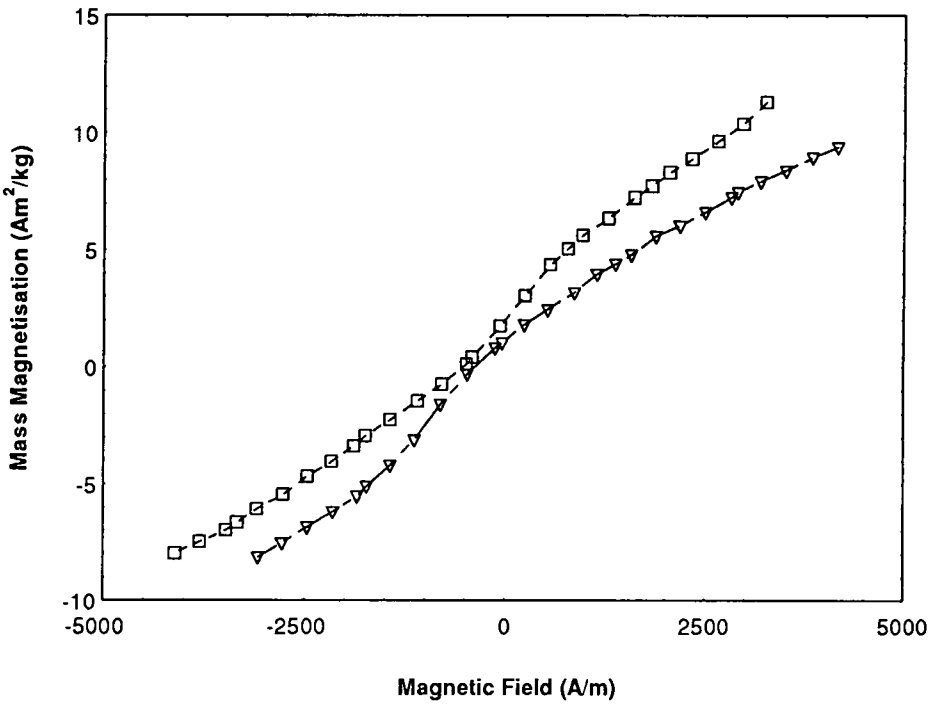

Fig.4.2c Low field region of a magnetic ink with a concentration of 6.4 kg/m^3.

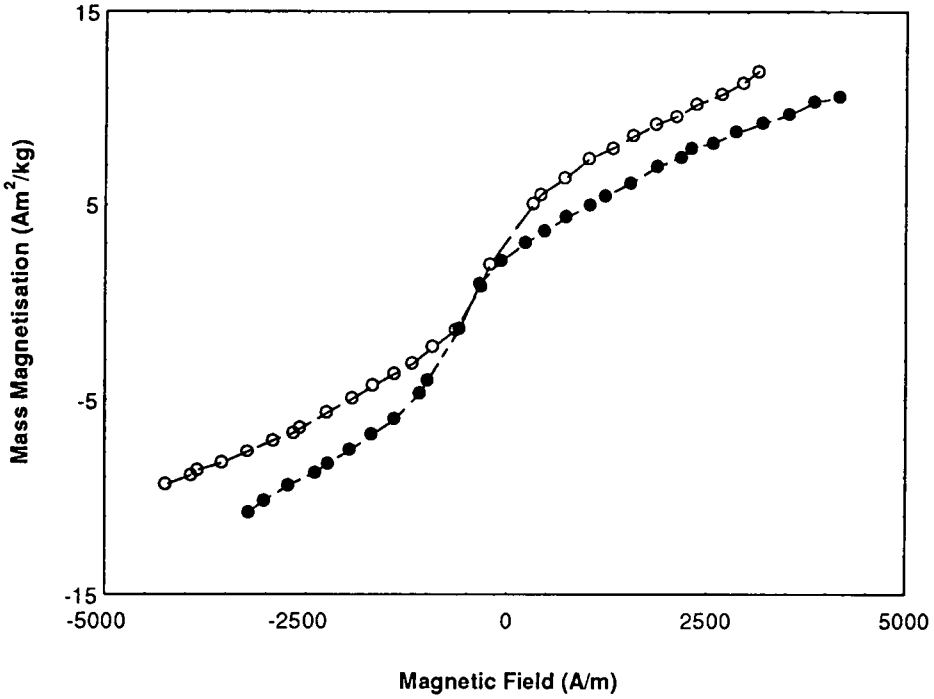

Fig.4.2d Low field region of a magnetic ink with a concentration of 7.1 kg/m^3.

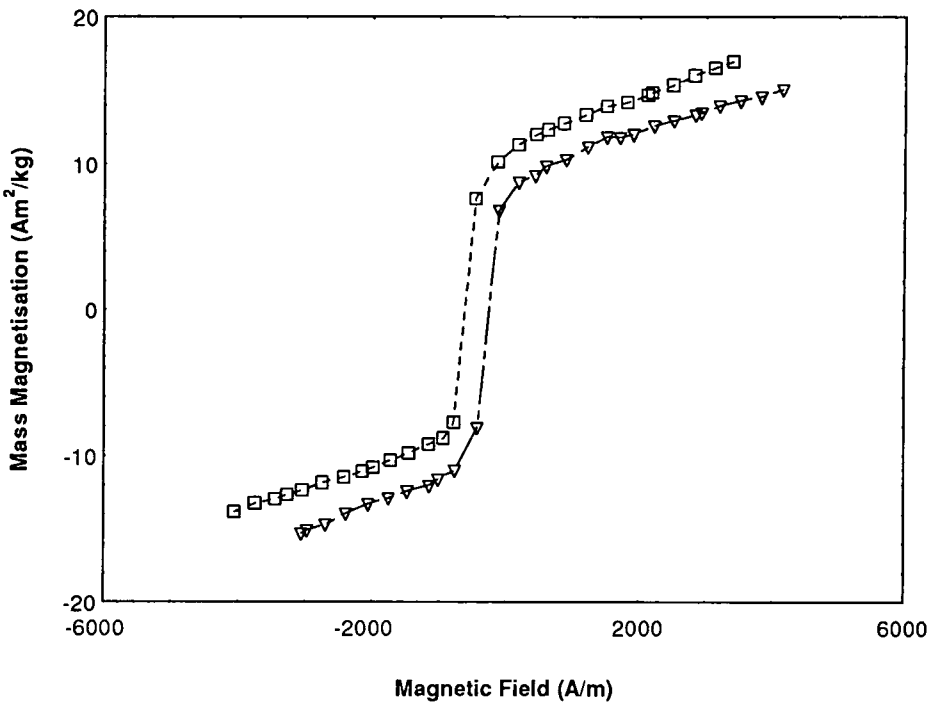

Fig.4.2e Low field region of a magnetic ink with a concentration of 63.1 kg/m^3.

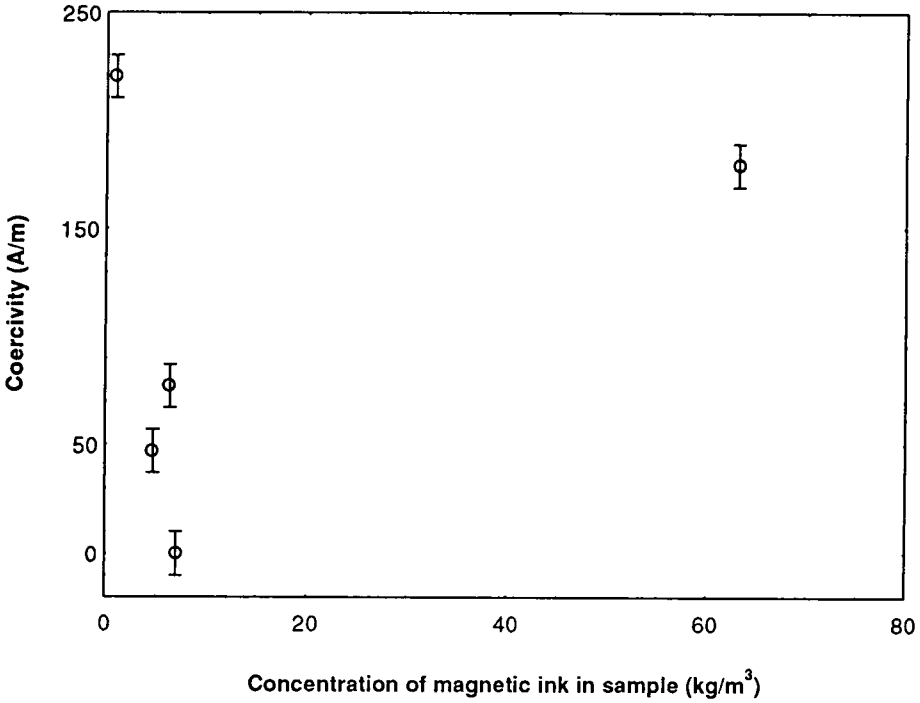

Fig.4.3 Variation of coercivity with concentration for a selection of magnetic inks.

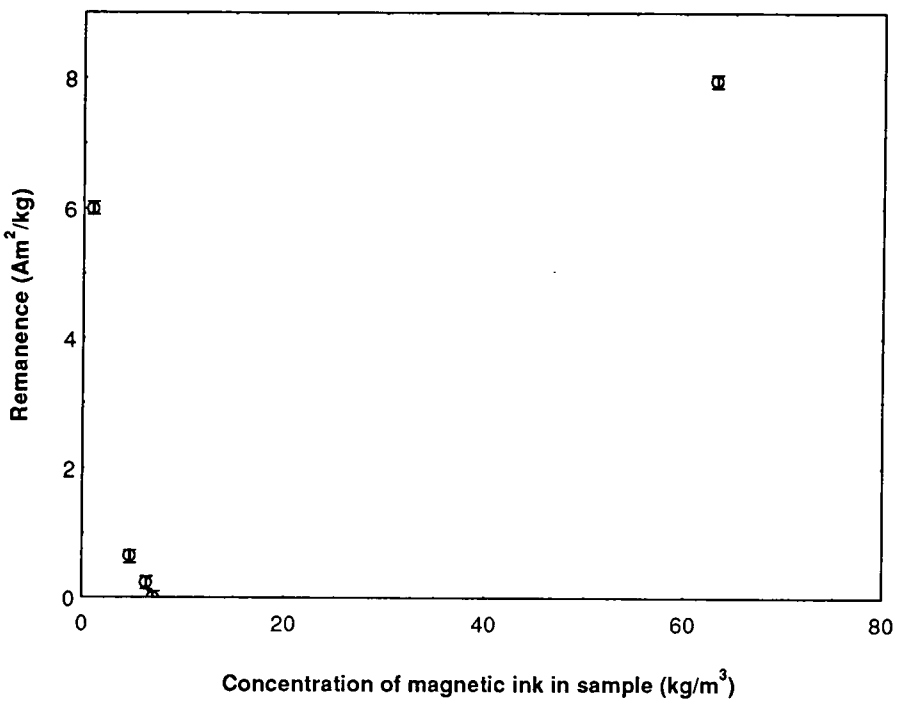

Fig.4.4 Variation of remanence with concentration for a selection of magnetic inks.

4.3 Low Field Measurements on Commercial Magnetic Inks

With the results in mind from the last section a Low Field Vibrating Sample Magnetometer was built. This allowed a maximum field of 4 kA/m and a step size of 2 A/m a gain of 120 on the VSM used in the last section. The maximum field possible from this instrument is typical of those experienced by an ink particle at the start of the inspection process.

4.3.1 Results of Low Field Measurements on Virgin Inks

The hysteresis loop for a freshly prepared magnetic ink is shown in Fig.4.5a. Upon examining the hysteresis loop of the sample in very small magnetic fields < 500 A/m as in Fig.4.5b it can be seen that the sample exhibits no coercivity or remanence. Therefore the effects of field induced agglomeration in fields up to 4 kA/m is not significant. The moment reversal mechanism is mainly by particle rotation. However there is a definitive hysteresis, this being shown clearly in Fig.4.5c. The mass of magnetic material in these samples was calculated by comparing its saturation moment with that of the bulk material after all the low field measurements had been undertaken. The susceptibility was found to be $5.5\pm0.2\text{x}10^{-4}$ m^3/kg.

By measuring the rate of decay of magnetisation as a function of reverse field after exposure to a positive field we expect the decay of the magnetisation to follow a ln(time) dependence[7]. The slope of this decay should have a maximum at the coercive field of the sample[8]. For the freshly prepared sample a magnetic field of 4 kA/m was applied for twenty seconds. Then the change in magnetisation was recorded as a reverse magnetic field was applied. Fig.4.6 shows the decay of magnetisation with respect to ln(time) in a reverse field of 40 A/m. The decay is apparently by Néel relaxation of the sample's moment as the magnetisation decays logarithmically. The particles on application of a negative field have rotated to align with new magnetic field direction. The time taken to do this is below the resolution of the instrument. Then the particle moment seems to relax by Néel relaxation. If we plot the slope of the decay with respect to ln (time) as a function of reverse field the decay was measured in, Fig.4.7 is obtained. It can be seen that a minimum rate of decay occurs in zero magnetic field. This is similar to the results presented by McCoy[9] who measured the time decay of the magnetisation as a function of magnetic field after exposure to a magnetic field of 800 kA/m.

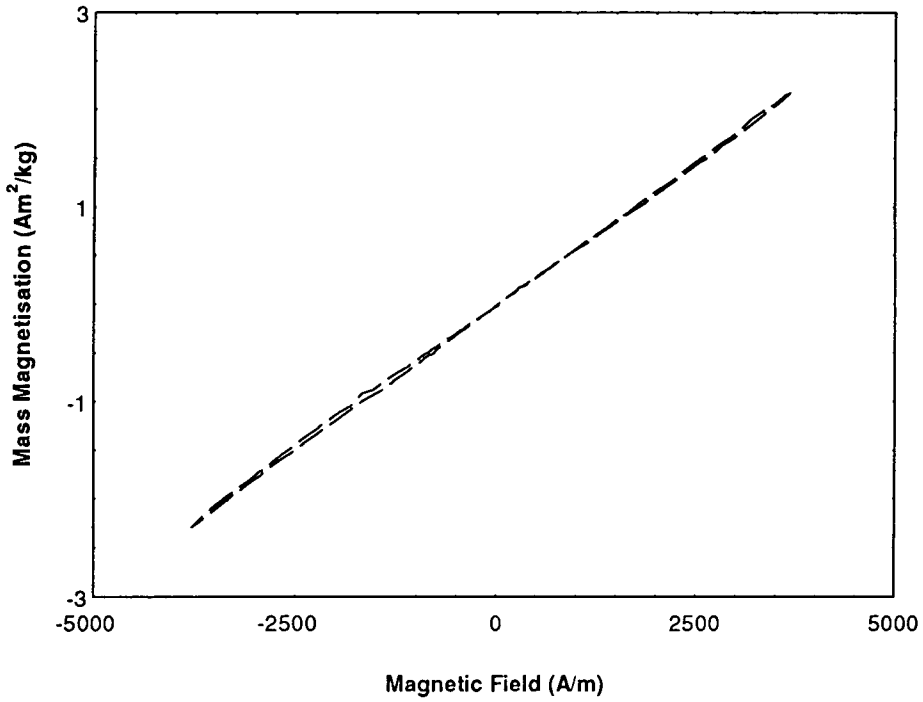

Fig.4.5a Low field Hysteresis loop of a freshly prepared black Magnetic ink.

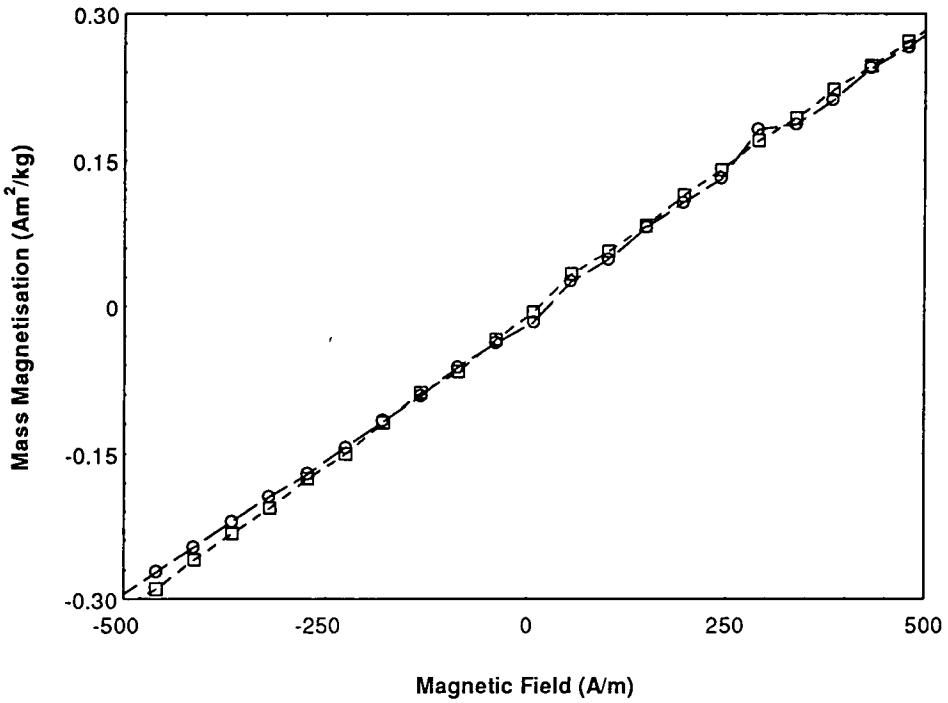

Fig.4.5b Hysteresis loop of the freshly prepared magnetic ink note the lack of coercivity and remanence indicating that the reversal mechanism is by particle rotation.

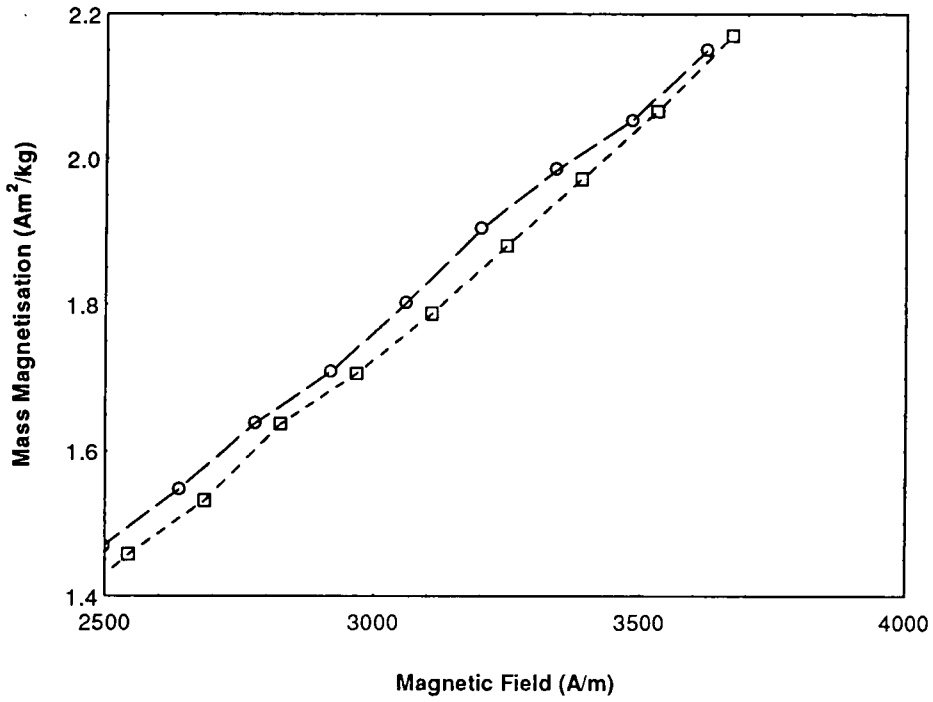

Fig.4.5c Showing the hysteresis present in a freshly prepared magnetic ink.

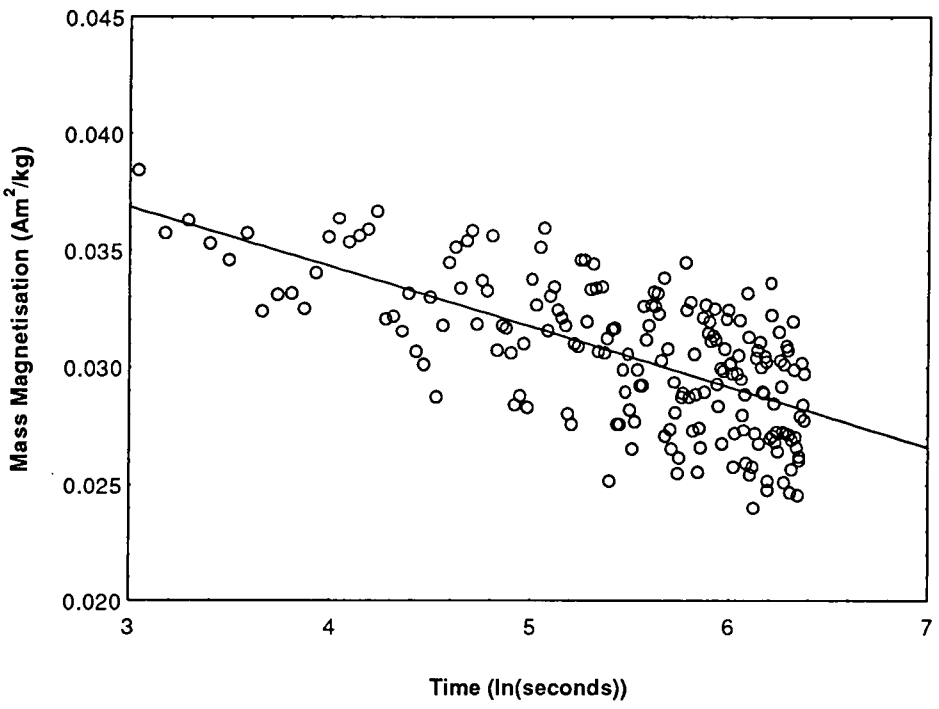

Fig.4.6 Magnetisation as a function of time in a negative magnetic field of 40 A/m after exposure to a magnetic field of 4 kA/m for twenty seconds for a freshly prepared magnetic ink indicating Néel reversal of the magnetic moment.

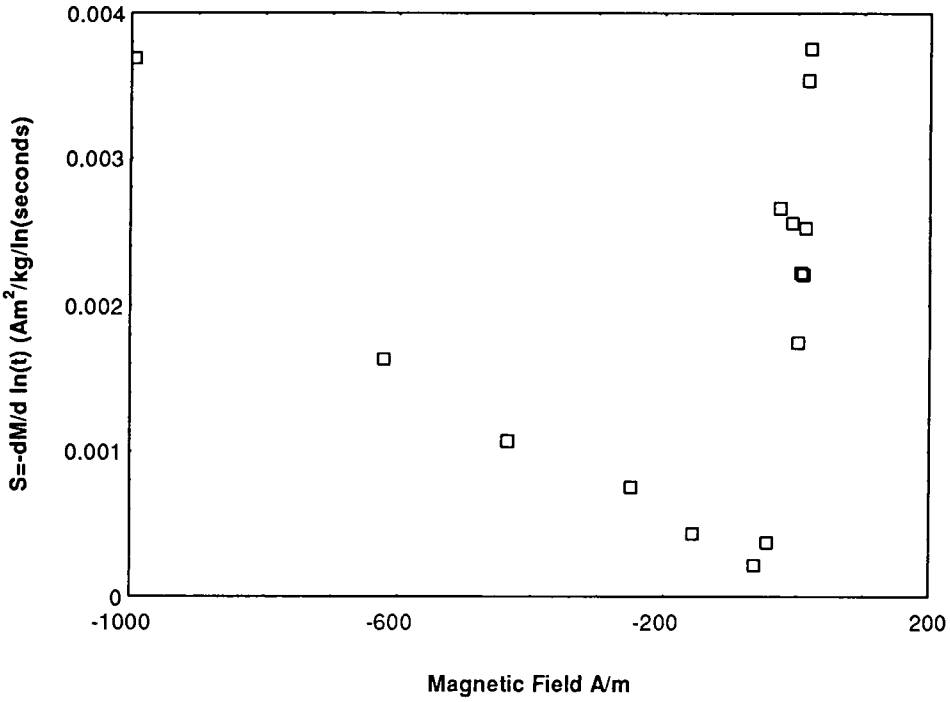

Fig.4.7 Rate of change of magnetisation as a function of Magnetic field for the unexposed magnetic ink.

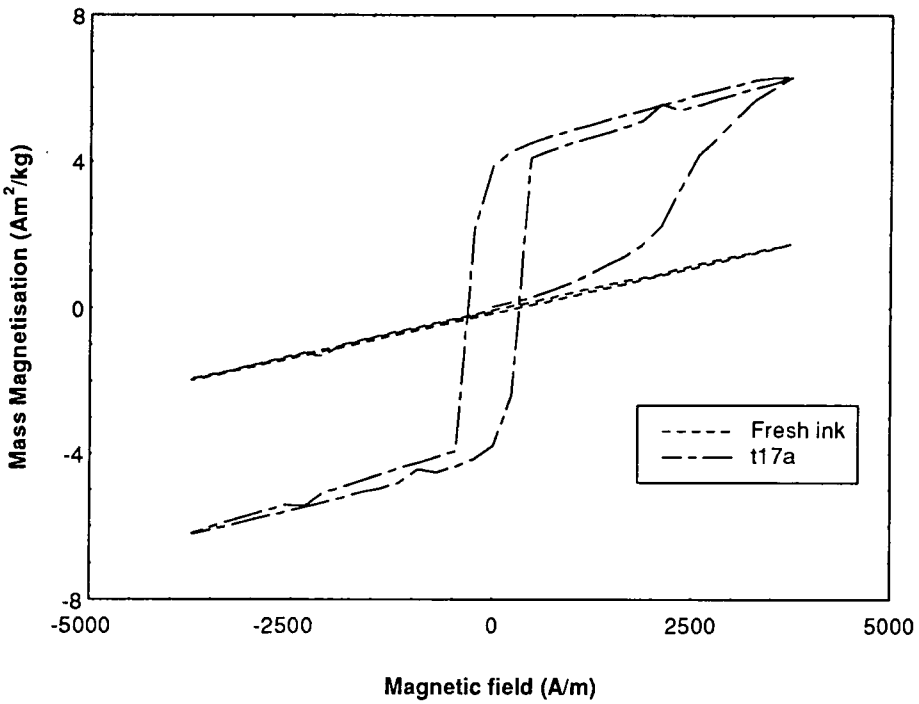

Fig.4.8 Hysteresis loops of sample T17 before and after exposure to a magnetic field of 80 kAm^{-1}.

4.3.2 Low Field Properties after Exposure to a Magnetic Field

From the measurements of the sample coercivity and remanence as a function of concentration it was seen that in a high enough magnetic field, field induced agglomeration occurs which changes the magnetic properties of the sample under investigation. The aim of this study was to see how field induced agglomeration affects the low field properties. Fig.4.8 shows the low field properties of sample t17 before and after exposure to a magnetic field of 80 kA/m . This shows that after exposure to a magnetic field the low field hysteresis properties are drastically different with a measurable coercivity and remanence. The interesting thing to note is that the susceptibility above the coercive region is the same before and after exposure to a magnetic field. We see also that the virgin curve is outside the main hysteresis loop for the exposed ink indicating that field induced agglomeration is now occurring at a much lower magnetic field.

The magnetisation loop however changes with respect to time. This is seen in Fig.4.9a where the hysteresis loops recorded over three days are shown. This change in magnetisation as a function of time was not observed for the unexposed ink. To obtain a better understanding how the magnetic properties are changing Fig.4.9b shows the coercivity changes after exposure to a magnetic field. Before exposure the sample had zero coercivity. Immediately after exposure the coercivity increases, having a maximum value 1 day after exposure and then decreases thereafter. Fig.4.9c shows the variation of the remanence magnetisation and the magnetisation at a field of 2500 A/m. These increase immediately after exposure to a magnetic field and then remain fairly constant.

Time decay measurements on the sample after exposure to a magnetic field indicate that the reversal mechanism can either be Néel or Brownian rotation or a combination of both. For the sample t17 immediately after exposure to a magnetic field of 80 kA/m, the time reversal mechanism in positive field is by Néel rotation as the magnetisation was found to decay logarithmically. However when the applied field becomes negative Brownian rotation occurs. Fig.4.10a shows a typical time decay curve in which Brownian relaxation is the dominant relaxation mechanism. This shows a sudden switch from positive magnetisation to negative magnetisation. However once the particles have rotated to align themselves with the new magnetic field direction, Néel relaxation of the magnetisation occurs. This can be seen in Fig.4.10b which shows an

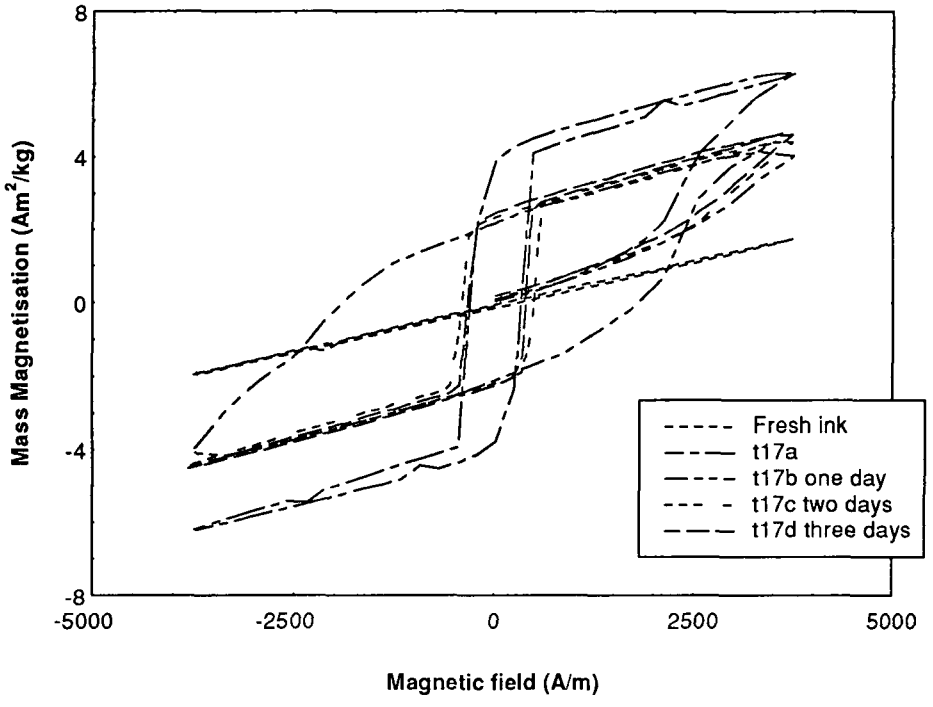

Fig.4.9a Hysteresis loops for sample T17 as a function of time.

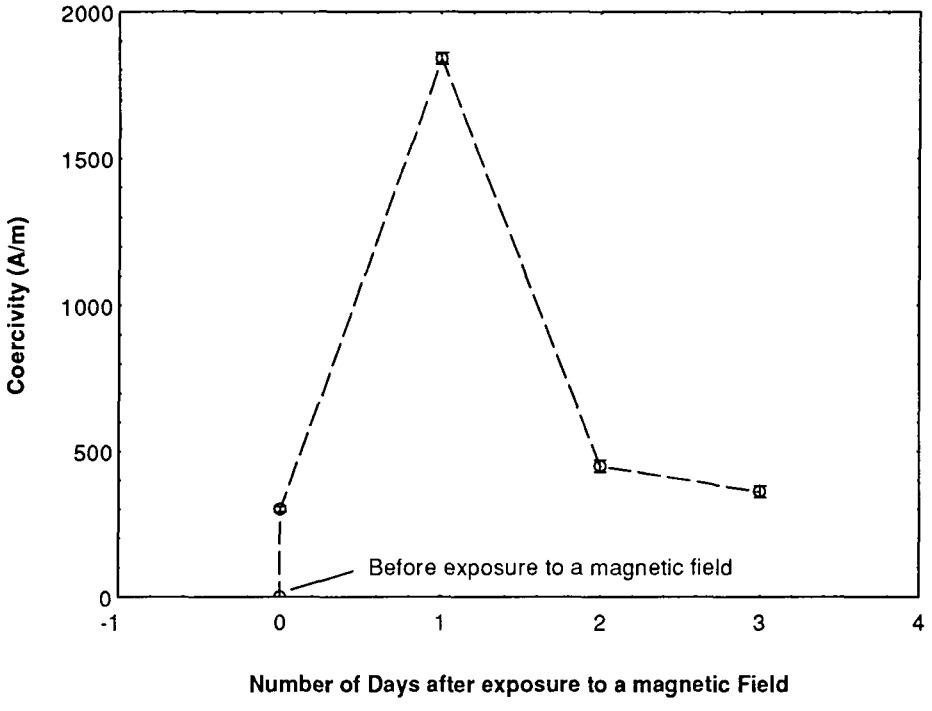

Fig.4.9b Variation of coercivity as a function of time after exposure to a magnetic field

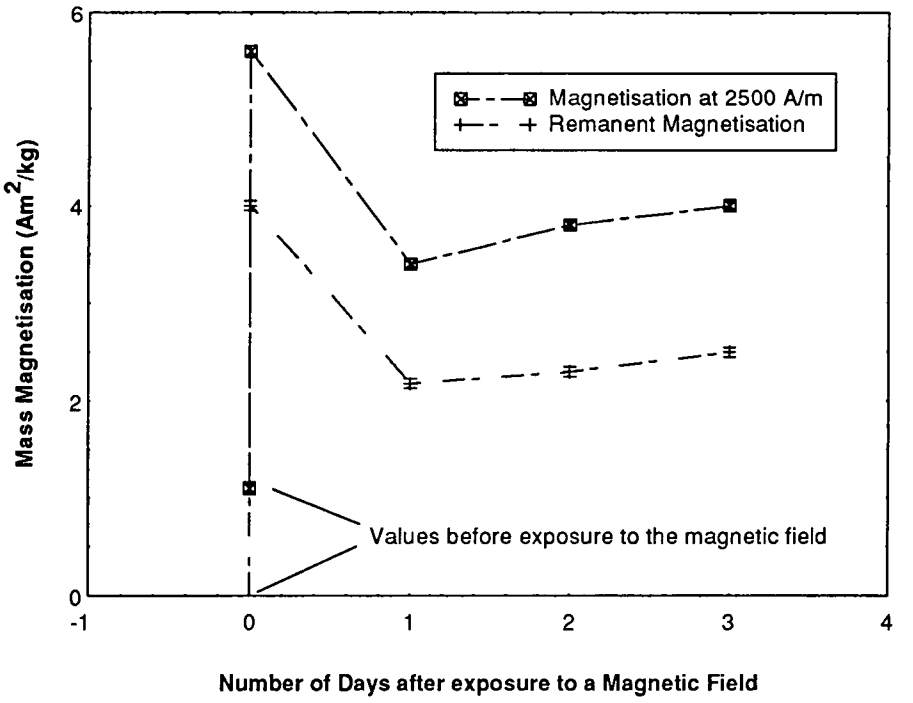

Fig.4.9c Variation of the remanent magnetisation and the magnetisation at a field of 2500 A/m for sample T17 after exposure to a magnetic field.

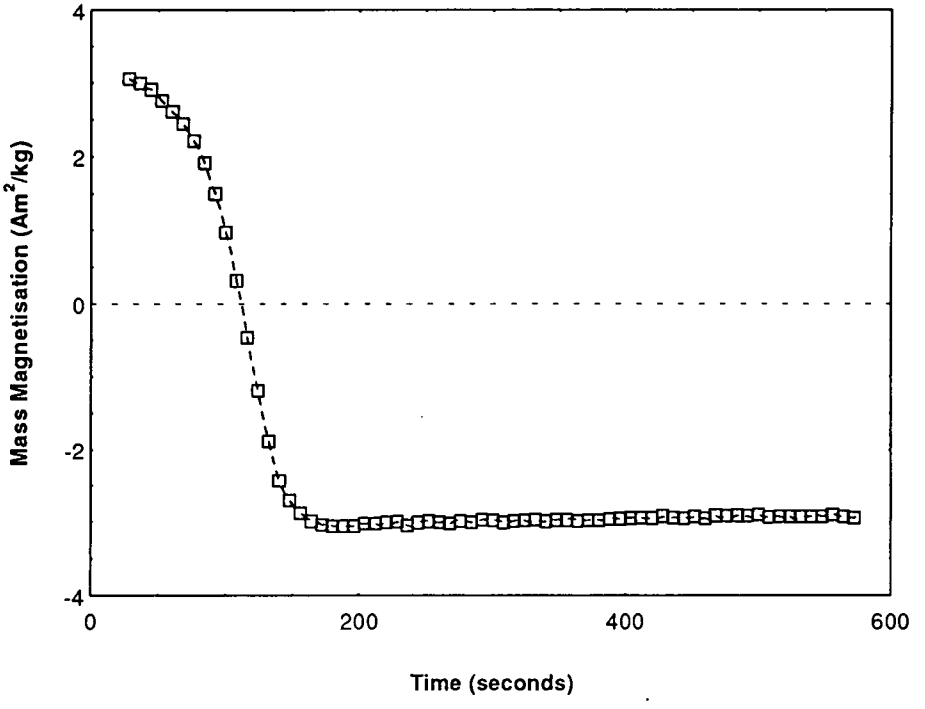

Fig.4.10a Magnetisation as a function of time for sample T17 in a negative magnetic field of 91 A/m after exposure to a positive magnetic field of 4 kA/m for 20 seconds indicating Brownian relaxation of the moment.

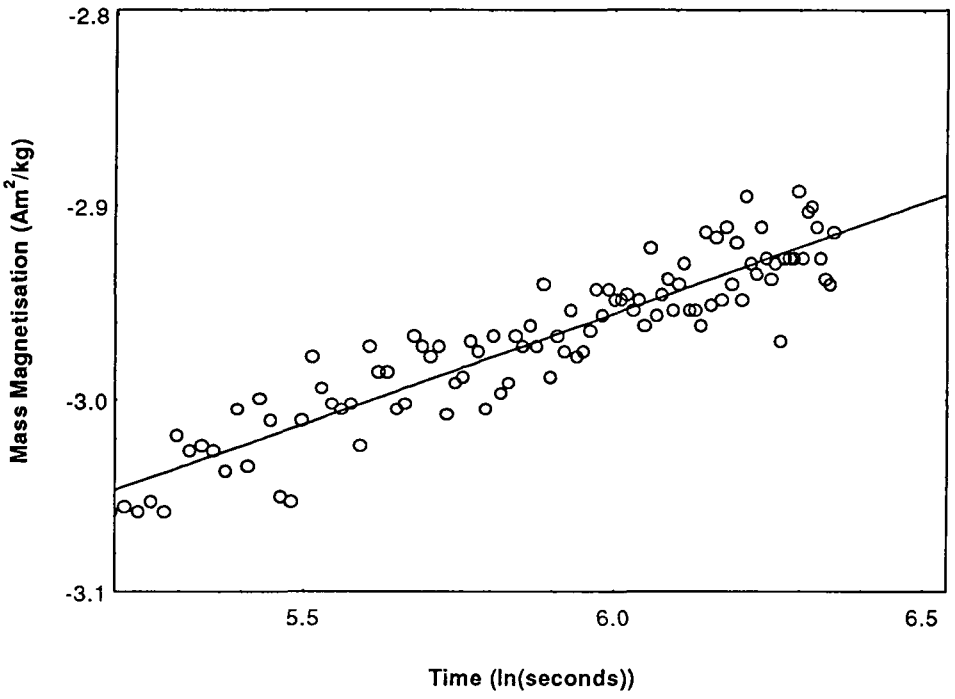

Fig.4.10b Diagram showing an expanded view of the decay of the magnetisation after the particles have bodily rotated from Fig.4.10a.

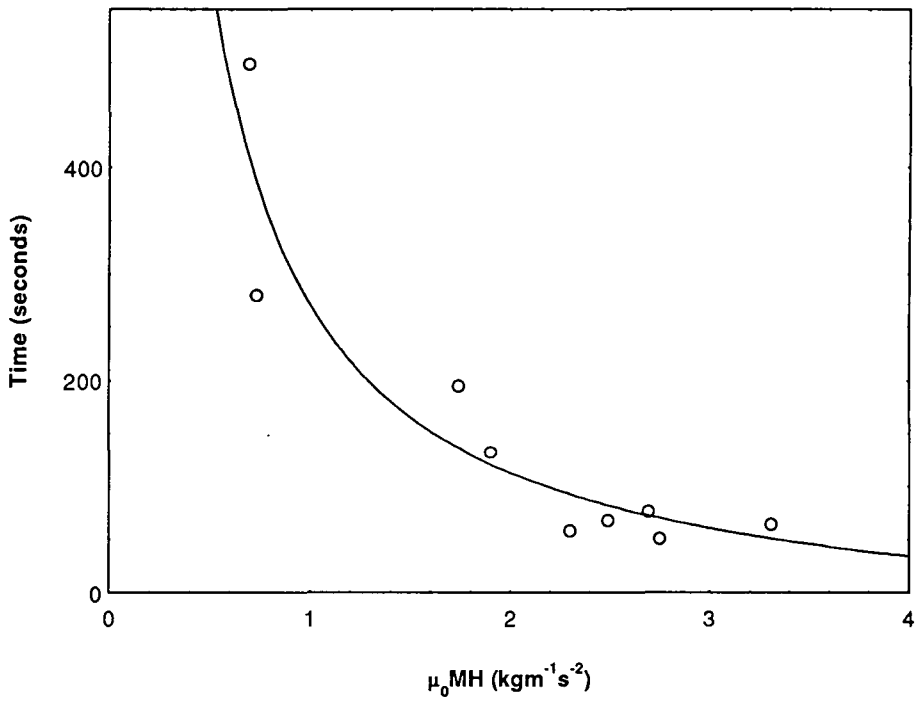

Fig.4.11 Time taken for the magnetisation to pass through zero as a function of the volume magnetisation and applied magnetic field. Fit shown is that of equation 4.1.

expanded view of the decay of the magnetisation from Fig.4.10a after 200 seconds. The magnetisation decays logarithmically.

Normally the Brownian relaxation mechanism is too quick to be seen so it is instructive to investigate the results from this study in greater detail. Shliomis stated that if the applied field is less than the anisotropy field then the relaxation time is given by

$$\tau = \frac{6\eta}{\mu_0 MH} \qquad 4.1$$

where M is the magnetisation before the application of a reverse field, H is the reverse magnetic field, μ_0 is the absolute permeability and η is the viscosity of the fluid. If we measure the time taken for the magnetisation to pass through zero and the magnetisation at the start of the decay as a function of applied field we would expect that the relaxation time would follow equation 4.1. Fig.4.11 shows the time taken to pass through zero as a function of MH and we find that the relation in 4.1 holds. However the value of the viscosity from the fit is a factor of 5×10^4 greater than the value of the carrier fluid water.

A possible reason for such a large discrepancy is that equation 4.1 was derived by neglecting the inertial term in the equation of motion for a particle subjected to a negative magnetic field. It was mentioned earlier that the reversal time for a 10 micron particle is less than 1 second. However once particle agglomeration has occurred then the radius increases and therefore the inertial term in the equation of motion cannot be neglected.

For the same sample measured the next day, as well as the hysteresis curve being radically different, i.e. squarer shape with a much higher coercivity, the reversal mechanism was found to be by Néel relaxation of the moment. Fig.4.12 shows the change of magnetisation against ln(time) for various reverse magnetic fields after being magnetised by a positive magnetic field of 4 kA/m for twenty seconds. The slope of these curves as a function of the applied magnetic field is shown in Fig.4.13. It can be seen that there is a definitive cusp at a field of 1000 A/m. Also shown is the coercivity of the sample. However the cusp is not at the same location as the coercivity measured earlier in the day from the static hysteresis loop.

The fact that the peak in the slope of the decay does not occur at the measured coercivity of the sample is due to the fact that the magnetic properties such as coercivity and remanence are changing as a function of time themselves. Therefore the

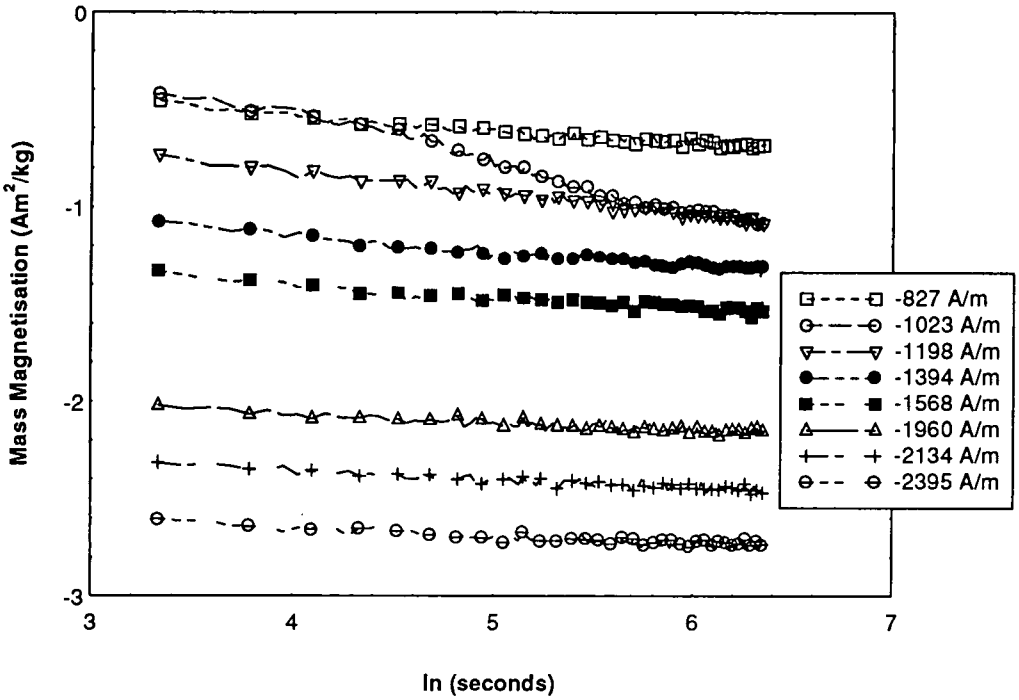

Fig.4.12 Magnetisation of sample T17 against ln(time) for various magnetic fields. Hysteresis loop is t17a in **Fig.4.9b**.

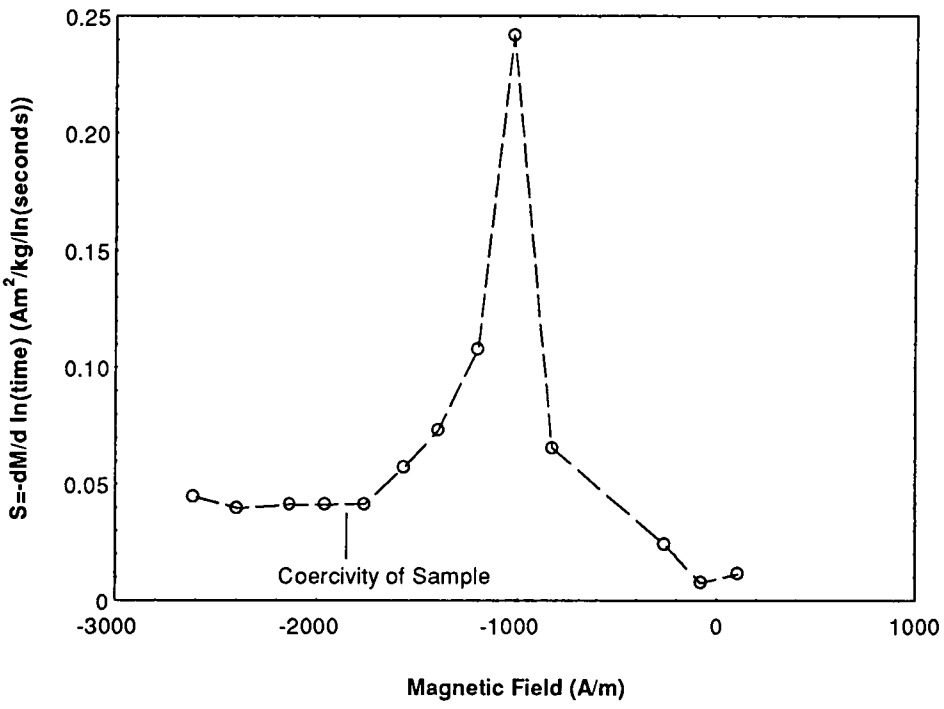

Fig.4.13 Rate of change of magnetisation as a function of magnetic field for sample T17b one day after exposure to a magnetic field of 80 k A/m .

coercivity measured earlier on the day is not the same as the coercivity when the time decay measurements were being performed. This hypothesis is in agreement with the fact that the peak occurs between the coercivities of day one (1850 A/m) when the measurements were performed and the coercivity on the next day (450 A/m).

4.4 Magnetic Characterisation of Individual Aggregates

Clustering of 10 micron particles in a magnetic field and gradient is the basis for successful MPI. This clustering occurs at the crack and shows the position of the crack. To date no measurements have been performed on individual aggregates. The aggregates chosen for this study were roughly 100 microns in size. Due to the small size of these aggregates and consequently their small magnet moment the measurements were performed on an Alternating Gradient Force Magnetometer at UCNW Bangor with the assistance of Mr V.Lewis and Dr K.O'Grady.

4.4.1 Hysteresis Loop of Individual Aggregates

Fig.4.14a shows the hysteresis loop for an aggregate of size 100x30x30 microns. As the masses of these samples are not known we have normalised the saturation moment of the aggregate to the mass magnetisation of the bulk material. Table 4.1 shows the static loop properties for all the samples investigated after the diamagnetic contribution of the substrate has been subtracted off. The coercivity of these samples was found to be 6.5±.4 kA/m and a maximum mass susceptibility of 5 kgm^{-3}. For comparison Fig.4.14b shows the hysteresis loop for a bulk sample of magnetic ink set in epoxy resin. Here the coercivity is 7 kA/m and the maximum mass susceptibility is 4.5 kgm^{-3}.

The similarity between the curves suggests that inter-aggregate interactions are a second order effect compared with the interactions within the aggregate. This means that the magnetic properties of the aggregate, which are active in the formation of the MPI indications, can be deduced from measurements on bulk samples.

Fig.4.15.a-b shows the variation of coercive force and squareness (M_r/M_s) for different aggregates as a function of their length measured in the direction of the magnetic field. It can be seen that there is no significant variation in any of these parameters with length which is not surprising considering the small changes.

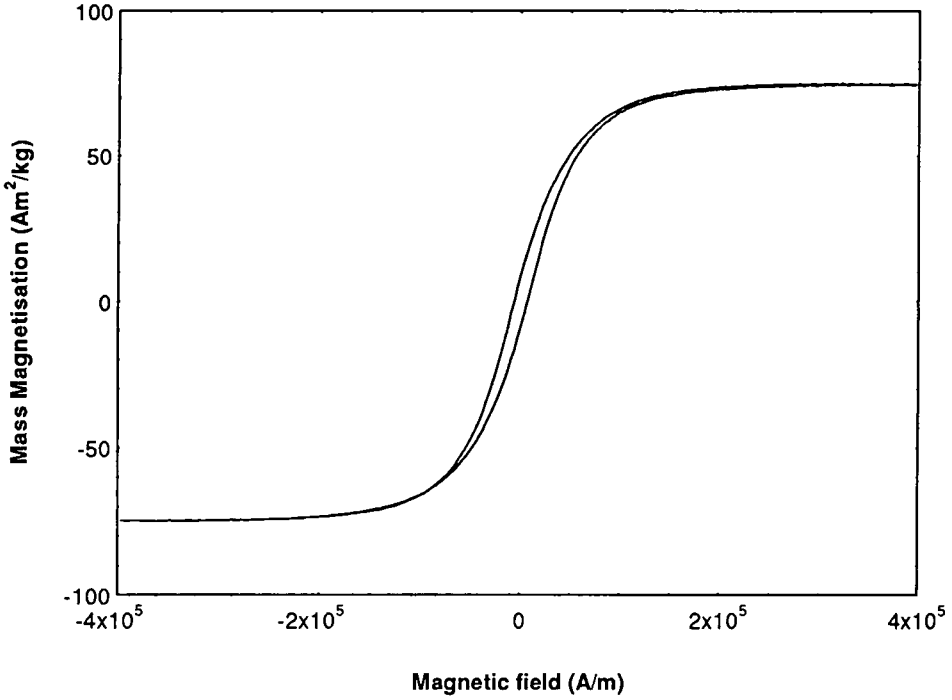

Fig.4.14a Hysteresis loop for an individual aggregate.

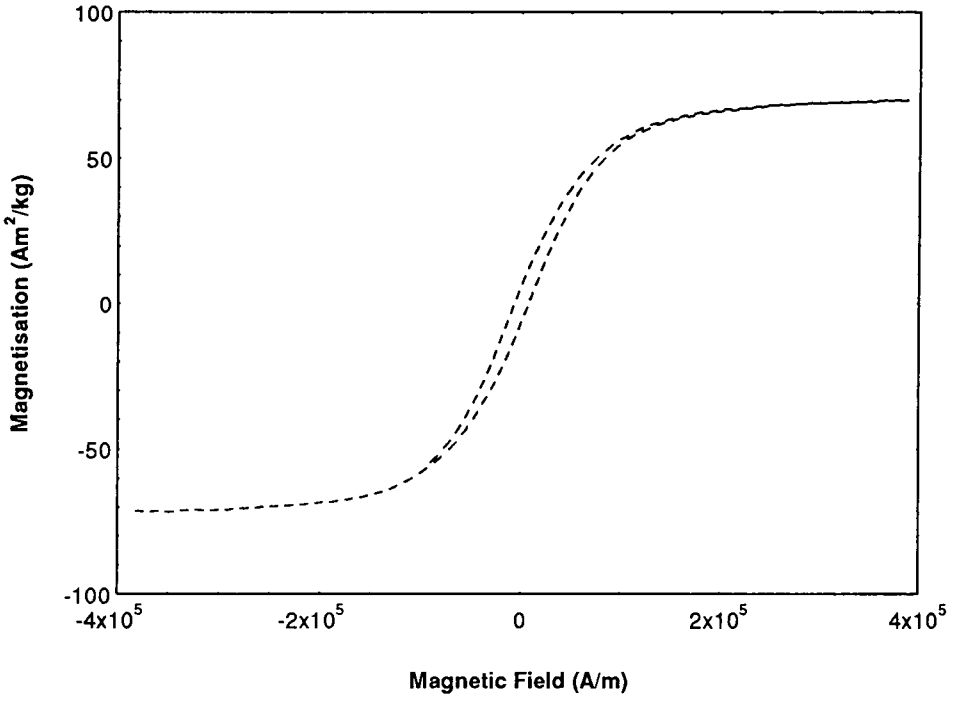

Fig.4.14b Hysteresis loop of a potted magnetic ink sample.

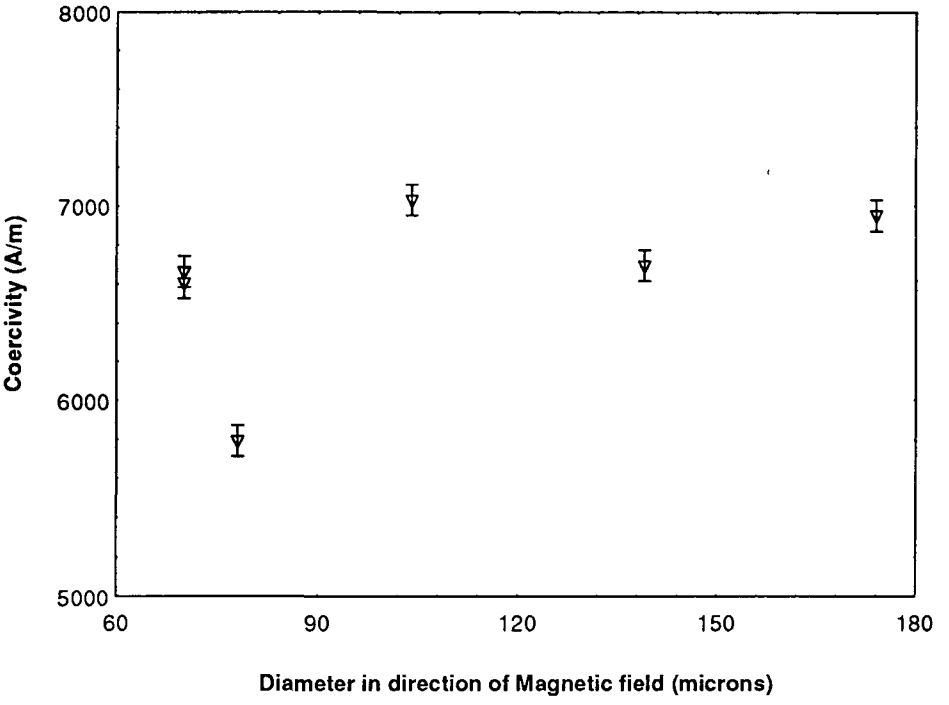

Fig.4.15a Variation of coercivity with respect to diameter in the magnetic field direction.

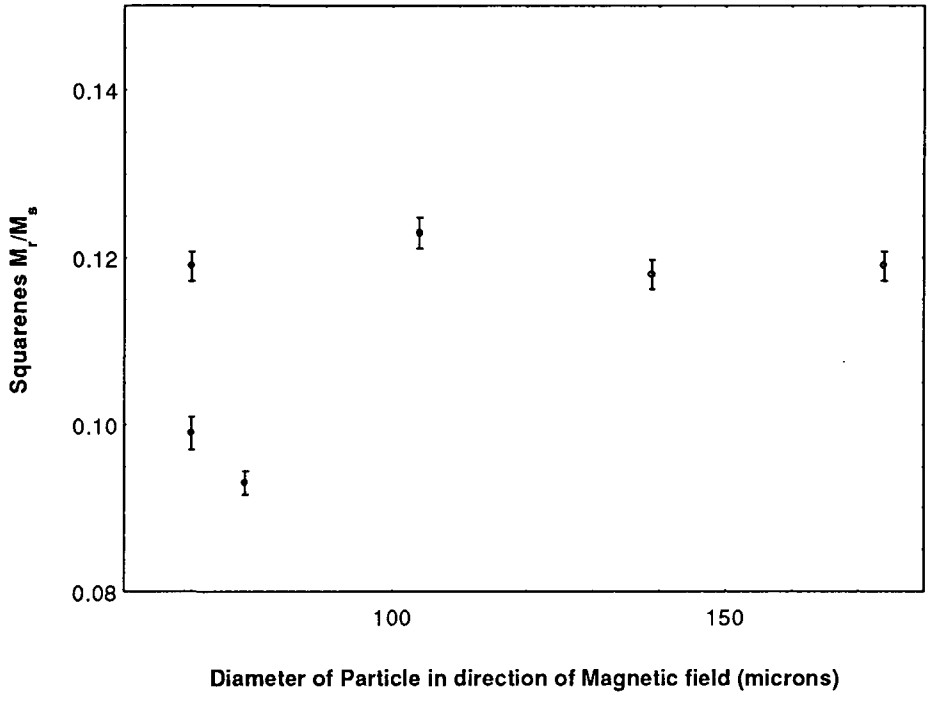

Fig.4.15b Variation of squareness with respect to direction in the magnetic field.

Table 4.1 Showing the magnetic and physical properties of the aggregates measured on the Alternating Gradient Force Magnetometer.

Sample No.	Size dimension in field given first (microns)	H_C (A/m)	Saturation Moment (10^{-9} Am^2)	Squareness (M_r/M_s)	Comments
A3	69x35	6664	21.1	0.119	Single Aggregate
A4	104x130	7032	12.3	0.123	Single Aggregate
A6	139x87	6696	38.9	0.117	Single Aggregate
A7	70x35	6608	9.74	0.098	One Aggregate
A10		6952	8.09	0.114	Two Aggregates
A13	Complex Shape	5792	5.11	0.093	Single Aggregate
A24	174x70	6952	29.6	0.119	Two Aggregates Dimensions given for largest one
A30		5936	88.4	0.082	Two Aggregates

4.4.2 Remanence Curves of Individual Aggregates

As these aggregates are composed of 20-200 nm single domain crystallites, a detailed study of different types of remanence curves has been undertaken to determine the effects interparticle interactions have on the aggregates' magnetisation. The two types of remanence curves are the isothermal remanence curve $M_r(H)$ in which the remanence is measured from the demagnetised state as the applied field is increased and the dc demagnetising curve $M_d(H)$ in which the sample is saturated positively and the remanence measured as a function of increasing negative field.

Analysis of the remanence curves [10,11] recorded under different magnetisation conditions is a well developed technique for studying interactions in magnetic recording media. The analysis, which has now been used on a variety of fine particle and thin film systems, starts from a theoretical relation due to Wohlfarth [12]. In the

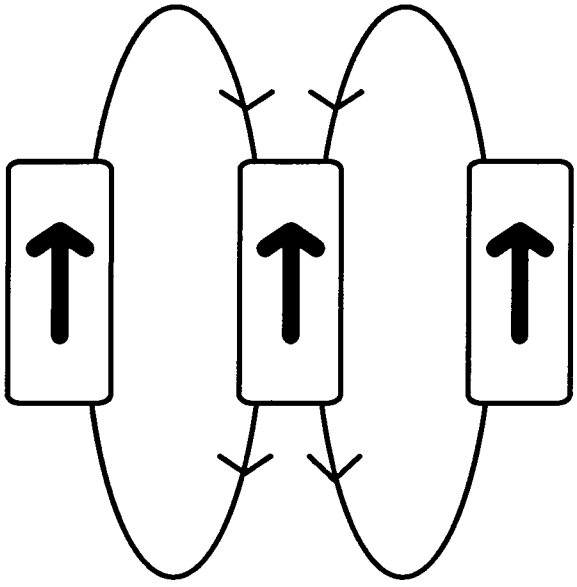

Fig.4.16a Diagram showing interparticle interactions destablizing the magnetisation.

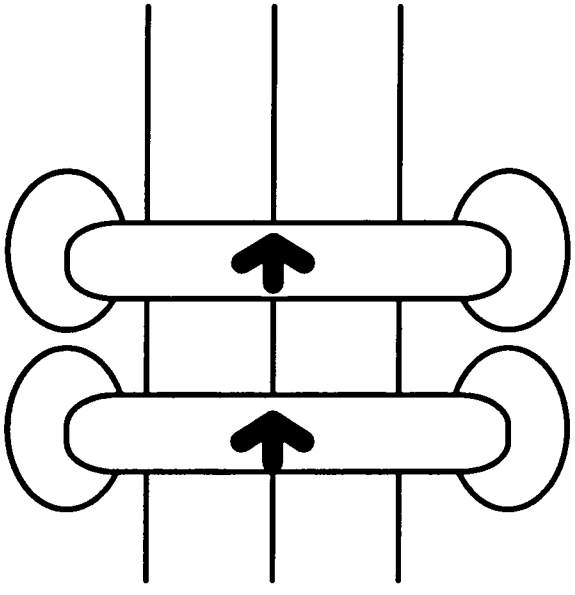

Fig.4.16b Diagram showing interparticle interactions which enhance the magnetisation.

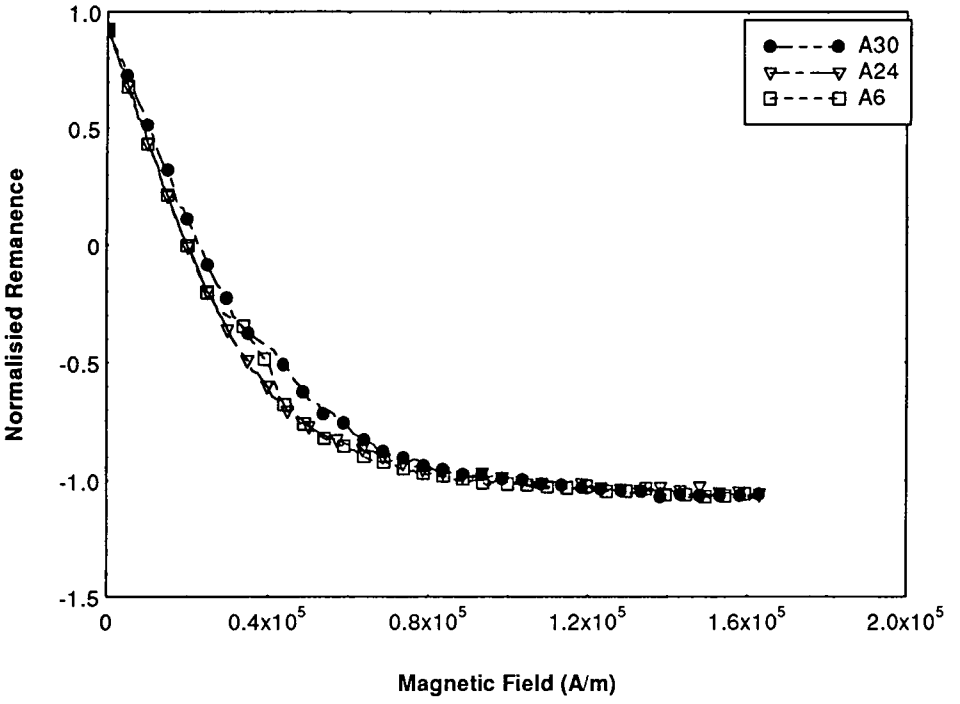

Fig.4.17 Dc demagnetising curves for samples A6,A24 and A30.

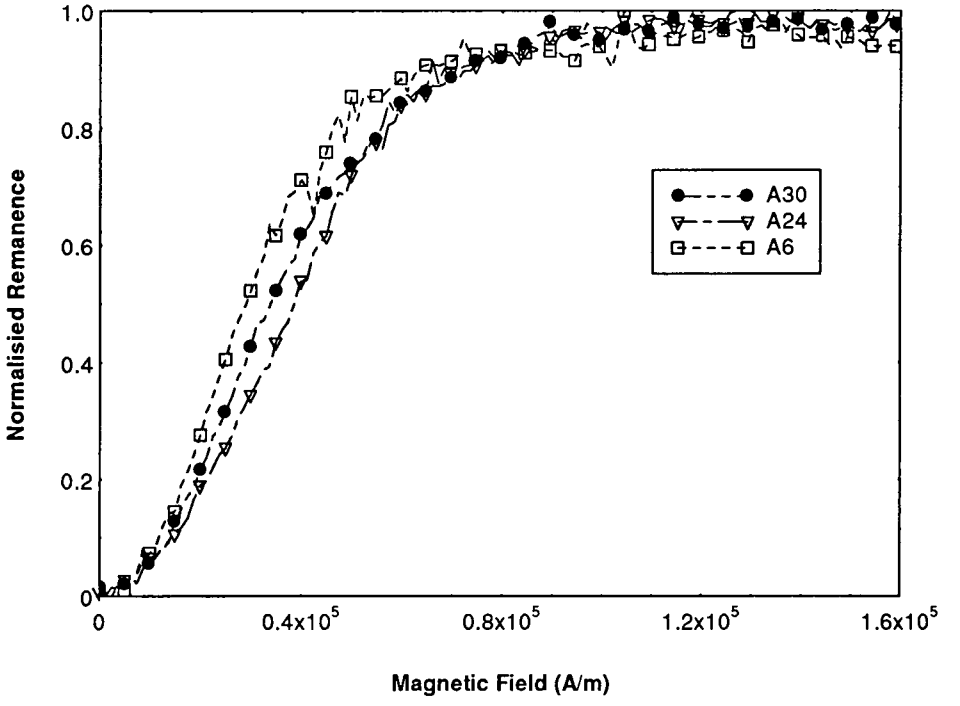

Fig.4.18 Isothermal remanence curves for samples A6,A24 and A30.

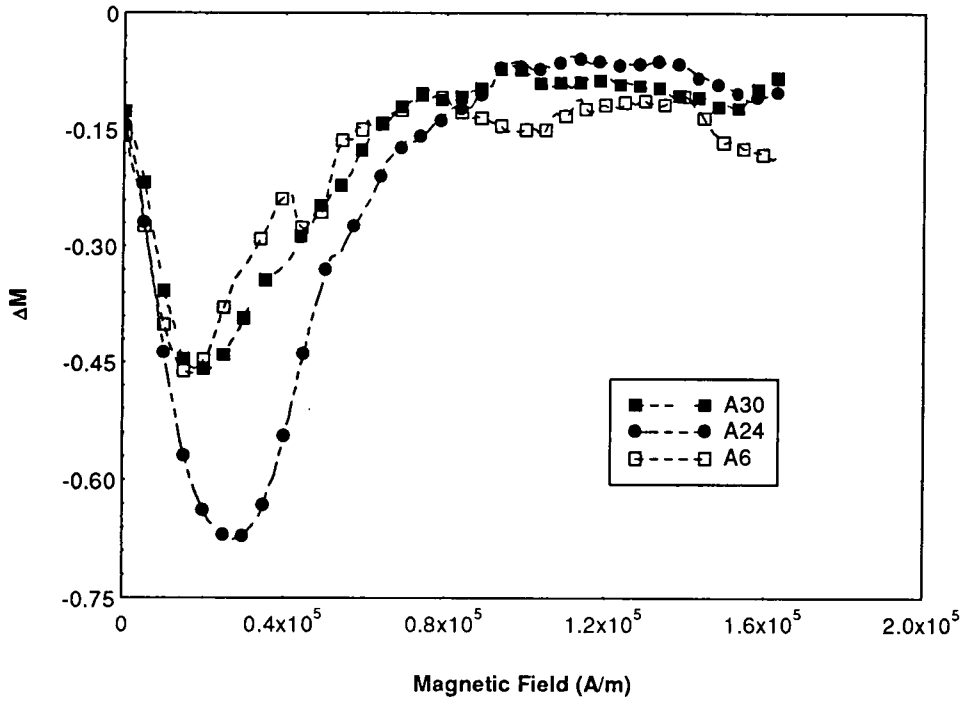

Fig.4.19 ΔM as a function of Magnetic field for samples A6,A24 and A30.

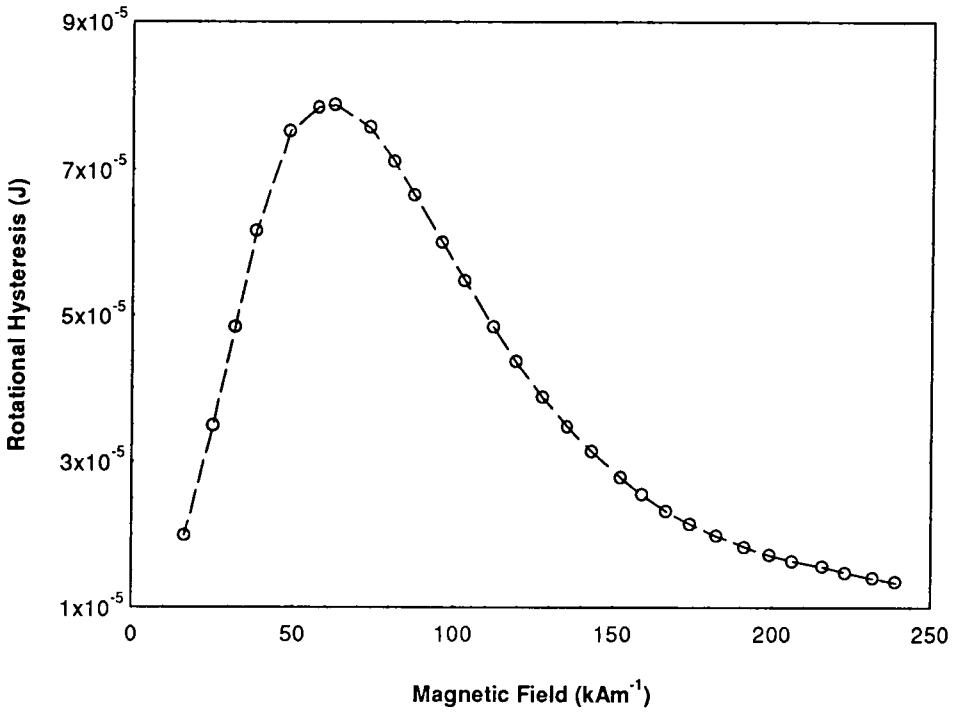

Fig.4.20 Rotational hysteresis as a function of magnetic field for a potted ink sample.

absence of inter-particle interactions the isothermal remanence magnetisation $M_r(H)$ is related to the demagnetisation remanence $M_d(H)$ by

$$M_d(H) = 1 - 2M_r(H) \qquad 4.2$$

Where both M_d and M_r are normalised to the value of the remanence after exposure to an infinite field. To determine the isothermal remanence $M_r(H)$, the sample is first ac demagnetised and the remanent magnetisation recorded after raising the magnetising field to a value H and then reducing to zero. By sequentially increasing the value of H, a series of remanence values are recorded as a function of H. In the $M_d(H)$ measurement the sample is initially saturated positively and taken to a negative field H before reduction to zero. Again the remanent magnetisation is measured as a function of increasing negative field to obtain the $M_d(H)$ curve.

Following Kelly *et al* [13], the nature of the interactions is determined from the deviation $\Delta M(H)$ between the measured $M_d(H)$ and the $M_d(H)$ calculated from the Wohlfarth relation. That is,

$$\Delta M(H) = M_d(H) - (1 - 2M_r(H)) \qquad 4.3$$

If the value of $\Delta M(H)$ is positive then the interparticle interactions tend to stabilise or enhance the magnetisation whereas if $\Delta M(H)$ is negative the interactions tend to destabilise the magnetisation, the effect of both positive and negative interactions on a array of single domain particles is shown in Fig.4.16

Fig.4.17 and Fig.4.18 show the dc demagnetisation and the isothermal remanence curves for three of the samples investigated. Dc demagnetisation curves starts from positive remanence and slowly at first goes towards the negative remanence. We note that the shape is the same for both curves. The isothermal remanence curve starts from zero and soon reaches the maximum value of remanence.

The variation of ΔM as a function of magnetic field is shown in Fig.4.19. The value of ΔM decreases to a maximum at a field between 20000 and 27000 A/m and then as the magnetic field is increased it approaches zero. This implies that interparticle interactions among the 20-200nm crystallites destabilise the aggregate magnetisation at low fields but at higher fields the effect of interparticle interaction can be ignored. This

result has important implications for MPI as the interparticle interactions among the 20-200 nm size crystallites lower the magnetisation of the mobile 10 micron particle as well as the aggregates which form at the crack and act as preferential trapping sites. The force of attraction between the mobile particles and the crack depends on the particles' magnetisation and the attraction between a particle and an aggregate already at the crack depends on the product of their magnetisation. As the magnetisation is lowered by these interactions therefore the attractive force is also lowered.

4.5. Determination of the Magnetic Components of Magnetic Inks

There has been discussion over which oxides of iron are used for black magnetic inks. McCoy[14] reported X-ray results that suggested that the ore was Fe_3O_4. However the manufacturers quote the magnetic components in their inks as a percentage of Fe_2O_3. This is because the test they use to determine the % of iron oxide in their inks is BS 3981 and this requires that the results obtained be expressed as a % of Fe_2O_3. However the test described works equally well for Fe_3O_4. To our knowledge no information is available as to the magnetic component of the fluorescent ink. In this study the mass magnetisation of Magnaflux MHF7 and Meccana a fluorescent ink are measured with the hope of determining their magnetic component. The exact magnetic component used in MPI is needed so that it can be included in the simulation results presented in the next chapter.

4.5.1 Mass Magnetisation of Commercial Magnetic Inks

Hysteresis curves were obtained for a known mass of MHF7 and Meccana. From a 1/H extrapolation we have determined the saturation mass magnetisation to be 75.5 Am^2/kg and 192 Am^2/kg respectively. The mass magnetisation of the fluorescent ink indicates that the ferromagnetic component is probably iron due to the large value of the mass magnetisation, the mass magnetisation of iron at room temperature is 218 Am^2/kg [15].

However for the black magnetic ink the mass magnetisation has a value between that of Fe_3O_4 (84 Am^2/kg) and γFe_2O_3 (74 Am^2/kg). The values for the mass magnetisation being taken from Wohlfarth[16]. This indicates that it could contain a mixture of Fe_3O_4, γFe_2O_3 and a non-magnetic material. However upon heating Fe_3O_4 in an oxidising atmosphere between 200 and 250 degrees the following transformation occurs[17].

$$2Fe_3O_4 + \frac{1}{2}O_2 \rightarrow 3Fe_2O_3 \qquad 4.4$$

Whereas γFe_2O_3 undergoes a transition to the antiferromagnet αFe_2O_3 in the region of 250 to 500 degrees[18]. It was therefore decided to oxidise the black magnetic ink at 220 degrees to convert all the Fe_3O_4 present to γFe_2O_3 but prevent any γFe_2O_3 present forming αFe_2O_3. The mass magnetisation after being oxidised was found to be 65.5 Am^2/kg. If the black magnetic ink consisted solely of Fe_3O_4 and a non magnetic component the mass magnetisation after the oxidation of Fe_3O_4 to γFe_2O_3 would be 66.5 Am^2/kg. Therefore the main ore used in black magnetic inks is Fe_3O_4 and not γFe_2O_3. The measured mass magnetisation after oxidation is close to that predicted if the ink just contained magnetite and a non magnetic component.

4.6 Determination of the Spin Reversal Mechanism in Potted Magnetic Inks

From measurements of the rotational hysteresis W_r the spin reversal mechanism in an array of single domain particles can be determined. Rotational hysteresis W_r is defined as the net work required to rotate a specimen slowly through 360° in a fixed magnetic field. It occurs in the field region where there are irreversible processes in the magnetisation of a sample. This technique was pioneered by Bean and Meiklejohn[19] who calculated the Rotational Hysteresis Integral for coherent rotation. The rotational hysteresis integral is defined as:

$$\int_0^{\infty} \frac{W_r}{M_s} d\left(\frac{1}{H}\right) \qquad 4.5$$

where M_S is the magnetisation and H is the applied magnetic field. Jacobs and Luborsky[20] extended the analysis to include chain of spheres coherent rotation and chain of spheres fanning. The values of the rotational hysteresis for the various spin reversal mechanisms are shown in Table.4.2.

The spin reversal mechanism of a sample can be determined from rotational hysteresis studies. These measurements were performed on a Bede Torque Magnetometer on a potted black magnetic ink sample. The rotational hysteresis measured was the difference between the two torque curves one in the forward direction and one in the reverse direction over 180°. This is the same as the work necessary to rotate the

specimen through 360°. Fig.4.20 shows the rotational hysteresis as a function of magnetic field. To determine the spin reversal mechanism we calculate the area under the curve of a graph of rotational hysteresis divided by the magnetic of the sample as a function of 1/H. This is shown in Fig.4.21.

Table.4.2 Showing the relationship between different reversal mechanism and the value of the rotational hysteresis integral. Taken from reference 20

Model of Spin rotation	**Alignment**	**Value**
Coherent Rotation	Random (sph.)	0.380±0.005
Coherent Rotation	Aligned or Random (pl.)	0.415±0.005
Chain-of-Spheres with Fanning	Random (sph.)	1.02±0.01
Chain-of-Spheres with Fanning	Aligned or Random (pl.)	1.54±0.01

From the area under the graph and the magnetisation of the sample determined by VSM measurements the rotational hysteresis integral was found to 1.04 and from Table 4.2 we can conclude that the spin reversal mechanism is by chain of sphere fanning.

4.7 Summary

From the measurements on the effect of concentration on the magnetic properties of a magnetic ink it was found that the virgin curve is outside the main hysteresis loop. This was attributed to particle agglomeration lowering the demagnetisation factor of the sample. Particle agglomeration was also believed to be responsible for the observed changes in the coercivity and remanence as a function of concentration. The magnetic measurements at low magnetic fields on fresh magnetic ink indicated that the mass susceptibility was independent of concentration and had a value of 5.5×10^{-4} m^3/kg. Hysteresis occurred in fields upto 4 kA/m however no coercivity or remanence was

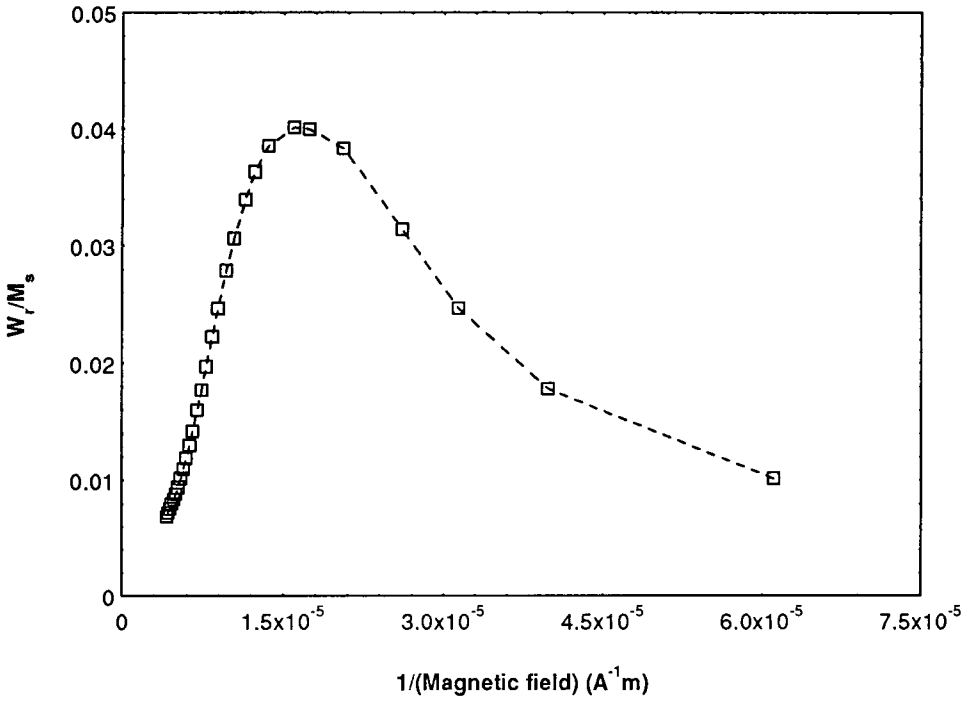

Fig.4.21 Rotational hysteresis/ magnetic moment as a function of (Magnetic field)$^{-1}$.

observed. This was because the particles rotated when the magnetic field changed its direction.

However upon exposure to a large enough magnetic field particle agglomeration occurs. This agglomeration affects quite drastically the magnetic properties inducing, a coercivity and remanence. This also affects the reversal mechanism. These properties change as a function of time indicating that the system is undergo changes in its structure.

Measurements on the aggregates indicate that interaction between single domain crystallites decreases the magnetisation of the aggregate. This lowers the force on the particle during MPI. Comparison between the measurements of bulk samples and the aggregates indicates that inter-aggregate interactions are a second order effect. Therefore the properties of the aggregates can be deduced from measurements on the bulk material. By measuring the mass magnetisation of a typical black ink and a fluorescent ink the magnetic component has been determined as Fe_3O_4 and Fe respectively. The spin reversal mechanism in the black magnetic ink was deduced to be by chain of spheres fanning.

References Chapter 4

[1] Magnaflux, South Dorcan Industrial Estate, Swindon, Wilts, SN3 5HE

[2] Shliomis, M.I., "Magnetic Fluids", *Sov. Phys.-Usp.*, **17**, 153-169 (1974)

[3] McCoy, J.M., and Tanner, B.K., "Magnetisation of inks for Magnetic Particle Inspection", *J. Phys. D: Appl. Phys.*, **22**, 1366-1371 (1989)

[4] Rosenweig, R.E., "Ferrohydrodynamics", *Cambridge University Press*, Cambridge (1985)

[5] O'Grady, K., Gilson, R.G., and Hobby, P.C., "Magnetic pigment dispersions (a tutorial review)", *J. Magn. Magn. Mater.*, **95** , 341-355 (1991)

[6] Flanders, P.J., and Sharrock, M.P., "An analysis of time-dependent Magnetization and coercivity and their relationship to print-through in Recording tapes", *J. Appl. Phys.*, **62,** 2918-2928 (1987)

[7] Cayless, A.T., Hoon, S.R., Tanner, B.K., Chantrell, R.W., and Kilner, M., "High sensitivity measurements of néel relaxation in fine particle ferromagnetic systems ", *J.Magn. Magn. Mater,* **30**, 303-311 (1983)

[8] O'Grady, K., Chantrell, R.W., Popplewell, J., and Charles, S.W., "Time dependent magnetisation of a system of fine cobalt particles", *IEEE Trans. Magn.*, **17**, 2943-2945 (1981)

[9] McCoy, J., PhD thesis, University of Durham (1988)

[10] Corradi, A.R., and Wolfarth, E.P., "Influence of densification on the remanence, the coercivities and the interaction field of elongated γ Fe_2O_3 powders ", *IEEE Trans. Magn.*, **14,** 861 (1978)

[11] Spratt, G.W.D., Bissell, P.R., Chantrell, R.W., and Wohlfarth, E.P., "Static and dynamic experimental studies of particulate recording media", *J. Magn. Magn Mater*, **75**, 309-318 (1988)

[12] Wohlfarth, E.P., "Relations between different modes of acquisition of the remanent magnetisation of ferromagnetic particles", *J.Appl. Phys.*, **29** ,595-596 (1958)

[13] Kelly, P.E., O'Grady, K., Mayo, P.I., and Chantrell, R.W., "Switching Mechanisms in cobalt-Phosphorus thin films", *IEEE Trans. Magn.*, **25**, 3881-3883 (1989)

[14] McCoy, J., PhD thesis, University of Durham (1988)

[15] Weast. R.C., "Handbook of Chemistry and Physics", *CRC Press*, E120 (1976)

16 Wohlfarth, E.P., "Ferromagnetic Materials", Vol 2, *North Holland Publishing Company*, 430-431 (1980)

17 Mee, C.D., "The physics of Magnetic Recording", *North Holland Publishing Company*, 179 (1964)

18 Craik, D.J., "Magnetic Oxides", *John Wiley and Sons,* 708 (1975)

19 Bean, C.P., and Meiklejohn, W.H., "Rotational hysteresis in ferromagnetic micropowders", *Bull. Am. Phys. Soc. Ser II,* **1**, 148 (1956)

20 Jacobs, I.S., and Luborsky, F.E., "Magnetic anisotropy and rotational hysteresis in elongated fine particle magnets", *J. Appl, Phys.*, **28,** 467-473 (1957)

Chapter 5

Computer Simulation of the Indication Process in MPI

5.0 Introduction

The motion of magnetic particles in a magnetic field gradient has relevance to a large area of physics apart from the area of magnetic particle inspection. These include the Bitter[1] technique used to detect domain walls in ferromagnetic crystals by application of a fine colloidal suspension of magnetite onto the crystal's surface and magnetic separation which is used in both industry and medicine to separate one component of a mixture from another due to their different magnetic properties. Consequently other people have modelled the motion of such a particle before, e.g. Kittel[2,3] and Watson[4]. We discuss this work first and then describe a model constructed for MPI by McCoy and Tanner[5]. Then results obtained from the model are discussed.

5.1.1 Bitter Technique

The Bitter technique is used to show the presence of domain walls in ferromagnetic crystals and is very similar to MPI but can detect regions of flux discontinuities which are much smaller due to the smaller particles that are used. In this technique it is essential that the surface of the crystal is suitably prepared before a colloidal suspension of magnetite of radius less than 1 micron is applied to the surface. These particles are attracted to regions of local maxima in the magnetic field intensity. The modelling work done by Kittel assumes that the particles are in thermal equilibrium, i.e. the magnetic force is comparable to the force due to Brownian motion, so that the particle distribution is predicted by a Boltzmann distribution.

Kittel considered two possible cases, depending on the magnetic properties of the particles used. If the particles are single domain with a magnetic moment m in a magnetic field H_O then the distribution function is given by

$$p(H_o) = p_o \frac{\sinh\left(\frac{mH_o}{kT}\right)}{\frac{mH_o}{kT}} \qquad 5.1$$

where p_O is the particle density in zero magnetic field, k is the Boltzmann constant and T is the temperature. However if the particles are multidomain then their magnetic moment is dependent upon the applied field. Kittel assumed a susceptibility of χ and the distribution function becomes:

$$p(H_o) = p_o \exp\left(\frac{\chi H_0^{\,2}}{kT}\right) \qquad 5.2$$

So the particle density at a particular field H is dependent on the particle moment and the magnitude and gradient of H. However the particles used in MPI are much larger and the effect of Brownian motion is negligible, therefore their distribution cannot be approximated to a Boltzmann distribution.

5.1.2 Magnetic Separation

Magnetic separation is used to separate micron size particles from fluids as the particles have a different susceptibility to that of the fluid. The fluid is passed through a magnetic filter, typically a magnetised steel wire. The particles are attracted to and remain at the filter leaving a purified liquid to pass through. The aim is to separate one component of the mixture from another. The more particles that are trapped by the filter the higher the efficiency of the filter is.

The use of these separators has increased recently due to the high magnetic fields and gradients possible from superconducting magnets. Currently work is concerned with the possibility of separating bone marrow from blood using this technique[6].

Watson considered a paramagnetic particle of susceptibility χ with radius R in a viscous fluid of viscosity η flowing with a velocity V_O. The particle is a distance r and θ from a ferromagnetic wire of radius a, which is magnetised by a magnetic field H_O and has a magnetisation M_S. This is shown in Fig.5.1. Watson reported that the equations of motion for such a particle were:

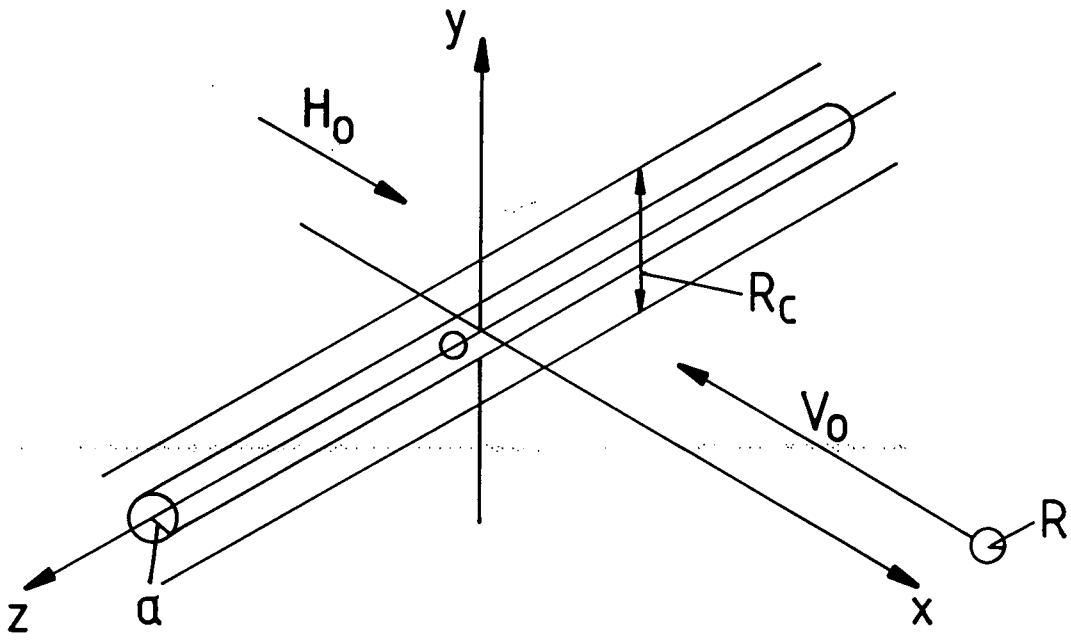

Fig.5.1 Diagram showing the geometry adopted by Watson for Magnetic Separation.

$$\frac{\partial r_a}{\partial t} = \left(\frac{V_o}{a}\right)\left(1 - \frac{1}{r_a^2}\right)\cos\theta - \left(\frac{V_m}{a}\right)\left(\frac{M_s}{2\mu_o H_o}\right)\frac{1}{r_a^5} - \left(\frac{V_m}{a}\right)\frac{\cos 2\theta}{r_a^3} \qquad 5.3$$

$$r_a\frac{\partial \theta}{\partial t} = -\left(\frac{V_0}{a}\right)\left(1 + \frac{1}{r_a^2}\right)\sin\theta - \left(\frac{V_m}{a}\right)\frac{\sin 2\theta}{r_a^3} \qquad 5.4$$

where

$$\left(\frac{V_m}{a}\right) = \frac{2}{9}\left(\frac{\chi M_s H_o R^2}{\eta a^2}\right) \qquad \text{and} \qquad r_a = \frac{r}{a}$$

Most of the modelling work in magnetic separation is used to calculate the capture radius R_C of the ferromagnetic wire. The capture radius is the radius around the wire in which all particles in it are attracted to the wire. From this capture radius the efficiency of a particular filter can be obtained and improved. For a more detail discussion see Gerber[7].

Magnetic separation mainly deals with either paramagnetic or diamagnetic particles. However Takayasu and Gerber[8] have modelled and experimentally verified results for ferromagnetic particles in suspension. These results indicate the existence of dendrites formed from the magnetic particles captured at the wire. These dendrites are aggregates of the ferromagnetic particles growing parallel to the field direction. These dendrites enhance the capture radius as they modify the magnetic field distribution and act as trapping sites themselves and therefore the efficiency of the filter is improved.

5.2.1. Modelling of the Indication Process in Magnetic Particle Inspection

This work relies heavily on the early work of McCoy and Tanner and as such only a brief description of the model will be given. Maeda[9] recently presented work on the modelling of the indication process in magnetic particle inspection however his work was for a limited number of simulations in which the main parameter that was varied was the angle the ink was applied to the surface at. This imparts the ink with a velocity and for the particle to be attracted towards the crack it needs to overcome this velocity. Khalileev and Alesksandrov[10] have calculated the trajectories of ferromagnetic particles in air falling

onto a magnetised specimen with a defect present. However the link between their calculations and the parameters such as applied magnetic field, crack width and crack depth is not obvious. Also they only calculated the trajectories for a limited number of cases.

McCoy and Tanner in their modelling work assumed a particle of radius r is suspended in a viscous fluid of viscosity η near a crack as shown in Fig.5.2. They considered that the three major forces acting on the particle were as follows.

The magnetic force is given by:

$$F_m = \frac{4\pi r^3 M \nabla B}{3} \qquad 5.5$$

where B is the magnetic field experienced by the particle and M is the particles magnetisation. The magnetic field B in this model is given by Edwards and Palmer[11] expressions for the magnetic field near a surface breaking elliptical crack. B is used in the subsequent equations to be consistent with McCoy and Tanner, who used B in deriving the following equations.

There will also be a viscous drag on the particle due to its velocity. In the model the particle is assumed to be spherical and of radius r. The viscous drag is then given by Stokes law:

$$F_{drag} = -6\pi\eta r\sqrt{(\dot{x}^2 + \dot{y}^2)} \qquad 5.6$$

where η is the viscosity of the carrier fluid and $\dot{x}$ $\dot{y}$ are the x and y components of the velocity.

The third force considered was the gravitational force. This acts only in the y direction and is given by:

$$F_g = \frac{4\pi r^3 g(\rho_p - \rho_w)}{3} \qquad 5.7$$

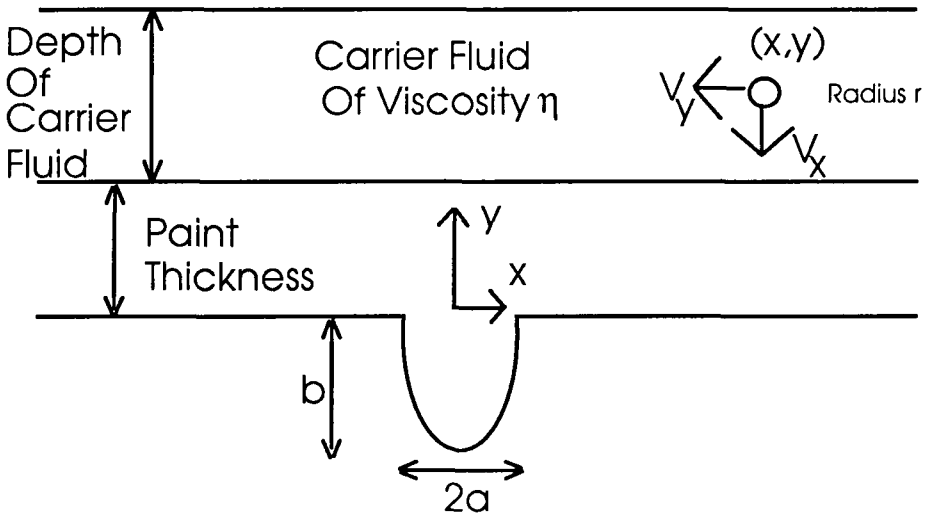

Fig.5.2 Diagram illustrating co-ordinate system used in McCoy's and Tanner's model of the indication mechanism in MPI.

where ρ_p and ρ_w are the densities of the particulate material and carrier fluid respectively and g is the acceleration due to gravity. Separating the forces into their x and y components respectively the following equations were obtained by McCoy and Tanner:

$$\ddot{x}_i + \frac{9\eta}{2r^2\rho_p}\dot{x}_i - \frac{M_i}{\rho_p}\left(\cos\theta_i \frac{\partial B_{ox}}{\partial x_i} + \sin\theta_i \frac{\partial B_{oy}}{\partial x_i}\right) = 0 \qquad 5.8$$

$$\ddot{y} + \frac{9\eta}{2r^2\rho_p}\dot{y} - \frac{M_i}{\rho_p}\left(\cos\theta_i \frac{\partial B_{ox}}{\partial y_i} + \sin\theta_i \frac{\partial B_{oy}}{\partial y_i}\right) + \frac{g(\rho_p - \rho_w)}{\rho_p} = 0 \qquad 5.9$$

$$\theta_i = \tan^{-1}\left(\frac{B_{oy}(x_i, y_i)}{\mu_o H_o + B_{ox}(x_i, y_i)}\right) \qquad 5.10$$

where θ is the angle the magnetic moment makes with the x axis.
These equations cannot be solved explicitly as the magnetic field and magnetic field gradient vary with the particle's position and therefore these equations must be solved numerically. However following the work of Gerber[12] and making the assumption that the magnetisation and the gradient have an average value of $<a_{mag}>$ over the particle's trajectory. Then the equation of motion in the x direction becomes:

$$\ddot{x}_i + \frac{9\eta}{2r^2\rho_p}\dot{x}_i - \frac{\langle a_{mag}\rangle}{\rho_p} = 0 \qquad 5.11$$

This equation can be solved and the solution is:

$$x_i(t) = x_i(0) + \frac{\langle a_{mag}\rangle 2r^2 t}{9\eta} + \frac{2r^2\rho_p}{9\eta}\left[\frac{\langle a_{mag}\rangle 2r^2}{9\eta} - \dot{x}_i(0)\right]\left(e^{-\frac{9\eta t}{2r^2\rho_p}} - 1\right) \qquad 5.12$$

where $\dot{x}_i(0)$ is the component of the velocity in the x direction at zero time and is assumed to have a value of zero henceforth.

Approximation can be made using this equation depending on the value of $\frac{9\eta t}{2r^2\rho_p}$. If this is greater than one, i.e. small radius and high viscosity then the equation of motion becomes:

$$x_i(t) - x_i(0) \approx \frac{2\langle a_{mag}\rangle r^2}{9\eta}\left(t - \frac{2r^2\rho_p}{9\eta}\right) \qquad 5.13$$

In this approximation the distance travelled by a particle is dependent on its size and the viscosity of the carrier fluid.

If on the other hand $\frac{9\eta t}{2r^2\rho_p}$ is less than 1, i.e. large radius and low viscosity then

$\exp\left(-\frac{9\eta t}{2\rho_p r^2}\right) \approx 1 - \frac{9\eta t}{2\rho_p r^2} + \frac{81\eta^2 t^2}{4\rho_p{}^2 r^4}$ and equation 5.12 becomes:

$$x_i(t) - x_i(0) \approx \frac{\langle a_{mag}\rangle t^2}{\rho_p} \qquad 5.14$$

Using this approximation the particle's displacement is independent of its size and the viscosity of the carrier fluid. These approximations will be discussed later as regards the effect of the particle radius and viscosity on the indication mechanism.

As was mentioned earlier to solve the full equations an numerical method must be used. This simulation uses a predictor-corrector algorithm to solve the equations of motion. In a predictor-corrector algorithm one equation is used to predict the new value of a quantity given the old value and then a corrector is used to correct this value. This carries on until some test criteria is met. The position and velocity of the particle are predicted by:

$$x_{m+1} = x_m + hv_{xm} \qquad 5.15$$

$$y_{m+1} = y_m + hv_{ym} \qquad 5.16$$

$$v_{x\,m+1} = v_{x\,m} - h\left(\frac{9\eta}{2r^2\rho_p}v_{x\,m} - \frac{M}{\rho_p}\left[\cos\theta_m \frac{\partial B_{ox}}{\partial x}(x_m, y_m) + \sin\theta \frac{\partial B_{oy}}{\partial x}(x_m, y_m)\right]\right) \qquad 5.17$$

$$v_{y\,m+1} = v_{y\,m} - h\left(\frac{9\eta}{2r^2\rho_p}v_{y\,m} - \frac{M}{\rho_p}\left[\cos\theta_m \frac{\partial B_{ox}}{\partial y}(x_m, y_m) + \sin\theta \frac{\partial B_{oy}}{\partial y}(x_m, y_m)\right] + \frac{g(\rho_p - \rho_w)}{\rho_p}\right)$$

5.18

where $m+1$ is the predicted value and m is the old value. Here h has the units of time and can be regarded as a small step. There will be an error associated with this prediction. The corrector algorithm is then used to produce a better estimate. This can then be fed back into the corrector to improve upon the estimate. The corrector equations are listed below and k is the number of estimates.

$$x_{m+1}^{(k)} = x_m + \frac{h}{2}\left(v_{x\,m} + v_{x\,m+1}^{(k-1)}\right) \qquad 5.19$$

$$y_{m+1}^{(k)} = y_m + \frac{h}{2}\left(v_{y\,m} + v_{y\,m+1}^{(k-1)}\right) \qquad 5.20$$

$$v_{x\,m+1}^{(k)} = v_{x\,m} - \frac{h}{2}\left(\begin{array}{l} \dfrac{9\eta}{2r^2\rho_p}\left[v_{x\,m} + v_{x\,m+1}^{(k-1)}\right] \\ -\dfrac{M}{\rho_p}\left[\begin{array}{l} \cos\theta_m \dfrac{\partial B_{ox}}{\partial x}(x_m, y_m) + \cos\theta_{m+1}^{(k-1)} \dfrac{\partial B_{ox}}{\partial x}\left(x_{m+1}^{(k-1)}, y_{m+1}^{(k-1)}\right) \\ +\sin\theta_m \dfrac{\partial B_{oy}}{\partial x}(x_m, y_m) + \sin\theta_{m+1}^{(k-1)} \dfrac{\partial B_{oy}}{\partial x}\left(x_{m+1}^{(k-1)}, y_{m+1}^{(k-1)}\right) \end{array}\right] \end{array}\right) \qquad 5.21$$

$$v_{y\,m+1}^{(k)} = v_{y\,m} - \frac{h}{2}\left(\begin{array}{l} \dfrac{9\eta}{2r^2\rho_p}\left[v_{y\,m} + v_{y\,m+1}^{(k-1)}\right] \\ -\dfrac{M}{\rho_p}\left[\begin{array}{l} \cos\theta_m \dfrac{\partial B_{ox}}{\partial y}(x_m, y_m) + \cos\theta_{m+1}^{(k-1)} \dfrac{\partial B_{ox}}{\partial y}\left(x_{m+1}^{(k-1)}, y_{m+1}^{(k-1)}\right) \\ +\sin\theta_m \dfrac{\partial B_{oy}}{\partial y}(x_m, y_m) + \sin\theta_{m+1}^{(k-1)} \dfrac{\partial B_{oy}}{\partial y}\left(x_{m+1}^{(k-1)}, y_{m+1}^{(k-1)}\right) \end{array}\right] + \dfrac{2g(\rho_p - \rho_w)}{\rho_p} \end{array}\right)$$

5.22

Obviously there is a limit to the number of corrections that can be calculated as the values from the corrector gradually approach the true value. The convergence of the corrected values are tested in both directions using the following criteria.

$$\left|x_{m+1}^{(k-1)} - x_{m+1}^{(k)}\right| < 1\mu m \text{ and } \left|y_{m+1}^{(k+1)} - y_{m+1}^{(k)}\right| < 1\mu m$$

Once these limits are reached the particle's displacement and velocity are assumed to have the correct value. In these simulations the value of the step size h is $5x10^{-6}$ seconds. The starting conditions are as follows, the particles are randomly distributed in the y direction between the paint layer and the liquid depth (typically 0.5 mm) and are distributed evenly in the x direction from zero to 0.8 mm. They have zero starting velocity in both the x and y directions.

In this model the trajectories of 160 particles are followed till the indication is complete. Interactions between the particles are ignored. The trajectories are followed for 0.4 second by which time the particles have effectively stopped moving. Simulations were run for greater periods of time however for almost all situations the indication was complete within 0.4 second. The particles are stopped whenever they reach the crack lip. However when they hit the paint liquid interface they are allowed to travel in the x direction only.

A figure of merit called contrast is defined by dividing the inspection piece into 8 areas of width 100 microns in the x direction and counting the number of particles in each area. Then subtracting from the highest number of particles in an area the lowest number of

particles in an area and this is then defined as the contrast. This allows comparisons to be made between different starting conditions.

In the model a wide range of parameters can be varied. These are the crack size, permeability of the inspection piece, magnetic properties of the particle, radius of the particles, density of the particles, the viscosity and density of the carrier fluid and the magnetising field are varied to see how they affect the contrast.

5.2.2. Particle Magnetisation

In this study the particles' magnetisation is either dependent upon the total field it is experiencing or it is fixed similar to the work of Kittel. The magnetisation of a spherical particle with a permeability of μ_r in a magnetic field B is given by Edwards and Palmer:

$$M = \frac{2B}{\mu_o}\left(\frac{\mu_r - 1}{\mu_r + 2}\right) \qquad 5.23$$

For large values of μ_r then this reduces to

$$M = \frac{2B}{\mu_o} \qquad \text{for } M < M_{sb} \qquad 5.24$$

and

$$M = M_{sb} \qquad \text{for } \frac{2B_o}{\mu_o} \geq M_{sb} \qquad 5.25$$

Where the saturation value for magnetite M_S is 4.71×10^5 A/m. Magnetite Fe_3O_4 is chosen as the magnetic material in the inks due to the results presented in Chapter 4 on the mass magnetisation of black magnetic inks and the X-ray results of McCoy[13]. Equations 5.24 and 5.25 are used throughout this simulation work apart from when the particles with a fixed magnetic moment are used in which case equation 5.26 is used.

The next case to consider is that when the particles' magnetisation is independent of the

applied field, i.e. a single domain particle or a group of such particles forming a flux closure aggregate in which case the magnetisation is lower than saturation magnetisation, i.e:

$$M = M_{var} \qquad 5.26$$

where the M_{var} in this study is varied between 0 and 10% of the saturation value of magnetite.

5.2.3. Parameters Used

Unless otherwise stated the following parameters were used throughout the simulation.

Particle radius	10 microns
Permeability of inspection piece	1400
Depth of crack	1 mm
Width of Crack	200 microns
Viscosity of Carrier fluid	0.5 mPas
Density of Carrier fluid	1000 kgm^{-3}
Density of Particle Material	5240 kgm^{-3}
Applied Magnetic Field	2400 A/m

5.2.4 Review of McCoys Results

It is worthwhile to consider the results obtained by McCoy as these were found to be in disagreement with the author's own results. The area of disagreement was over the number of particles arriving at the crack and the time taken for the simulation to form. For the test case with the parameters described above, McCoy reported a contrast of 18 on a time scale of 1.4 seconds whereas the author using the same parameters found a contrast of 120 on a time scale of 0.4 seconds. The author has re-run all of McCoy simulations and generally found that the value of the contrast was greater than that obtained by McCoy.

The author has tried all combinations of the starting conditions used by McCoy and has not been able to replicate McCoy results. The calculations have been carried out by hand and were found to agree with the values from the simulation. One explanation for the

discrepancy is that the value used for the volume magnetisation by McCoy was lower than the reference value. This would explain the fact that the indication took longer as the magnetic force on the particle was lower.

5.2.5 Programs Used

The programs used are listed in Appendix A1, they are identical to those of McCoys apart from slight modifications to encompass time varying waveforms and particles with a fixed magnetic moment. These programs are written in FORTRAN 77 and are run on a 486 Personnel computer with a clock speed of 33 MHz. A typical simulation taking 3 hours. Also listed are the programs used to generate the starting conditions for the simulation and one that is used to analyse the simulation data. Both of these are written in Microsoft Qbasic. A description of all the programs is given in the relevant appendix.

The starting co-ordinates for the particles' in the y direction are selected randomly. The effect of various random distributions on the simulation data has been investigated and was found to have little or no effect. On the graphs that follow, the lines that are drawn are a guide for the eye only.

5.3 Time Varying Waveforms

As mentioned in Chapter 2 time varying waveforms are often used in MPI, i.e. thyristor, AC and rectified AC. In the simulations that follow the effect of skin depth is neglected. This is because it is unimportant when current flow methods are being used to magnetise the specimen, as the magnetisation at the surface is unaffected by time varying waveforms. Also the effects of hysteresis in the magnetic particle and specimen under investigation are ignored. This assumption is valid provided that the specimen under investigation is a low remanent steel, this is because in high remanent steels the magnetisation and therefore the flux leakage is not a linear function of the magnetic field. Which is what this model assumes. It is also assumed that the magnetic moment of the particle aligns itself to the new field direction either through rotation of the moment or the particle aligning itself to the new field direction.

The purpose of this study is to determine which parameter of the waveform affects the indication in the same way for all waveforms as currently there is some confusion over this

issue. British standard BS 6072 states *'The peak current value is the relevant quantity used for the calculation of magnetic field intensity'* and the draft European Standard rms. The British Standard then goes onto list conversion factors between the rms. and peak for various waveforms. However for thyristor waveforms there is no simple relation between peak and rms. In this study the contrast is measured for various waveforms as the peak and rms. is varied.

5.3.1 D.C. Waveforms

In these simulations the value of the DC applied magnetic H_O is increased from 100 to 3000 A/m and the effect this has on the contrast is recorded. As expected there was an increase in contrast with applied field. Fig.5.3a shows the time contrast plots for various values of DC applied magnetic field. The contrast has saturated within 0.4 second and the shape of the curves is the same for all the magnetic field values, the magnetic field values affects the absolute value of the contrast. This is to be expected as the magnetic force depend on the gradient of the magnetic field and the particle's magnetisation. Both of these increase with the magnetic field. Fig.5.3b shows the final contrast as a function of the DC field. The final contrast is the value of the contrast at 0.4 seconds. This shows that the relationship between contrast and applied field is not a linear one. However above 500 A/m the relationship between the two is linear and during an actual inspection the applied field will almost certainly be greater than 500 A/m. In which case the relationship between contrast and applied magnetic field is linear.

5.3.2 AC and Rectified AC

The value of the AC and rectified AC applied magnetic field H_O is increased from 100 to 3000 A/m. The waveform used is of the type $H=H_O sin(wt)$ and $H=|H_O sin(wt)|$ for the AC and rectified AC waveforms respectively. The frequency of the oscillation was 50Hz as this is the UK mains frequency. The results for the rectified AC and AC waveforms are identical and for convenience they are plotted as one. These are shown in Fig.5.4. These results show the same slow saturation as the DC waveforms also the fact that the contrast increases as the value of H_O increases.

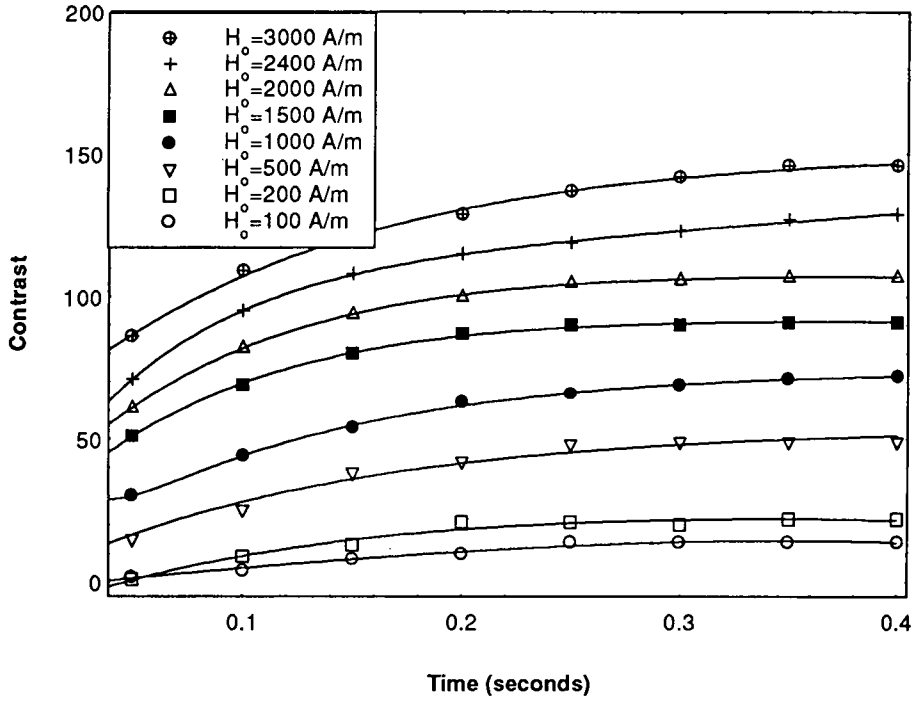

Fig.5.3a Variation of contrast with respect to time for various values of applied dc magnetic field.

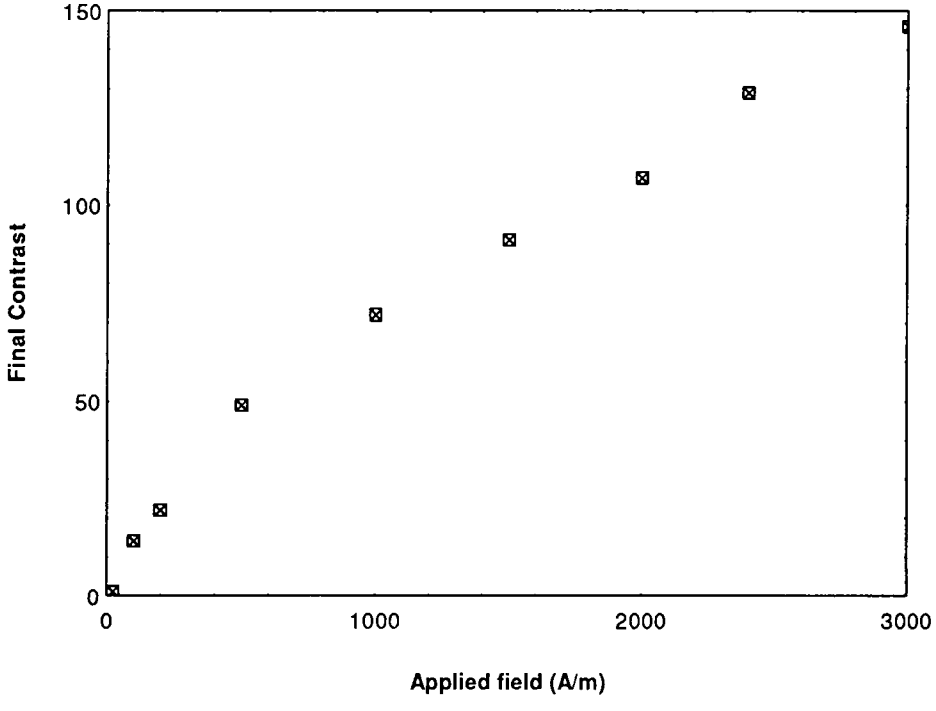

Fig.5.3b Final contrast as a function of applied magnetic field.

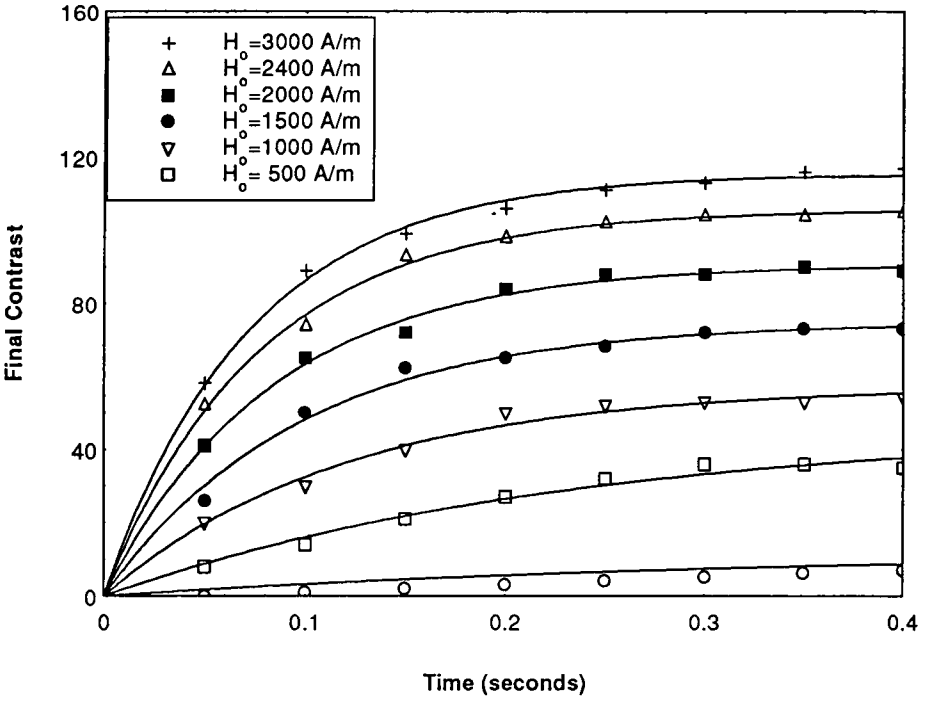

Fig.5.4 Variation of Contrast with time for Ac. and rectified Ac. Waveforms at various magnetic fields.

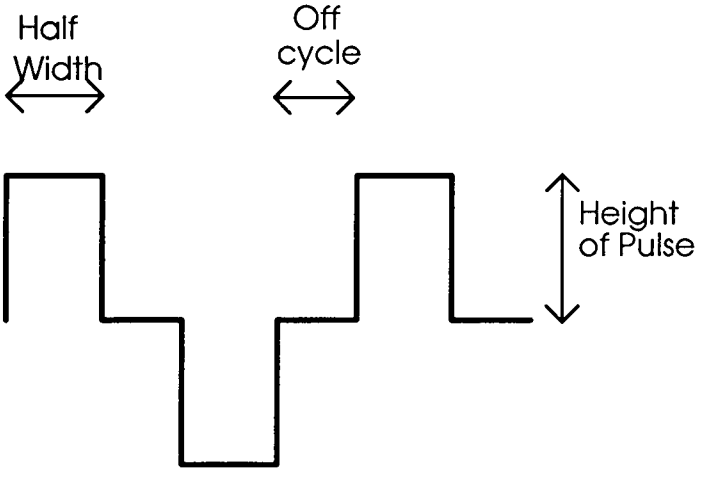

Fig.5.5 Diagram illustrating waveform used to model a thyristor waveform. Both the pulse height and width can be varied.

5.3.3 Thyristor Waveform

The use of thyristor waveforms is becoming more common in magnetising power supplies, they work by switching the power on and off for a certain amount of time regulated by the operator. The waveforms generated by such devices are discussed in Chapter 6. The simplest way to model such a complex waveform was to use a square wave with variable width and height. Such a waveform is shown in Fig.5.5. Simulations were run in which both the width and height of the pulse were varied. In Fig.5.6 the width of the thyristor waveform remained constant and the height of the pulse was increased. Increasing the pulse height causes the contrast to increase steadily as is to be expected. In Fig.5.7 the peak height of the thyristor waveform remained constant but the width of this peak was increased. The maximum width was 0.02 seconds which is a pure square wave with no off cycle. These results show that as the width is increased the contrast is enhanced. This is because the magnetic particles are experiencing the magnetic field for longer periods of time. Therefore the magnetic force on the particle is greater.

5.3.4 Peak, Mean or rms ?

At the moment there is confusion over which quantity should be specified as the requirement to magnetise the specimen under investigation. As BS 6072 recommends the peak of the field whereas the draft European standard suggests the rms. of the field and some manufactures calibrate their devices to the mean of the field. To see which factor affects the contrast in a constant way in our simulation, final contrast is plotted as a function of mean, rms. and peak applied magnetic field.

Fig.5.8 shows the variation of the final contrast as a function of the mean of the waveform. This graph shows that the thyristor waveform has the best contrast with the mean of the applied field. The AC and rectified AC results are similar and the DC results are the worse. The main point to note is that the mean of the field should not be specified when consistent results from various power supplies are wanted. Fig.5.9 shows the variation of final contrast with the peak of the applied field. For the thyristor waveform with the peak height fixed the contrast increases regardless of the peak of the waveform this is because the width of the pulse is being increased and this affects the contrast and causes the increase. When the peak of the applied field is plotted against the contrast the DC waveform results are above the AC and rectified AC. This graph shows that contrary

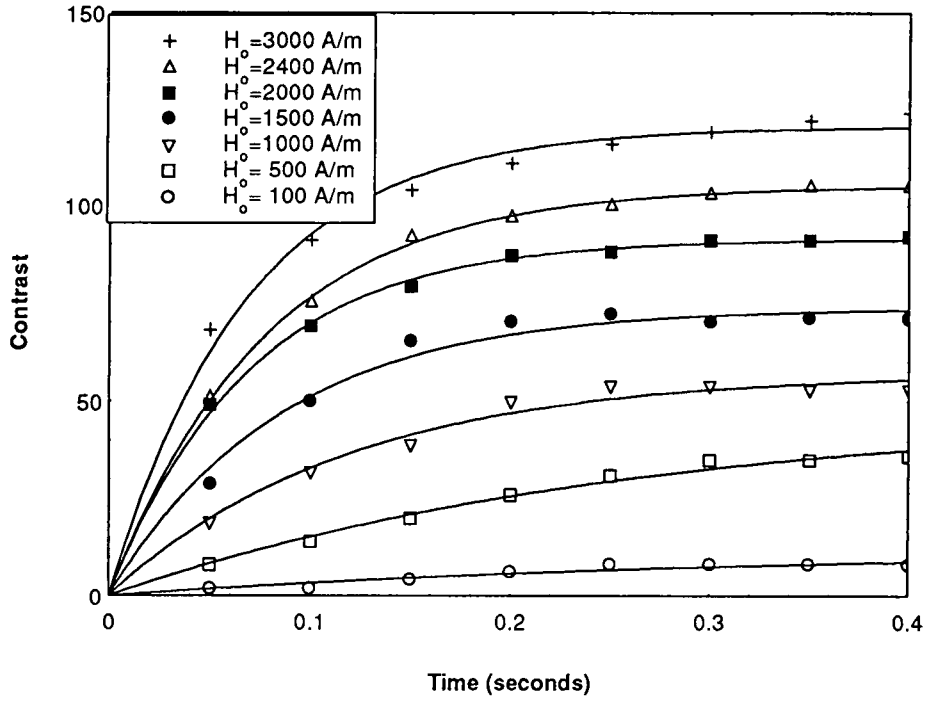

Fig.5.6 Variation of Contrast with time for a thyristor waveform as the peak is increased at a constant width of .01.

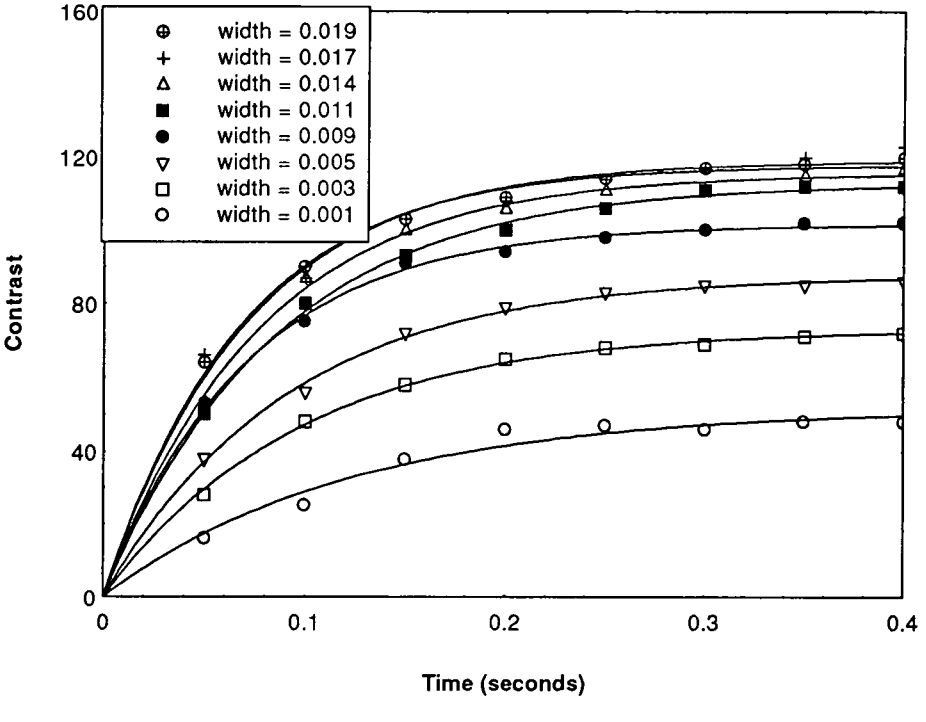

Fig.5.7 Variation of contrast with time for a thyristor waveform as the width is varied at a constant peak height of 2400 A/m.

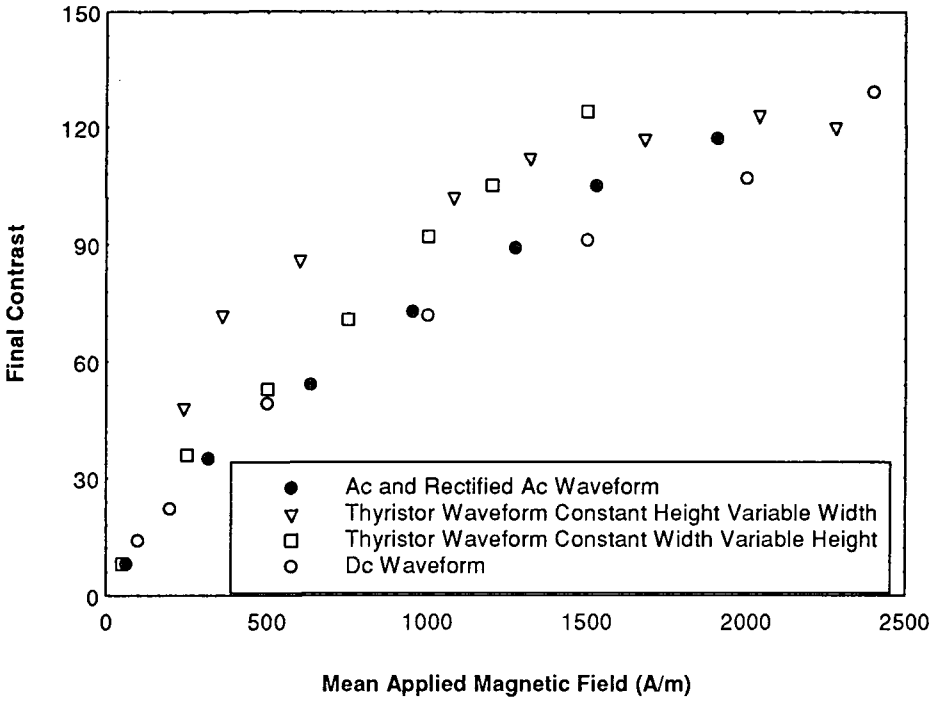

Fig.5.8 Variation of Final contrast with the mean of the applied magnetic field for various waveforms.

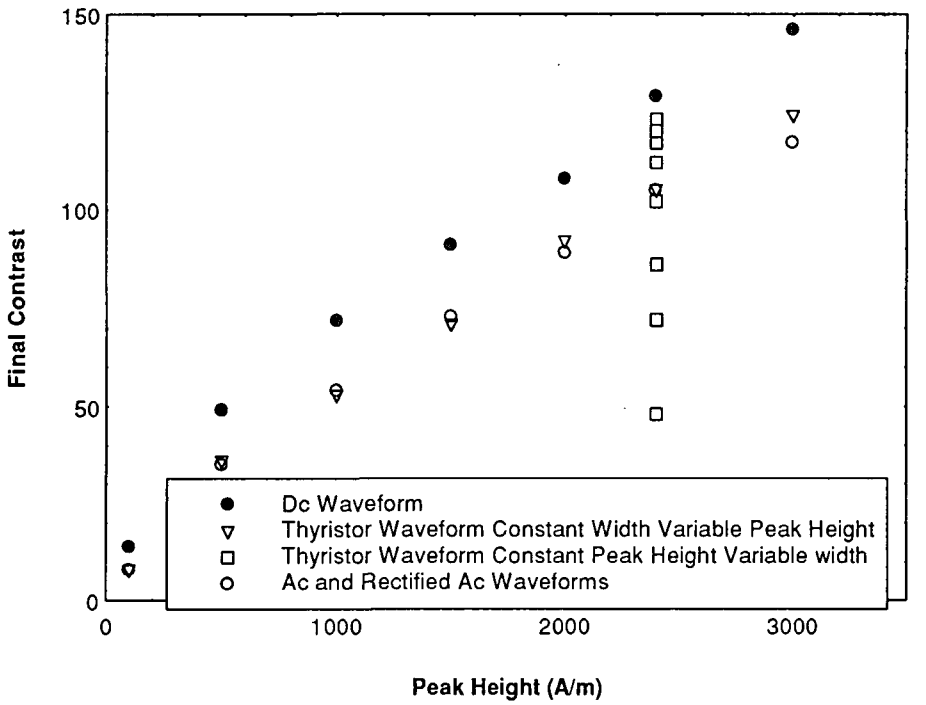

Fig.5.9 Variation of final contrast with the peak of applied magnetic field for various waveforms.

to BS 6072 the peak of the waveform is not the relevant quantity for calculation of the magnetic field in Magnetic Particle Inspection. This is because it affects the contrast in different ways depending on the waveform used and therefore the ability to detect defects will depend upon the waveform used. Therefore the peak and the mean of the applied field should not be used when specifying field values if consistent results are wanted. Fig.5.10 shows the variation of the final contrast as a function of the rms. of the applied field it can be seen that the contrast increases in the same manner for all waveforms as the rms. is increased. This suggests that the rms. of the applied field should be used when specifying field values for use in MPI across a wide range of power supplies, this is in agreement with the draft European standard. However these results are true only for specimen which exhibit no hysteresis as the magnetic field is altered. These conditions are met to some degree in low remanent steels and in this respect these results are in agreement with the experimental work of Stadhaus[14] and MacDonald[15].

5.4 The Effect of Viscosity and Particle Size

In magnetic particle inspection the inks used typically have a mean diameter of 10 microns with a standard deviation of 18 microns[16]. However to show finer defects the use of smaller particles that remain in suspension longer is common cf. Bitter technique. To see the effects that particles of different radius r have on the contrast simulation were run for particles of radius 2,5,10,20 microns over a viscosity range of .1 to 1.1mPas.

Fig.5.11a-d shows the contrast as a function of time as both the radii and viscosity are varied. In Fig.5.11a shows the time contrast plots for the 2 micron radius particles as the viscosity is increased. It can be seen that for the low viscosity 0.1 mPas simulation the contrast does not seem to saturate with time whereas for the other simulations does. This is due to the terminal velocity of the particles' being dependent upon the viscosity of the carrier fluid. This has important implication for manufactures of magnetic inks, as they lower the particle size in an attempt to reveal smaller discontinuities they must also take into account the viscosity of the carrier fluid. The results for the particles with a radius of 5 microns are shown in Fig.5.11b, it can be seen that as the viscosity decreases the contrast increases. The contrast also seems to saturate as the time is increased. The effect of viscosity on contrast is still important for particles of this size. However as the particle's radius is increased the effect of viscosity becomes less important as the magnetic force on a particle starts to dominate the indication process. This can be seen in Fig.5.11c,d. Which shows the time contrast plots for particles of radii 10 and 20 microns respectively. If the

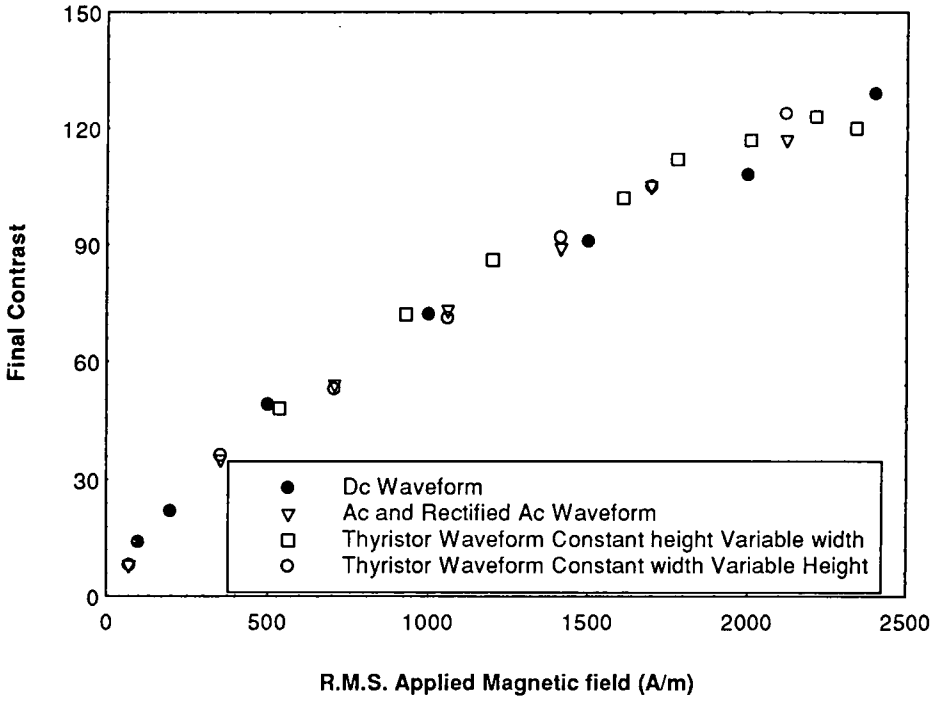

Fig.5.10 Variation of final Contrast with the rms. of magnetic field for various waveforms.

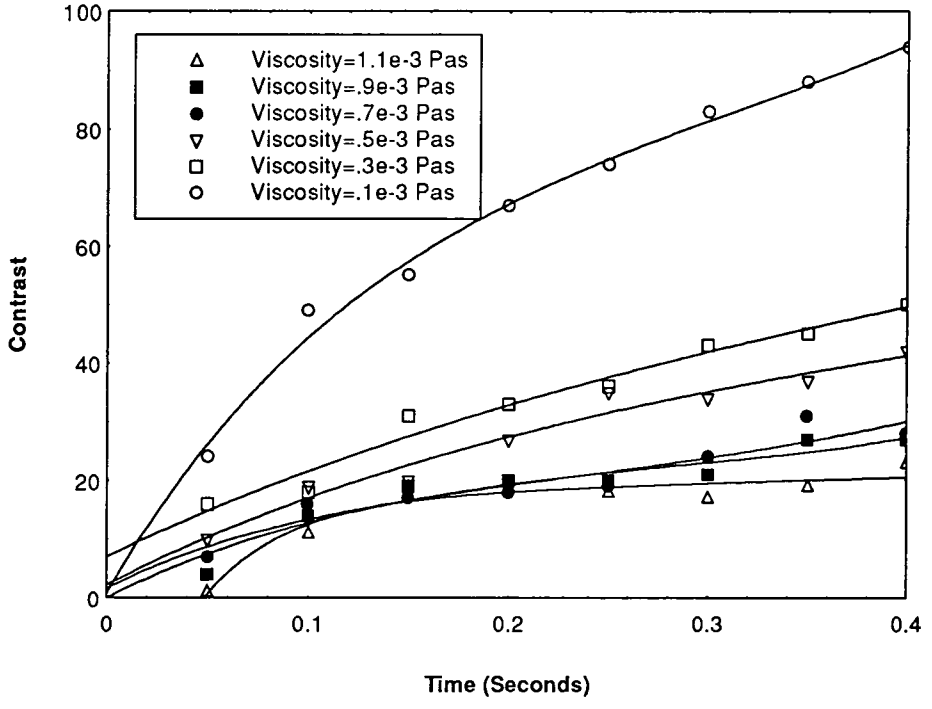

Fig.5.11a Contrast as a function of time and viscosity for particles with a 2 micron radius.

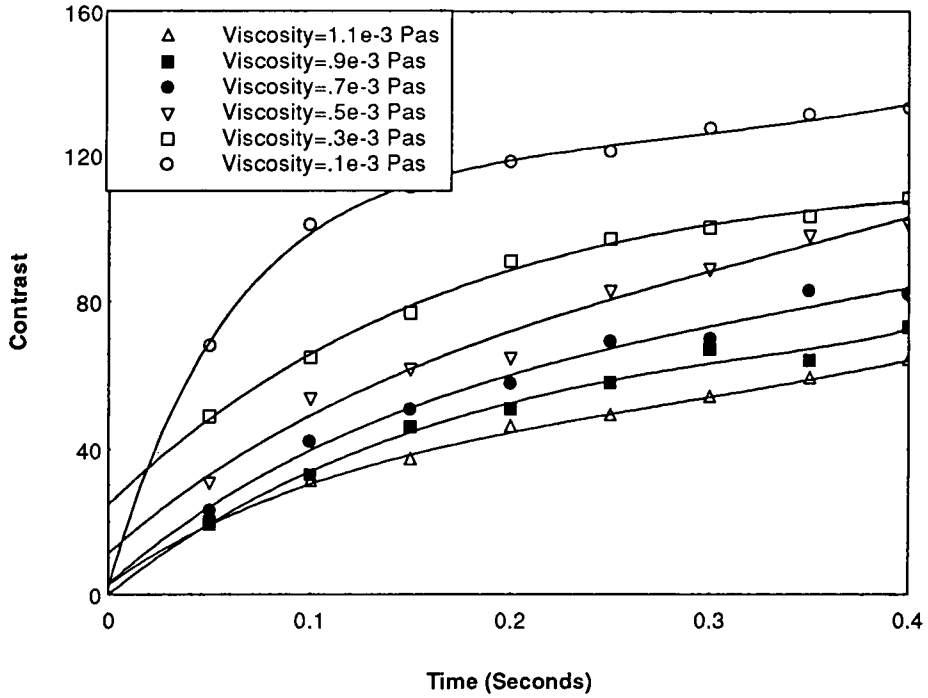

Fig.5.11b Contrast as a function of time and viscosity for particles with a 5 micron radius.

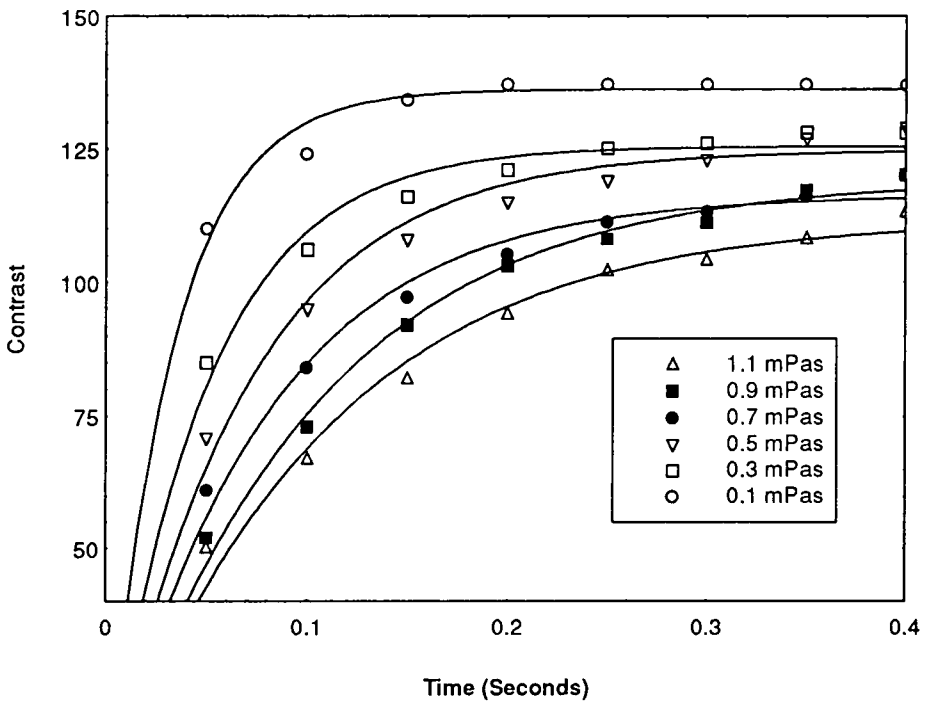

Fig.5.11c Contrast as a function of time and viscosity for particles with a 10 micron radius.

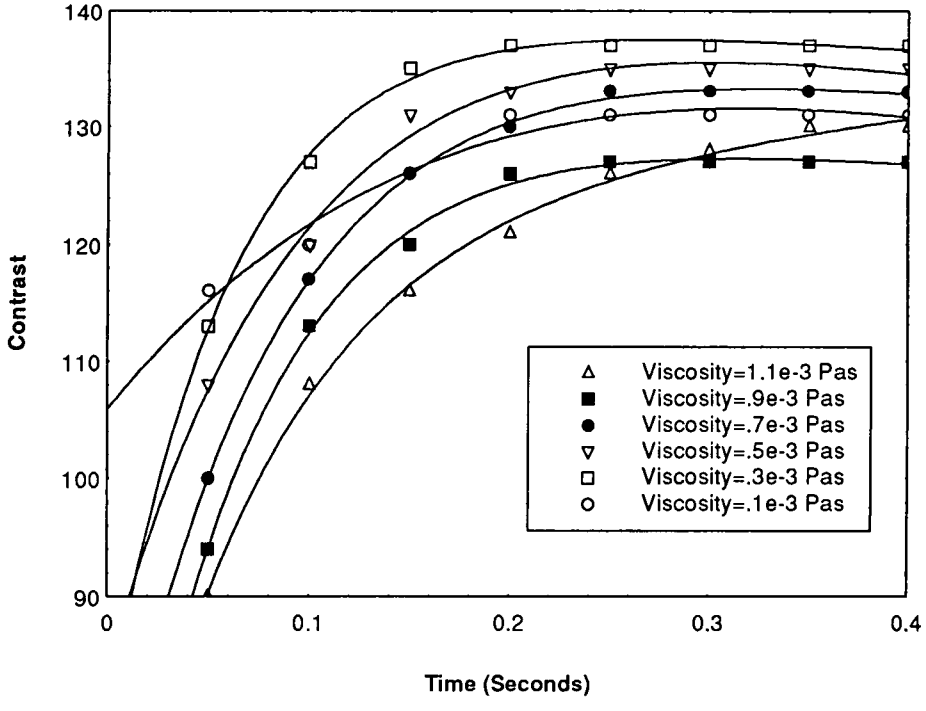

Fig.5.11d Contrast as a function of time and viscosity for particles with a 20 micron radius.

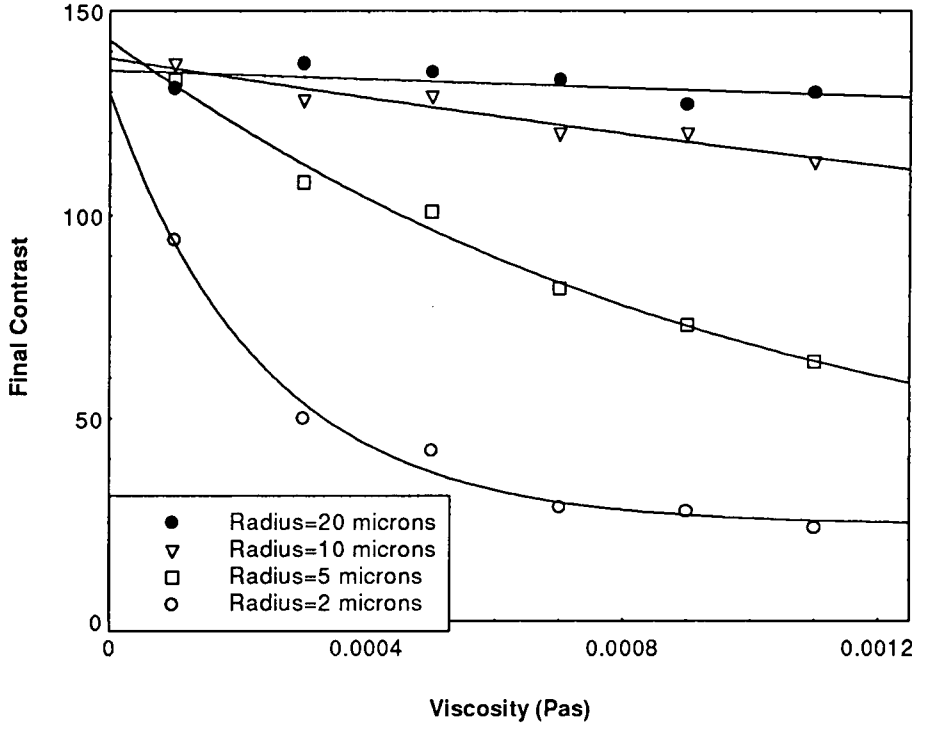

Fig.5.12 Final contrast as a function of viscosity and radius.

final contrast is plotted as a function of viscosity for the various radii Fig.5.12 is obtained. This shows that for larger particles (radius greater than 10 microns) the contrast is essentially independent of viscosity of the carrier fluid. However as the particle's radius is lowered the viscosity contribution becomes significant and the contrast falls as $(\text{viscosity})^{-1}$.This is the same result as the approximation mentioned earlier.

These results indicate that as the manufactures decrease the particle size then equal care should be taken with the viscosity of the carrier fluid to obtain a significant indication. The viscosity of the carrier fluid will also change if the temperature of the carrier fluid changes. This will occur in the inspection of boilers, etc. The manufacturers normally use water or kerosene as the carrier fluid. The viscosity of these changes rapidly as a function of temperature (water from 1.78 mPas at 0^{oc} to 0.4665 mPas at 60^{oc} and kerosene changes from 0.82 mPas at 0^{oc} to 0.403 mPas at 50^{oc}). Fig.5.12 indicates that for the larger particles, changes in viscosity do not affect the contrast. Therefore inspection can be carried out at higher temperatures without a significant change in contrast however the contrast will deteriorate at these temperatures if smaller particles are used.

These results indicate that the larger the particle the better it is at detecting cracks. However this arises from the program in that it assumes that any particle travelling over the crack will stop there. Which is not always the case as large particles will not be arrested by small cracks.

5.5 Paint Thickness

It was mentioned in an earlier chapter that a white paint layer is often applied to the surface of the specimen to increase the visibility of the indication. In this simulation the thickness of the paint layer was altered and the effect this had on contrast was recorded. The results are shown in Fig.5.13. This shows that the contrast decreases rapidly with paint layer thickness. Also shown in Fig.5.13 is the variation of B_{ox} for the crack used in the simulation. It can be seen that the contrast decreases in a similar manner to that of B_{ox}. The British Standard recommends a paint layer thickness of less than 25 microns, even at this thickness the contrast has decreased by 10 % for a half crack width of 100 microns. For narrower cracks the decrease in contrast will be greater and the increase in visibility of the particles due to the paint layer would be completely offset by the decrease in the number of particles at the crack. Fig.5.14 shows the magnetic field at the surface of a paint layer of 25 microns compared to that at the crack surface for various crack widths

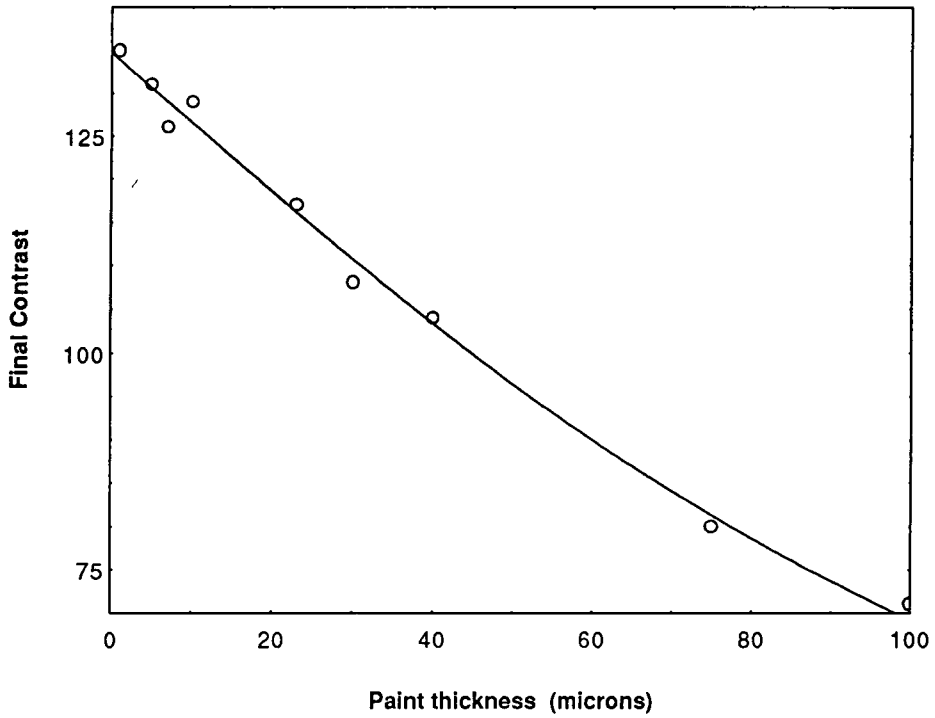

Fig.5.13 Variation of final contrast as the paint layer thickness is increased. Line is the variation of B_{ox} as the paint thickness is varied..

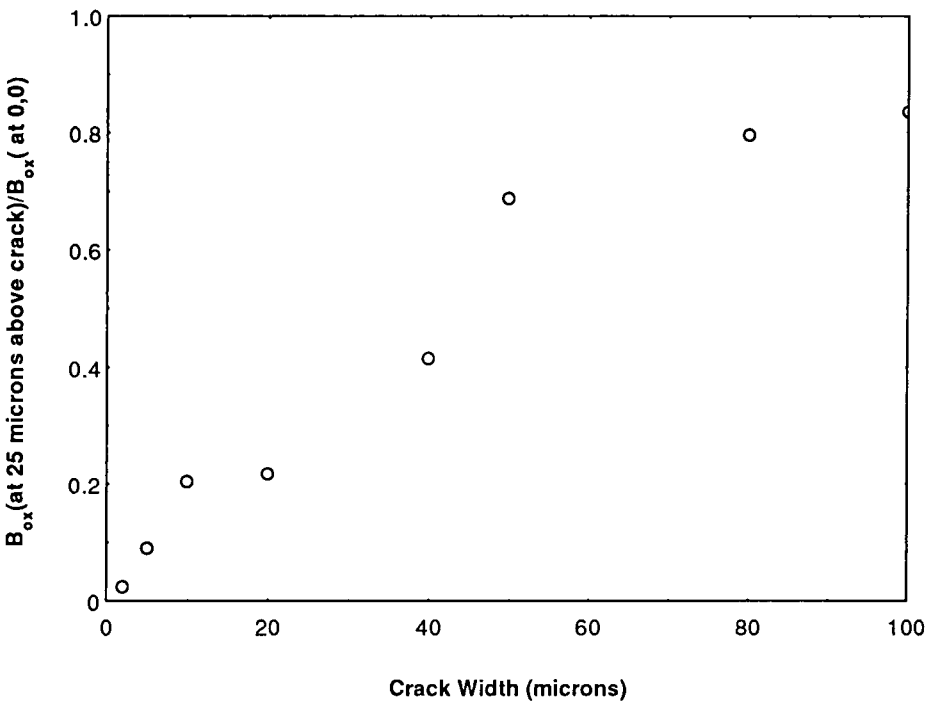

Fig.5.14 Variation of the magnetic field at a height of 25 microns compared to that a the surface for various crack width assuming a constant aspect ratio of 10.

assuming a constant crack aspect ratio of 10. This shows that for smaller cracks the chance of detecting them decreases quite rapidly when a paint layer of 25 microns is applied. In which case the MPI practitioner may be better using a fluorescent ink in which case no paint layer needs to be applied.

5.6 Particles with a Fixed Magnetic Moment

In the previous simulations the particles magnetic moment was assumed to be dependent upon the applied field via equation 5.23. In the following studies the magnetic moment of the particles was fixed at values between 100 and 5000 A/m which corresponds to a maximum of 10% of the saturation volume magnetisation of magnetite. The reason such a low value was chosen was that single domain particles agglomerate to form flux closure structures and therefore the magnetic moment of such an aggregate is going to be lower than the saturation value.

Fig.5.15a-b shows the variation in contrast as a function of time as the magnetic moment of the particles is increased and the final contrast as a function of the magnetic moment. The contrast is increased as the magnetic moment of the particles is increased as is to be expected.

5.7 Variation of Contrast with Crack Depth and Crack Width

So far the half crack width and crack depth has remained constant at 100 microns and 1 mm respectively. In this section the dependence of the contrast on crack depth and width was investigated. The results of this investigation are shown in Fig.5.16a-e which shows the contrast as a function of crack depth for various crack widths from 20-100 microns. It shows that for all the crack widths investigated as the crack depth is increased so the contrast is enhanced.

Fig.5.17 shows the variation of final contrast plotted against both the crack width and depth, it indicates that the as the crack depth and crack width increases so does the contrast associated with the crack. This is to be expected as increasing the width and depth increases both the magnetic field and the magnetic field gradient which influences the magnetic force on a particle.

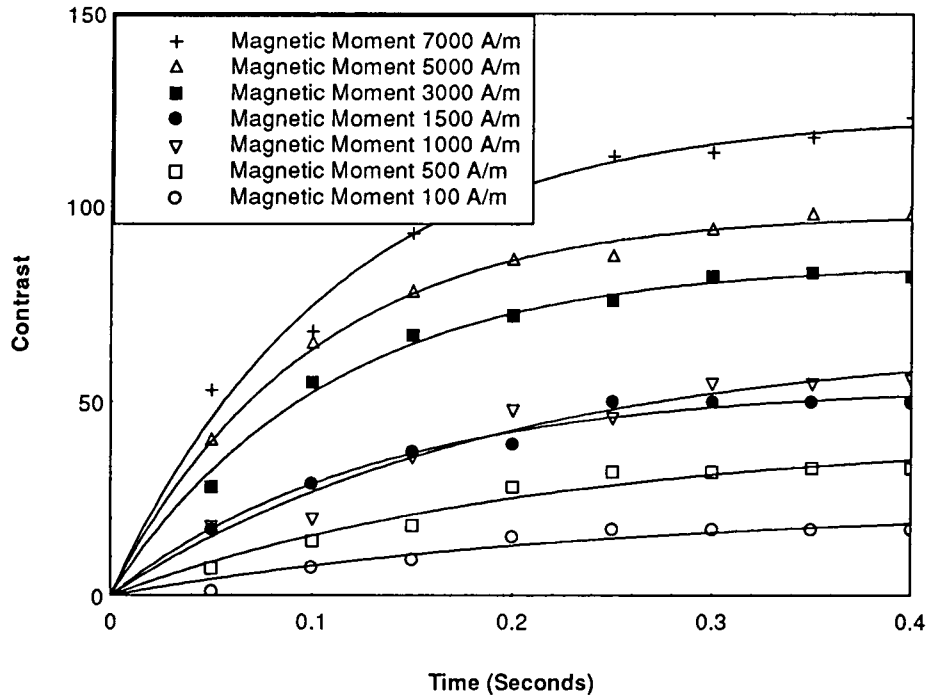

Fig.5.15a Variation of contrast as a function of time for particles with various fixed magnetic moments.

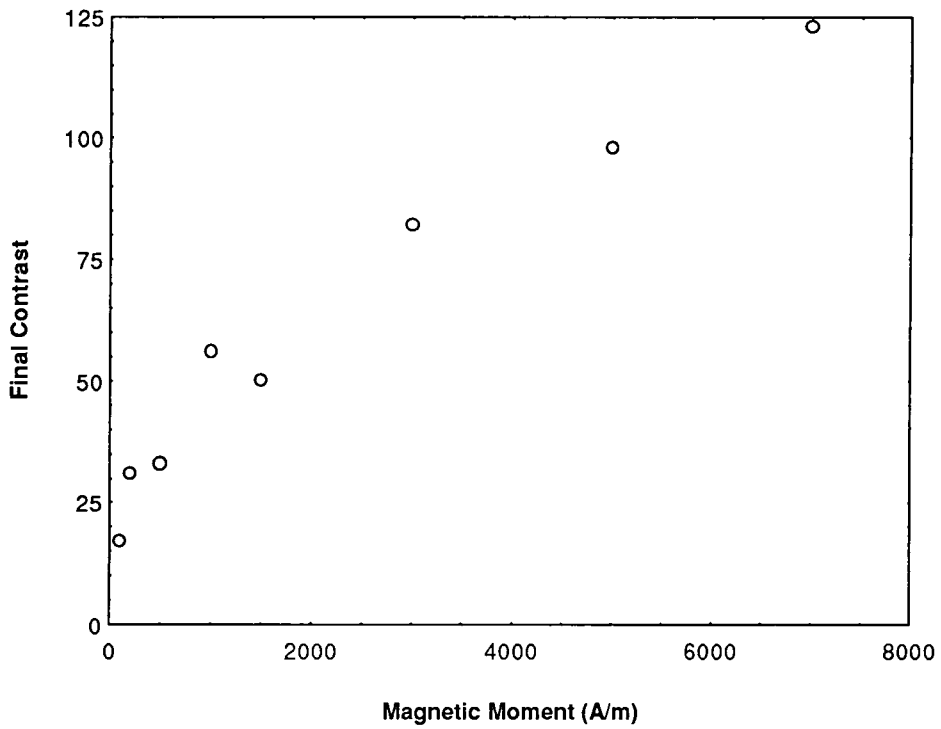

Fig.5.15b Variation of final contrast as a function of the magnetic moment of the particles.

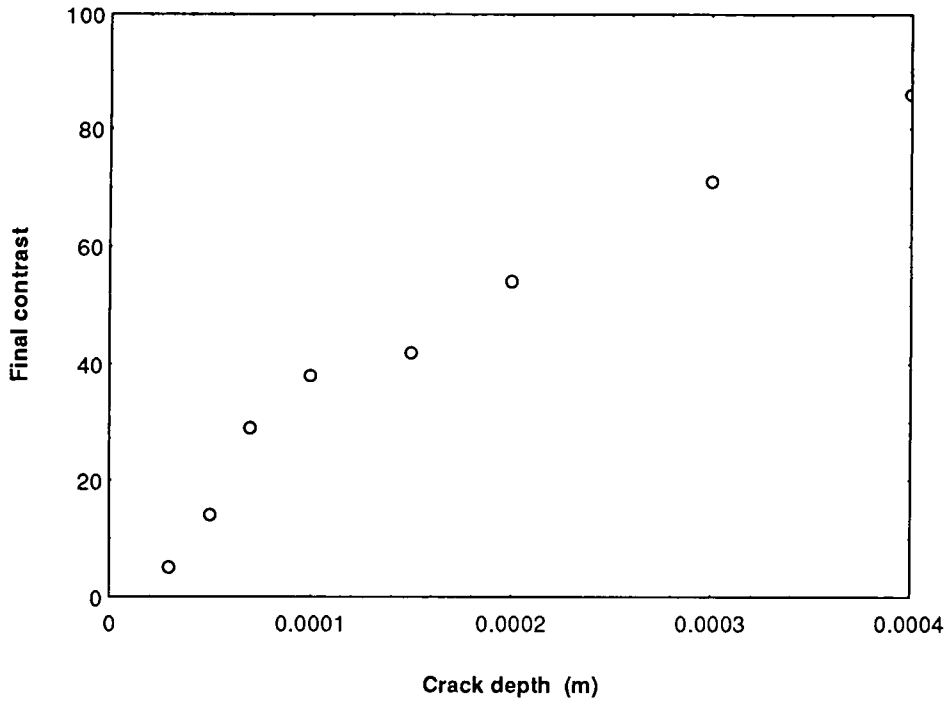

Fig.5.16a Variation of contrast as a function of crack depth, the half crack width a=20 microns.

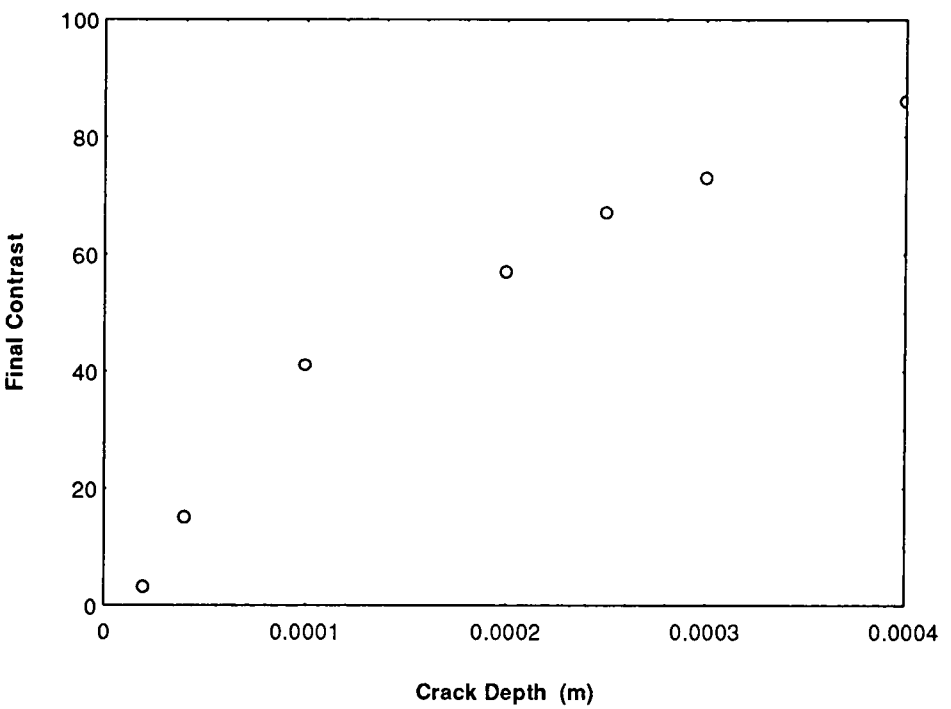

Fig.5.16b Variation of contrast as a function of crack depth, the half crack width a=40 microns.

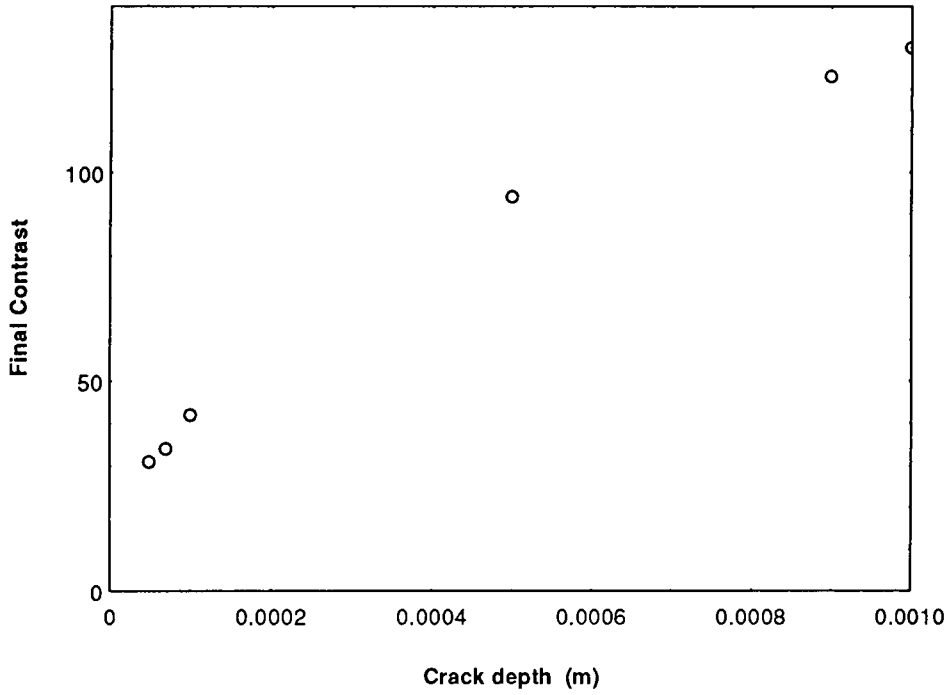

Fig.5.16c Variation of contrast as a function of crack depth, the half crack width a=50 microns.

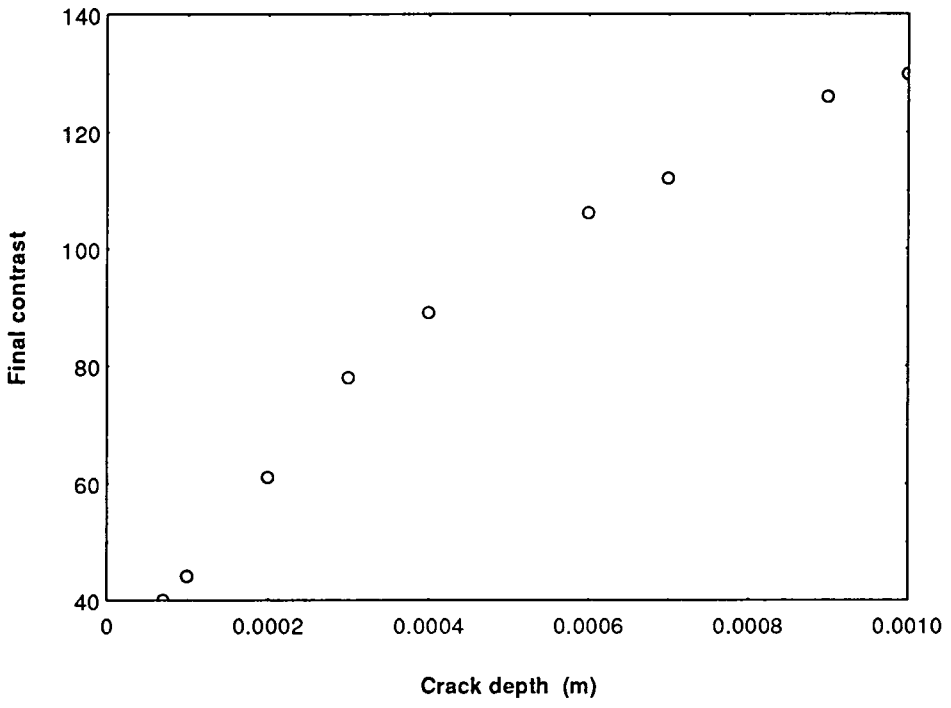

Fig.5.16d Variation of contrast as a function of crack depth, the half crack width a=70 microns.

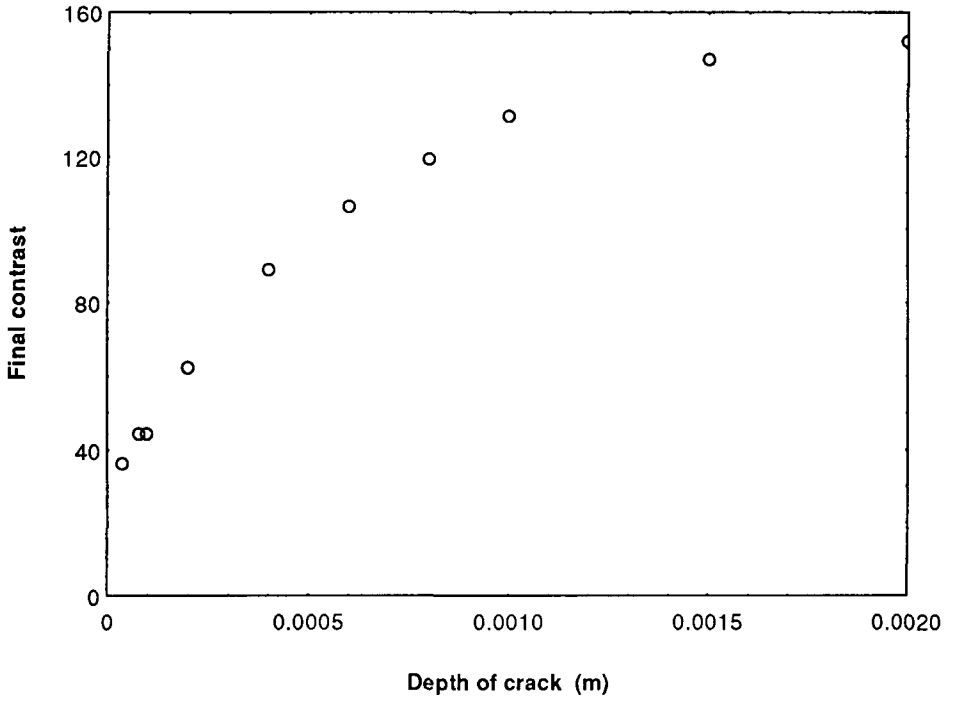

Fig.5.16e Variation of contrast as a function of crack depth, the half crack width a=40 microns.

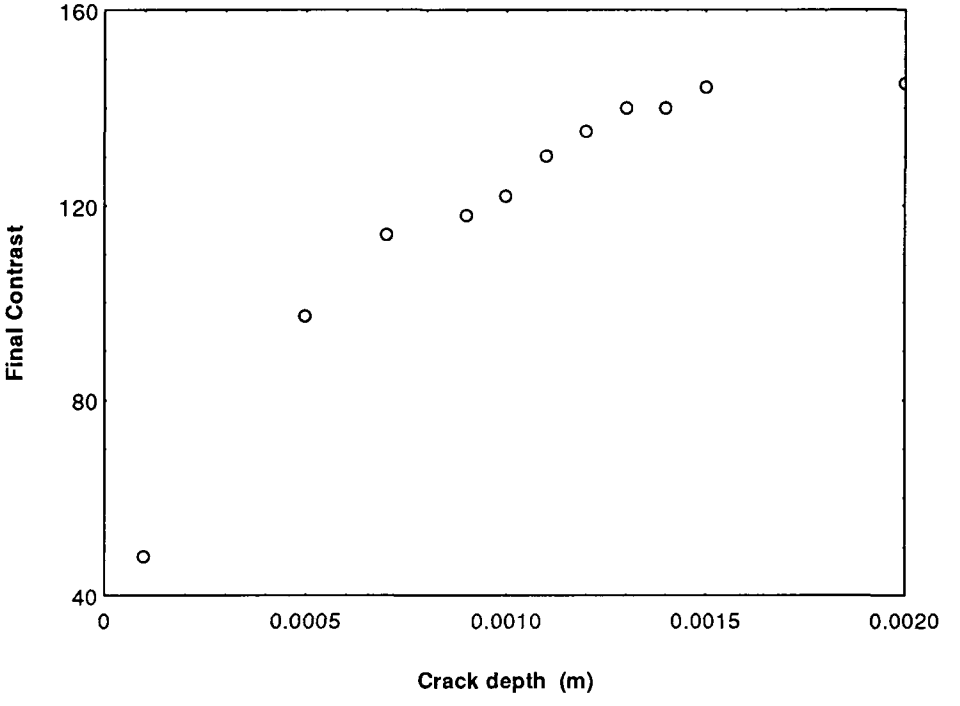

Fig.5.16f Variation of contrast as a function of crack depth, the half crack width a=40 microns.

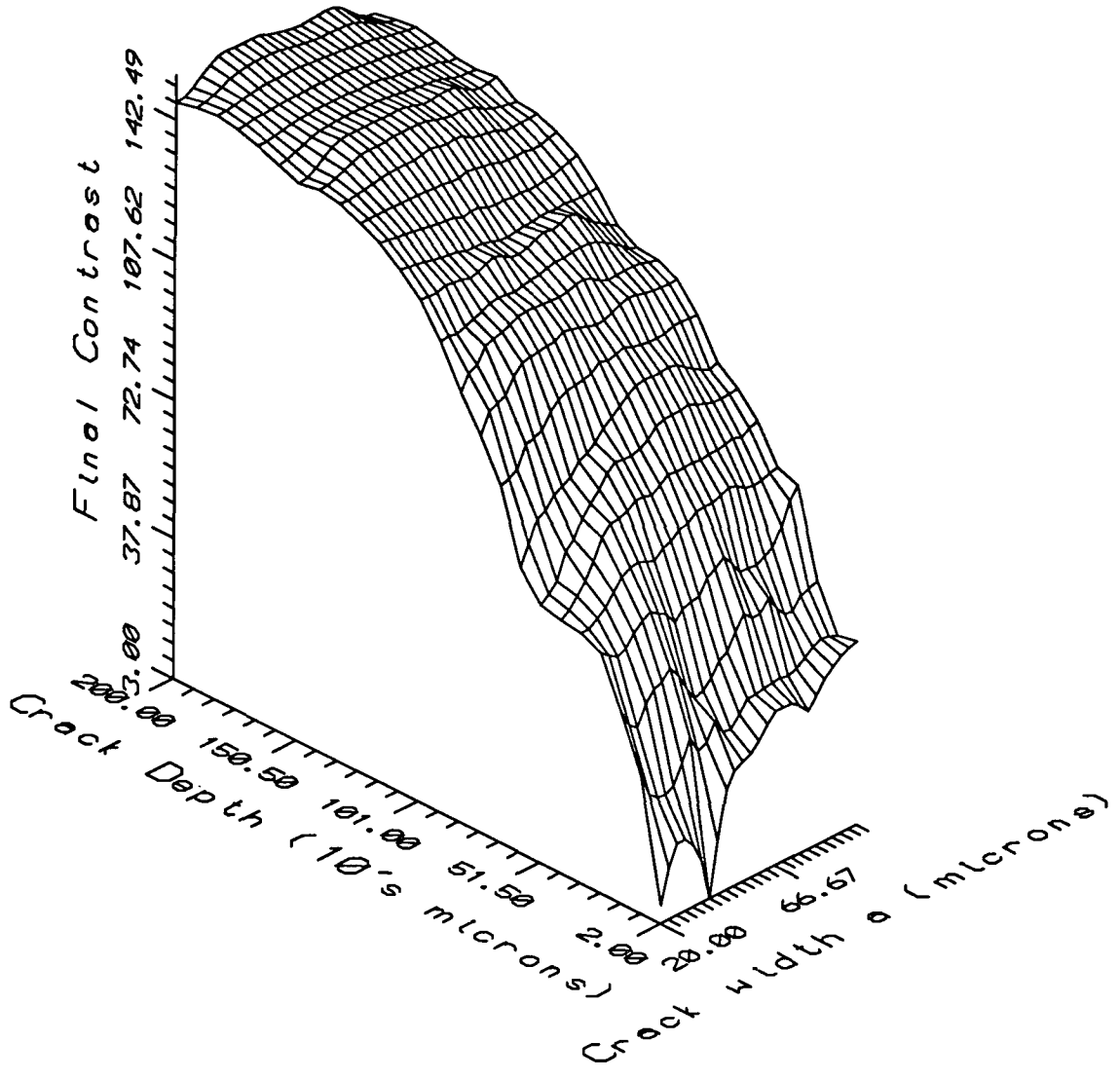

Fig.5.17 Diagram showing final contrast as a function of both crack width and crack depth

5.8 Summary

The motion of particles under the influence of a magnetic field and gradient in a viscous carrier fluid has been investigated with particular regard to the situation which occurs in magnetic particle inspection. The results from these simulations are summarised below.

The number of particles arriving at the crack is dependent upon the magnetic field was found to be linear above 500 A/m. If the magnetic field varies with time then it is the rms. value of the magnetic field which is crucial for reliable MPI. These results are valid only for low remanence steels. The experimental work of Stadhaus and MacDonald confirm these results. This is in disagreement with the recommendations of the British standards but is in agreement with the draft European standard.

Upon decreasing the particle size care must be taken with the viscosity of the carrier fluid otherwise the terminal velocity of the particles will be too low and the time taken to form an indication will be too long. These results also indicate that inspections can be carried out at elevated temperatures with no lost in contrast for the larger particles.

A layer of white contrast paint is often applied to the surface of an inspection piece to increase the contrast. By altering this paint layer thickness in the model it was found that the contrast decreased in a similar way to the variation of B_{ox} for the crack under investigation. Therefore by applying a paint layer thickness of 25 microns you are increasing the chances of detecting big cracks due to the increased contrast but decreasing the chance of detecting smaller cracks.

From the studies of the effect of crack depth and width we see that by increasing the depth of the crack we increase the contrast the same applies to the effect of crack width on contrast.

References Chapter 5

[1] Bitter, F., "On inhomogeneities in the magnetisation of ferromagnetic materials", *Phys. Rev.* ,**38** ,1903 (1931)

[2] Kittel, C., "Physical theory of ferromagnetic domains", *Rev. Mod. Phys.* ,**21** , 541-583 (1949)

[3] Kittel, C., "Theory of the formation of powder patterns on ferromagnetic crystals", *Phys. Rev.*, **76**, 1527 (1949)

[4] Watson, J.H.P., "Magnetic filtration", *J.Appl. Phys.*, **44**, 4209-4213 (1973)

[5] McCoy, J.M., and Tanner, B.K., "Computer simulation of indications in magnetic particle inspection", *J.Phys. D:Appl. Phys.*, **23**, 593-599 (1990)

[6] Roath, S., Smith, A.R., and Watson, J.H.P, "High-Gradient magnetic separation in blood and bone-marrow processing", *J. Magn. Mag. Mater.*, **85**, 285-289 (1992)

[7] Gerber, R., and Birss, R.R., "High gradient Magnetic Separation", *J.Wiley and Sons/Research Studies Press*, Chicester (1983)

[8] Takayasu, M., Gerber, R., and Friedlaender, F.J., "The collection of strongly magnetic particles in HGMS", *J.Magn. Mag. Mater.*, **40**, 204-214 (1983)

[9] Maeda, N., "Computer Simulation of Magnetic particle behaviour", *Mater. Eval.*, **51**, 290-293 (1993)

[10] Khalileev, P.A., and Alesksandrov, A.G., "Dynamics of Deposition of Ferromagnetic powder particles from suspension in air in crack detection in magnetised parts", *Defektoskopiya*, **5**, 3-28 (1989)

[11] Edwards, C., and Palmer, S.B., "The magnetic leakage field of surface breaking cracks", *J.Phys. D:Appl. Phys.*, **19**, 657-673 (1986)

[12] Gerber, R., and Watmough, M.H., "Linear superconducting OGMS system: optimum configuration and performance", *J.Phys. D: Appl. Phys.*, **22** 440-448 1989

[13] McCoy, J.M., PhD Thesis, University of Durham (1988)

[14] Stadthaus, M., Dichaut, E., and Prestel, W., "System performance in magnetic particle inspection", WCNDT, London (1987)

15 MacDonald, E., "Significance of Magnetising Current Waveform in Magnetic Particle Inspection", *University of Strathclyde 2nd Year for Nuclear Electric, Wyntheshaw*, (1993)

16 Westwood, S.M., Lewis, V.J., O'Grady, K., and Tanner, B.K., "Measurement of Interparticle Interactions in a Single Magnetic Ink Aggregate", *J. Magn. Magn. Mater.*, **125**, L247-250 (1993)

Chapter 6

Practical MPI Measurements

6.0 Introduction

In this chapter results will be presented on work more directly related to practical MPI. These include characterisation of the waveform properties of thryistor power supplies that are commonly used to magnetise specimen for use in MPI. Determining the relationship between the rms. of a waveform and the peak of a waveform is important if the MPI operator wishes to remain within the British Standards. Also included is an experimental verification of some of the simulation results presented in Chapter 5, an offshoot of this is a possible method of sizing cracks using MPI. Finally results from the viewing of MPI indications under a microscope are presented these indicate that the magnetic flux leakage from a crack changes its direction as the magnetic field is increased and also when the applied field is decreased.

6.1 Waveform Characterisation of Thyristor Controlled Power Supplies

Thyristor controlled power supplies are increasingly being used in Magnetic Particle Inspection as a convenient way of generating the large currents necessary for successful MPI. The waveform produced by a thyristor controlled power supply has been studied as a function of effective current. The manufacturers[1] of the thyristor power supply used stated that the meter on the device measured effective current upon further investigation they reported that the effective current was equivalent to the mean modulus of the current.

The relationship between the peak and rms. of a waveform is important in the practical use of MPI as the British Standards specify that the peak current is the relevant quantity to use for the calculation of magnetic field intensity. However as most meters measure either rms. or mean current there is a need to know the relationship between these two to be able to calculate the magnetic field intensity as per British Standard. At present there is much debate about the relevant property of the waveform as Stadthaus[2] has presented results for low remanence steels which indicate that the rms. value is the pertinent property. Work by MacDonald [3] on the current necessary to bring up an indication agree with Stadthaus results for low remanent steels but for high remanent steel no conclusion

could be made. In addition McCoy's[4] model which uses Edwards and Palmer's[5] equations for flux leakage indicates that the average magnetic force on the particle and hence the indication mechanism is an average of the applied field. The exact average is dependent on the magnetic properties of the particle.

In Thyristor controlled power supplies the relationship between peak and rms. is not obvious and depends on the detailed shape of the waveform. Consequently it was decided to investigate this dependence. Experiments were performed using a thyristor controlled power supply and measurements were made for effective currents from 50 to 900 Amps.

6.1.1 Experimental Method

The Power supply was a Tiede 1400 Ferrotest unit used for prod magnetisation of a flat steel plate using prods of 15cm in length and a prod spacing of 186mm. The output voltage across the prods when under load was fed into a digital storage oscilloscope. Then the mean, rms. and peak height as well as the Fourier components of the waveform were measured from the stored digital data. The mean in this case is defined as the mean modulus of the waveform.

6.1.2 Results

Fig.6.1 and Fig.6.2 shows the waveform produced at an effective current of 250 and 900 Amps. Clearly the shapes of these waveforms are radically different. At 900 Amps the waveform is almost sinusoidal whereas at 250 Amps the waveform consists of non sinusoidal short pulses. It is obvious that there is no simple relationship between peak height and rms.

The variation of the amplitude of the Fourier components of the waveform as a function of effective current is shown in Fig.6.3. This shows that as the current is increased the amplitude of the Fourier components of the frequencies close to 50 Hz increase while the higher frequencies decrease. This is a consequence of a chopped waveform with an increasing 'on' period. The variation of measured rms. and mean from the waveform were plotted against effective current and are shown in Fig. 6.4. Both of these reveal a linear dependence. This shows that the meter could indeed be measuring the mean. There is a slight offset on both these curves at zero current.

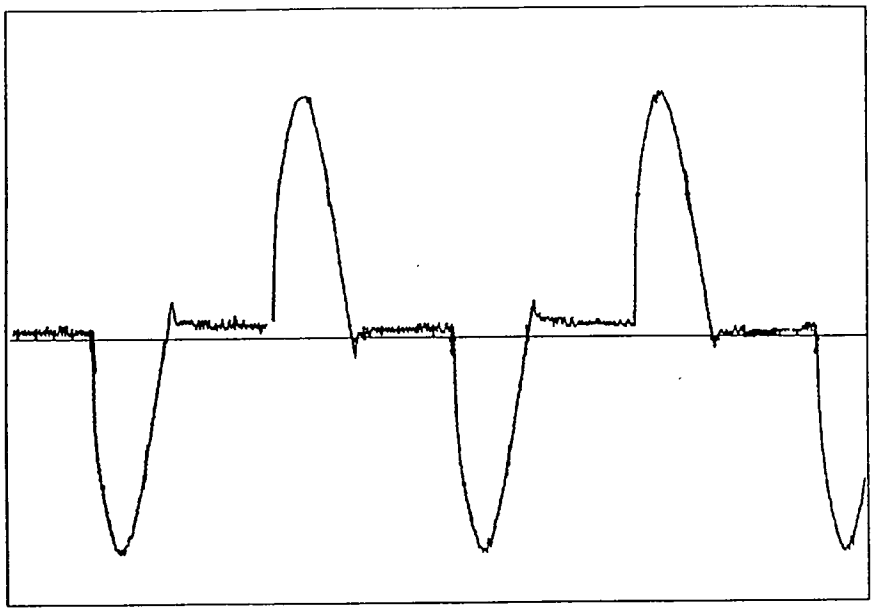

Fig.6.1 Waveform at an effective current of 250 Amps

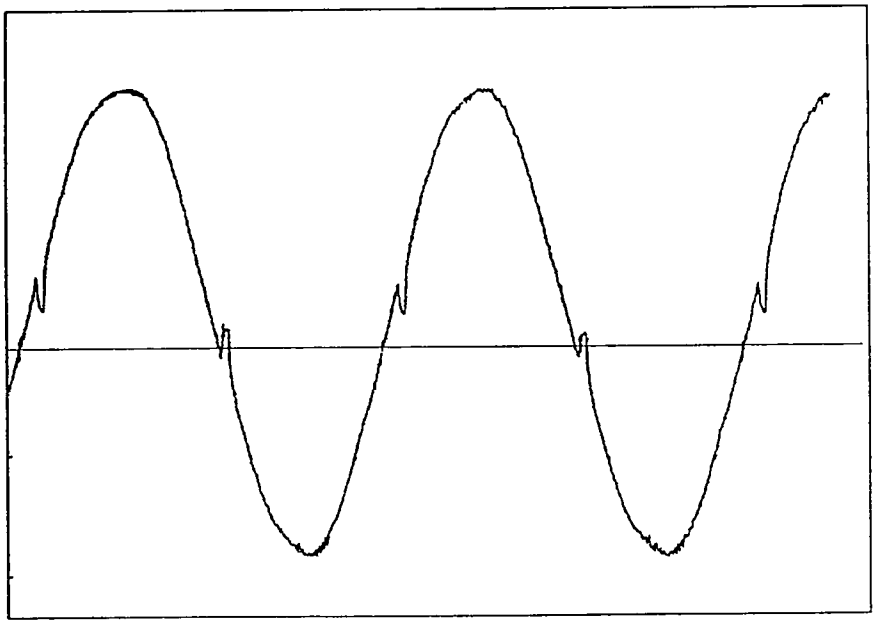

Fig.6.2 Waveform at an effective current of 900 Amps

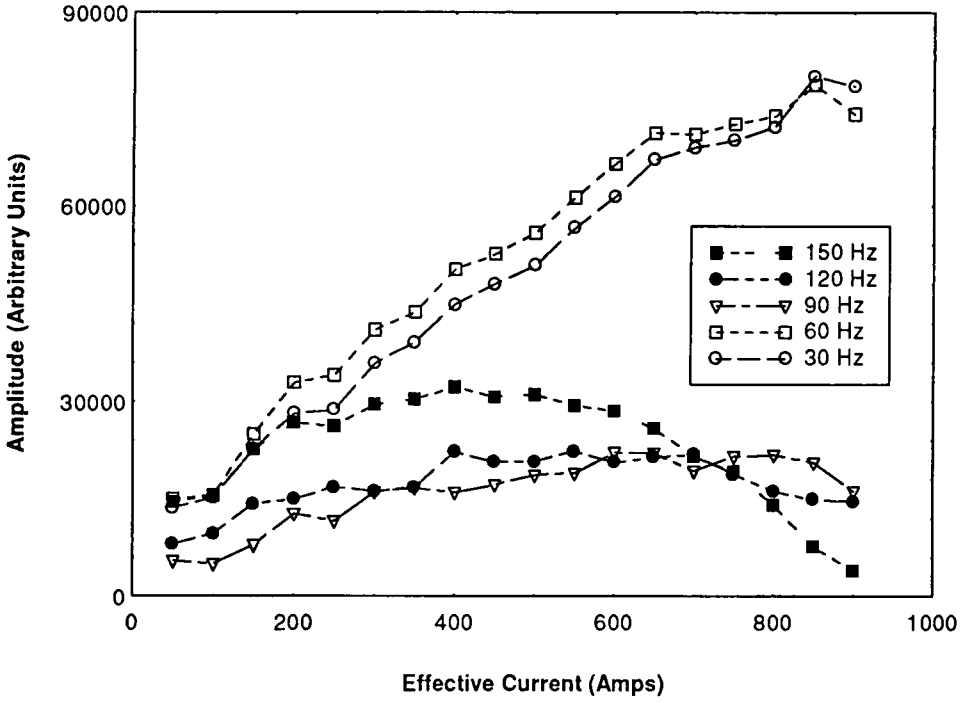

Fig.6.3 Variation in the amplitude of various frequencies as a function of effective current.

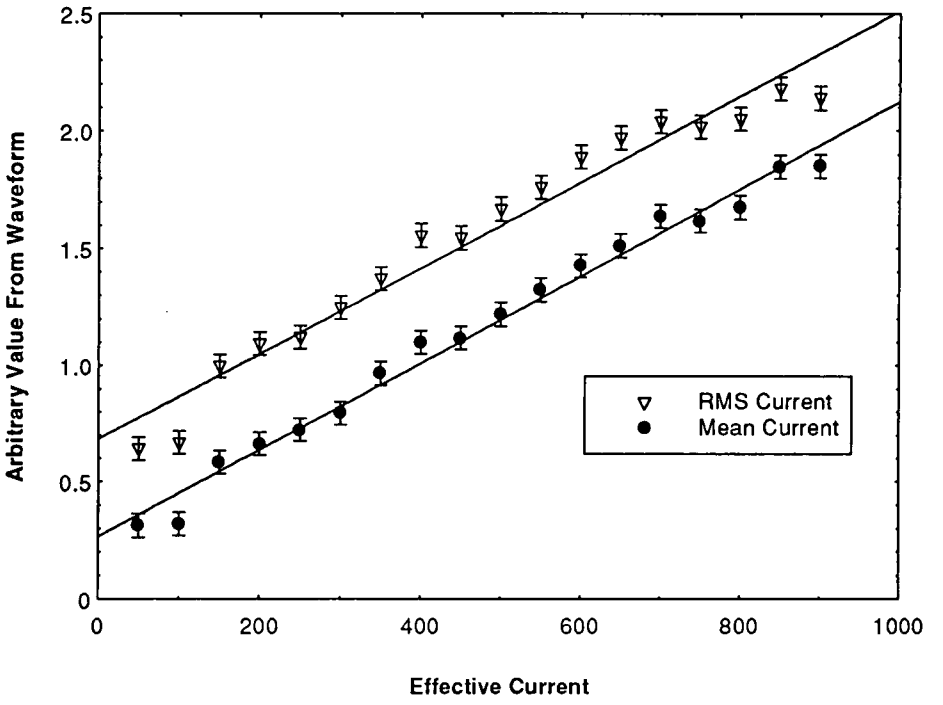

Fig.6.4 Variation of the mean and rms. of a thyristor waveform as a function of effective current.

There is a discrepancy between the size of the negative peak and the positive peak for all currents. This is due to there being a slight DC level produced by the power supply. Both peak heights saturate at a maximum value and remain relatively fixed regardless of any change in effective current. The variation of both peak heights with effective current is shown in Fig.6.5. BS 6072 supplies linear conversion factors between peak height and rms. for various waveforms but this does not supply one for thyristor controlled devices.

The variation of the measured peak height and rms. is compared with other waveforms using the formula quoted BS 6072 in Fig.6.6. Yet again this shows quite clearly the non linear dependence of rms. and peak height for thyristor controlled devices this is because the shape of the waveform is changing. However the other power supplies with AC or rectified AC waveforms have a linear dependence.

6.1.3 Implication for MPI

Thyristor controlled devices produce waveforms which vary dramatically as a function of the current being supplied for a constant load. The peak height rapidly saturates while the rms. and mean increases steadily due to the fact the by increasing the effective current the power supply has a longer on period and therefore the mean and rms. increase. Therefore when using thyristor controlled power supplies special calibration procedures may be necessary to comply with BS 6072. However thyristor power supplies will conform to the new European Standard.

6.2 Variation of Indication Width with Paint Thickness in a Fixed Magnetic Field

In practical MPI a paint layer is often applied to increase the visibility of the particles. This paint layer also affects the magnetic leakage field the particles experience by altering the distance between the particle and the crack. Consequently if too much paint is applied the indication no longer becomes visible. In this study the width of the indication was measured as a function of paint thickness for various cracks.

The experimental set-up used was as follows. The test specimens (30 cm length, 8 cm width and 1 cm height) with machined cracks in them, had a layer of white paint applied to the surface. This paint layer was measured using a Elecometer[6] 145 which uses an eddy current method to measure the paint thickness. The test specimen was placed in a set of

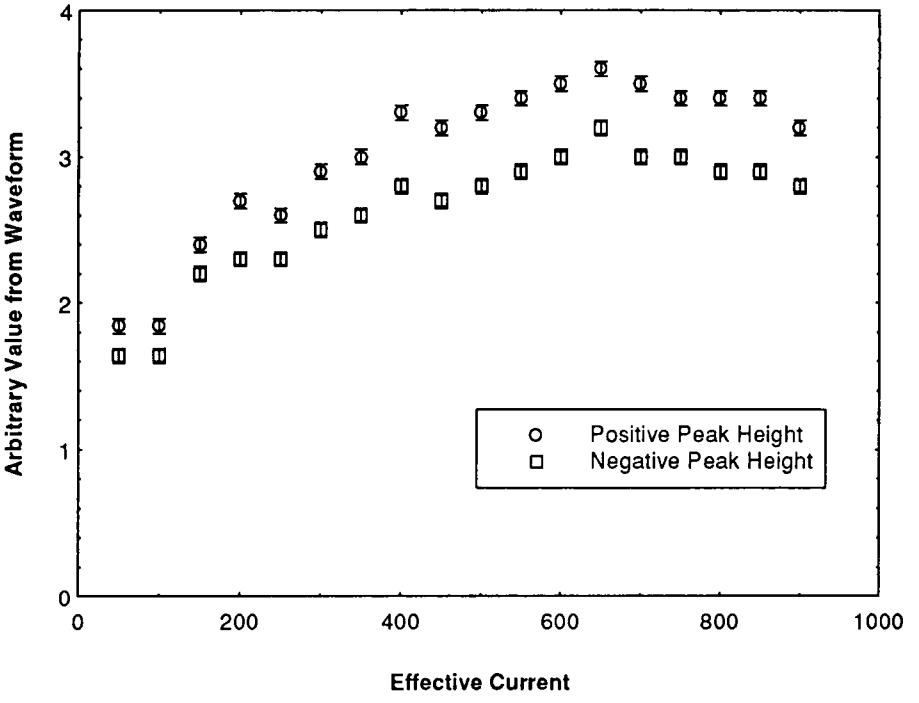

Fig.6.5 Variation of Peak height with effective current.

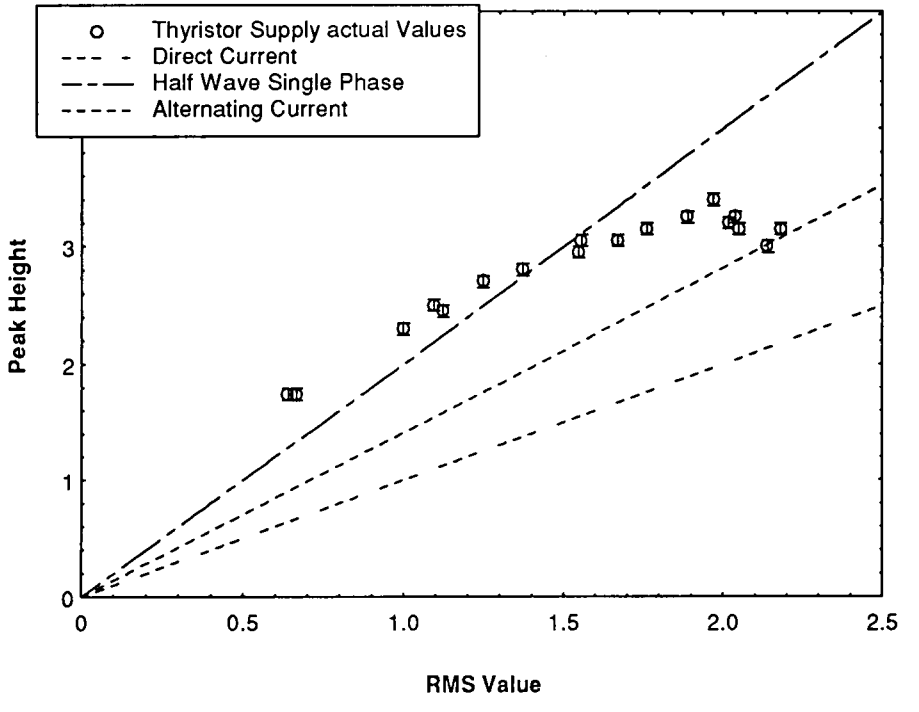

Fig.6.6 RMS versus Peak height for various waveforms

rectangular coils which could generate a magnetic field up to 3000 A/m. It was then placed on a microscope stage and a magnetic field applied using the coils. While the field was applied a black magnetic ink was sprayed onto the surface. The particles agglomerate at the crack and the width of the indication formed was measured. The specimen was then cleaned and a different paint layer was applied. Then the process was repeated.

6.2.1 Experimental Results

The results of this study are shown in Fig.6.7a-b. Each measurement of the indication width was the average of 50 readings. It can be seen that the indication width as a function of paint thickness has a definite dip. During the experiments it was noted that the density of the particles was decreasing at the crack as the paint thickness was increasing but this had little effect on the indication width. Computer simulations have been run in an effort to replicate this dip in indication width with no success. However in the computer model the number of particles at the crack decreases with increasing paint thickness as was observed above. This effect is mentioned in the next section.

6.3 Experimental Verification of the Simulation Results

In the previous chapter results were presented from a computer simulation of the indication mechanism in MPI in which a wide variety of parameters could be varied. However very little experimental work has been reported to verify the results of the model. McCoy[7] presented data on the velocity of magnetic ink particles in a magnetic field and gradient. He found a linear dependence between the (particle volume/Stokes radius) and velocity. This is one of the predictions from the model. The particles however moved slower than predicted by the model. This was attributed to the problems of calculating the particle magnetisation, the presence of voids and the problems of assigning a Stokes radius to a non-spherical particle. It does also explain why in the simulation the indication is complete in 0.4 second but in practical MPI the indication can take a few seconds to form. The motivation behind this research was to provide a more realistic test of the model.

6.3.1 Variation of Contrast with a Variable Magnetic Field

If the magnetic field varies over the crack length and an ink is applied to the surface the particles will delineate the crack. The particle density will then vary over the length of the crack due to the variation in the magnetic field and field gradient. The indication length r

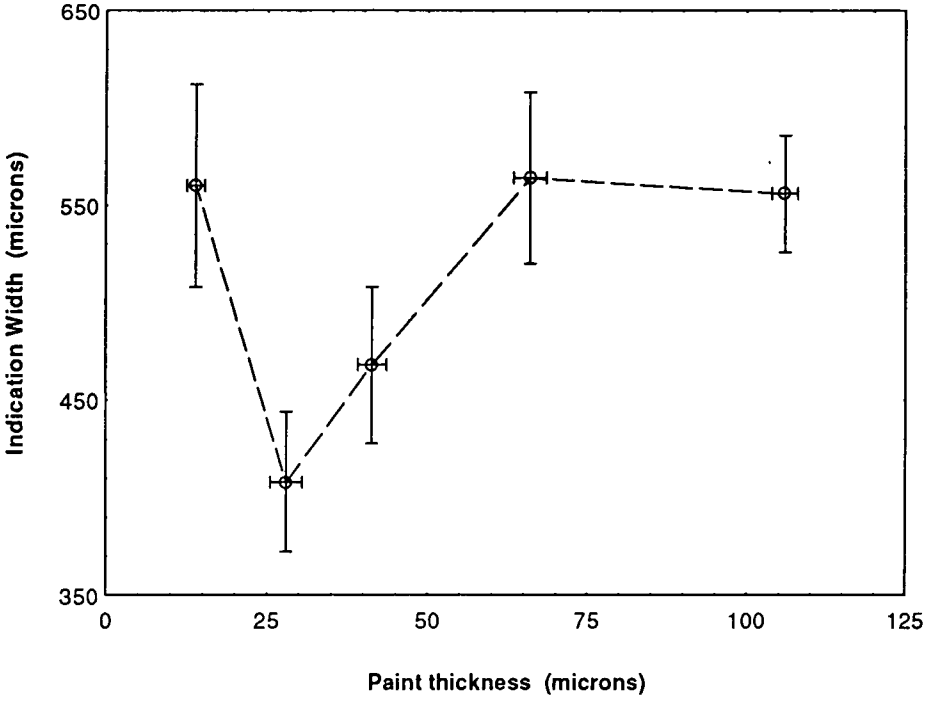

Fig.6.7a Variation of Indication width with paint thickness for test piece B.

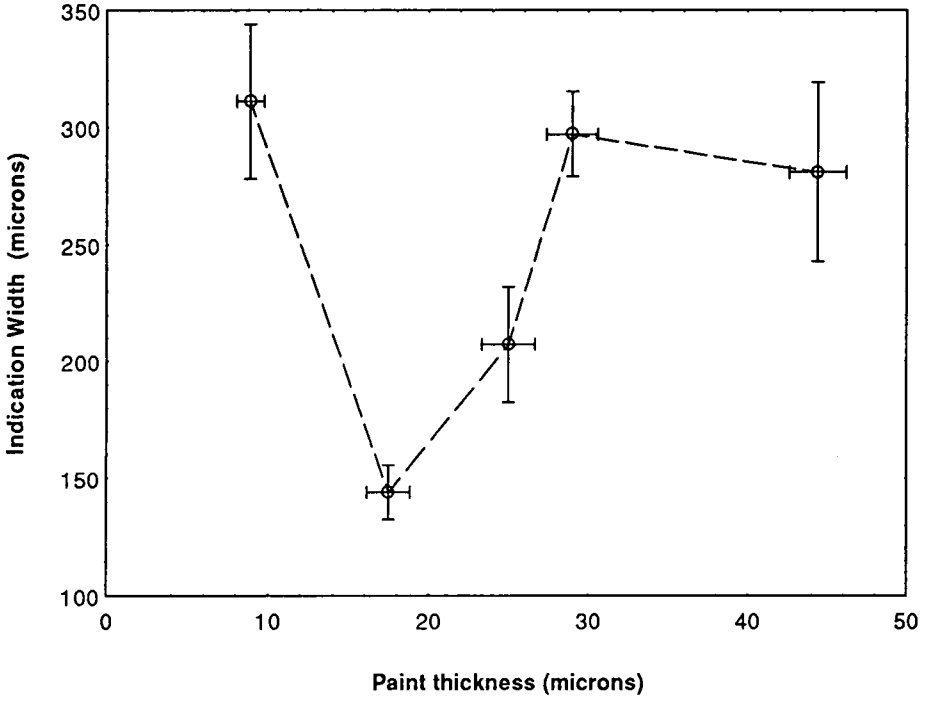

Fig.6.7b Variation of Indication width with paint thickness for test piece C.

is defined as the length at which the indication stops being visible along the crack length to the operators eye. This indication length r is determined by the number of particles present and therefore is related to the value of the contrast from the computer simulation. The exact relationship between the two is given in the next section.

To achieve a variable magnetic field along the length of the crack the test blocks shown in Fig.6.8 are used. These are the Fluxa[8] test block more commonly used to give qualitative measurements between different magnetic inks, and consist of two iron blocks bolted together with a magnet at one end. The magnetic field varies over its length and the indication length r can be read off the ruler. The second test piece is a normal test block with a horseshoe magnet with the crack at the centre of it. The indication length is measured along the crack. A layer of paint is applied to the surface and the paint thickness is measured using the Elecometer. Then the ink is applied to the surface and the length of the indication formed measured. Then the process was repeated.

6.3.2 Simulation Results

In chapter 5 it was stated that the dependence of contrast with paint thickness y has the same functional dependence as the variation of B_{ox}. However when the applied magnetic field $H_o(r)$ varies over the crack length r, then the contrast C is given by:

$$C = K_1 H_o(r)\left(\tan^{-1}\frac{ba}{a^2 + y(y+b)}\right) \qquad 6.1$$

Assuming permeability and crack aspect ratio remain constant. This assumes a linear dependence between the applied magnetic field and contrast which was seen to be the case in Chapter 5 if the applied magnetic field was greater than 500 A/m. By defining a critical contrast C^+ as the number of particles necessary for the operator to see an indication, occurring at an indication length r. Therefore the indication length and the critical contrast are related by:

$$C^+ = K_1 H_o(r)\left(\tan^{-1}\frac{ba}{a^2 + y(y+b)}\right) \qquad 6.2$$

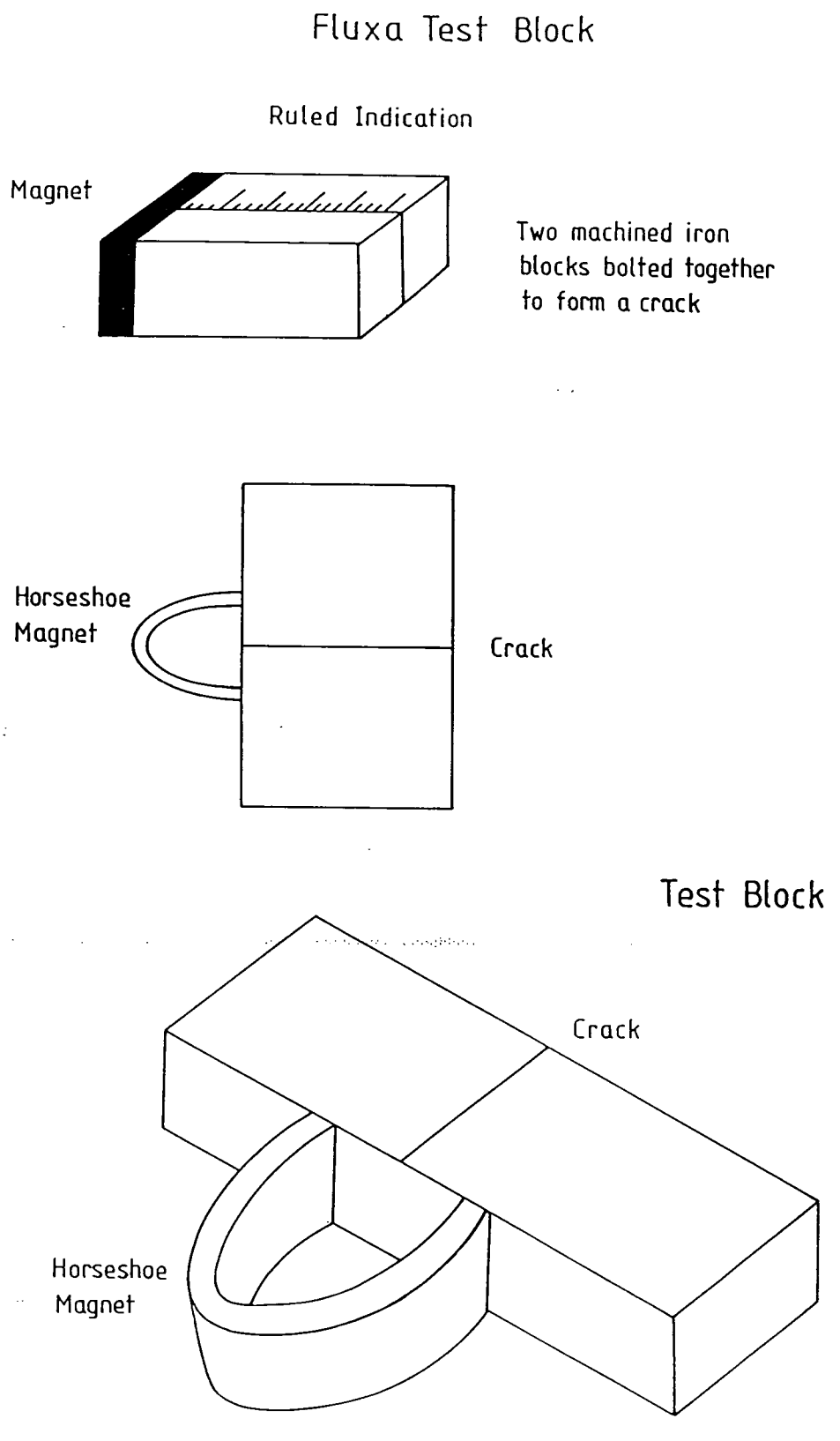

Fig.6.8 Test blocks used to achieve a variable magnetic field along the crack length.

where K_1 is a constant. So if $H_O(r)$ is known and r is measured as a function of paint thickness y then the crack width and depth can be determined. To determine the half crack width a and crack depth b we define the Indication Power P as:

$$P = \frac{C^+}{H_o(r)} = K_1\left(\tan^{-1}\frac{ab}{a^2 + y(y+b)}\right) \qquad 6.3$$

so the variation in indication power as a function of paint thickness should follow equation 6.3. Therefore from the experimental data information about the crack can be determined.

6.3.3 Experimental Results

Measurements were performed on the fluxa test piece twice and on two separate test blocks using the horseshoe magnet. The variation in magnetic field along the specimens is shown in Fig.6.9a-b. Magnetic field measurements were performed using a Group 3 Hall Probe fitted to an x-y micrometer stage. The magnetic field was found to decay exponentially for both test blocks, the best fits being for the fluxa test piece:

$$H_o(r) = C\exp(Br) \qquad 6.4$$

$$C = 284 \pm 44\ A/m$$
$$B = -0.376 \pm 0.028\ mm^{-1}$$

It would seem that the applied magnetic field for the fluxa test block is less than 500 A/m. However the magnetic fields measured in this section were measured with a Hall Probe and the active element was situated 2mm from its edge. Therefore the magnetic field measured with the Hall probe is less than the magnetic field at the surface. From the variation with magnetic field as a function of height above the fluxa test block we can extrapolate back and determine the magnetic field at the surface. This was found to be greater than 500 A/m for all indication lengths. This applies equally to the measurements performed with the horseshoe magnet.

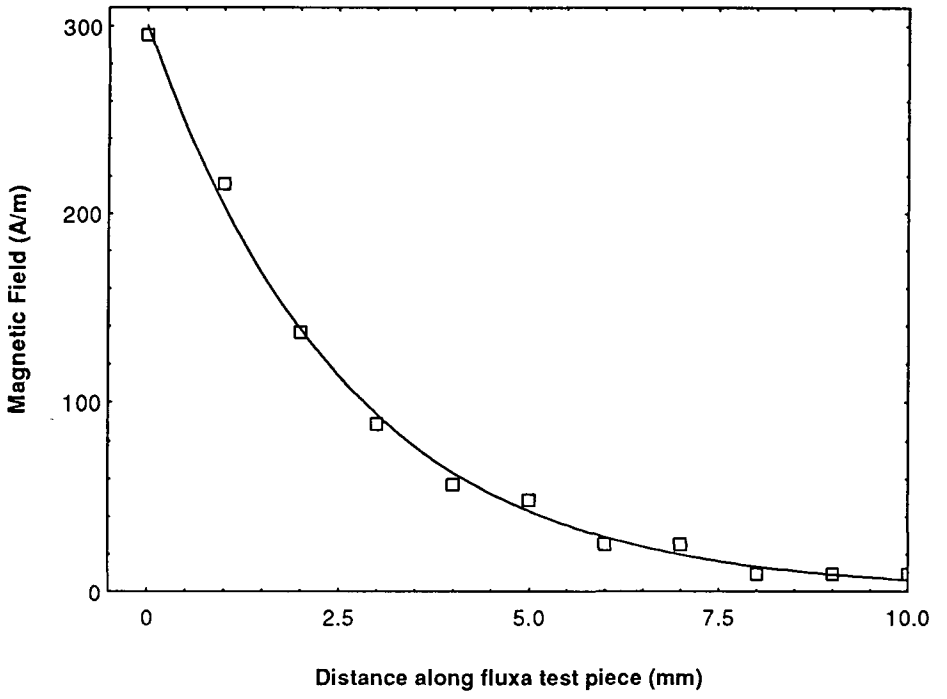

Fig.6.9a Magnetic field variation along the fluxa test piece.

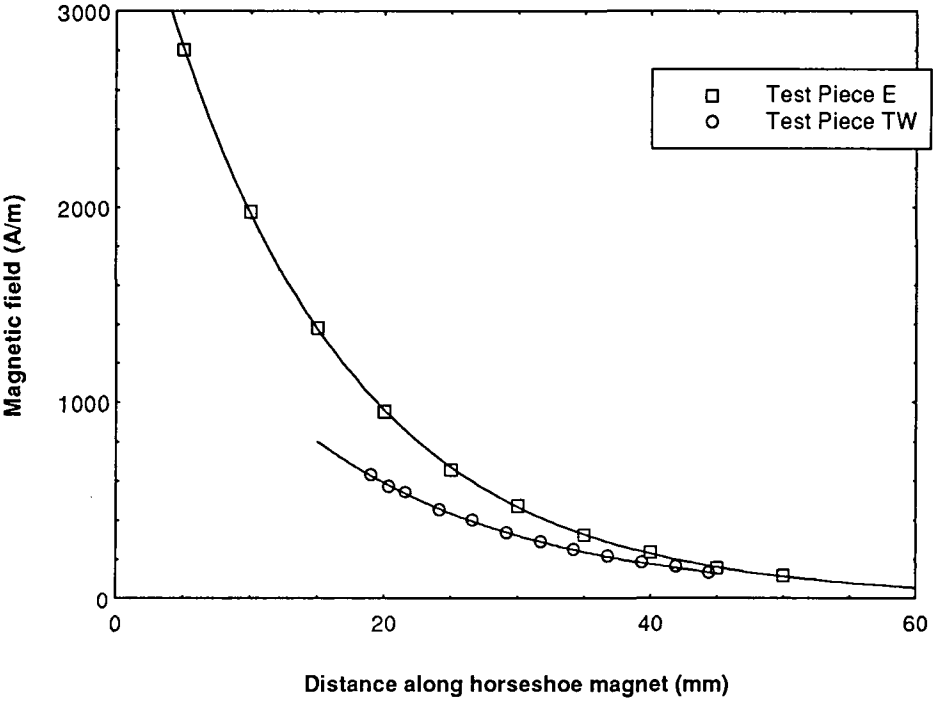

Fig.6.9b Magnetic field variation for the two test pieces using the horseshoe magnet

For the horseshoe magnet on the two separate test pieces the variation of magnetic field was found to be:

$$H_o(r) = C\exp(Br) \qquad 6.5$$

$C = 1998 \pm 40 A/m$	$C = 3983 \pm 164\ A/m$
$B = -0.0608 \pm .0006\ mm^{-1}$	$B = -0.0716 \pm .001\ mm^{-1}$
Test piece TW	Test piece E

The variation in indication length with respect to paint thickness for the fluxa test block is shown in Fig6.10a-b and in Fig.6.11a-b for the two other test specimens. These show a decrease in indication length with increasing paint thickness. Taking the variation in magnetic field into account for all the test pieces, we can then plot the Indication Power as a function of paint thickness. This is shown in Fig6.12a-b for the fluxa test piece and Fig6.13a-b for the two other test pieces. Also shown are fits using equation 6.3.

Table 6.1 shows the values of the crack depth and width for all the cracks calculated using equation 6.3 along with optical microscopy measurements of the crack width only as optical microscopy can not determine the crack depth. Optical microscopy is not always possible on the specimen used in MPI due to the surface finish on some of the specimens. The correlation between the optical microscopy measurement of crack width and the crack width measured using the above measurement is reasonable. The values of crack depth derived using equation 6.3 are not reliable because the fit is very insensitive to changes in b assuming $b \gg a$ which is normally the case.

When considering the satisfactory agreement between the crack width measured optically and those measured by this technique it is instructive to consider the possible sources of error on the measurement and the assumptions used in deriving equation 6.3. There are errors in the measurement of paint thickness, in the variation of the applied field along the crack length and in the measurement of the indication length. Assumptions used are that the aspect ratio remains constant and that the permeability does not change with applied field and the contrast is a linear function of applied magnetic field.

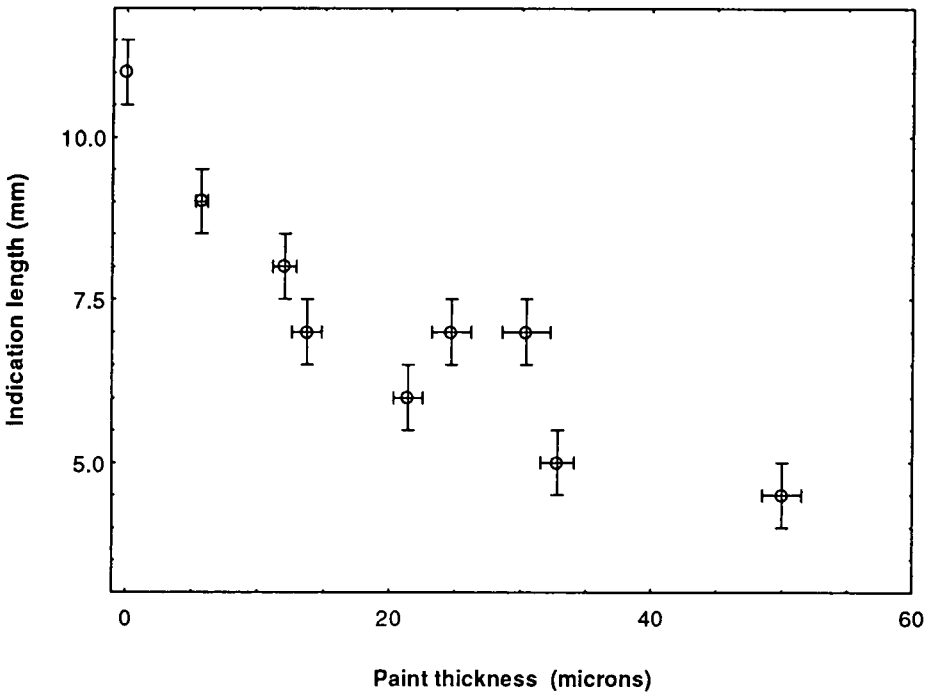

Fig.6.10a Indication length as the paint thickness is varied for the fluxa test piece.

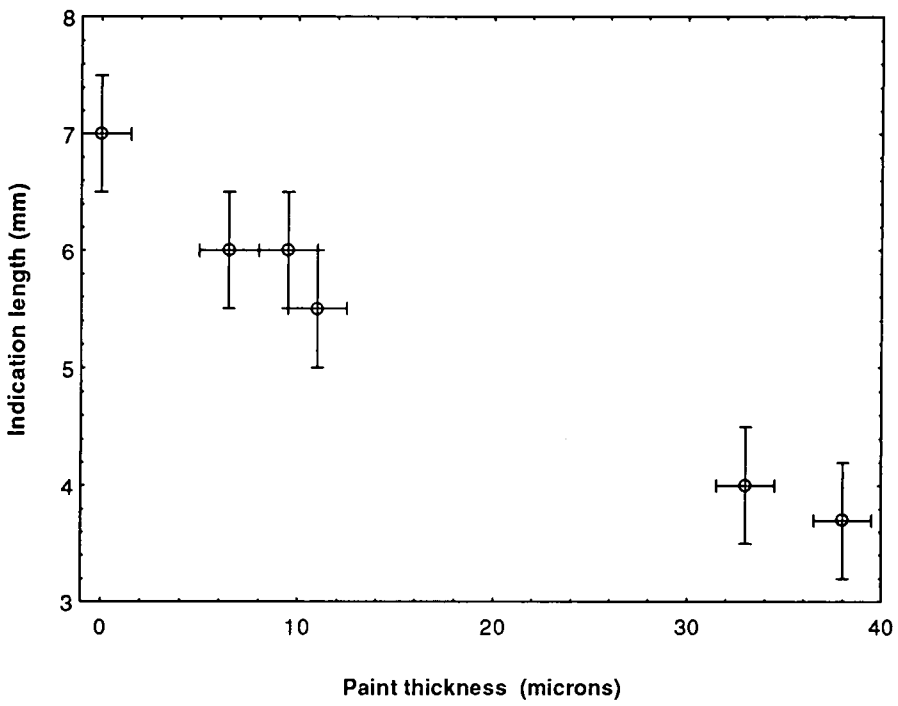

Fig.6.10b Indication length as paint thickness is varied for fluxa test piece.

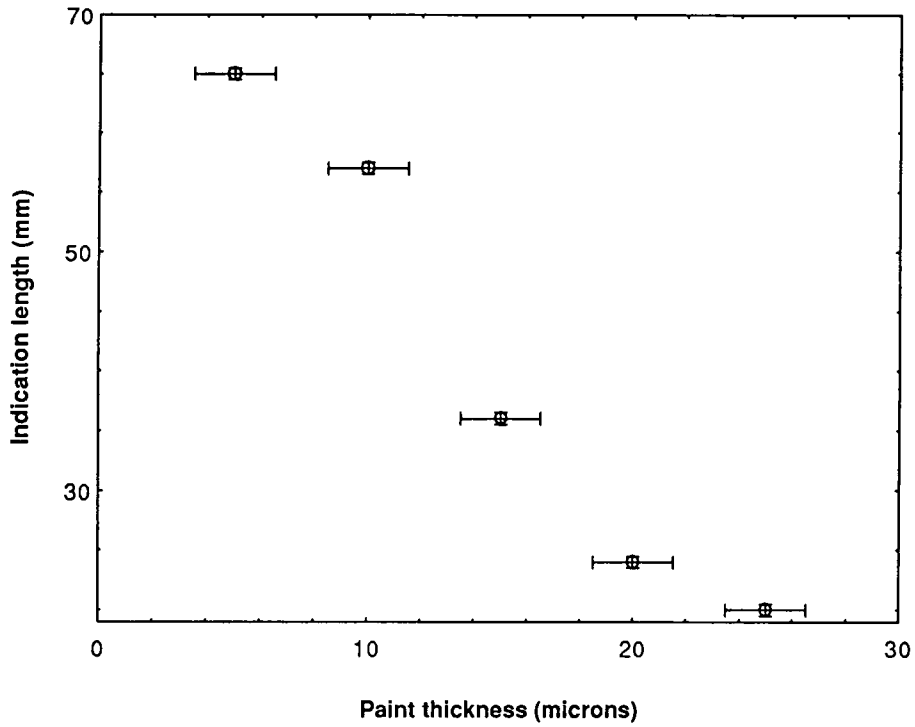

Fig.6.11a Indication length as paint thickness is varied for test piece E.

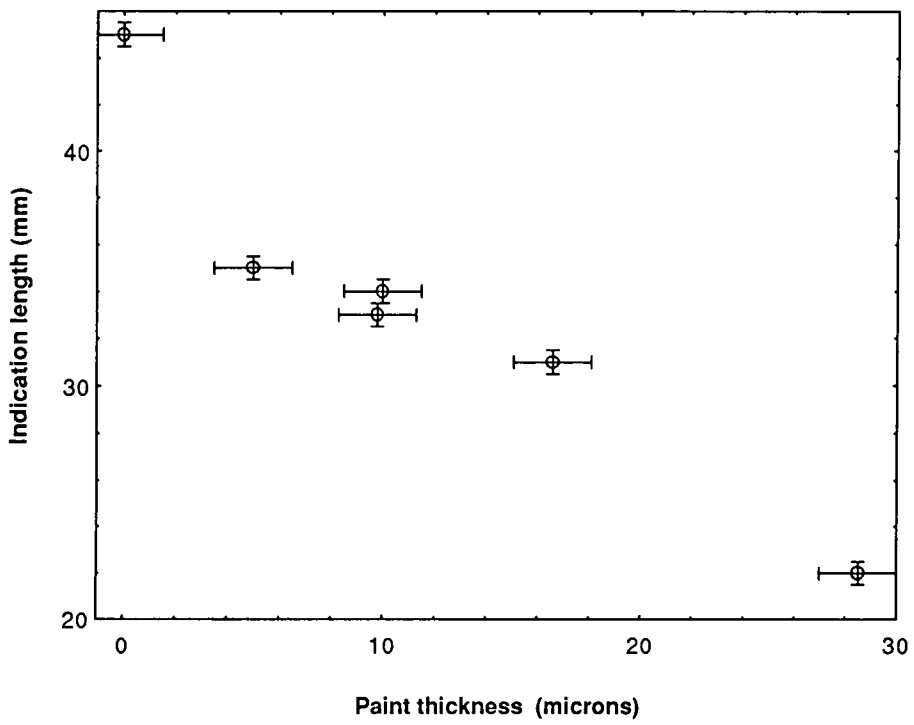

Fig.6.11b Indication length as paint thickness is varied for test piece TW.

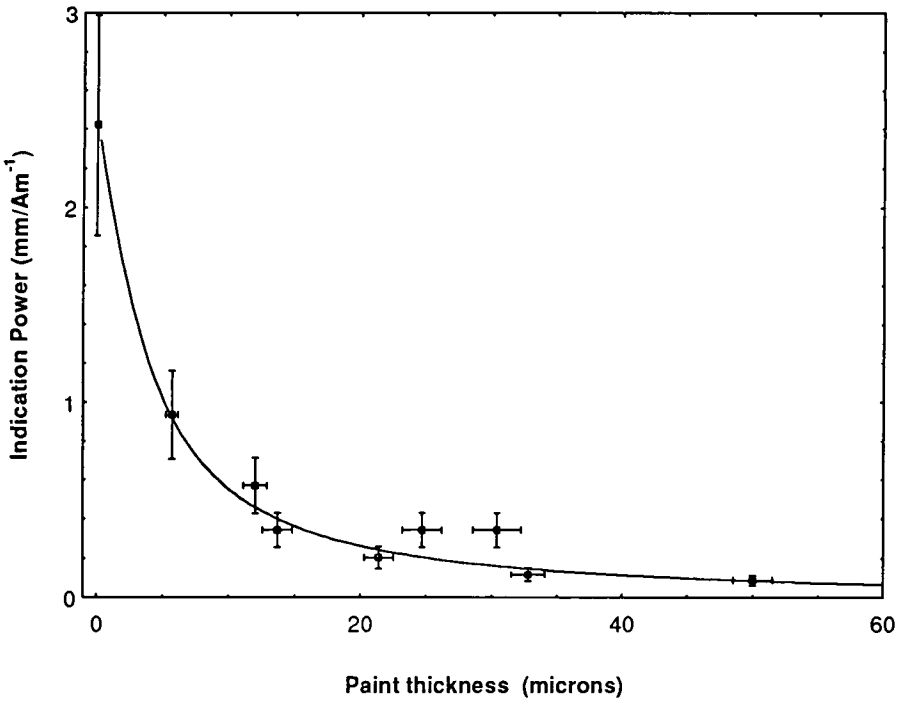

Fig.6.12a Indication Power as a function of paint thickness for the fluxa test block. Fit shown is equation 6.3.

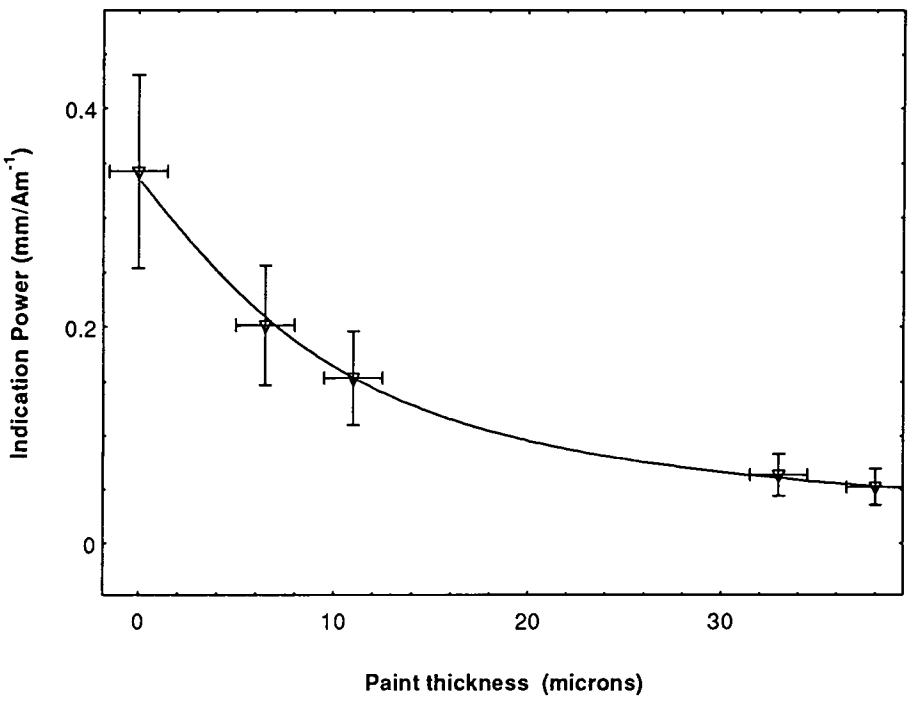

Fig.6.12b Indication Power as a function of paint thickness for the fluxa test block. Fit shown is equation 6.3.

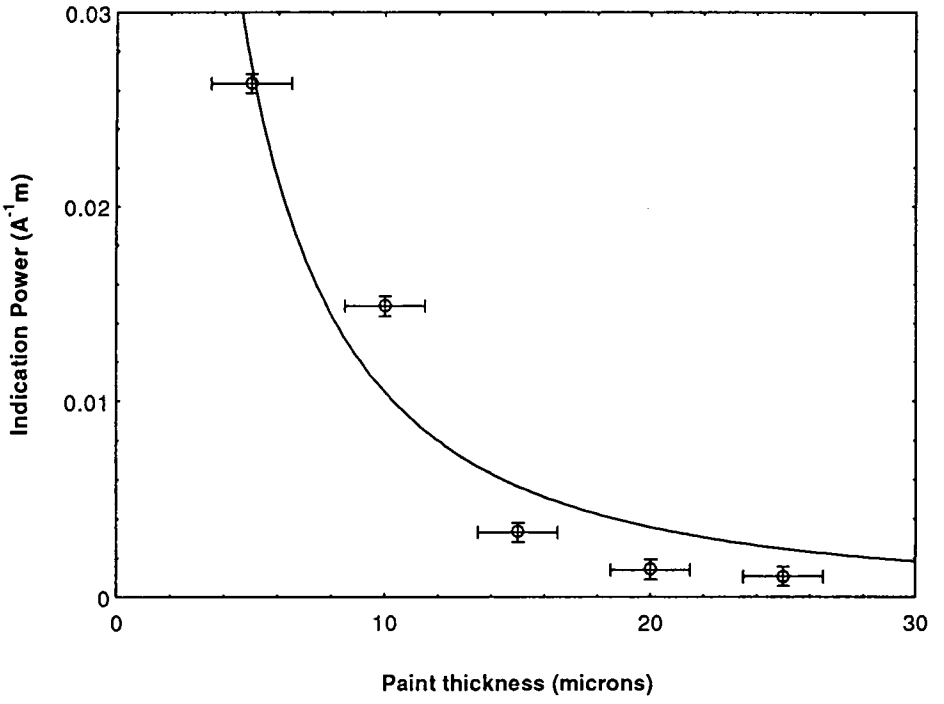

Fig.6.13 Indication Power as a function of paint thickness for the test piece E. Fit shown is equation 6.3.

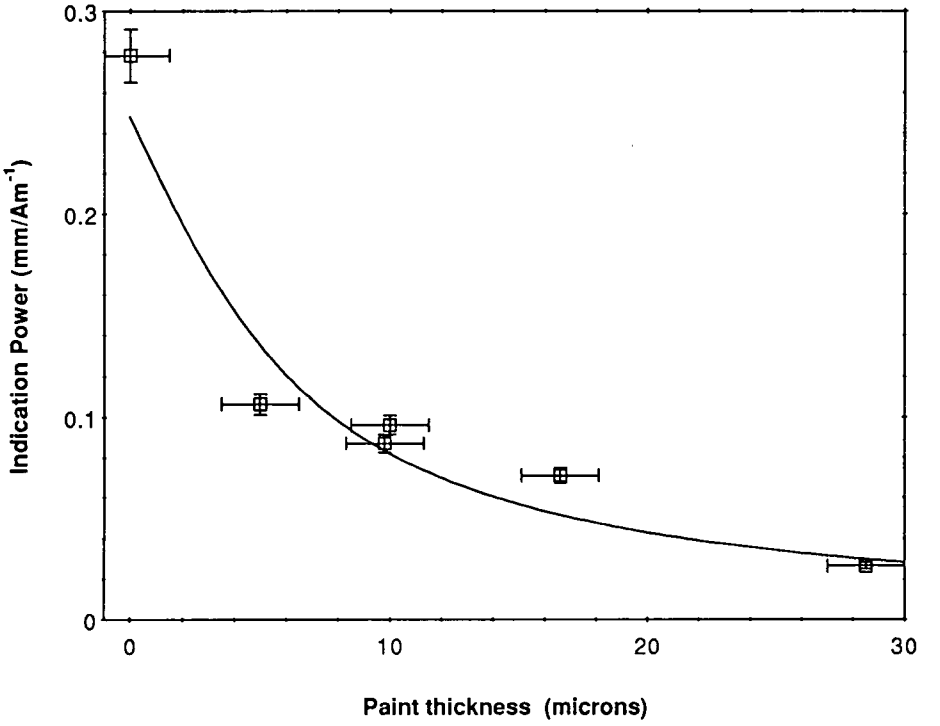

Fig.6.13b Indication Power as a function of paint thickness for the test piece TW. Fit shown is equation 6.3.

Table.6.1 Comparison of optical microscopy measurements of half crack width with half crack width and depth measured using the technique outlined in section 6.2.4

Test Piece	Crack half width measured by MPI (microns)	Crack depth measured by MPI (microns)	Crack half width measured by optical microscopy (microns)
Fluxa	6±3	$7x10^8±7x10^8$	3±1
Fluxa	20±3	$1x10^{10}±1x10^{10}$	3±1
E	6±3	$1x10^6±1x10^6$	5±2
TW	10±3	$1x10^4±1x10^4$	8±2

However measurements on certain test pieces have revealed that if the aspect ratio changes significantly then the preceding analysis does not hold. The effect of a non constant aspect ratio along the crack length is that indication is not continuous and splits into two or more separate indications which appear along the crack length. This is due to the variation of the magnetic leakage field along its length because of the non constant aspect ratio.

6.3.4 Implications for Practical MPI

Magnetic Particle Inspection is routinely used to detect the presence of surface breaking cracks in ferrous metals and as such is the most sensitive technique available but requires good access and fairly good surface preparation. However up to now the only information available about the crack parameters when using this technique is the crack length as this is the length of indication formed. Ultrasonics[9] however can give such information as the

depth and length of the crack assuming the defect is in the material and not at the surface. AC Potential Drop[10] techniques allow the crack depth of surface breaking cracks to be measured once the crack has been detected and assuming the width of the crack is small compared to its depth. The results presented in the last section indicate the possibility of sizing crack width using this technique if certain assumptions are made. Therefore by using ACPD, standard MPI and this technique all the parameters of a crack can be determined.

Perhaps more importantly these results also verify the simulation data presented in Chapter 5. Which means that the results presented in Chapter 5 have some experimental basis.

6.4 Flipping Fields

Whilst measuring the indication width as a function of paint thickness it was noticed that if the ink was applied first and the magnetic field gradually increased from zero the particles and aggregates at the crack rotated through 180° at the same applied magnetic field. Also while decreasing the magnetic field the particles switched their direction again but not at the same magnetic field as before. This difference between the two flipping fields is probably attributable to the magnetic properties of the inspection piece. As the particles indicate the direction of the magnetic field they are experiencing the fact that the particles rotate as the magnetic field applied to the specimen is increased indicates that the magnetic field changes its direction. Upon increasing the magnetic field from zero, the leakage field should not change its direction. Also upon decreasing the applied magnetic field the direction of the leakage field should not change. It is for these reasons we have investigated this effect. Fig.6.14a shows a magnetic particle in a crack as the magnetic field is being increased upto the magnetic field required for it to flip whereas Fig.6.14b shows the same magnetic particle after the flip.

6.4.1 Experiments on Flipping Fields

From preliminary experiments on the flipping field it was noticed that all the particles in the crack that were still in suspension flipped as the applied magnetic field was altered. For the particles to flip the magnetic field must change direction. As the flipping of the particles was independent of the particle size it was decided to investigate the dependence of the flipping field on height above the crack. The height above the crack was altered by

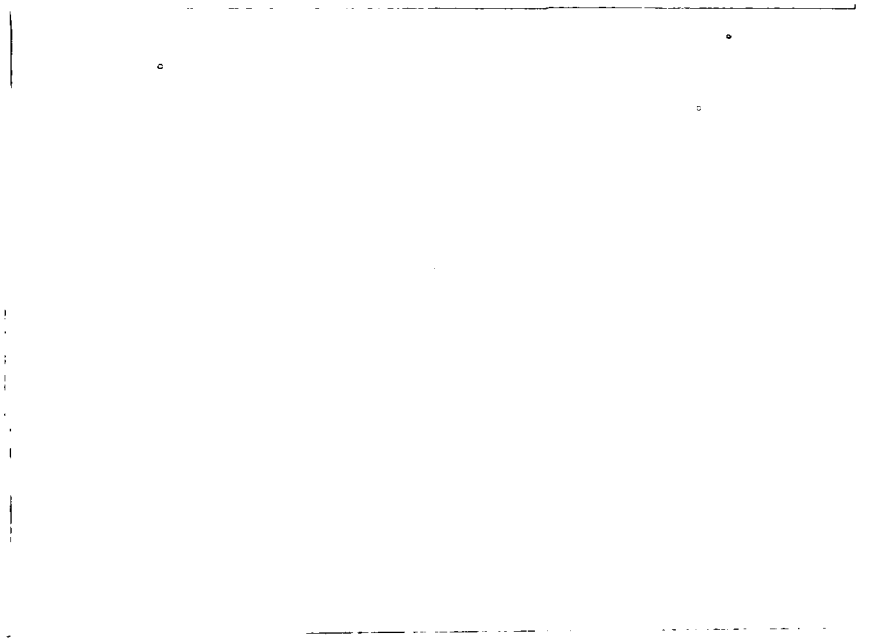

Fig.6.14a Magnetic Particle in a crack, below its top flipping field.

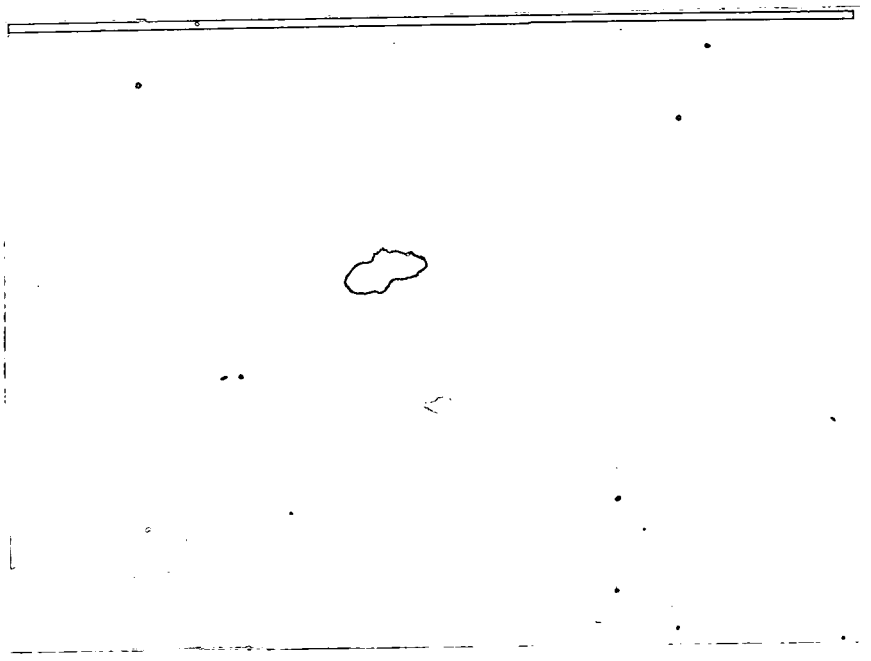

Fig.6.14b Same partice once the applied magnetic field is greater than the flipping field. The particle has rotated through 180°.

applying different layers of paint thickness. The flipping field was measured as the paint thickness was increased. Measurements of the flipping fields of the particles were only performed on particles which were well isolated from other magnetic particles to lessen the magnetic field contribution from other particles.

Fig.6.15 and Fig.6.16 shows the flipping fields for two different cracks. The top field is the magnetic field at which the particles flip when increasing the magnetic field from zero. The bottom field is the magnetic field at which the particles flip when decreasing the magnetic field. It is seen that the flipping field remains independent of the paint thickness.

6.5 Analysis of Flipping Fields

In this section the various possible mechanism that cause the particles to flip will be discussed and compared to the experimental results presented above.

6.5.1 Contaminated Crack

The first case to consider is that the crack is filled with a material of permeability μ_C. This affects the magnetic field within the crack, the magnetic field within the contaminated crack is given by [11]:

$$H_i = \frac{H_0}{1+\left(\frac{\mu_c-\mu}{\mu}\right)\left(\frac{n}{n+1}\right)} \qquad 6.6$$

Where H_O is the applied magnetic field, n is the aspect ratio of the crack and the permeability of the parent material is μ, the worst possible case is that the permeability of the contaminant μ_C is greater than μ, and the magnetic field within the crack becomes:

$$H_i \approx \frac{H_o\mu}{\mu_c} \qquad 6.7$$

This reduces the magnetic field within the crack and therefore the leakage field but does not change its direction and therefore contamination of the crack cannot be responsible for the flipping of the particles.

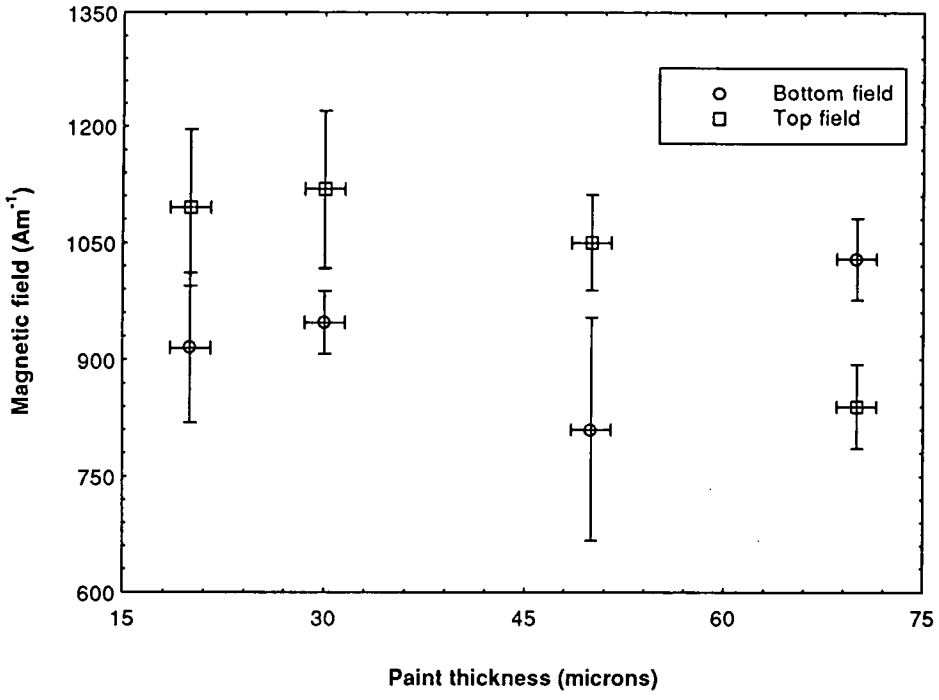

Fig.6.15 Variation of flipping fields with respect to paint thickness for test piece A

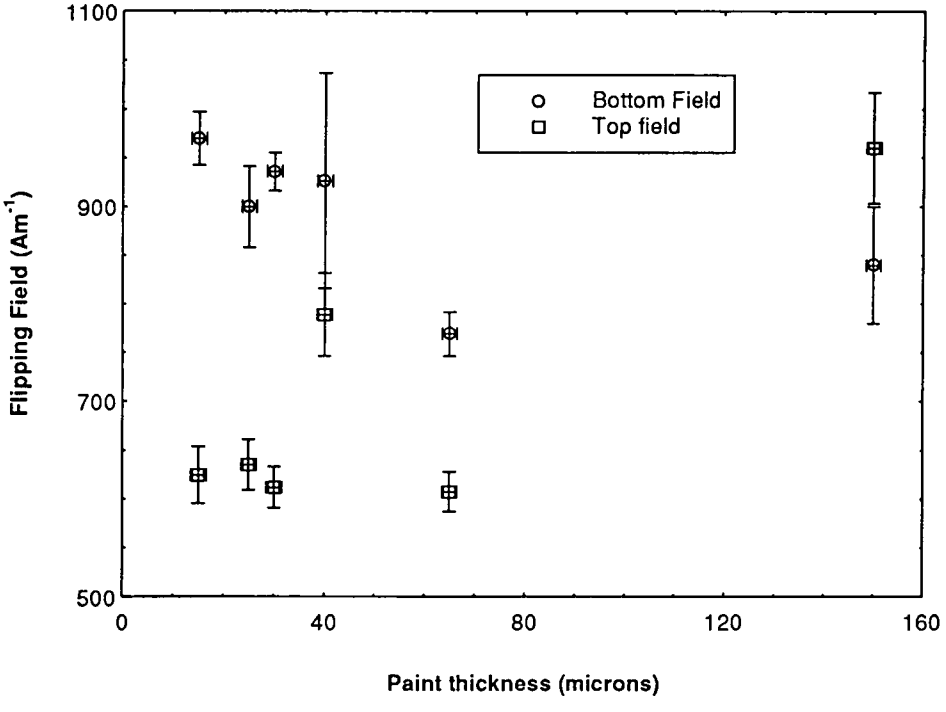

Fig.6.16 Variation of flipping fields with respect to paint thickness for test piece B

6.5.2 Demagnetising Field of the Inspection Piece

Another possible mechanism for the reversal of the particle is that the remanent magnetisation of the inspection piece creates a demagnetising field in the opposite direction to the applied magnetic field. If the applied magnetic field is sufficiently low then the demagnetising field is greater than the applied field. In which case the permeability becomes negative. This negative permeability arises from the fact the permeability is given by:

$$\mu_{eff} = \frac{M + H_0 - DM}{H_o - DM} \qquad 6.8$$

where D is the demagnetising factor dependent only upon the specimen geometry and M is the magnetisation of the specimen. If the demagnetising field is greater than the applied magnetic field then the permeability will be negative. A negative permeability in equation 6.8 would cause the magnetic leakage field to be in the opposite direction to the applied magnetic field, until the applied magnetic field became greater than the demagnetising field. Once this occurred the particle would flip into the new field direction. However this negative permeability is the effective permeability and not the intrinsic permeability of the specimen. Whereas the permeability in equation 6.8 is the intrinsic permeability. Therefore this can not be the mechanism responsible for the particles flipping.

6.5.3 Demagnetising Field of Other Particles

The particles that flip are the ones that remain in suspension at the crack and not the ones trapped at the interface between the fluid and the paint layer. However the particles that are at this interface have associated with them a demagnetising field shown schematically in Fig.6.17. This is in the opposite direction to their magnetisation and the magnetic leakage field of the crack. The magnetic field experienced by a particle in suspension at the crack is given by:

$$H = H_{crack} - DM \qquad 6.9$$

where DM is the demagnetising field of the particle stranded at the crack and H_{crack} is the leakage magnetic field and comprises of the leakage field of the crack and the applied magnetic field. Therefore H can change its sign as the applied magnetic field is increased, this increases H_{crack} and once this becomes greater than the demagnetising field of the

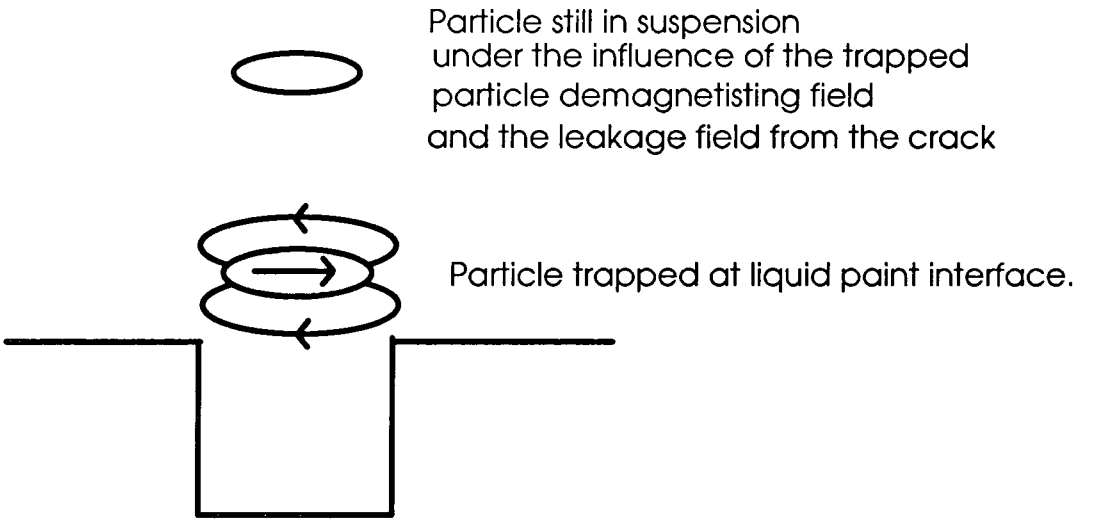

Fig.6.17 Simplified diagram showing the demagnetising field from a particle sitting above the crack during Magnetic Particle Inspection. The demagnetising field from a particle above a crack opposes the magnetic leakage field of the crack, so the magnetic field above this particle is the sum of the demagnetising field of the particle below it and the leakage field from this crack.

particles which are stranded then the particles in the fluid will flip. Decreasing the applied magnetic field the particles will flip once the demagnetising field of the particles stranded at the crack is greater than the magnetic field from the crack.

However the particles that flip are below the particles trapped at the interface, this was determined by optical microscopy. Therefore these particles will experience a demagnetising field but this will be in the same direction as the magnetic leakage field and therefore this can not be the mechanism by which the particles flip.

6.5.4 Remanent Magnetisation of the Inspection Piece

The remanent state of the inspection piece will consist of domains pointing in various directions. The calculation of the exact domain structure is a complex and computationally extensive exercise. One possible domain structure at the crack interface is shown in Fig.6.18, this consists of spike domains[12] which point in the opposite direction to that of the bulk magnetisation. Consequently there will be flux leakage between these spike domains and the other domains as well as across the crack. The magnetic flux leakage between the spike domains and the bulk material can be in the opposite direction to that of the flux leakage across the crack. If the magnetic leakage field associated with the spike domains is greater than the magnetic leakage field associated with the crack, then this would align the particles in the opposite direction to that of the applied magnetic field.

As the magnetic field is increased these spike domains will reorientate themselves towards the magnetic field direction. Once the magnetic leakage field from the crack becomes greater than the leakage field from the spike domains then the magnetic particles will flip to align itself with the direction of the applied magnetic field. When the magnetic field is decreased these spike domains will form again and oppose the direction of the magnetic field. This will cause the particles to flip. The existence of these spike domains in the remanent state of the inspection piece, we believe is responsible for the flipping of the magnetic particles as the magnetic field is altered.

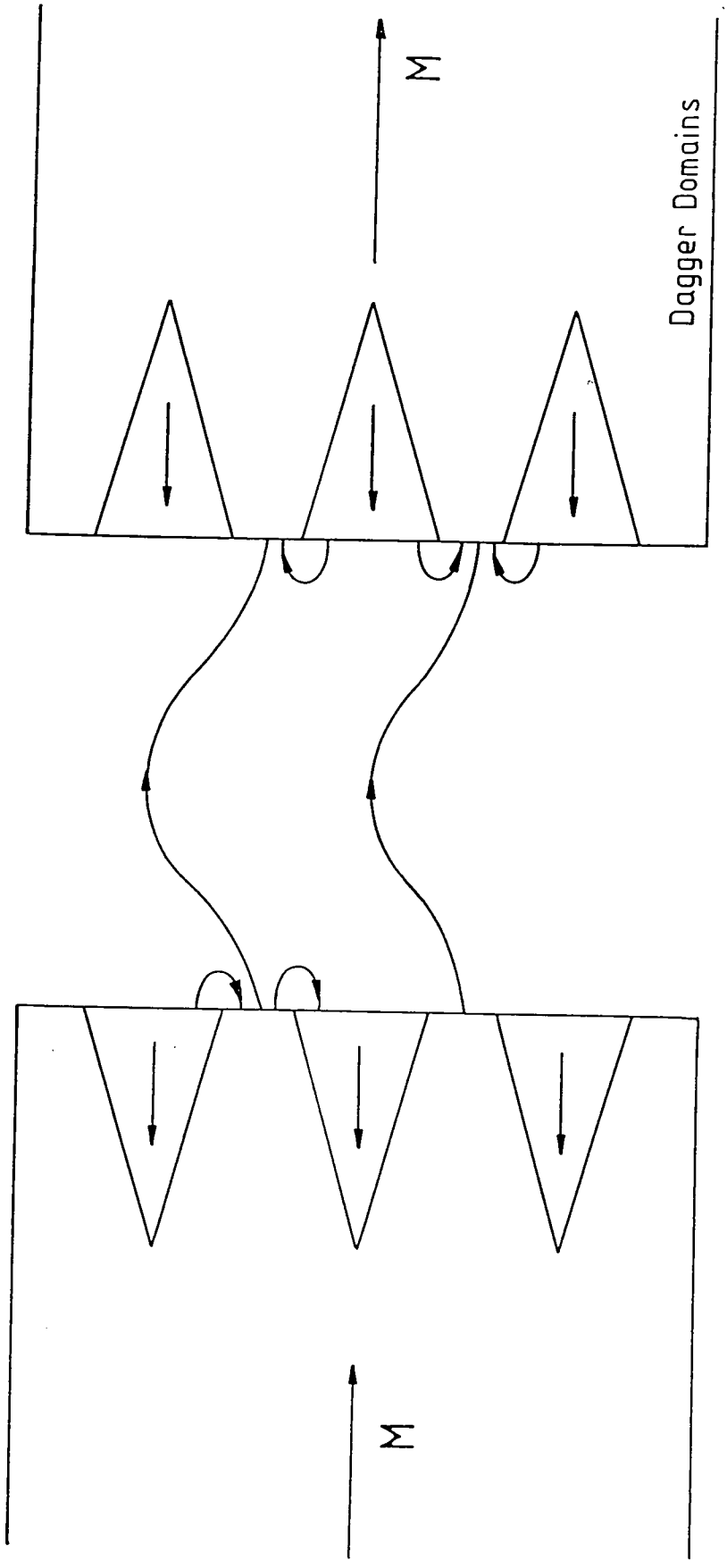

Fig.6.18 Diagram showing a possible domain structure for the remanent state of the inspection piece. The presence of these spike domains we believe are responsible for the flipping of the particles as the magnetic field is increased. In zero magnetic field, the leakage field from these domains is greater than the leakage field from the crack and therefore the particle are aligned in the opposite direction to the remanent magnetisation. Increasing the magnetic field causes the particle to flip once these domains are reoriented.

6.6 Summary

The relationship between the peak and rms. for a thyristor power supply has been determined and this has implications for the British Standard. By measuring the indication width as a function of paint thickness layer it was noted that the indication width went through a minimum. This we can not explain. Measurement of the indication length in a variable magnetic field provided a valuable test of the simulation results and also a possible mechanism for determining the crack width. The observation that the particles in suspension flip as the magnetic field is altered, could be due to the existence of spike domains in the remanent state of the material.

References Chapter 6

[1] Tiede, U.K. agents are Wells Krautkrammer, Sutton Coldfield, Birmingham

[2] Stadthaus, M., Dichaut, E., and Prestel, W., "System performance in magnetic particle inspection", WCNDT, London (1987)

[3] MacDonald, E., "Significance of Magnetising Current Waveform in Magnetic Particle Inspection", *University of Strathclyde 2nd Year for Nuclear Electric, Wyntheshaw*, (1993)

[4] McCoy, J.M., and Tanner, B.K., "Computer simulation of indications in magnetic particle inspection", *J.Phys. D:Appl. Phys.*, **23**, 593-599 (1990)

[5] Edwards, C., and Palmer, S.B., "The magnetic leakage field of surface breaking cracks", *J.Phys. D:Appl. Phys.*, **19**, 657-673 (1986)

[6] Elecometer Instruments, Edge Lane, Droysden, Manchester, M35 6BU, U.K

[7] McCoy, J.M., PhD thesis, University of Durham (1988)

[8] Fluxa test block made by Karl Deutsch, U.K. agents are Teledictor Ltd., Tipton, West Midlands, U.K

[9] Blitz, J., "Fundamentals of Ultrasonics", *Butterworths*, London, 185-189, (1963)

[10] Frise, P.R., and Bell, R., "Improved probe array for ACPD crack measurements", *The British Journal of Non-Destructive Testing*, **34**, 15-19 (1992)

[11] Edwards, C., PhD Thesis, University of Hull (1986)

[12] Craik, D.J., and Tebble, R.S., "Ferromagnetism and Ferromagnetic Domains",*North Holland Publishing Company*, 103-110 (1965)

Chapter 7

Conclusion and Suggestions for Further Work

7.0 Introduction

The results of a study in the physics of Magnetic Particle Inspection will be discussed. These results give us a better understanding of the processes involved and provide justification for some of the statements in the new European Standard. Then ideas for further work on the subject of Magnetic particle Inspection will be discussed.

7.1 Results

The three areas of work which have been undertaken are the magnetic properties of the inks and powders used in MPI, a computer simulation of the indication process and work of a more practical nature concerning MPI. This includes determining the relationship between the rms and peak values for a thyristor waveform and the viewing of the indications formed in MPI.

An extensive study of the magnetic properties of the inks and powders used in MPI was undertaken. It was found from magnetic measurements that field induced agglomeration occurs, this imparts the inks with a measurable coercivity and remanence. The particles form needle shaped aggregates. The formation of these needle shaped aggregates lowers the demagnetisation factor of the sample during the measurement and for this reason the virgin curve is outside the main hysteresis curve. Low field measurements on magnetic inks unexposed to large magnetic fields indicate a susceptibility of $5.5 \pm .2.10^{-4}$ m^3/kg. Hysteresis is observed but no coercivity or remanence. Time decay measurements indicate that the decay in low magnetic field is by Néel relaxation of the particles magnetic moment. However upon exposure to a large magnetic field, the low field properties change dramatically as a coercivity and remanence is induced. The coercivity and remanence of the ink after exposure to a magnetic field change as a function of time. The time decay measurements now indicate that the moment decays by a combination of Néel and Brownian relaxation.

Measurements using a AGFM and torque magnetometer have told us about the properties of the single domain crystallites that form the ink particles. Analysis of the remanence curves measured on the AGFM using the ΔM technique pioneered by Kelly indicate that interactions between the crystallites lower the magnetisation of the aggregate. This lowering of the magnetisation lowers the magnetic force on a particle during an inspection

and therefore affects the indication process. From the studies using the torque magnetometer to determine the rotational hysteresis integral, the spin reversal mechanism was found to be by chain of spheres fanning.

The active magnetic component of a typical fluorescent and black magnetic ink has been determined. These were Fe and Fe_3O_4 respectively.

From the computer simulation of the indication mechanism it was found that the number of particles at the crack increased with applied magnetic field. This is to be expected as the force on the particle depends on its magnetisation and the strength of the gradient field. Both of which increase with applied magnetic field for permeable particles. When time varying magnetic fields are used for low remanent materials it was found that the rms of the waveform gave consistent results for all the waveforms used. This is in agreement with the draft European Standard.

Manufacturers are decreasing the size of the particles used in the ink to increase its sensitivity, in the Bitter technique which allows domain walls to be viewed ferrofluids are routinely used. The decreasing of the particle size affects the terminal velocity of the particles, as does the viscosity of the carrier fluid. The variation in the number of particles at the crack was recorded for various radii and carrier fluid viscosity. It was found that for particles greater than 10 micron radius the contrast was essentially independent of the viscosity. Whereas for smaller particles the contrast increased as the viscosity decreased. This study also provides some physical basis for MPI to be carried out at high temperatures, as the viscosity of the carrier fluid changes with temperature. However for the larger particles this change in viscosity had little effect on the contrast obtained.

White contrast paint is often applied to the surface to increase the contrast of the particles against the background. The effect of various layers of paint thickness was to lower the number of particles present at the crack. The rate of this decrease was found to be similar to the variation of B_{ox} at the crack centre with increasing paint layer thickness. The fact that the number of particles at the crack decreases with the variation of the leakage field implies that applying a paint layer increases the chances of detecting large cracks due to the increase in contrast but lowers the chance of detecting small cracks due to the rapid decrease in the magnetic leakage field.

Investigation of the waveform properties of thyristor controlled power supplies found that the relationship between the rms of the waveform and its peak was non linear. This has important implications if the user wishes to remain within the British Standard. However the simulation results presented above indicate that the British Standard is wrong in this respect at least for low remanent steels.

By allowing the magnetic field to vary along the crack length then the length of the indication formed will change with increasing paint thickness. This indication length can be related to contrast predicted by the computer simulation. The indication power was found

to vary in the same way as the leakage field. By performing a fit to the experimental data the crack width can be determined. The crack width calculated in this way was compared to optical microscopy measurements and found to give reasonable agreement. Therefore we suggest that this is a possible method for sizing crack by using MPI.

The last measurements performed were on the magnetic field required to flip the particles in a crack. It was found during the viewing of indications under a microscope that increasing the magnetic field from zero caused the particles at the crack to rotate through 180 degrees. Upon decreasing the magnetic field the particles flipped back to their original direction. This flipping of the particles implies that the leakage field experienced by the particle changes its direction. Possible mechanisms for this were examined, the most likely one being the existence of spike domains in the remanent state of the inspection piece. These domains are in the opposite direction to the leakage field of the crack and cause the magnetic particles to align in the opposite direction to that of the applied magnetic field. As the magnetic field is increased these domains switch their magnetisation which causes the particles to flip. When the magnetic field is decreased these domains are formed again. They are still in the opposite direction to the applied magnetic field and the particle will flip again.

7.2 Suggestions for Further Work

The magnetic measurements made on the inks were essential static measurements it would be instructive to look at the magnetic properties of the ink as the frequency of the ac field used as the magnetisation source was varied. This would see whether the particles when subjected to an 50 Hz ac signal, bodily rotated or the magnetic moment rotated this has implications for the modelling process. The ΔM technique could also be extended to a wider range of magnetic inks to see the variation in it across the different manufacturers. It would be interstring to try and relate ΔM measurements to a measurement of the inks' sensitivity. The structure of the fluorescent ink particles could also be investigated to determine the size of the iron based core in these particles. This could then be accommodated in the computer simulation of the indication mechanism.

On the computer simulations side the improvements which could be made are to allow the permeability of the inspection piece to vary. This will allow the effect of time varying waveforms on high remanent steels to be investigated. For low remanent steels Stadhaus found that the rms was the pertinent property and the modelling work in this thesis agree with his results. However no results concerning high remanet steels have been obtained. In magnetic separation the use of multi-wire filters is common and magnetic field and field gradient from these have been successfully calculated. It would be instructive to see if this approach could be used to model the effect of surface roughness on a particles' trajectory.

In Chapter 6 a method was mentioned for sizing the cracks using MPI this was done for a limited number of man made cracks. It would be instructive to increase the number of cracks in this survey to include natural cracks and find out if the method can be extended and be of practical use. The observation that the magnetic leakage field changes its

direction as the magnetic field is increased from zero should be explored further. The idea that the flipping fields was due to spike domains could be examined by the use of the Bitter technique. Another possible way to this is to measure the magnetic field profile of the crack by using a magnetic force microscope.

Appendix A1

In this appendix there are complete listings of the programs used to simulate the indication mechanism in Magnetic Particle Inspection. The programs are:

MPI.FOR This is Jim McCoys original program of the indication mechanism.

TMPIA.FOR This program is identical to MPI.FOR but uses a thyristor waveform instead of a DC waveform to magnetise the inspection piece

SINMPIA.FOR This is identical to MPI.FOR but uses a sine waveform to magnetise the inspection piece it can easily be adapted to allow a rectified sine waveform to be used.

MAGX.FOR Allows the particles in the simulation to have a fixed magnetic moment.

The other programs were written in Qbasic by the author they are:

RND.BAS Generates the starting conditions for the above programs

ANAN.BAS Analyses the data from the simulation programs.

MPI.FOR

```
C123457

      DIMENSION X(1000), Y(1000), VX(1000), VY(1000), T(1000)
      DIMENSION XB(1000), YB(1000), VXB(1000), VYB(1000)
      COMMON ALPHA,BETA,ASPECT,GAMMA,DELTA,H,A,B,RADIUS,HO,MU,PNTTHK
      H=5E-6


C  INPUT SYSTEM DATA
C123457
      OPEN(7,FILE='e:\STEPHEN\RESULTS.NUM')
      DO 97 LL=1,8
      OPEN (4,file='e:\stephen\number1.num')
      READ(4,*) RADIUS, RHOP, RHOC, ETA, HO, BDEF, ADEF
      READ(4,*) MU, NPARTS,PNTTHK
      DO 33 I=1,160
      READ(4,*) XB(I), YB(I), VXB(I), VYB(I)
   33 CONTINUE
      CLOSE (4)
      NEVAL=10

C EVALUATE CLUSTERS OF CONSTANTS IN DIFFERENTIAL EQUATIONS
C123457

      ASPECT=BDEF / ADEF
      ALPHA=(9*ETA) / (2*RHOP*(RADIUS ** 2))
      BETA=4*3.14159265*1.0E-7*HO*ASPECT*(MU-1)
      BETA=BETA / (2*RHOP*ATAN(ASPECT)*(ASPECT+MU))
      GAMMA=(9.80655*(RHOP-RHOC)) / RHOP

C SOLVE TRAJECTORY FOR EACH PARTICLE ONE AT A TIME


      DO 600 L=1,160
      A=ADEF
      B=BDEF
      X(1)=XB(L)
      Y(1)=YB(L)
      VX(1)=VXB(L)
      VY(1)=VYB(L)
      T(1)=0


      IF (Y(1).LT.PNTTHK) THEN
      JJ=1
      GOTO 50
      END IF
      JJ=NEVAL
      IFAIL=0
      CALL PRCOXY(X, Y, VX, VY, T, JJ, IFAIL)
      IF (JJ.GE.NEVAL) THEN
```

```
      NEVAL=JJ
      GOTO 60
      END IF

C123467

   50 IFAIL=0
      CALL PRCOX(X, Y, VX, VY, T, JJ, NEVAL, IFAIL)
   60 XB(L)=X(NEVAL)
      YB(L)=Y(NEVAL)
      VXB(L)=VX(NEVAL)
      VYB(L)=VY(NEVAL)
  600 CONTINUE

C123457

      OPEN(4,FILE='e:\STEPHEN\NUMBER1.NUM')
      WRITE(4,*) RADIUS, RHOP, RHOC, ETA, HO, BDEF, ADEF
      WRITE(4,*) MU, NPARTS,PNTTHK
      WRITE(7,*) RADIUS,RHOP,RHOC,ETA,HO,BDEF,ADEF
      WRITE(7,*) MU,NPARTS,PNTTHK
      DO 69 I=1,160
      WRITE(4,*) XB(I), YB(I), VXB(I), VYB(I)
      WRITE(7,*)XB(I),YB(I),VXB(I),VYB(I)
   69 CONTINUE
      CLOSE (4)
   97 CONTINUE
      CLOSE(7)
      STOP
      END


      FUNCTION THET(XX, YY, AA, BB)
      DOUBLE PRECISION C1,C2,C3,C4
      COMMON ALPHA,BETA,ASPECT,GAMMA,DELTA,H,A,B,RADIUS,HO,MU,PNTTHK
      C1=ATAN(BB*(XX+AA) / ((XX+AA) ** 2+YY*(YY+BB)))
      C2=ATAN(BB*(XX-AA) / ((XX-AA) ** 2+YY*(YY+BB)))
      HX=HO*ASPECT*(MU-1)*(C1-C2) / (2*ATAN(ASPECT)*(ASPECT+MU))
      C3=((XX+AA) ** 2+(YY+BB)**2)*((XX-AA)**2+YY**2)
      C4=((XX+AA) ** 2+YY ** 2)*((XX-AA) ** 2+(YY+BB)**2)
      HY=(MU-1)*(LOG(C3/C4))/(4*ATAN(ASPECT)*(ASPECT+MU))
      HY=HY*ASPECT*HO
      THET=ATAN(HY / (HX+HO))
      RETURN
      END

      FUNCTION MAG(XX, YY, AA, BB)
      DOUBLE PRECISION C1,C2,C3,C4
      COMMON ALPHA,BETA,ASPECT,GAMMA,DELTA,H,A,B,RADIUS,HO,MU,PNTTHK
      C1=ATAN(BB*(XX+AA)/((XX+AA)**2+YY*(YY+BB)))
      C2=ATAN(BB*(XX-AA)/((XX-AA)**2+YY*(YY+BB)))
      HX=HO*ASPECT*(MU-1)*(C1-C2) / (2*ATAN(ASPECT)*(ASPECT+MU))
      C3=((XX+AA)**2+(YY+BB)**2)*((XX-AA)**2+YY**2)
      C4=((XX+AA)**2+YY**2)*((XX-AA)**2+(YY+BB)**2)
```

```
HY=(MU-1)*(LOG(C3/C4))/(4*ATAN(ASPECT)*(ASPECT+MU))
HY=HO*HY*ASPECT
MAG=2*SQRT(HY**2+(HO+HX)**2)
IF (ABS(MAG).GT.4.71E5) THEN
MAG=4.71E5
END IF
RETURN
END

FUNCTION DHXBDX(XX, YY, AA, BB)
DOUBLE PRECISION C1,C2,C3,C4
XX=1000000*XX
YY=1000000*YY
AA=1000000*AA
BB=1000000*BB
C1=(YY+BB) / ((XX-AA) ** 2+(YY+BB)** 2)
C2=(YY+BB) / ((XX+AA) ** 2+(YY+BB) ** 2)
C3=YY / ((XX+AA) ** 2+YY ** 2)
C4=YY / ((XX-AA) ** 2+YY ** 2)
XX=.000001*XX
YY=.000001*YY
AA=.000001*AA
BB=.000001*BB
DHXBDX=(C1-C2+C3-C4)*1000000
RETURN
END

FUNCTION DHYBDX(XX, YY, AA, BB)
DOUBLE PRECISION C1,C2,C3,C4
XX=1000000*XX
YY=YY*1000000
AA=AA*1000000
BB=1000000*BB
C1=(XX+AA) / ((XX+AA) ** 2+(YY+BB) ** 2)
C2=(XX-AA) / ((XX-AA) ** 2+(YY+BB) ** 2)
C3=(XX-AA) / ((XX-AA) ** 2+YY ** 2)
C4=(XX+AA) / ((XX+AA) ** 2+YY ** 2)
XX=.000001*XX
YY=.000001*YY
AA=.000001*AA
BB=.000001*BB
DHYBDX=(C1-C2+C3-C4)*1000000
RETURN
END


SUBROUTINE PRCOX(X, Y, VX, VY, T, JJ, NEVAL, IFAIL)
DIMENSION X(1000), Y(1000), VX(1000), VY(1000), T(1000)
DIMENSION XX(1001), YY(1001), VXX(1001), VYY(1001), TT(1001)
COMMON ALPHA,BETA,ASPECT,GAMMA,DELTA,H,A,B,RADIUS,HO,MU,PNTTHK
CX1=0
CY1=0
CVX1=0
CVY1=0
```

```
      XX(1)=X(JJ)
      YY(1)=Y(JJ)
      VXX(1)=VX(JJ)
      VYY(1)=0
      TT(1)=T(JJ)
      YYCST=Y(JJ)
      VYYCST=0
      IF (Y(1).LT.PNTTHK.OR.ABS(XX(1)).LT.A) THEN
      X(1)=X(JJ)
      NPTS=1
      GOTO 207
      END IF
      NEVAL=NEVAL-1
      DO  195 N=JJ,NEVAL
      DO 190 M=1,1000
C PREDICT X,Y,VX,VY

      XX(M+1)=XX(M)+H*VXX(M)
      YY(M+1)=YYCST
      VYY(M+1)=0
      E1=DHXBDX(XX(M), YYCST, A, B)
      E2=DHYBDX(XX(M), YYCST, A, B)
      ANG=THET(XX(M), YYCST, A, B)
      FLD=MAG(XX(M), YYCST, A, B)
      U1=FLD*(E1*COS(ANG)+E2*SIN(ANG))
      U2=FLD*(E1*SIN(ANG)-E2*COS(ANG))
      VXX(M+1)=VXX(M)+H*(-1*ALPHA*VXX(M)+BETA*U1)

C STORES FIRST PREDICTION

      FIRSX=XX(M+1)
      FIRSVX=VXX(M+1)
      ITN=1

C CORRECT X,VX
C123457
  200 CX1=XX(M)+.5*H*(VXX(M)+VXX(M+1))
      E3=DHXBDX(XX(M+1), YYCST, A, B)
      E4=DHYBDX(XX(M+1), YYCST, A, B)
      ANG=THET(XX(M+1), YYCST, A, B)
      FLD=MAG(XX(M+1), YYCST, A, B)
      U3=FLD*(E3*COS(ANG)+E4*SIN(ANG))
      U4=FLD*(E3*SIN(ANG)-E4*COS(ANG))
      CVX1=VXX(M)-.5*H*(ALPHA*(VXX(M+1)+VXX(M))-BETA*(U3+U1))

C CHANGE ITERATION COUNTER AND CHECK LIMIT ON ITERATIONS

      Q1=ABS(XX(M+1)-CX1)
      IF (Q1.LT..000001) THEN

C CORRECT USING TRUNCATION ESTIMATE

      XX(M+1)=CX1+.2*(FIRSX-CX1)
      VXX(M+1)=CVX1+.2*(FIRSVX-CVX1)
```

```
      TT(M+1)=TT(M)+H
      IF (ABS(XX(M+1)).LT.A) THEN
      XX(1001)=XX(M+1)
      YY(1001)=YYCST
      VXX(1001)=VXX(M+1)
      VYY(1001)=0
      TT(1001)=TT(M+1)
      GOTO 191
      END IF
      GOTO 190
      ELSE
      ITN=ITN+1
      END IF
      IF (ITN.GT.10) THEN
      IFAIL=1
      X(N+1)=X(N)
      Y(N+1)=Y(N)
      VX(N+1)=VX(N)
      VY(N+1)=VY(N)
      NPTS=N+1
      GOTO 209
      ELSE
C ELSE RECORRECT
      XX(M+1)=CX1
      VXX(M+1)=CVX1
      END IF
      GOTO 200
  190 CONTINUE
  191 X(N+1)=XX(1001)
      Y(N+1)=YYCST
      VX(N+1)=VXX(1001)
      VY(N+1)=0
      T(N+1)=TT(1001)
      XX(1)=XX(1001)
      YY(1)=YYCST
      VXX(1)=VXX(1001)
      VYY(1)=0
      TT(1)=TT(1001)
      NPTS=N+1
      IF (ABS(X(N+1)).LT.A) THEN
      NPTS=N+1
      GOTO 199
      END IF
  195 CONTINUE
  199 IF (ABS(X(NPTS)).LT.A) THEN

C PARTICLE TRAPPED AT DEFECT TAKE LAST VALUE
C123457
  207 NEVAL=NEVAL-1
      DO 201 I=NPTS ,NEVAL
      X(I+1)=X(NPTS)
      Y(I+1)=YYCST
      VX(I+1)=0
      VY(I+1)=0
```

```
      T(I+1)=T(I)+(1000*H)
  201 CONTINUE
      NEVAL=NEVAL+1
      END IF

  209 RETURN

      END

      SUBROUTINE PRCOXY(X, Y, VX, VY, T, JJ, IFAIL)
      DIMENSION X(1000), Y(1000), VX(1000), VY(1000), T(1000)
      DIMENSION XX(1001), YY(1001), VXX(1001), VYY(1001), TT(1001)
      COMMON ALPHA,BETA,ASPECT,GAMMA,DELTA,H,A,B,RADIUS,HO,MU,PNTTHK
      CX1=0
      CY1=0
      CVX1=0
      CVY1=0
      XX(1)=X(1)
      YY(1)=Y(1)
      VXX(1)=VX(1)
      VYY(1)=VY(1)
      TT(1)=T(1)
      JJ=JJ-1
      DO 95  N=1, JJ
      DO 90 M=1 , 1000
      XX(M+1)=XX(M)+H*VXX(M)
      YY(M+1)=YY(M)+H*VYY(M)
      E1=DHXBDX(XX(M), YY(M), A, B)
      E2=DHYBDX(XX(M), YY(M), A, B)
      ANG=THET(XX(M), YY(M), A, B)
      FLD=MAG(XX(M), YY(M), A, B)
      U1=FLD*(E1*COS(ANG)+E2*SIN(ANG))
      U2=FLD*(E1*SIN(ANG)-E2*COS(ANG))
      VXX(M+1)=VXX(M)+H*(-1*ALPHA*VXX(M)+BETA*U1)
      VYY(M+1)=VYY(M)+H*(-1*ALPHA*VYY(M)-BETA*U2-GAMMA)
      FIRSX=XX(M+1)
      FIRSY=YY(M+1)
      FIRSVX=VXX(M+1)
      FIRSVY=VYY(M+1)
      ITN=1
  100 CX1=XX(M)+.5*H*(VXX(M)+VXX(M+1))
      CY1=YY(M)+.5*H*(VYY(M)+VYY(M+1))
      E3=DHXBDX(XX(M+1), YY(M+1), A, B)
      E4=DHYBDX(XX(M+1), YY(M+1), A, B)
      ANG=THET(XX(M+1), YY(M+1), A, B)
      FLD=MAG(XX(M+1), YY(M+1), A, B)

C123457
      U3=FLD*(E3*COS(ANG)+E4*SIN(ANG))
      U4=FLD*(E3*SIN(ANG)-E4*COS(ANG))
      CVX1=VXX(M)-.5*H*(ALPHA*(VXX(M+1)+VXX(M))-BETA*(U3+U1))
      CVY1=VYY(M)-.5*H*(ALPHA*(VYY(M+1)+VYY(M))+BETA*(U2+U4)+2*GAMMA)
      Q1=ABS(XX(M+1)-CX1)
      Q2=ABS(YY(M+1)-CY1)
```

```
      IF (Q1.LT..000001.AND.Q2.LT..000001) THEN
      XX(M+1)=CX1+.2*(FIRSX-CX1)
      YY(M+1)=CY1+.2*(FIRSY-CY1)
      VXX(M+1)=CVX1+.2*(FIRSVX-CVX1)
      VYY(M+1)=CVY1+.2*(FIRSVY-CVY1)
      TT(M+1)=TT(M)+H
      IF (YY(M+1).LT.PNTTHK.OR.ABS(XX(M+1)).LT.A) THEN
      XX(1001)=XX(M+1)
      YY(1001)=YY(M+1)
      VXX(1001)=VXX(M+1)
      VYY(1001)=VYY(M+1)
      TT(1001)=TT(M+1)
      GOTO 91
      END IF
      GOTO 90
      ELSE
      ITN=ITN+1
      END IF
      IF (ITN.GT.10) THEN
      IFAIL=1
      X(N+1)=X(N)
      Y(N+1)=Y(N)
      VX(N+1)=VX(N)
      VY(N+1)=VY(N)
      NPTS=N+1
      GOTO 99
      ELSE
      XX(M+1)=CX1
      YY(M+1)=CY1
      VXX(M+1)=CVX1
      VYY(M+1)=CVY1
      END IF

C ELSE RECORRECT
      GOTO 100
   90 CONTINUE
   91 X(N+1)=XX(1001)
      Y(N+1)=YY(1001)
      VX(N+1)=VXX(1001)
      VY(N+1)=VYY(1001)
      T(N+1)=TT(1001)
      XX(1)=XX(1001)
      YY(1)=YY(1001)
      VXX(1)=VXX(1001)
      VYY(1)=VYY(1001)
      TT(1)=TT(1001)
      NPTS=N+1


C IF PARTICLE HAS HIT INTERFACE OR TRAPPED THEN RETURN
C123457
      IF (Y(N+1).LT.PNTTHK.OR.ABS(X(N+1)).LT.A) THEN
      NPTS=N+1
      GOTO 99
```

```
  END IF
95 CONTINUE
99 JJ=NPTS
  RETURN
  END
```

TMPIA.FOR

```
C PROGRAM TMPIA
C CALCULATES MPI INDICATIONS USING A THYRISTOR WAVEFORM
C Modified from J.M.McCoy MPI.for to accomadate thyristor waveforms by S.M.Westwood.

      DIMENSION X(1000), Y(1000), VX(1000), VY(1000), T(1000)
      DIMENSION XB(1000), YB(1000), VXB(1000), VYB(1000)
      COMMON ALPHA,BETA,ASPECT,GAMMA,DELTA,H,A,B,RADIUS,HO,MU,PNTTHK
      COMMON WIDTH
      H=5E-6


C  INPUT SYSTEM DATA
      OPEN(7,file='e:\stephen\results.num')
      DO 90 II=1,8
      OPEN (4,file='e:\stephen\number1.num')
      READ(4,*) RADIUS, RHOP, RHOC, ETA, HO, BDEF, ADEF
      READ(4,*) MU, NPARTS,PNTTHK,WIDTH
      DO 33 I=1,160
      READ(4,*) XB(I), YB(I), VXB(I), VYB(I)
   33 CONTINUE
      CLOSE (4)
      NEVAL=10

C EVALUATE CLUSTERS OF CONSTANTS IN DIFFERENTIAL EQUATIONS

      ASPECT=BDEF / ADEF
      ALPHA=(9*ETA) / (2*RHOP*RADIUS ** 2)
      BETA=4*3.14159265*.0000001*HO*ASPECT*(MU-1)
      BETA=BETA / (2*RHOP*ATAN(ASPECT)*(ASPECT+MU))
      GAMMA=9.80655*(RHOP-RHOC) / RHOP

C SOLVE TRAJECTORY FOR EACH PARTICLE ONE AT A TIME

      DO 600 L=1,160
      A=ADEF
      B=BDEF
      X(1)=XB(L)
      Y(1)=YB(L)
      VX(1)=VXB(L)
      VY(1)=VYB(L)
      T(1)=0


      IF (Y(1).LT.PNTTHK) THEN
      JJ=1
      GOTO 50
      END IF
      JJ=NEVAL
      IFAIL=0
      CALL PRCOXY(X, Y, VX, VY, T, JJ, IFAIL)
      IF (JJ.GE.NEVAL) THEN
```

```
   NEVAL=JJ
   GOTO 60
   END IF

 50 IFAIL=0
   CALL PRCOX(X, Y, VX, VY, T, JJ, NEVAL, IFAIL)
 60 XB(L)=X(NEVAL)
   YB(L)=Y(NEVAL)
   VXB(L)=VX(NEVAL)
   VYB(L)=VY(NEVAL)
600 CONTINUE

   OPEN(4,FILE='e:\STEPHEN\NUMBER1.NUM')
   WRITE(4,*) RADIUS, RHOP, RHOC, ETA, HO, BDEF, ADEF
   WRITE(4,*) MU, NPARTS,PNTTHK,WIDTH
   WRITE(7,*)RADIUS,RHOP,RHOC,ETA,HO,BDEF,ADEF
   WRITE(7,*)MU,NPARTS,PNTTHK,WIDTH
   DO 69 I=1,160
   WRITE(4,*) XB(I), YB(I), VXB(I), VYB(I)
   WRITE(7,*)XB(I),YB(I),VXB(I),VYB(I)
 69 CONTINUE
   CLOSE (4)
 90 CONTINUE
   CLOSE(7)
   STOP
   END

   FUNCTION THET(XX, YY, AA, BB,TIME)
   DOUBLE PRECISION C1,C2,C3,C4
   COMMON ALPHA,BETA,ASPECT,GAMMA,DELTA,H,A,B,RADIUS,HO,MU,PNTTHK
   COMMON WIDTH
   IF (TIME.GT..02.AND.TIME.LT..04)  TIME=TIME-.02
   IF (TIME.GT..04.AND.TIME.LT..06)  TIME=TIME-.04
   IF (TIME.GT..06.AND.TIME.LT..08)  TIME=TIME-.06
   IF (TIME.GT..08.AND.TIME.LT..1)  TIME=TIME-.08
   HO1=1

   SPACE=(.02-WIDTH)/2
   HO1=1
   IF (TIME.LT.(WIDTH/2)) HO1=HO
   IF (TIME.GT.(WIDTH/2).AND.TIME.LT.((WIDTH/2)+SPACE)) HO1=1
   IF (TIME.GT.((WIDTH/2)+SPACE).AND.TIME.LT.(WIDTH+SPACE)) HO1=-1*HO
   IF (TIME.GT.(WIDTH+SPACE)) HO1=1
   C1=ATAN(BB*(XX+AA) / ((XX+AA) ** 2+YY*(YY+BB)))
   C2=ATAN(BB*(XX-AA) / ((XX-AA) ** 2+YY*(YY+BB)))
   HX=HO1*ASPECT*(MU-1)*(C1-C2) / (2*ATAN(ASPECT)*(ASPECT+MU))
   C3=((XX+AA) ** 2+(YY+BB)**2)*((XX-AA)**2+YY**2)
   C4=((XX+AA) ** 2+YY ** 2)*((XX-AA) ** 2+(YY+BB)**2)
   HY=HO1*ASPECT*(MU-1)*(LOG(C3/C4))/(4*ATAN(ASPECT)*(ASPECT+MU))
   THET=ATAN(HY / (HX+HO1))
   RETURN
   END

   FUNCTION MAG(XX, YY, AA, BB,TIME)
```

```
DOUBLE PRECISION C1,C2,C3,C4
COMMON ALPHA,BETA,ASPECT,GAMMA,DELTA,H,A,B,RADIUS,HO,MU,PNTTHK
COMMON WIDTH
IF (TIME.GT..02.AND.TIME.LT..04)  TIME=TIME-.02
IF (TIME.GT..04.AND.TIME.LT..06)  TIME=TIME-.04
IF (TIME.GT..06.AND.TIME.LT..08)  TIME=TIME-.06
IF (TIME.GT..08.AND.TIME.LT..1)  TIME=TIME-.08
SPACE=(.02-WIDTH)/2
HO1=1
IF (TIME.LT.(WIDTH/2)) HO1=HO
IF (TIME.GT.(WIDTH/2).AND.TIME.LT.((WIDTH/2)+SPACE)) HO1=1
IF (TIME.GT.((WIDTH/2)+SPACE).AND.TIME.LT.(WIDTH+SPACE)) HO1=-1*HO
IF (TIME.GT.(WIDTH+SPACE)) HO1=1

C1=ATAN(BB*(XX+AA)/((XX+AA)**2+YY*(YY+BB)))
C2=ATAN(BB*(XX-AA)/((XX-AA)**2+YY*(YY+BB)))
HX=HO1*ASPECT*(MU-1)*(C1-C2) / (2*ATAN(ASPECT)*(ASPECT+MU))
C3=((XX+AA)**2+(YY+BB)**2)*((XX-AA)**2+YY**2)
C4=((XX+AA)**2+YY**2)*((XX-AA)**2+(YY+BB)**2)
HY=HO1*ASPECT*(MU-1)*(LOG(C3/C4))/(4*ATAN(ASPECT)*(ASPECT+MU))
MAG=2*SQRT(HY**2+(HO1+HX)**2)
IF (ABS(MAG).GT.471380) THEN
MAG=471380
END IF
RETURN
END

FUNCTION DHXBDX(XX, YY, AA, BB)
DOUBLE PRECISION C1,C2,C3,C4
XX=1000000*XX
YY=1000000*YY
AA=1000000*AA
BB=1000000*BB
C1=(YY+BB) / ((XX-AA) ** 2+(YY+BB)** 2)
C2=(YY+BB) / ((XX+AA) ** 2+(YY+BB) ** 2)
C3=YY / ((XX+AA) ** 2+YY ** 2)
C4=YY / ((XX-AA) ** 2+YY ** 2)
XX=.000001*XX
YY=.000001*YY
AA=.000001*AA
BB=.000001*BB
DHXBDX=(C1-C2+C3-C4)*1000000
RETURN
END

FUNCTION DHYBDX(XX, YY, AA, BB)
DOUBLE PRECISION C1,C2,C3,C4
XX=1000000*XX
YY=YY*1000000
AA=AA*1000000
BB=1000000*BB
C1=(XX+AA) / ((XX+AA) ** 2+(YY+BB) ** 2)
C2=(XX-AA) / ((XX-AA) ** 2+(YY+BB) ** 2)
C3=(XX-AA) / ((XX-AA) ** 2+YY ** 2)
```

```
C4=(XX+AA) / ((XX+AA) ** 2+YY ** 2)
XX=.000001*XX
YY=.000001*YY
AA=.000001*AA
BB=.000001*BB
DHYBDX=(C1-C2+C3-C4)*1000000
RETURN
END

FUNCTION BET(TIME)
DOUBLE PRECISION C1,C2,C3,C4
COMMON ALPHA,BETA,ASPECT,GAMMA,DELTA,H,A,B,RADIUS,HO,MU,PNTTHK
COMMON WIDTH
IF (TIME.GT..02.AND.TIME.LT..04)  TIME=TIME-.02
IF (TIME.GT..04.AND.TIME.LT..06)  TIME=TIME-.04
IF (TIME.GT..06.AND.TIME.LT..08)  TIME=TIME-.06
IF (TIME.GT..08.AND.TIME.LT..1)  TIME=TIME-.08
HO1=1

SPACE=(.02-WIDTH)/2
HO1=1
IF (TIME.LT.(WIDTH/2)) HO1=HO
IF (TIME.GT.(WIDTH/2).AND.TIME.LT.((WIDTH/2)+SPACE)) HO1=1
IF (TIME.GT.((WIDTH/2)+SPACE).AND.TIME.LT.(WIDTH+SPACE)) HO1=-1*HO
IF (TIME.GT.(WIDTH+SPACE)) HO1=1
BET=4*3.14159265*.0000001*HO*ASPECT*(MU-1)
BET=BET / (2*5240*ATAN(ASPECT)*(ASPECT+MU))
RETURN
END

SUBROUTINE PRCOX(X, Y, VX, VY, T, JJ, NEVAL, IFAIL)
DIMENSION X(1000), Y(1000), VX(1000), VY(1000), T(1000)
DIMENSION XX(1001), YY(1001), VXX(1001), VYY(1001), TT(1001)
COMMON ALPHA,BETA,ASPECT,GAMMA,DELTA,H,A,B,RADIUS,HO,MU,PNTTHK
COMMON WIDTH
CX1=0
CY1=0
CVX1=0
CVY1=0
XX(1)=X(JJ)
YY(1)=Y(JJ)
VXX(1)=VX(JJ)
VYY(1)=0
TT(1)=T(JJ)
TIME=T(JJ)
YYCST=Y(JJ)
VYYYCST=0
IF (Y(1).LT.PNTTHK.OR.ABS(XX(1)).LT.A) THEN
X(1)=X(JJ)
NPTS=1
GOTO 207
END IF
NEVAL=NEVAL-1
DO  195 N=JJ,NEVAL
```

```
      DO 190 M=1,1000

C PREDICT X,Y,VX,VY

      XX(M+1)=XX(M)+H*VXX(M)
      YY(M+1)=YYCST
      VYY(M+1)=0
      E1=DHXBDX(XX(M), YYCST, A, B)
      E2=DHYBDX(XX(M), YYCST, A, B)
      ANG=THET(XX(M), YYCST, A, B,TIME)
      FLD=MAG(XX(M), YYCST, A, B,TIME)
      U1=FLD*(E1*COS(ANG)+E2*SIN(ANG))
      U2=FLD*(E1*SIN(ANG)-E2*COS(ANG))
      BETA=BET(TIME)
      VXX(M+1)=VXX(M)+H*(-1*ALPHA*VXX(M)+BETA*U1)

C STORES FIRST PREDICTION

      FIRSX=XX(M+1)
      FIRSVX=VXX(M+1)
      ITN=1

C CORRECT X,VX

  200 CX1=XX(M)+.5*H*(VXX(M)+VXX(M+1))
      E3=DHXBDX(XX(M+1), YYCST, A, B)
      E4=DHYBDX(XX(M+1), YYCST, A, B)
      ANG=THET(XX(M+1), YYCST, A, B,TIME)
      FLD=MAG(XX(M+1), YYCST, A, B,TIME)
      BETA=BET(TIME)
      U3=FLD*(E3*COS(ANG)+E4*SIN(ANG))
      U4=FLD*(E3*SIN(ANG)-E4*COS(ANG))
      CVX1=VXX(M)-.5*H*(ALPHA*(VXX(M+1)+VXX(M))-BETA*(U3+U1))

C CHANGE ITERATION COUNTER AND CHECK LIMIT ON ITERATIONS

      Q1=ABS(XX(M+1)-CX1)
      IF (Q1.LT..000001) THEN

C CORRECT USING TRUNCATION ESTIMATE

      XX(M+1)=CX1+.2*(FIRSX-CX1)
      VXX(M+1)=CVX1+.2*(FIRSVX-CVX1)
      TT(M+1)=TT(M)+H
      TIME=TIME+H
      IF (ABS(XX(M+1)).LT.A) THEN
      XX(1001)=XX(M+1)
      YY(1001)=YYCST
      VXX(1001)=VXX(M+1)
      VYY(1001)=0
      TT(1001)=TT(M+1)
      GOTO 191
      END IF
      GOTO 190
```

```
      ELSE
      ITN=ITN+1
      END IF
      IF (ITN.GT.10) THEN
      IFAIL=1
      X(N+1)=X(N)
      Y(N+1)=Y(N)
      VX(N+1)=VX(N)
      VY(N+1)=VY(N)
      NPTS=N+1
      GOTO 209
      ELSE

C ELSE RECORRECT

      XX(M+1)=CX1
      VXX(M+1)=CVX1
      END IF
      GOTO 200
  190 CONTINUE
  191 X(N+1)=XX(1001)
      Y(N+1)=YYCST
      VX(N+1)=VXX(1001)
      VY(N+1)=0
      T(N+1)=TT(1001)
      XX(1)=XX(1001)
      YY(1)=YYCST
      VXX(1)=VXX(1001)
      VYY(1)=0
      TT(1)=TT(1001)
      NPTS=N+1
      IF (ABS(X(N+1)).LT.A) THEN
      NPTS=N+1
      GOTO 199
      END IF
  195 CONTINUE
  199 IF (ABS(X(NPTS)).LT.A) THEN

C PARTICLE TRAPPED AT DEFECT TAKE LAST VALUE

  207 NEVAL=NEVAL-1
      DO 201 I=NPTS ,NEVAL
      X(I+1)=X(NPTS)
      Y(I+1)=YYCST
      VX(I+1)=0
      VY(I+1)=0
      T(I+1)=T(I)+(1000*H)
  201 CONTINUE
      NEVAL=NEVAL+1
      END IF

  209 RETURN

      END
```

```
      SUBROUTINE PRCOXY(X, Y, VX, VY, T, JJ, IFAIL)
      DIMENSION X(1000), Y(1000), VX(1000), VY(1000), T(1000)
      DIMENSION XX(1001), YY(1001), VXX(1001), VYY(1001), TT(1001)
      COMMON ALPHA,BETA,ASPECT,GAMMA,DELTA,H,A,B,RADIUS,HO,MU,PNTTHK
      COMMON WIDTH
      CX1=0
      CY1=0
      CVX1=0
      CVY1=0
      XX(1)=X(1)
      YY(1)=Y(1)
      VXX(1)=VX(1)
      VYY(1)=VY(1)
      TT(1)=T(1)
      TIME=T(1)
      JJ=JJ-1
      DO 95  N=1, JJ
      DO 90 M=1 , 1000
      TIME=TT(M)
      XX(M+1)=XX(M)+H*VXX(M)
      YY(M+1)=YY(M)+H*VYY(M)
      E1=DHXBDX(XX(M), YY(M), A, B)
      E2=DHYBDX(XX(M), YY(M), A, B)

      ANG=THET(XX(M), YY(M), A, B,TIME)
      FLD=MAG(XX(M), YY(M), A, B,TIME)
      U1=FLD*(E1*COS(ANG)+E2*SIN(ANG))
      U2=FLD*(E1*SIN(ANG)-E2*COS(ANG))
      BETA=BET(TIME)
      VXX(M+1)=VXX(M)+H*(-1*ALPHA*VXX(M)+BETA*U1)
      VYY(M+1)=VYY(M)+H*(-1*ALPHA*VYY(M)-BETA*U2-GAMMA)
      FIRSX=XX(M+1)
      FIRSY=YY(M+1)
      FIRSVX=VXX(M+1)
      FIRSVY=VYY(M+1)
      ITN=1
  100 CX1=XX(M)+.5*H*(VXX(M)+VXX(M+1))
      CY1=YY(M)+.5*H*(VYY(M)+VYY(M+1))
      E3=DHXBDX(XX(M+1), YY(M+1), A, B)
      E4=DHYBDX(XX(M+1), YY(M+1), A, B)
      ANG=THET(XX(M+1), YY(M+1), A, B,TIME)
      FLD=MAG(XX(M+1), YY(M+1), A, B,TIME)
      BETA=BET(TIME)
      U3=FLD*(E3*COS(ANG)+E4*SIN(ANG))
      U4=FLD*(E3*SIN(ANG)-E4*COS(ANG))
      CVX1=VXX(M)-.5*H*(ALPHA*(VXX(M+1)+VXX(M))-BETA*(U3+U1))
      CVY1=VYY(M)-H*(ALPHA*(VYY(M+1)+VYY(M))+BETA*(U2+U4)+2*GAMMA) / 2
      Q1=ABS(XX(M+1)-CX1)
      Q2=ABS(YY(M+1)-CY1)
      IF (Q1.LT..000001.AND.Q2.LT..000001) THEN
      XX(M+1)=CX1+.2*(FIRSX-CX1)
      YY(M+1)=CY1+.2*(FIRSY-CY1)
      VXX(M+1)=CVX1+.2*(FIRSVX-CVX1)
```

```
      VYY(M+1)=CVY1+.2*(FIRSVY-CVY1)
      TT(M+1)=TT(M)+H
      TIME=TIME+H
      IF (YY(M+1).LT.PNTTHK.OR.ABS(XX(M+1)).LT.A) THEN
      XX(1001)=XX(M+1)
      YY(1001)=YY(M+1)
      VXX(1001)=VXX(M+1)
      VYY(1001)=VYY(M+1)
      TT(1001)=TT(M+1)
      GOTO 91
      END IF
      GOTO 90
      ELSE
      ITN=ITN+1
      END IF
      IF (ITN.GT.10) THEN
      IFAIL=1
      X(N+1)=X(N)
      Y(N+1)=Y(N)
      VX(N+1)=VX(N)
      VY(N+1)=VY(N)
      NPTS=N+1
      GOTO 99
      ELSE
      XX(M+1)=CX1
      YY(M+1)=CY1
      VXX(M+1)=CVX1
      VYY(M+1)=CVY1
      END IF

C ELSE RECORRECT

      GOTO 100
   90 CONTINUE
   91 X(N+1)=XX(1001)
      Y(N+1)=YY(1001)
      VX(N+1)=VXX(1001)
      VY(N+1)=VYY(1001)
      T(N+1)=TT(1001)
      XX(1)=XX(1001)
      YY(1)=YY(1001)
      VXX(1)=VXX(1001)
      VYY(1)=VYY(1001)
      TT(1)=TT(1001)
      NPTS=N+1


C IF PARTICLE HAS HIT INTERFACE OR TRAPPED THEN RETURN

      IF (Y(N+1).LT.PNTTHK.OR.ABS(X(N+1)).LT.A) THEN
      NPTS=N+1
      GOTO 99
      END IF
   95 CONTINUE
```

```
99 JJ=NPTS
   RETURN
   END
```

MAGX.FOR

```
C ALLOWS THE MAGNETISATION TO BE FIXED
C Modified from McCoy Code by S.M.Westwood to allow the magnetic moment of the particles to be
C fixed

      DIMENSION X(1000), Y(1000), VX(1000), VY(1000), T(1000)
      DIMENSION XB(1000), YB(1000), VXB(1000), VYB(1000)
      COMMON ALPHA,BETA,ASPECT,GAMMA,DELTA,H,A,B,RADIUS,HO,MU,PNTTHK
      COMMON MAGX
      H=5E-6


C  INPUT SYSTEM DATA
C123457
      OPEN(7,FILE='E:\STEPHEN\RESULTS.NUM')
      DO 97 LL=1,8
      OPEN (4,file='E:\stephen\number1.num')
      READ(4,*) RADIUS, RHOP, RHOC, ETA, HO, BDEF, ADEF
      READ(4,*) MU, NPARTS,PNTTHK,MAGX
      DO 33 I=1,160
      READ(4,*) XB(I), YB(I), VXB(I), VYB(I)
   33 CONTINUE
      CLOSE (4)
      NEVAL=10

C EVALUATE CLUSTERS OF CONSTANTS IN DIFFERENTIAL EQUATIONS
C123457
      ASPECT=BDEF / ADEF
      ALPHA=(9*ETA) / (2*RHOP*(RADIUS ** 2))
      BETA=4*3.14159265*1.0E-7*HO*ASPECT*(MU-1)
      BETA=BETA / (2*RHOP*ATAN(ASPECT)*(ASPECT+MU))
      GAMMA=(9.80655*(RHOP-RHOC)) / RHOP
C SOLVE TRAJECTORY FOR EACH PARTICLE ONE AT A TIME


      DO 600 L=1,160
      A=ADEF
      B=BDEF
      X(1)=XB(L)
      Y(1)=YB(L)
      VX(1)=VXB(L)
      VY(1)=VYB(L)
      T(1)=0


      IF (Y(1).LT.PNTTHK) THEN
      JJ=1
      GOTO 50
C     Change to 600 to allow viscoity effect to be modelled
      END IF
      JJ=NEVAL
```

```
      IFAIL=0
      CALL PRCOXY(X, Y, VX, VY, T, JJ, IFAIL)
      IF (JJ.GE.NEVAL) THEN
      NEVAL=JJ
      GOTO 60
      END IF
C123467
   50 IFAIL=0
      CALL PRCOX(X, Y, VX, VY, T, JJ, NEVAL, IFAIL)
   60 XB(L)=X(NEVAL)
      YB(L)=Y(NEVAL)
      VXB(L)=VX(NEVAL)
      VYB(L)=VY(NEVAL)
  600 CONTINUE

C123457
      OPEN(4,FILE='E:\STEPHEN\NUMBER1.NUM')
      WRITE(4,*) RADIUS, RHOP, RHOC, ETA, HO, BDEF, ADEF
      WRITE(4,*) MU, NPARTS,PNTTHK,MAGX
      WRITE(7,*) RADIUS,RHOP,RHOC,ETA,HO,BDEF,ADEF
      WRITE(7,*) MU,NPARTS,PNTTHK,MAGX
      DO 69 I=1,160
      WRITE(4,*) XB(I), YB(I), VXB(I), VYB(I)
      WRITE(7,*)XB(I),YB(I),VXB(I),VYB(I)
   69 CONTINUE
      CLOSE (4)
   97 CONTINUE
      CLOSE(7)
      STOP
      END


      FUNCTION THET(XX, YY, AA, BB)
      DOUBLE PRECISION C1,C2,C3,C4
      COMMON ALPHA,BETA,ASPECT,GAMMA,DELTA,H,A,B,RADIUS,HO,MU,PNTTHK
      COMMON MAGX
      C1=ATAN(BB*(XX+AA) / ((XX+AA) ** 2+YY*(YY+BB)))
      C2=ATAN(BB*(XX-AA) / ((XX-AA) ** 2+YY*(YY+BB)))
      HX=HO*ASPECT*(MU-1)*(C1-C2) / (2*ATAN(ASPECT)*(ASPECT+MU))
      C3=((XX+AA) ** 2+(YY+BB)**2)*((XX-AA)**2+YY**2)
      C4=((XX+AA) ** 2+YY ** 2)*((XX-AA) ** 2+(YY+BB)**2)
      HY=(MU-1)*(LOG(C3/C4))/(4*ATAN(ASPECT)*(ASPECT+MU))
      HY=HY*ASPECT*HO
      THET=ATAN(HY / (HX+HO))
      RETURN
      END

      FUNCTION MAG(XX, YY, AA, BB)
      DOUBLE PRECISION C1,C2,C3,C4
      COMMON ALPHA,BETA,ASPECT,GAMMA,DELTA,H,A,B,RADIUS,HO,MU,PNTTHK
      COMMON MAGX
      MAG=MAGX
      RETURN
      END
```

```
      FUNCTION DHXBDX(XX, YY, AA, BB)
      DOUBLE PRECISION C1,C2,C3,C4
      XX=1000000*XX
      YY=1000000*YY
      AA=1000000*AA
      BB=1000000*BB
      C1=(YY+BB) / ((XX-AA) ** 2+(YY+BB)** 2)
      C2=(YY+BB) / ((XX+AA) ** 2+(YY+BB) ** 2)
      C3=YY / ((XX+AA) ** 2+YY ** 2)
      C4=YY / ((XX-AA) ** 2+YY ** 2)
      XX=.000001*XX
      YY=.000001*YY
      AA=.000001*AA
      BB=.000001*BB
      DHXBDX=(C1-C2+C3-C4)*1000000
      RETURN
      END

      FUNCTION DHYBDX(XX, YY, AA, BB)
      DOUBLE PRECISION C1,C2,C3,C4
      XX=1000000*XX
      YY=YY*1000000
      AA=AA*1000000
      BB=1000000*BB
      C1=(XX+AA) / ((XX+AA) ** 2+(YY+BB) ** 2)
      C2=(XX-AA) / ((XX-AA) ** 2+(YY+BB) ** 2)
      C3=(XX-AA) / ((XX-AA) ** 2+YY ** 2)
      C4=(XX+AA) / ((XX+AA) ** 2+YY ** 2)
      XX=.000001*XX
      YY=.000001*YY
      AA=.000001*AA
      BB=.000001*BB
      DHYBDX=(C1-C2+C3-C4)*1000000
      RETURN
      END


      SUBROUTINE PRCOX(X, Y, VX, VY, T, JJ, NEVAL, IFAIL)
      DIMENSION X(1000), Y(1000), VX(1000), VY(1000), T(1000)
      DIMENSION XX(1001), YY(1001), VXX(1001), VYY(1001), TT(1001)
C     DOUBLE PRECISION X,Y,VX,T,XX,YY,VXX,VYY,TT,CX1,CY1,CVX1,CVY1
C     DOUBLE PRECISION YYCST,VYYCST
      COMMON ALPHA,BETA,ASPECT,GAMMA,DELTA,H,A,B,RADIUS,HO,MU,PNTTHK
      COMMON MAGX
      CX1=0
      CY1=0
      CVX1=0
      CVY1=0
      XX(1)=X(JJ)
      YY(1)=Y(JJ)
      VXX(1)=VX(JJ)
      VYY(1)=0
      TT(1)=T(JJ)
```

```
      YYCST=Y(JJ)
      VYYCST=0
      IF (Y(1).LT.PNTTHK.OR.ABS(XX(1)).LT.A) THEN
      X(1)=X(JJ)
      NPTS=1
      GOTO 207
      END IF
      NEVAL=NEVAL-1
      DO  195 N=JJ,NEVAL
      DO 190 M=1,1000
C PREDICT X,Y,VX,VY

      XX(M+1)=XX(M)+H*VXX(M)
      YY(M+1)=YYCST
      VYY(M+1)=0
      E1=DHXBDX(XX(M), YYCST, A, B)
      E2=DHYBDX(XX(M), YYCST, A, B)
      ANG=THET(XX(M), YYCST, A, B)
      FLD=MAG(XX(M), YYCST, A, B)
      U1=FLD*(E1*COS(ANG)+E2*SIN(ANG))
      U2=FLD*(E1*SIN(ANG)-E2*COS(ANG))
      VXX(M+1)=VXX(M)+H*(-1*ALPHA*VXX(M)+BETA*U1)

C STORES FIRST PREDICTION

      FIRSX=XX(M+1)
      FIRSVX=VXX(M+1)
      ITN=1

C CORRECT X,VX
C123457
  200 CX1=XX(M)+.5*H*(VXX(M)+VXX(M+1))
      E3=DHXBDX(XX(M+1), YYCST, A, B)
      E4=DHYBDX(XX(M+1), YYCST, A, B)
      ANG=THET(XX(M+1), YYCST, A, B)
      FLD=MAG(XX(M+1), YYCST, A, B)
      U3=FLD*(E3*COS(ANG)+E4*SIN(ANG))
      U4=FLD*(E3*SIN(ANG)-E4*COS(ANG))
      CVX1=VXX(M)-.5*H*(ALPHA*(VXX(M+1)+VXX(M))-BETA*(U3+U1))

C CHANGE ITERATION COUNTER AND CHECK LIMIT ON ITERATIONS

      Q1=ABS(XX(M+1)-CX1)
      IF (Q1.LT..000001) THEN

C CORRECT USING TRUNCATION ESTIMATE

      XX(M+1)=CX1+.2*(FIRSX-CX1)
      VXX(M+1)=CVX1+.2*(FIRSVX-CVX1)
      TT(M+1)=TT(M)+H
      IF (ABS(XX(M+1)).LT.A) THEN
      XX(1001)=XX(M+1)
      YY(1001)=YYCST
      VXX(1001)=VXX(M+1)
```

```
      VYY(1001)=0
      TT(1001)=TT(M+1)
      GOTO 191
      END IF
      GOTO 190
      ELSE
      ITN=ITN+1
      END IF
      IF (ITN.GT.10) THEN
      IFAIL=1
      X(N+1)=X(N)
      Y(N+1)=Y(N)
      VX(N+1)=VX(N)
      VY(N+1)=VY(N)
      NPTS=N+1
      GOTO 209
      ELSE
C ELSE RECORRECT
      XX(M+1)=CX1
      VXX(M+1)=CVX1
      END IF
      GOTO 200
  190 CONTINUE
  191 X(N+1)=XX(1001)
      Y(N+1)=YYCST
      VX(N+1)=VXX(1001)
      VY(N+1)=0
      T(N+1)=TT(1001)
      XX(1)=XX(1001)
      YY(1)=YYCST
      VXX(1)=VXX(1001)
      VYY(1)=0
      TT(1)=TT(1001)
      NPTS=N+1
      IF (ABS(X(N+1)).LT.A) THEN
      NPTS=N+1
      GOTO 199
      END IF
  195 CONTINUE
  199 IF (ABS(X(NPTS)).LT.A) THEN

C PARTICLE TRAPPED AT DEFECT TAKE LAST VALUE
C123457
  207 NEVAL=NEVAL-1
      DO 201 I=NPTS ,NEVAL
      X(I+1)=X(NPTS)
      Y(I+1)=YYCST
      VX(I+1)=0
      VY(I+1)=0
      T(I+1)=T(I)+(1000*H)
  201 CONTINUE
      NEVAL=NEVAL+1
      END IF
```

```
 209 RETURN

     END

     SUBROUTINE PRCOXY(X, Y, VX, VY, T, JJ, IFAIL)
     DIMENSION X(1000), Y(1000), VX(1000), VY(1000), T(1000)
     DIMENSION XX(1001), YY(1001), VXX(1001), VYY(1001), TT(1001)
C    DOUBLE PRECISION X,Y,VX,VY,T,XX,YY,VXX,VYY,TT,CX1,CY1,CVX1,CVY1
     COMMON ALPHA,BETA,ASPECT,GAMMA,DELTA,H,A,B,RADIUS,HO,MU,PNTTHK
     COMMON MAGX
     CX1=0
     CY1=0
     CVX1=0
     CVY1=0
     XX(1)=X(1)
     YY(1)=Y(1)
     VXX(1)=VX(1)
     VYY(1)=VY(1)
     TT(1)=T(1)
     JJ=JJ-1
     DO 95  N=1, JJ
     DO 90 M=1 , 1000
     XX(M+1)=XX(M)+H*VXX(M)
     YY(M+1)=YY(M)+H*VYY(M)
     E1=DHXBDX(XX(M), YY(M), A, B)
     E2=DHYBDX(XX(M), YY(M), A, B)
     ANG=THET(XX(M), YY(M), A, B)
     FLD=MAG(XX(M), YY(M), A, B)
     U1=FLD*(E1*COS(ANG)+E2*SIN(ANG))
     U2=FLD*(E1*SIN(ANG)-E2*COS(ANG))
     VXX(M+1)=VXX(M)+H*(-1*ALPHA*VXX(M)+BETA*U1)
     VYY(M+1)=VYY(M)+H*(-1*ALPHA*VYY(M)-BETA*U2-GAMMA)
     FIRSX=XX(M+1)
     FIRSY=YY(M+1)
     FIRSVX=VXX(M+1)
     FIRSVY=VYY(M+1)
     ITN=1
 100 CX1=XX(M)+.5*H*(VXX(M)+VXX(M+1))
     CY1=YY(M)+.5*H*(VYY(M)+VYY(M+1))
     E3=DHXBDX(XX(M+1), YY(M+1), A, B)
     E4=DHYBDX(XX(M+1), YY(M+1), A, B)
     ANG=THET(XX(M+1), YY(M+1), A, B)
     FLD=MAG(XX(M+1), YY(M+1), A, B)

C123457
     U3=FLD*(E3*COS(ANG)+E4*SIN(ANG))
     U4=FLD*(E3*SIN(ANG)-E4*COS(ANG))
     CVX1=VXX(M)-.5*H*(ALPHA*(VXX(M+1)+VXX(M))-BETA*(U3+U1))
     CVY1=VYY(M)-.5*H*(ALPHA*(VYY(M+1)+VYY(M))+BETA*(U2+U4)+2*GAMMA)
     Q1=ABS(XX(M+1)-CX1)
     Q2=ABS(YY(M+1)-CY1)
     IF (Q1.LT..000001.AND.Q2.LT..000001) THEN
     XX(M+1)=CX1+.2*(FIRSX-CX1)
     YY(M+1)=CY1+.2*(FIRSY-CY1)
```

```
      VXX(M+1)=CVX1+.2*(FIRSVX-CVX1)
      VYY(M+1)=CVY1+.2*(FIRSVY-CVY1)
      TT(M+1)=TT(M)+H
      IF (YY(M+1).LT.PNTTHK.OR.ABS(XX(M+1)).LT.A) THEN
      XX(1001)=XX(M+1)
      YY(1001)=YY(M+1)
      VXX(1001)=VXX(M+1)
      VYY(1001)=VYY(M+1)
      TT(1001)=TT(M+1)
      GOTO 91
      END IF
      GOTO 90
      ELSE
      ITN=ITN+1
      END IF
      IF (ITN.GT.10) THEN
      IFAIL=1
      X(N+1)=X(N)
      Y(N+1)=Y(N)
      VX(N+1)=VX(N)
      VY(N+1)=VY(N)
      NPTS=N+1
      GOTO 99
      ELSE
      XX(M+1)=CX1
      YY(M+1)=CY1
      VXX(M+1)=CVX1
      VYY(M+1)=CVY1
      END IF

C ELSE RECORRECT
      GOTO 100
   90 CONTINUE
   91 X(N+1)=XX(1001)
      Y(N+1)=YY(1001)
      VX(N+1)=VXX(1001)
      VY(N+1)=VYY(1001)
      T(N+1)=TT(1001)
      XX(1)=XX(1001)
      YY(1)=YY(1001)
      VXX(1)=VXX(1001)
      VYY(1)=VYY(1001)
      TT(1)=TT(1001)
      NPTS=N+1


C IF PARTICLE HAS HIT INTERFACE OR TRAPPED THEN RETURN
C123457
      IF (Y(N+1).LT.PNTTHK.OR.ABS(X(N+1)).LT.A) THEN
      NPTS=N+1
      GOTO 99
      END IF
   95 CONTINUE
   99 JJ=NPTS
```

```
RETURN
END
```

SINMPI.FOR

```
C PROGRAM SINMPI
C CALCULATES MPI INDICATIONS USING A SIN WAVE
C Modified from J.M.McCoy code to accomadate time varying waveforms by S.M.Westwood

      DIMENSION X(1000), Y(1000), VX(1000), VY(1000), T(1000)
      DIMENSION XB(1000), YB(1000), VXB(1000), VYB(1000)
      COMMON ALPHA,BETA,ASPECT,GAMMA,DELTA,H,A,B,RADIUS,HO,MU,PNTTHK
      H=5E-6


C  INPUT SYSTEM DATA
      OPEN(7,file='E:\stephen\results.num')
      DO 90 II=1,8
      OPEN (4,file='E:\stephen\number1.num')
      READ(4,*) RADIUS, RHOP, RHOC, ETA, HO, BDEF, ADEF
      READ(4,*) MU, NPARTS,PNTTHK
      DO 33 I=1,160
      READ(4,*) XB(I), YB(I), VXB(I), VYB(I)
 33   CONTINUE
      CLOSE (4)
      NEVAL=10

C EVALUATE CLUSTERS OF CONSTANTS IN DIFFERENTIAL EQUATIONS

      ASPECT=BDEF / ADEF
      ALPHA=(9*ETA) / (2*RHOP*RADIUS ** 2)
      BETA=4*3.14159265*.0000001*HO*ASPECT*(MU-1)
      BETA=BETA / (2*RHOP*ATAN(ASPECT)*(ASPECT+MU))
      GAMMA=9.80655*(RHOP-RHOC) / RHOP

C SOLVE TRAJECTORY FOR EACH PARTICLE ONE AT A TIME

      DO 600 L=1,160
      A=ADEF
      B=BDEF
      X(1)=XB(L)
      Y(1)=YB(L)
      VX(1)=VXB(L)
      VY(1)=VYB(L)
      T(1)=0


      IF (Y(1).LT.PNTTHK) THEN
      JJ=1
      GOTO 50
      END IF
      JJ=NEVAL
      IFAIL=0
      CALL PRCOXY(X, Y, VX, VY, T, JJ, IFAIL)
      IF (JJ.GE.NEVAL) THEN
      NEVAL=JJ
```

```
   GOTO 60
   END IF

 50 IFAIL=0
   CALL PRCOX(X, Y, VX, VY, T, JJ, NEVAL, IFAIL)
 60 XB(L)=X(NEVAL)
   YB(L)=Y(NEVAL)
   VXB(L)=VX(NEVAL)
   VYB(L)=VY(NEVAL)
600 CONTINUE

   OPEN(4,FILE='E:\STEPHEN\NUMBER1.NUM')
   WRITE(4,*) RADIUS, RHOP, RHOC, ETA, HO, BDEF, ADEF
   WRITE(4,*) MU, NPARTS,PNTTHK
   WRITE(7,*)RADIUS,RHOP,RHOC,ETA,HO,BDEF,ADEF
   WRITE(7,*)MU,NPARTS,PNTTHK
   DO 69 I=1,160
   WRITE(4,*) XB(I), YB(I), VXB(I), VYB(I)
   WRITE(7,*)XB(I),YB(I),VXB(I),VYB(I)
 69 CONTINUE
   CLOSE (4)
 90 CONTINUE
   CLOSE(7)
   STOP
   END

   FUNCTION THET(XX, YY, AA, BB,TIME)
   DOUBLE PRECISION C1,C2,C3,C4
   COMMON ALPHA,BETA,ASPECT,GAMMA,DELTA,H,A,B,RADIUS,HO,MU,PNTTHK
   IF (TIME.GT..02.AND.TIME.LT..04)  TIME=TIME-.02
   IF (TIME.GT..04.AND.TIME.LT..06)  TIME=TIME-.04
   IF (TIME.GT..06.AND.TIME.LT..08)  TIME=TIME-.06
   IF (TIME.GT..08.AND.TIME.LT..1)  TIME=TIME-.08
   HO1=HO*(SIN(100*3.14159265*TIME))+1
   MU=(.1*80*1E4+(.62*80*1E4*HO1)/HO)/HO1
   C1=ATAN(BB*(XX+AA) / ((XX+AA) ** 2+YY*(YY+BB)))
   C2=ATAN(BB*(XX-AA) / ((XX-AA) ** 2+YY*(YY+BB)))
   HX=HO1*ASPECT*(MU-1)*(C1-C2) / (2*ATAN(ASPECT)*(ASPECT+MU))
   C3=((XX+AA) ** 2+(YY+BB)**2)*((XX-AA)**2+YY**2)
   C4=((XX+AA) ** 2+YY ** 2)*((XX-AA) ** 2+(YY+BB)**2)
   HY=HO1*ASPECT*(MU-1)*(LOG(C3/C4))/(4*ATAN(ASPECT)*(ASPECT+MU))
   THET=ATAN(HY / (HX+HO1))
   RETURN
   END

   FUNCTION MAG(XX, YY, AA, BB,TIME)
   DOUBLE PRECISION C1,C2,C3,C4
   COMMON ALPHA,BETA,ASPECT,GAMMA,DELTA,H,A,B,RADIUS,HO,MU,PNTTHK
   IF (TIME.GT..02.AND.TIME.LT..04)  TIME=TIME-.02
   IF (TIME.GT..04.AND.TIME.LT..06)  TIME=TIME-.04
   IF (TIME.GT..06.AND.TIME.LT..08)  TIME=TIME-.06
   IF (TIME.GT..08.AND.TIME.LT..1)  TIME=TIME-.08
   HO1=HO*(SIN(100*3.14159265*TIME))+1
   MU=(.1*80*1E4+(.62*80*1E4*HO1)/HO)/HO1
```

```
C1=ATAN(BB*(XX+AA)/((XX+AA)**2+YY*(YY+BB)))
C2=ATAN(BB*(XX-AA)/((XX-AA)**2+YY*(YY+BB)))
HX=HO1*ASPECT*(MU-1)*(C1-C2) / (2*ATAN(ASPECT)*(ASPECT+MU))
C3=((XX+AA)**2+(YY+BB)**2)*((XX-AA)**2+YY**2)
C4=((XX+AA)**2+YY**2)*((XX-AA)**2+(YY+BB)**2)
HY=HO1*ASPECT*(MU-1)*(LOG(C3/C4))/(4*ATAN(ASPECT)*(ASPECT+MU))
MAG=2*SQRT(HY**2+(HO1+HX)**2)
IF (ABS(MAG).GT.471380) THEN
MAG=471380
END IF
RETURN
END

FUNCTION DHXBDX(XX, YY, AA, BB)
DOUBLE PRECISION C1,C2,C3,C4
XX=1000000*XX
YY=1000000*YY
AA=1000000*AA
BB=1000000*BB
C1=(YY+BB) / ((XX-AA) ** 2+(YY+BB)** 2)
C2=(YY+BB) / ((XX+AA) ** 2+(YY+BB) ** 2)
C3=YY / ((XX+AA) ** 2+YY ** 2)
C4=YY / ((XX-AA) ** 2+YY ** 2)
XX=.000001*XX
YY=.000001*YY
AA=.000001*AA
BB=.000001*BB
DHXBDX=(C1-C2+C3-C4)*1000000
RETURN
END

FUNCTION DHYBDX(XX, YY, AA, BB)
DOUBLE PRECISION C1,C2,C3,C4
XX=1000000*XX
YY=YY*1000000
AA=AA*1000000
BB=1000000*BB
C1=(XX+AA) / ((XX+AA) ** 2+(YY+BB) ** 2)
C2=(XX-AA) / ((XX-AA) ** 2+(YY+BB) ** 2)
C3=(XX-AA) / ((XX-AA) ** 2+YY ** 2)
C4=(XX+AA) / ((XX+AA) ** 2+YY ** 2)
XX=.000001*XX
YY=.000001*YY
AA=.000001*AA
BB=.000001*BB
DHYBDX=(C1-C2+C3-C4)*1000000
RETURN
END

FUNCTION BET(TIME)
DOUBLE PRECISION C1,C2,C3,C4
COMMON ALPHA,BETA,ASPECT,GAMMA,DELTA,H,A,B,RADIUS,HO,MU,PNTTHK
IF (TIME.GT..02.AND.TIME.LT..04)  TIME=TIME-.02
IF (TIME.GT..04.AND.TIME.LT..06)  TIME=TIME-.04
```

```
      IF (TIME.GT..06.AND.TIME.LT..08)  TIME=TIME-.06
      IF (TIME.GT..08.AND.TIME.LT..1)  TIME=TIME-.08
      HO1=HO*ABS((SIN(100*3.14159265*TIME)))+1
      MU=1400
      BET=4*3.14159265*.0000001*HO1*ASPECT*(MU-1)
      BET=BET / (2*5240*ATAN(ASPECT)*(ASPECT+MU))
      RETURN
      END

      SUBROUTINE PRCOX(X, Y, VX, VY, T, JJ, NEVAL, IFAIL)
      DIMENSION X(1000), Y(1000), VX(1000), VY(1000), T(1000)
      DIMENSION XX(1001), YY(1001), VXX(1001), VYY(1001), TT(1001)
      COMMON ALPHA,BETA,ASPECT,GAMMA,DELTA,H,A,B,RADIUS,HO,MU,PNTTHK
      CX1=0
      CY1=0
      CVX1=0
      CVY1=0
      XX(1)=X(JJ)
      YY(1)=Y(JJ)
      VXX(1)=VX(JJ)
      VYY(1)=0
      TT(1)=T(JJ)
      YYCST=Y(JJ)
      VYYYCST=0
      IF (Y(1).LT.PNTTHK.OR.ABS(XX(1)).LT.A) THEN
      X(1)=X(JJ)
      NPTS=1
      GOTO 207
      END IF
      NEVAL=NEVAL-1
      DO  195 N=JJ,NEVAL
      DO 190 M=1,1000

C PREDICT X,Y,VX,VY

      TIME=TT(M)
      XX(M+1)=XX(M)+H*VXX(M)
      YY(M+1)=YYCST
      VYY(M+1)=0
      E1=DHXBDX(XX(M), YYCST, A, B)
      E2=DHYBDX(XX(M), YYCST, A, B)
      ANG=THET(XX(M), YYCST, A, B,TIME)
      FLD=MAG(XX(M), YYCST, A, B,TIME)
      BETA=BET(TIME)
      U1=FLD*(E1*COS(ANG)+E2*SIN(ANG))
      U2=FLD*(E1*SIN(ANG)-E2*COS(ANG))
      VXX(M+1)=VXX(M)+H*(-1*ALPHA*VXX(M)+BETA*U1)

C STORES FIRST PREDICTION

      FIRSX=XX(M+1)
      FIRSVX=VXX(M+1)
      ITN=1
```

```
C CORRECT X,VX

  200 CX1=XX(M)+.5*H*(VXX(M)+VXX(M+1))
      E3=DHXBDX(XX(M+1), YYCST, A, B)
      E4=DHYBDX(XX(M+1), YYCST, A, B)
      ANG=THET(XX(M+1), YYCST, A, B,TIME)
      FLD=MAG(XX(M+1), YYCST, A, B,TIME)
      BETA=BET(TIME)
      U3=FLD*(E3*COS(ANG)+E4*SIN(ANG))
      U4=FLD*(E3*SIN(ANG)-E4*COS(ANG))
      CVX1=VXX(M)-.5*H*(ALPHA*(VXX(M+1)+VXX(M))-BETA*(U3+U1))

C CHANGE ITERATION COUNTER AND CHECK LIMIT ON ITERATIONS

      Q1=ABS(XX(M+1)-CX1)
      IF (Q1.LT..000001) THEN

C CORRECT USING TRUNCATION ESTIMATE

      XX(M+1)=CX1+.2*(FIRSX-CX1)
      VXX(M+1)=CVX1+.2*(FIRSVX-CVX1)
      TT(M+1)=TT(M)+H
      IF (ABS(XX(M+1)).LT.A) THEN
      XX(1001)=XX(M+1)
      YY(1001)=YYCST
      VXX(1001)=VXX(M+1)
      VYY(1001)=0
      TT(1001)=TT(M+1)
      GOTO 191
      END IF
      GOTO 190
      ELSE
      ITN=ITN+1
      END IF
      IF (ITN.GT.10) THEN
      IFAIL=1
      X(N+1)=X(N)
      Y(N+1)=Y(N)
      VX(N+1)=VX(N)
      VY(N+1)=VY(N)
      NPTS=N+1
      GOTO 209
      ELSE

C ELSE RECORRECT

      XX(M+1)=CX1
      VXX(M+1)=CVX1
      END IF
      GOTO 200
  190 CONTINUE
  191 X(N+1)=XX(1001)
      Y(N+1)=YYCST
      VX(N+1)=VXX(1001)
```

```
      VY(N+1)=0
      T(N+1)=TT(1001)
      XX(1)=XX(1001)
      YY(1)=YYCST
      VXX(1)=VXX(1001)
      VYY(1)=0
      TT(1)=TT(1001)
      NPTS=N+1
      IF (ABS(X(N+1)).LT.A) THEN
      NPTS=N+1
      GOTO 199
      END IF
  195 CONTINUE
  199 IF (ABS(X(NPTS)).LT.A) THEN

C PARTICLE TRAPPED AT DEFECT TAKE LAST VALUE

  207 NEVAL=NEVAL-1
      DO 201 I=NPTS ,NEVAL
      X(I+1)=X(NPTS)
      Y(I+1)=YYCST
      VX(I+1)=0
      VY(I+1)=0
      T(I+1)=T(I)+(1000*H)
  201 CONTINUE
      NEVAL=NEVAL+1
      END IF

  209 RETURN

      END

      SUBROUTINE PRCOXY(X, Y, VX, VY, T, JJ, IFAIL)
      DIMENSION X(1000), Y(1000), VX(1000), VY(1000), T(1000)
      DIMENSION XX(1001), YY(1001), VXX(1001), VYY(1001), TT(1001)
      COMMON ALPHA,BETA,ASPECT,GAMMA,DELTA,H,A,B,RADIUS,HO,MU,PNTTHK
      CX1=0
      CY1=0
      CVX1=0
      CVY1=0
      XX(1)=X(1)
      YY(1)=Y(1)
      VXX(1)=VX(1)
      VYY(1)=VY(1)
      TT(1)=T(1)
      JJ=JJ-1
      DO 95  N=1, JJ
      DO 90 M=1 , 1000
      TIME=TT(M)
      XX(M+1)=XX(M)+H*VXX(M)
      YY(M+1)=YY(M)+H*VYY(M)
      E1=DHXBDX(XX(M), YY(M), A, B)
      E2=DHYBDX(XX(M), YY(M), A, B)
```

```
  ANG=THET(XX(M), YY(M), A, B,TIME)
  FLD=MAG(XX(M), YY(M), A, B,TIME)
  BETA=BET(TIME)
  U1=FLD*(E1*COS(ANG)+E2*SIN(ANG))
  U2=FLD*(E1*SIN(ANG)-E2*COS(ANG))
  VXX(M+1)=VXX(M)+H*(-1*ALPHA*VXX(M)+BETA*U1)
  VYY(M+1)=VYY(M)+H*(-1*ALPHA*VYY(M)-BETA*U2-GAMMA)
  FIRSX=XX(M+1)
  FIRSY=YY(M+1)
  FIRSVX=VXX(M+1)
  FIRSVY=VYY(M+1)
  ITN=1
100 CX1=XX(M)+.5*H*(VXX(M)+VXX(M+1))
  CY1=YY(M)+.5*H*(VYY(M)+VYY(M+1))
  E3=DHXBDX(XX(M+1), YY(M+1), A, B)
  E4=DHYBDX(XX(M+1), YY(M+1), A, B)
  ANG=THET(XX(M+1), YY(M+1), A, B,TIME)
  FLD=MAG(XX(M+1), YY(M+1), A, B,TIME)
  BETA=BET(TIME)
  U3=FLD*(E3*COS(ANG)+E4*SIN(ANG))
  U4=FLD*(E3*SIN(ANG)-E4*COS(ANG))
  CVX1=VXX(M)-.5*H*(ALPHA*(VXX(M+1)+VXX(M))-BETA*(U3+U1))
  CVY1=VYY(M)-H*(ALPHA*(VYY(M+1)+VYY(M))+BETA*(U2+U4)+2*GAMMA) / 2
  Q1=ABS(XX(M+1)-CX1)
  Q2=ABS(YY(M+1)-CY1)
  IF (Q1.LT..000001.AND.Q2.LT..000001) THEN
  XX(M+1)=CX1+.2*(FIRSX-CX1)
  YY(M+1)=CY1+.2*(FIRSY-CY1)
  VXX(M+1)=CVX1+.2*(FIRSVX-CVX1)
  VYY(M+1)=CVY1+.2*(FIRSVY-CVY1)
  TT(M+1)=TT(M)+H
  IF (YY(M+1).LT.PNTTHK.OR.ABS(XX(M+1)).LT.A) THEN
  XX(1001)=XX(M+1)
  YY(1001)=YY(M+1)
  VXX(1001)=VXX(M+1)
  VYY(1001)=VYY(M+1)
  TT(1001)=TT(M+1)
  GOTO 91
  END IF
  GOTO 90
  ELSE
  ITN=ITN+1
  END IF
  IF (ITN.GT.10) THEN
  IFAIL=1
  X(N+1)=X(N)
  Y(N+1)=Y(N)
  VX(N+1)=VX(N)
  VY(N+1)=VY(N)
  NPTS=N+1
  GOTO 99
  ELSE
  XX(M+1)=CX1
  YY(M+1)=CY1
```

```
      VXX(M+1)=CVX1
      VYY(M+1)=CVY1
      END IF

C ELSE RECORRECT

      GOTO 100
   90 CONTINUE
   91 X(N+1)=XX(1001)
      Y(N+1)=YY(1001)
      VX(N+1)=VXX(1001)
      VY(N+1)=VYY(1001)
      T(N+1)=TT(1001)
      XX(1)=XX(1001)
      YY(1)=YY(1001)
      VXX(1)=VXX(1001)
      VYY(1)=VYY(1001)
      TT(1)=TT(1001)
      NPTS=N+1


C IF PARTICLE HAS HIT INTERFACE OR TRAPPED THEN RETURN

      IF (Y(N+1).LT.PNTTHK.OR.ABS(X(N+1)).LT.A) THEN
      NPTS=N+1
      GOTO 99
      END IF
   95 CONTINUE
   99 JJ=NPTS
      RETURN
      END
```

RND.BAS

```
REM Program used to calculate the starting conditions for the simulations
REM Writes the data to a file called S100.num
REM Written in Qbasic

n$ = "E:\stephen\mpi\S100.num"
OPEN n$ FOR OUTPUT AS #1

REM Declares the parameters to be used in the to generate the simulation data

        radius = .00001
        rhop = 5240
        rhoc = 1000
        eta = .0005
        ho = 100
        bdef = .001
        adef = .0001
        mu = 1400
        nparts = 160
        pntthk = .00001

REM If using this program to generate data for simulations program which uses fixed magnetic moment
REM or the Thyristor Waveform TMPIA.FOR. You need to declare a parameter mom=xxx or wid=xxx
REM Where xxx is the value wanted for the simulation it also need to be added after pntthk in the
REM PRINT #1

        x = 0
PRINT #1, radius, rhop, rhoc, eta, ho, bdef, adef
PRINT #1, mu, nparts, pntthk
FOR f = 1 TO 160
        y = RND * .0005 + pntthk
        x = x + .000005
        vx = 0
        vy = 0
        PRINT #1, x, y, vx, vy
NEXT f
CLOSE #1
```

ANAN.BAS

```
REM analyses data from the simulation program
REM written in Qbasic
REM Data from the simulation is in wid3000.num

CLS
n$ = "E:\stephen\mpi\wid3000.num"
OPEN n$ FOR INPUT AS #1
FOR g = 1 TO 8
INPUT #1, radius, rhop, rhoc, eta, ho, bdef, adef
INPUT #1, mu, nparts, pnt, widh
IF g = 1 THEN
PRINT radius, rhop, rhoc, eta, ho, bdef, adef, mu, nparts, pnt, widh
END IF
FOR f = 1 TO 160
 INPUT #1, x, y, vx, vy
 x = x * 10000!
 IF x < 1 THEN x1 = x1 + 1
 IF x < 2 AND x > 1 THEN x2 = x2 + 1
 IF x < 3 AND x > 2 THEN x3 = x3 + 1
 IF x < 4 AND x > 3 THEN x4 = x4 + 1
 IF x < 5 AND x > 4 THEN x5 = x5 + 1
 IF x < 6 AND x > 5 THEN x6 = x6 + 1
 IF x < 7 AND x > 6 THEN x7 = x7 + 1
 IF x < 8 AND x > 7 THEN x8 = x8 + 1
NEXT f

REM Prints out the number of particles in each bin after 0.05 second

PRINT
PRINT x1; " "; x2; " "; x3; " "; x4; " "; x5; " "; x6; " "; x7; " "; x8
x1 = 0
x2 = 0
x3 = 0
x4 = 0
x5 = 0
x6 = 0
x7 = 0
x8 = 0
NEXT g
```

Appendix A2

In this appendix are the papers published by the author not directly related to the subject of this thesis. The author was responsible for the magnetic measurements in these papers. This work would not have been possible without the help and assistance of Dr. Z.Blazina of the Ruder Boskovic Institute of Solid State Chemistry, Zagreb, Croatia. In these troubled times the author wishes him and his family the best.

It is instructive to consider the motivation behind this research. In most systems of interest the electrons responsible for the magnetic moments are not localised. This being the case theories have to be developed which take into account the itinerant nature of the electrons responsible for the magnetisation of the system. Cerium based intermetallics are of interest as they can lead to a better understanding of the magnetic and electronic properties of solids. This is because the 4f electrons in cerium are nearly at the same energy as the outer valence electrons. Therefore only a small amount of energy is needed to change the occupancy of these electronic levels. This gives rise to a whole array of electronic properties observable in cerium based systems. These include magnetic ordering, heavy fermion behaviour with or without a transition to a superconducting state at a low temperature (<1K), and several types of intermediate behaviour (Kondo, spin fluctuation and intermediate valence states).

Interesting results have been encountered during the magnetic and structural studies of the system $CePt_{5-x}Al_x$. It was found that the platinum in $CePt_5$ can be replaced by aluminium upto the composition $CePt_2Al_3$ without changing the hexagonal structure of $CePt_5$. Aluminium atoms replace platinum atoms in the interleaving layer containing small atoms only (Kagome net). An ordering within this net starts at the composition $CePt_3Al_2$, when the resulting structure can be considered as a superstructure of the prototype compound $CePt_5$. The results of magnetic measurements indicate a Curie Weiss behaviour for all the alloys. The effective magnetic moments correspond to the value of the value of free Ce^{3+} ion for $CePt_2Al_3$ and decrease monotonically with the decreasing concentration of aluminium. The different nature of the crystal structure of $CePt_3Al_2$ is clearly reflected in the deviation of its magnetic behaviour.

It is known that many intermetallic compounds react reversibly and absorb large quantities of hydrogen. Studies of such metal-hydrogen system are of great interest because drastic modification in the electronic properties sometimes occur. Examples of the profound changes that can occur upon absorbing hydrogen can be found in the suppression of ferromagnetism in ferromagnetic alloys or conversion of Pauli paramagnetism to ferromagnetism. It is known that partial substitution of Cr in $ZrCr_2$ by other 3d metals, as well as addition of these metals considerably affects the hydrogen capacity, hydrogen dissociation pressure and the magnetic properties of $ZrCr_2$. Magnetisation measurements on $Zr(Cr_{1-x}Cu_x)$ alloys and their hydrides, as well as the hyperstoichiometric $ZrCr_2T_{0.8}$ (T=Fe, Co, Ni) and their hydrides represents a continuation of Dr Z.Blazina studies on $ZrCr_2$ systems with the aim to obtain further information on their electronic structure.

In the system $Zr(Cr_{1-x}Cu_x)_2$ it was found that the sample exhibit beside the Pauli paramagnetism a ferromagnetic contribution to the total magnetisation. Both contributions being enhanced by hydrogen absorption. Addition of ferromagnetic materials (Fe, Co, Ni) to $ZrCr_2$ do not show the corresponding ferromagnetism in the alloys indicating that these ferromagnetic metals incorporated in the crystal structure. Interesting the strongest magnetisation is observed for the alloy $ZrCr_2Ni$

The papers in this appenix are as follows:

Blazina, Z., and Westwood, S.M., "On The Structural and Magnetic Properties of the $CePt_{5-x}Al_x$ System", *To be published in The Journal of Alloys and Compounds*

Westwood, S.M., Blazina, Z., and Drasner, A., "Magnetic Characterisation of Some Hypersoichmetric $ZrCr_2$ based Alloys and Their Hydrides", *Submitted to the Journal of Material Science Letters*

Westwood, S.M., Blazina, Z., and Drasner, A., "Magnetic Characterisation of $Zr(Cr_{1-x}Cu_x)^2$ and Hydrides", *Submitted to the Journal of Material Science Letters*

ON THE STRUCTURAL AND MAGNETIC PROPERTIES OF THE $CePt_{5-x}Al_x$ SYSTEM

Z. Blazina(*) , and S.M. Westwood

Department of Physics, University of Durham, Durham DH1 3LE, U.K.

ABSTRACT

The structural and magnetic properties of the $CePt_{5-x}Al_x$ system have been studied. It was found that platinum in $CePt_5$ can be replaced by aluminium up to the composition $CePt_2Al_3$. The hexagonal unit cell of the prototype $CePt_5$ compound is preserved and substitution takes place in the interleaving layer (Kagome net) only. At the composition $CePt_3Al_2$ as a result of partial ordering of aluminium atoms within the Kagome net a much larger unit cell which can be considered as a superstructure of the $CaCu_5$ type was observed. Magnetic susceptibility for all samples follows a Curie-Weiss behaviour with effective magnetic moments close to that of Ce^{3+} ion, providing that a temperature indepedent susceptibility is subtracted from the total susceptibility. The valency for cerium ion is briefly discussed in terms of possible electron transfer and difference in electronegativity. The structural change at the composition $CePt_2Al_3$ is also clearly reflected in a deviation of the magnetic behaviour of this alloy from the observed trend of the system in whole.

(*) On leave from the Ruder Boskovic Institute, POB 1016, 41001 Zagreb, Croatia

INTRODUCTION

It is well-known that the AB_5 intermetallic compounds crystallize either as a hexagonal $CaCu_5$ structure type (space group P6/mmm) or as a cubic $AuBe_5$ structure type (space group Fd3m). Substitution of the B component in these compounds by some other metals or metalloids results sometimes in interesting structural transformations. For example, a series of crystal structures related to the hexagonal $CaCu_5$ structure type was determined by the ordered replacement of cobalt atoms by boron in RCo_5 (R=rare earth) in the basal mixed layer (R + Co) of the prototype alloy RCo_5 [1]. Some other $CaCu_5$ related structures of the composition AB_3Ga_2 can be obtained by replacement of B atoms by gallium atoms in the interleaving layer containing small atoms only [2-6]. Substitution of the B component in cubic AB_5 compounds does not exceed the composition AB_4B', but results sometimes with an ordered structure of the $MgSnCu_4$ type [7-9].

Results of our studies on the systems $ThT_{5-x}Al_x$ (T=transition metal) [10] and $UCu_{5-x}Al_x$ [11] indicated the self-consistent properties of the interleaving layer in the hexagonal structures, and on the possibility to replace one nickel atom in cubic $ZrNi_5$ and UNi_5 with a "pseudosilicon", i.e. with the combination of some elements of the IIIa-Va and IIb-VIa group [12].

The physical, especially the magnetic properties of many binary and ternary AB_5 compounds have been extensively investigated. Among many interesting findings in the AB_5 intermetallics based on rare earth and noble metals it was observed that $CePt_5$ orders antiferromagnetically with a Neel temperature of 1K [13], and that the magnetic properties of $CePt_5$ are strongly affected by substitution of a platinum atom by Cu, Ga, Rh, Pd or In [14-16].

The investigation of the structural and magnetic properties of the $CePt_{1-x}Al_x$ system described in this paper was carried out with the aim to obtain further information on the interesting behaviour of ternary compounds based on $CePt_5$.

EXPERIMENTAL PROCEDURE

Samples of the composition $CePt_{5-x}Al_x$ were prepared from metals of the highest available commercial purity (Johnson Matthey, UK, min. 99.99 wt.%) in a water-cooled copper boat under ultra-high vacuum, using high frequency induction melting. To ensure homogeneity samples were turned upside down and remelted several times and then annealed at 800 oC for 7 days. X-ray powder diffraction patterns were obtained with a computerised Siemens D-5000 diffractometer; nickel filtered CuKα radiation was employed. Line positions were corrected according to silicon which was used as an internal standard. Intensities were calculated with the "Lazy Pulverix" program [17].

Magnetic measurements were performed on a Vibrating Sample Magnetometer (VSM) in Physics Department, University of Durham, Durham, U.K. described in details in references [18,19] and fitted with an Oxford Instruments CF 1200 helium gas flow cryostat. Two types of measurement were made: 1) Susceptibility dependence on temperature over the range 16 - 300 K, at a field strength of 5.5 kOe, and 2) Magnetization measurements over field strengths -5.5 to +5.5 kOe at various temperatures. Pure nickel was used as the calibrant.

RESULTS AND DISCUSSION

Structure

X-ray powder diffraction data of the alloys $CePt_{1-x}Al_x$ indicated that single phase samples exist up to the composition $CePt_2Al_3$. It was found that all single phase compounds crystallise with the hexagonal $CaCu_5$ type of structure, i.e. the same structure in which the prototype $CePt_5$ compound crystallises. In the $CePt_5$ structure there exist two crystallographically inequivalent platinum sites; 2(c) in the basal plane layer of mixed atoms (Ce+Pt) and 3(g) in the interleaving layer known also as Kagome net [20]. A detailed diffraction intensity data analysis was carried out and it was unequivocally determined that aluminium atoms replace the platinum atoms preferentially in the Kagome net only. Substitution takes place until all platinum atoms in the Kagome net are replaced by aluminium atoms thus correspond to the formula $CePt_2Al_3$. The most interesting feature of the system investigated seems to be the rather high and unexpected

increase of the unit cell parameters (Table I) observed at the composition $CePt_3Al_2$. It was found that the crystal structure for this particular compound can be better described with a larger hexagonal unit cell derived from the $CaCu_5$ type of structure as shown in Fig.1. The space group remains the same (P6/mmm) as well as the parameter c, while the parameter a is increased by a factor of $\sqrt{3}$. Comparison between observed and calculated intensity values showed the best agreement if the following atomic positions are assumed:

1 Ce in 1(a),
2 Ce in 2(c),
6 Pt in 6(j) (x=1/3),
3 Al in 3(g) and
(3 Al + 3 Pt, statistically) in 6(m) (x=1/6).

The corresponding intensity values are given in Table II, and the calculated intensity values for the smaller $CaCu_5$ type lattice with the statistical distribution of (Al+Pt) atoms in the Kagome net (the best agreement with the observed values) are included for comparison. However, for a final conformation of this structure a neutron diffraction study and/or a system containing carefully chosen components with atomic factors to give rise to stronger intensities would be necessary.

It should be mentioned that the structure of $CePt_3Al_2$ is the same as $TbCo_3Ga_2$ [3,5], $NdCo_3Ga_2$ [6] and some other rare earth-transition metal-gallium analogues [4]. The characteristic of all these structures is the partially ordered arrangement of gallium (aluminium) atoms within the Kagome net. In the system $CePt_{5-x}Al_x$ the appearance of such partially ordered arrangement of aluminium atoms is easy understandable. Namely, substitution of platinum by aluminium is taking place until the whole net is occupied by aluminium atoms only and the resulting structure is an ordered one. In this trend the $CePt_3Al_2$ should be regarded as the intermediate stage to the full ordering.

It should also be noted that the RCo_3Ga_2 (R=rare earth) structure proposed by Fremy et al.[2] (a similar structure related to $CaCu_5$ in which rare earth atoms are shifted along the c axis, and the arrangement of smaller atoms is slightly different than in the above mentioned structures) was rejected for $CePt_3Al_2$, because of the disagreement between the calculated and observed values of intensity. We assume that the formation of the

Table I. Unit cell parameters and the magnetic data for the $CePt_{5-x}Al_x$ system

Composition	a (Å)	c (Å)	χ_{app} at 16K (emu/mol)	χ_0 at 16K (emu/mol)	Paramagnetic Curie temperature (K)	Curie Constant C_m (emu K/mol)	Effective Magnetic Moment (μ_B/ Ce atom)
$CePt_5$	5.366	4.377	$2.20.10^{-2}$	$9.37.10^{-4}$	-9.44	0.500	2.00
$CePt_4Al$	5.369	4.389	$2.87.10^{-2}$	$8.05.10^{-4}$	-5.13	0.640	2.37
$CePt_3Al_2$	5.428 9.403	4.414 4.414	$2.18.10^{-2}$	$9.73.10^{-4}$	-4.72	0.459	1.92
$CePt_3Al_3$	5.368	4.406	$3.88.10^{-2}$	$1.24.10^{-4}$	-2.92	0.830	2.57

Table II. Intensity values for the $CePt_3Al_2$ compound

		Larger cell a=9.403Å c=4.414Å		$CoCu_5$ type a=5.428 Å c=4.414Å	
a	I_O	hkl	I_O	hkl	I_C
8.143	6	100	3	-	-
4.702	5	110	4	100	14
4.414	11	001	12	001	21
4.072	8	200	5	-	-
2.993	9	201	4	-	-
2.714	55	300	57	110	64
2.351	5	220	3	200	2
2.312	100	301	100	111	100
2.207	7	002	4	002	25
2.075	21	221	19	201	21
1.998	6	112	4	102	3
1.777	5	410	3	210	2
1.712	22	302	20	112	21
1.609	6	222	4	202	3
1.567	10	330	8	300	7
1.496	5	402	3	-	-
1.477	23	331	25	301,003	20
1.463	5	510	3	-	-
1.453	5	421	3	-	-

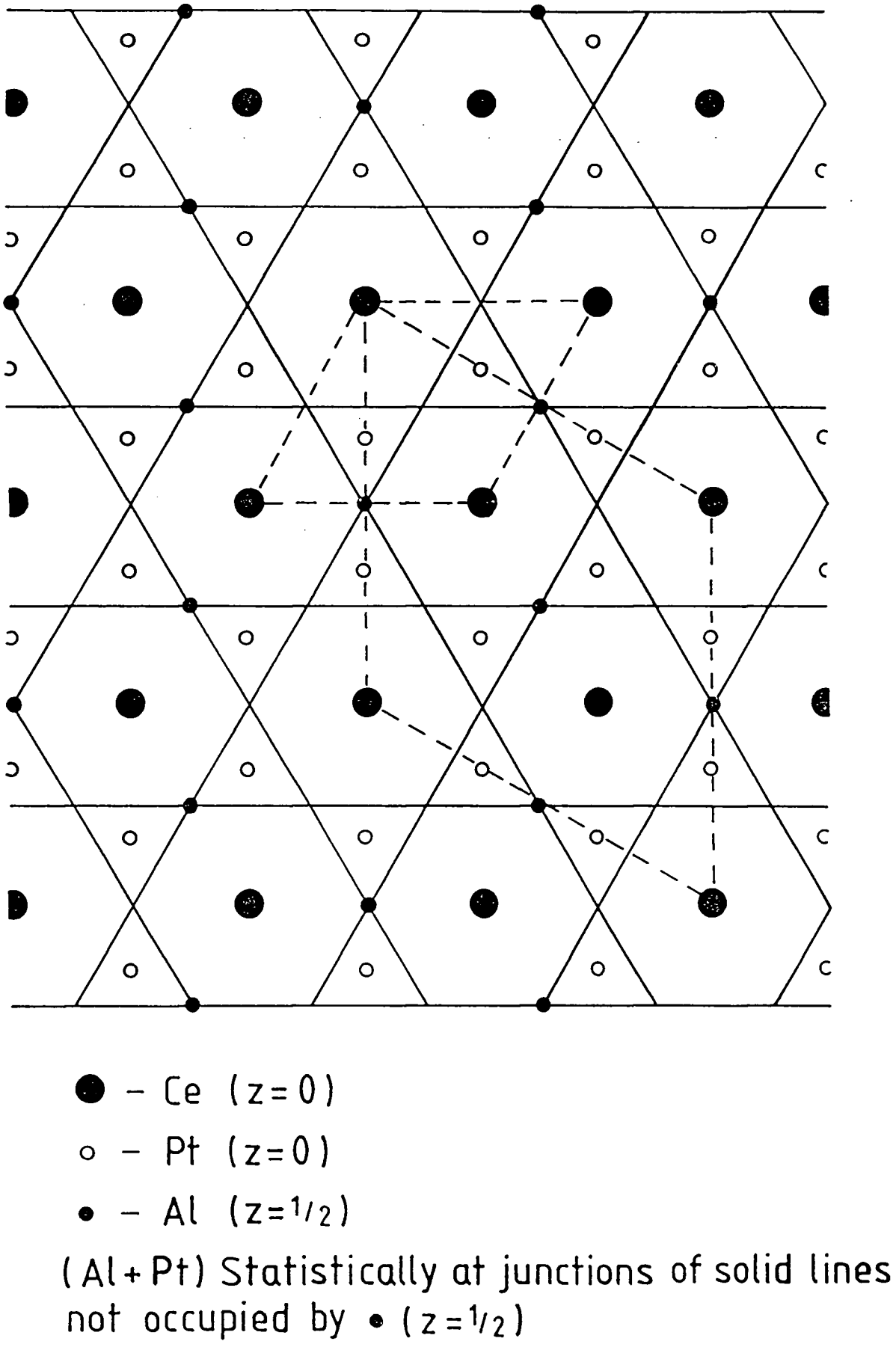

Fig.1. Projection of the crystal structure of the $CePt_3Al_2$ compound along the c axis. Broken lines indicate the smaller and the larger unit cell respectively. (Note in the smaller cell a statistical arrangement of Al + Pt atoms at all junctions of solid lines)

structure proposed by Fremy occurs if substitution of B atoms also takes place in the basal plane layers rather than in Kagome layers only.

It is worth mentioning that the virtually unchanged lattice parameter a and the monotonically increase in lattice parameter c with the increased content of aluminium (except for $CrPt_3Al_2$) reflects the preferential substitution of the platinum atoms in the Kagome net. Namely, the atomic radius of aluminium (1.43 Å) is larger than that of platinum (1.39 Å) which in the case of a preferred substitution results in a larger expansion of the c axis.

Magnetic Properties

The results of magnetic susceptibility measurements for selected compounds (x=0, 1, 2, 3) of the system $CePt_{5-x}Al_x$ over temperature region 16 - 300 K at 5.5 kOe are presented in Figs.2,3 and the magnetization versus field strength at 6K in Fig.4.The results indicate that the susceptibility of all alloys investigated follow a Curie-Weiss behaviour provided that a temperature independent term was subtracted from the total susceptibility. The susceptibility results have been fitted to $\chi_{app}= \chi_o+C/(T-\theta_p)$. χ_{app} represents the total susceptibility, χ_o is the temperature independent term, C is the Curie constant and θ_p is the paramagnetic Curie temperature. The effective paramagnetic moment was calculated from the Curie constant. All the results are summarised in Table I.

Before we attempt to discuss the results of the magnetic measurements it is well to be mentioned that the values obtained from the magnetic data for binary $CePt_5$ are in good agreement with the literature data [13,14] although the effective paramagnetic moment per cerium atom was found to be smaller (2.00 μ_B/Ce compared to 2.40 μ_B/Ce in reference[14]).

The magnetic features of the investigated $CePt_{5-x}Al_x$ system can be summarised as follows: All the alloys investigated are paramagnetic and the Curie-Weiss behaviour indicates on localised magnetic moments. The effective magnetic moments are close to that of the free trivalent Ce ion value and the negative Curie temperature indicates antiferromagnetism. The apparent susceptibility increases with x, while the paramagnetic Curie temperature and the Curie constant decrease with x. However, this is true for all

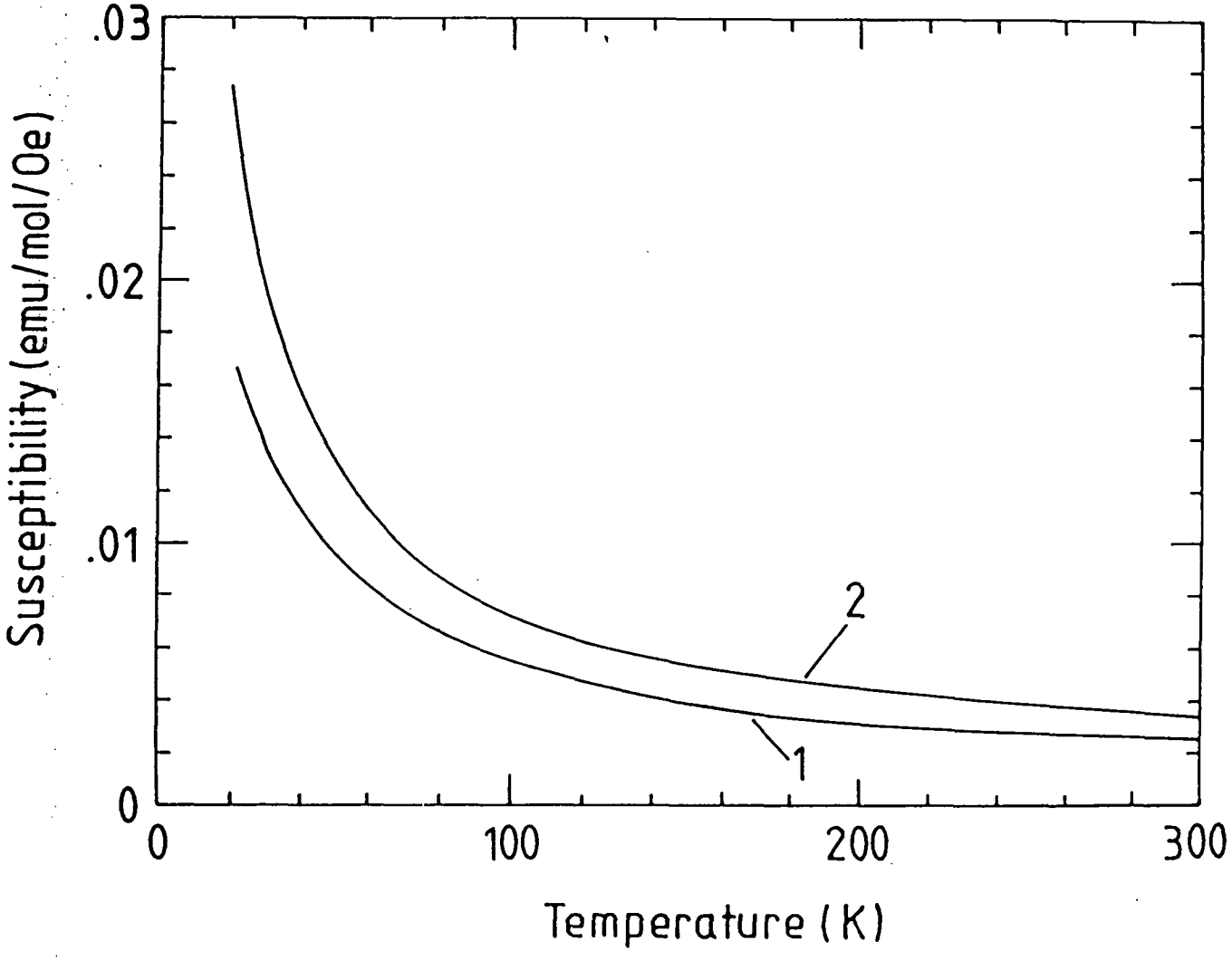

Fig.2. Magnetic Susceptibility versus temperature at 5.5 kOe for 1) $CePt_5$ and 2)$CePt_4Al$.

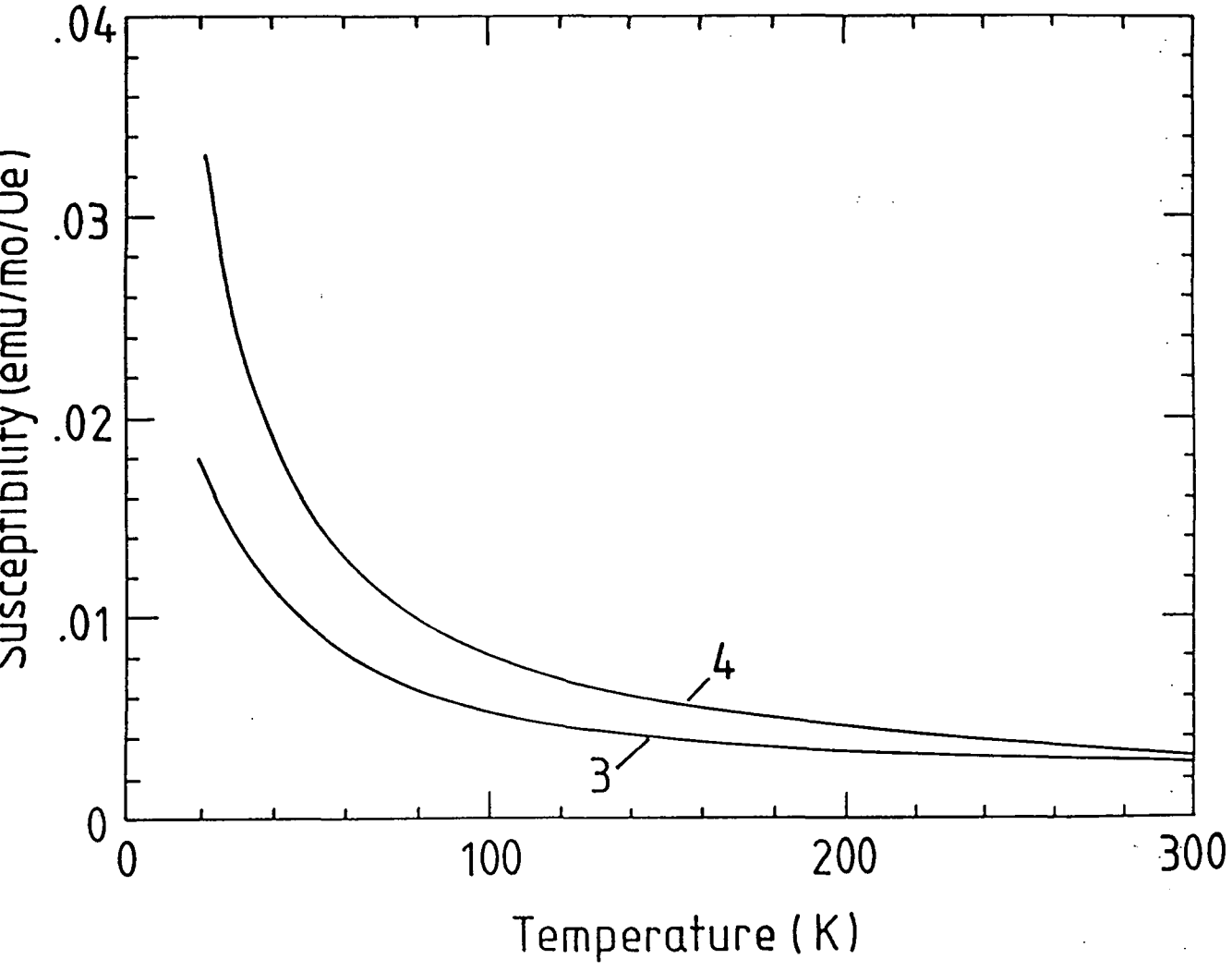

Fig.3. Magnetic susceptibility versus temperature at 5.5 kOe for 3) $CePt_3Al_2$ and 4) $CePt_2Al_3$.

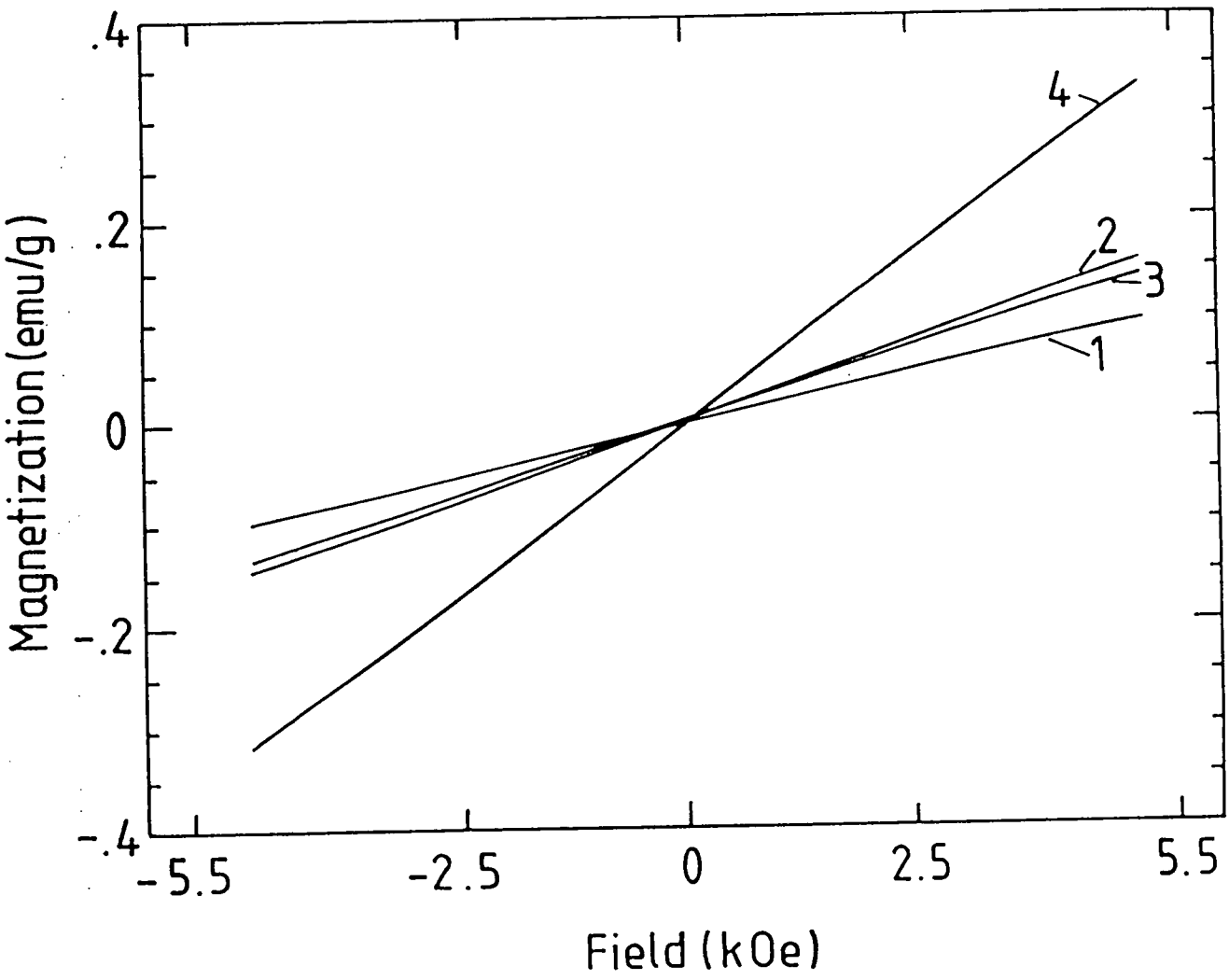

Fig.4. Magnetisation versus field strength at 16K for 1) $CePt_5$, 2) $CePt_4Al$, 3) $CePt_3Al_2$ and 4) $CePt_2Al_3$.

alloys except for $CePt_3Al_2$, which shows a minimum in the apparent susceptibility value, positive deviation in Curie temperature but negative deviation in effective moments from the observed trend in this system. The odd behaviour of this compound should be attributed to the different electron structure as a result of the observed significant increase in the lattice constants. This is also a further confirmation that a crystal structure transformation that includes partially ordering of aluminium atoms within the Kagome net takes place at this composition.

The magnetic behaviour of the $CePt_{5-x}Al_x$ system could be explained following the concept of electron transfer from rare earth atoms to 5d atoms [21] due to the significant difference in electronegativity. The electronegativity of aluminium is lower than that of platinum but higher than that of cerium. Therefore as substitution proceeds the difference in electronegativity between Ce and B atoms (Pt+Al) becomes less pronounced and the electron transfer from Ce to B atoms weakens. As a result the average valency of cerium which is higher than 3+ in $CePt_5$ (2.00 μ_B/Ce compared to 2.54 μ_B/Ce for Ce^{3+} ion) decreases with the increasing concentration of aluminium and reaches very close the value for Ce^{3+} ion at the composition $CePt_2Al_3$, when the substitution is terminated. As a consequence the temperature independent term of the susceptibility which reflects the Ce^{4+} decreases with increasing aluminium concentration. The behaviour of the sample $CePt_3Al_2$ may look some what puzzling because the electron transfer should be weaker due to the larger interatomic distances. A possible explanation could be that the increase in lattice parameters gives rise to an increase in Ce-Ce separation which results in reduced hybridisation between Ce-4f and conduction electrons and a virtually decrease in f electron concentration.

Alternatively one can assume that aluminium acts as an electron donor into the system which results in an increase of the average f electron concentration of Ce which is bellow 1 in $CePt_5$ but very close to 1 at the end of the single phase ternary region.

CONCLUSION

As a conclusion of the structural and magnetic investigation of the system $CePt5_{1-x}Al_x$ we can say that the substitution of platinum by aluminium takes place up to the composition $CePt_2Al_3$. Aluminium atoms statistically replace platinum atoms in the interleaving Kagome net only. Ordering of aluminium atoms in the Kagome net begins at

the composition $CePt_3Al_2$ when an drastic increase in the unit cell was observed. The results of magnetic measurements follow the structural changes very well. Susceptibility values follow the Curie-Weiss law with an effective magnetic moment close to that for Ce^{3+} ion. A decrease in valency of cerium from above 3+ in $CePt_5$ to 3+ in $CePt_2Al_3$ was observed. The different nature of the crystal structure of $CePt_3Al_2$ is reflected in deviation in magnetic behaviour of this sample from the observed trend for the system $CePt_{5-x}Al_x$ in whole.

Acknowldegements

The authors would like to thank Dr Nick Bernhoeft who made these measurements possible and Paul Foley for his technical expertise.

LITERATURE

[1] Yu.B. Kuzma and N.S. Bilonizhko, Sov. Phys. Crystallogr. 18 (1974) 447.

[2] M.A.Fremy, D.Gignoux, J.M. Moreau, D. Paccard and L. Paccard, J. Less-Common Met. 106 (1985) 251.

[3] I. Felner, A. Grayevsky and N. Kaplan, J. Magn. Magn. Mater. 81 (1989) 179.

[4] Ch.D. Routsi, J.K. Jakinthos and E. Gamari-Seale, J. Magn. Magn. Mater. 102 (1991) 275.

[5] Ch.D. Routsi, J.K. Yakinthos and E. Gamari-Seale, J. Magn. Magn. Mater. 102 (1991) 266.

[6] Ch.D. Routsi, J.K. Yakinthos and E. Gamari-Seale, J. Magn. Magn. Mater. 116 (1992) 99.

[7] A.E. Dwight, J. Less-Common Met. 43 (1975) 117.

[8] T. Takeshita, S.K. Malik and W.E. Wallace, J. Solid State Chem. 23 (1978) 225.

[9] E.I. Gladisevskij, P.I. Kripjakevich and M.Ju. Tesljuk, Dokl. Akad. Nauk SSSR, 85 (1952) 81.

[10] Z. Blazina and Z. Ban, J. Less-Common Met. 64 (1979) 167.

[11] Z. Blazina and Z. Ban, Z. Naturforsch. 35b (1980) 1162.

[12] Z. Blazina and Z. Ban, J. Nucl. Mater. 136 (1985) 136.

[13] A. Schroeder, R.van den Berg, H.V. Loehneysen, W. Paul and H. Leuken, Solid State Commun. 65 (1988) 99.

[14] D.T. Adroja, S.K. Malik, B.D. Padalia and R. Vijayaraghavan, Solid State Commun. 71 (1989) 649.

[15] S.K. Malik, D.T. Adroja, M. Salski, B.D. Dunlap and A. Umezawa, Phys.

Rev.B, 40 (1989) 9378.

[16] S.K. Malik, R. Vijayaraghavan, D.T. Adroja, B.D. Padalia and A.S. Edelstein, J. Magn. Magn. Mater. 92 (1990) 80.

[17] K. Yvon, W. Jeitschko and E. Parthe, J. Appl. Crystallogr. 10 (1977) 73.

[18] R.S. Hoon, Eur. J. Phys. 4 (1983) 61.

[19] R.S. Hoon and S.N.M. Willoock, J. Phys. E. Sci. Instrum. 21 (1988) 772.

[20] F.C. Frank and J.S. Kasper, Acta Crystallogr. 12 (1959) 483.

[21] K.H.J. Buschow, Rep. Prog. Phys. 42 (1979) 1373.

MAGNETIC CHARACTERISATION OF SOME HYPERSTOICHIOMETRIC $ZrCr_2$-BASED ALLOYS AND THEIR HYDRIDES

S.M. Westwood(1), Z. Blazina(1,2) and A. Drasner(2)

(1) Department of Physics, University of Durham, Durham DH1 3LE, U.K.

(2) Laboratory for Solid State Chemistry, Institute "Ruder Boskovic",

POB 1016, 41001 Zagreb, Croatia.

It is well known that many zirconium-based Laves phase intermetallics react reversibly and absorb large quantities of hydrogen. They have therefore attracted a great deal of attention as possible hydrogen storage materials[1-5]. Although $ZrCr_2$ reacts reversibly and absorbs more than three hydrogen atoms per formula unit this compound is not technologically interesting because of its low hydrogen equilibrium dissociation pressure [6]. However, it was found that partial substitution of chromium by other transition metals and/or addition of these metals to $ZrCr_2$ may considerably affect the hydrogen dissociation pressure of $ZrCr_2$ [1,5,7-11]. Apart from their possible practical applications, these materials are also of great interest because profound changes in the electronic properties can occur. This is a concomitant of the substitution of one metal in

binary compounds by a third metal, addition of a third metal to binary compounds (hyperstoichiometry) and/or hydrogen absorption. For example, it was found that the Pauli paramagnetism of $ZrCr_2$ is changed into ferromagnetism in the system $Zr(Cr_{1-x}Fe_x)_2$, strongly enhanced in the system $Zr(Cr_{1-x}Co_x)_2$, only moderate enhanced in the system $Zr(Cr_{1-x}Ni_x)_2$ and in the system $Zr(Cr_{1-x}Cu_x)_2$ a ferromagnetic contribution to the total magnetisation is developed. Hydrogen uptake acts in favour of these effects [12-15].

In this paper the results of the magnetisation measurements for $ZrCr_2$ when subjected to addition of selected quantities of iron, cobalt or nickel are reported and represent the continuation of our studies of the hydrogen sorption and magnetic properties of the $ZrCr_2$-based alloys.

The intermetallic compounds corresponding to the stoichiometry $ZrCr_2T_{0.8}$ (T=Fe,Co,Ni) were prepared by arc melting of the high purity constituent metals (Ventron, at least 99.9 wt.%), and then charged with hydrogen. The details on alloy preparation, the hydrogen absorption procedure, the hydrogen pressure-composition desorption measurements, as well as the apparatus used, have been described previously [7].

X-ray powder diffraction patterns of alloys and their hydrides were obtained using a Philips PW 1050 diffractometer equipped with a pulse height analyser; nickel filtered Cu Kα radiation was employed.

Magnetisation measurements were performed on a vibrating sample magnetometer (VSM) in Physics Department, University of Durham, Durham, U.K. in the temperature range 4.2 - 300 K and in applied fields up to 12 kOe.

The predominance of the hexagonal crystal structure of the $MgZn_2$ type was observed for all the $ZrCr_2T_{0.8}$ (T=Fe,Co,Ni) alloys and their hydrides as reported earlier [8]. It was also suggested that in the structure of $ZrCr_2$ some of the chromium atoms are replaced by the T metal atoms and that zirconium atoms are partially substituted by chromium and/or T atoms. It was also reported that the dissociation equilibrium pressure of the hyperstoichiometric alloys is considerably higher than the equilibrium pressure of $ZrCr_2$, and that the alloys $ZrCr_2Fe_{0.8}$ and $ZrCr_2Co_{0.8}$ could even have technological potential as hydrogen storage material due to the convenient dissociation pressure plateau around 0.1 MPa.

The magnetisation versus field measurements are illustrated in Fig.1., and Figs. 2-3. present the susceptibility versus temperature at a field strength of 5.8 kOe.

The alloys and the hydrides are paramagnetic, but the non-linear dependence of magnetisation versus field in all samples indicates beside this paramagnetism there is the presence of a ferromagnetic contribution to the total magnetisation.

The saturation magnetisation (σ_S) of the ferromagnetic contribution was determined by extrapolation of the linear behaviour of magnetisation versus field (H) at high fields to zero field. Magnetic susceptibility is temperature dependent only for the samples containing nickel, and the corresponding susceptibility curves can be fitted to a Curie-Weiss behaviour according to $\chi_{app}= C/(T-\theta_p)+ \sigma_S /H$. C is the Curie constant, θ_p the paramagnetic Curie temperature, and σ_S/H is the susceptibility corresponding to ferromagnetism. In this procedure it is assumed that the saturation magnetisation of nickel does not change with temperature. The molar fraction of the ferromagnetic component was calculated using the saturation magnetisation for pure iron, cobalt or nickel. The

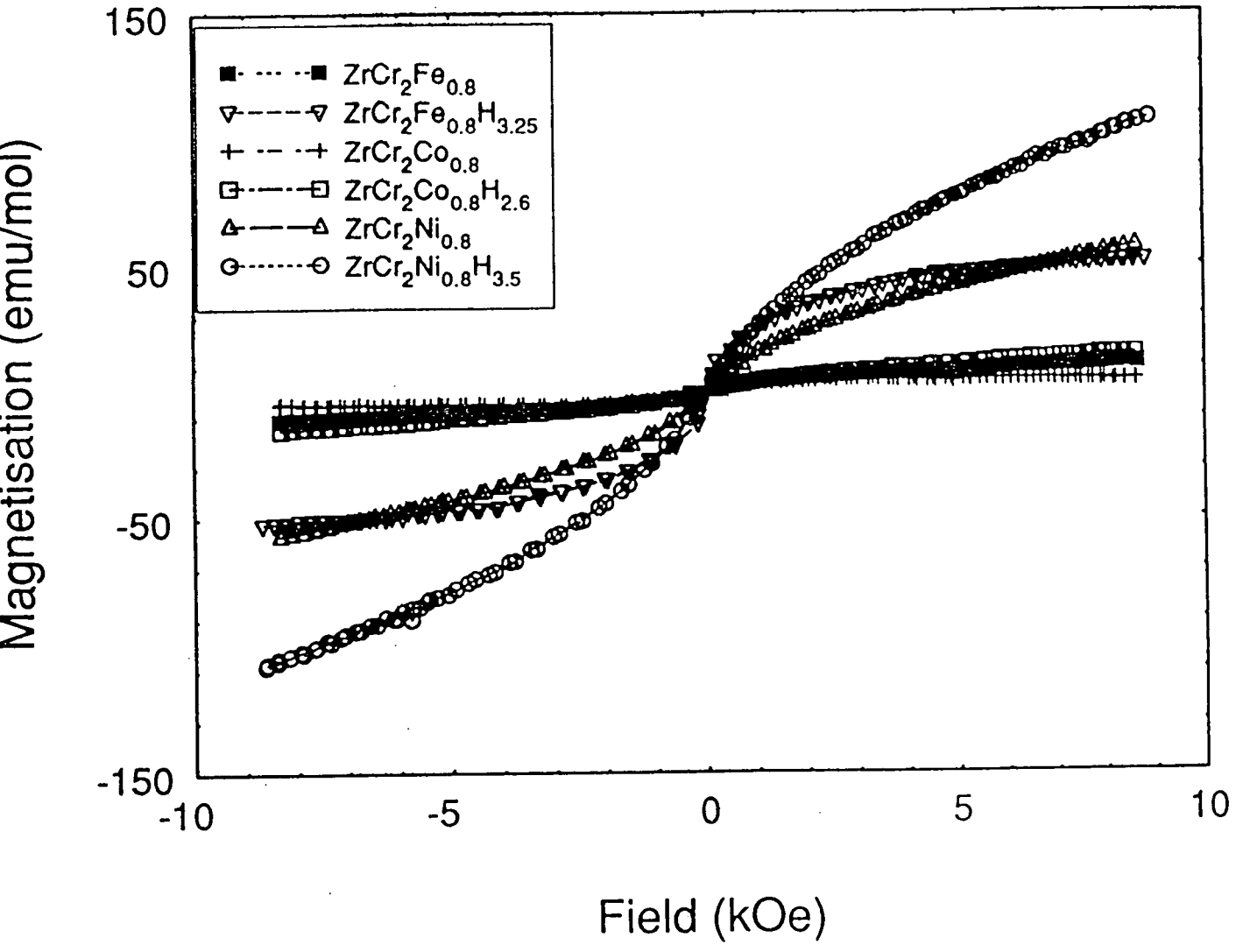

Fig.1. Magnetisation versus field for the alloys $ZrCr_2T_{0.8}$ (T=Fe,Co,Ni) and their hydrides at 300 k.

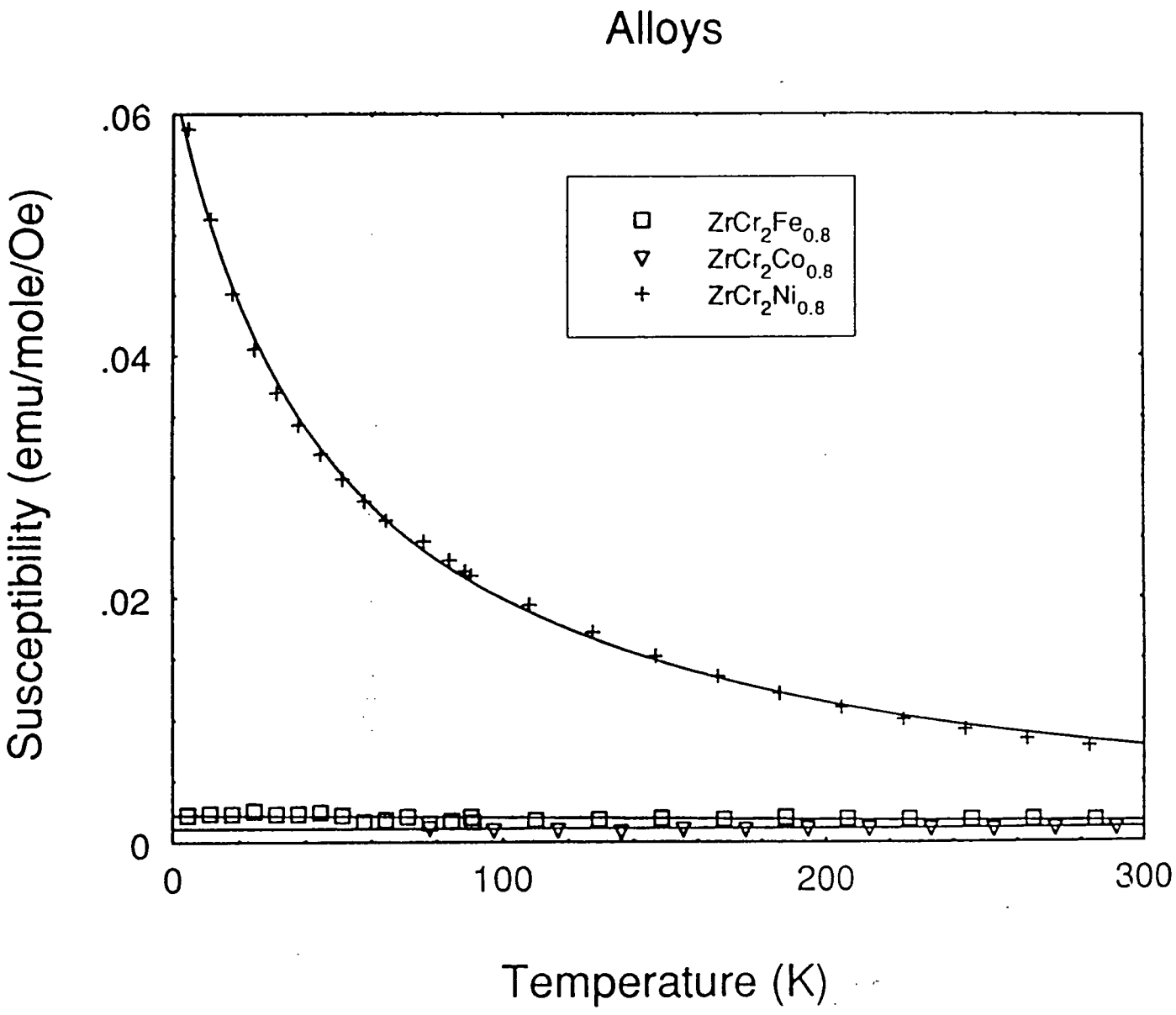

Fig.2. Magnetic susceptibility for $ZrCr_2T_{0.8}$ alloys at 5.8 kOe.

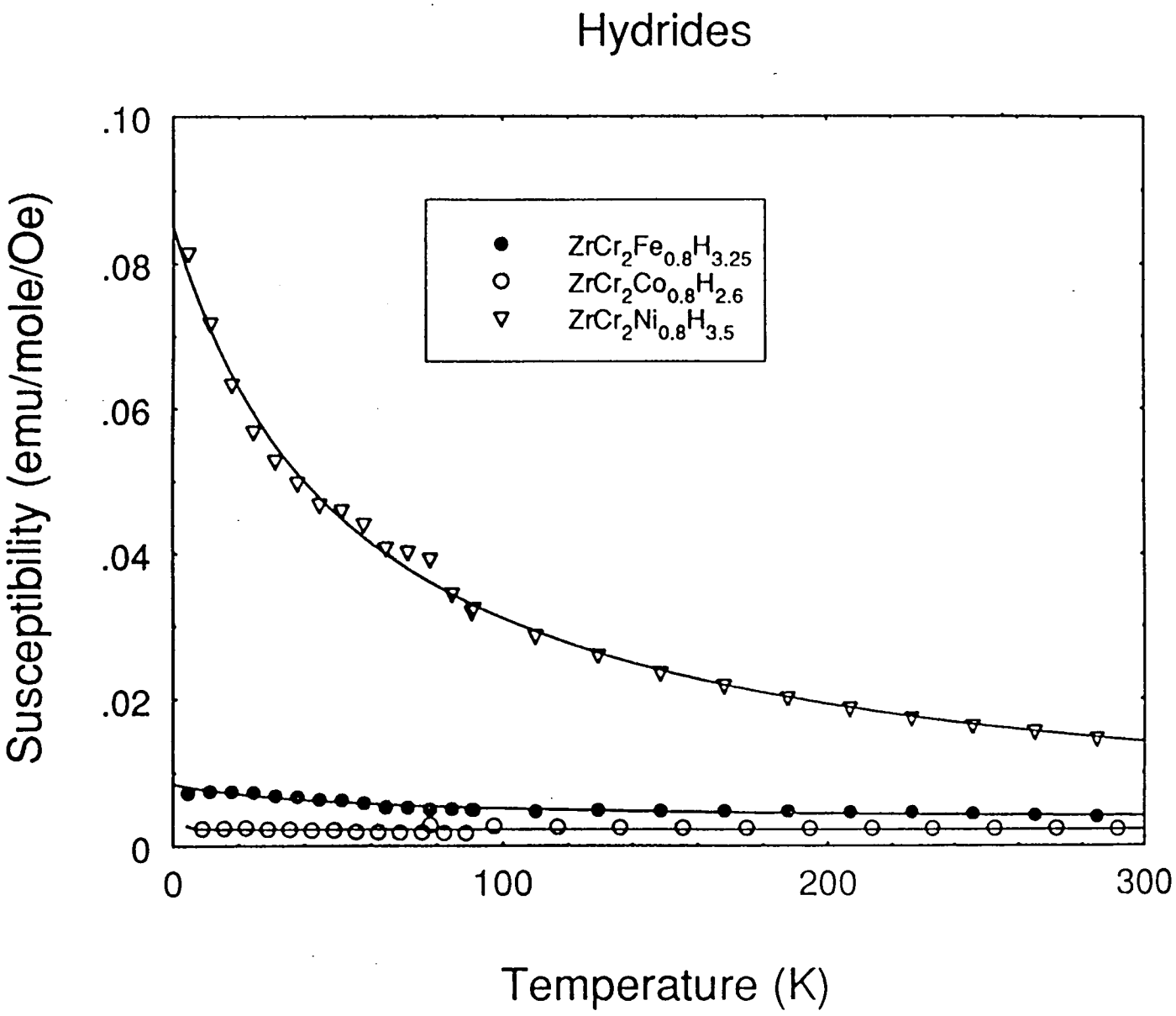

Fig.3. Magnetic susceptibility for $ZrCr_2T_{0.8}$ hydrides at 5.8 kOe.

relevant magnetic data are summarised in Table I., and the data for the binary hexagonal $ZrCr_2$ and its hydride [14] are included for comparison.

It is interesting to point out that the ferromagnetism of the samples, as well as the paramagnetism is increased on going from Co to Fe to Ni, and is exactly opposite from the observed trend in the hydrogen equilibrium pressure which decreases in the same direction.

The magnetic features of the investigated hyperstoichiometric $ZrCr_2$ based systems can be summarised as follows. The susceptibility values of the samples (alloys and hydrides) are enhanced if compared to the values of the prototype $ZrCr_2$/$ZrCr_2$-hydride samples. All the alloys investigated exhibit a ferromagnetism (T_C>300 K) superimposed either on the temperature independent paramagnetism (alloys with iron and cobalt) or on a Curie-Weiss type of paramagnetism (alloy with nickel). The observed ferromagnetism presents only a small fraction of the added amount of the ferromagnetic metal (the highest value of 0.7 at.% is found for the nickel containing alloy), this clearly indicates that the ferromagnetic metals are completely incorporated in the crystal structure of $ZrCr_2$. Hydrogen absorption increases the ferromagnetism in all systems, while the paramagnetism is increased in the systems with Co and Ni but decreased in the system containing Fe, while on the other hand the highest increase in ferromagnetism is observed after hydrogenation for the system containing Fe.

A rational explanation of the magnetic behaviour of these alloys and their hydrides present some difficulties. The Curie-Weiss behaviour with a negative Curie temperature indicating antiferromagnetism (systems with nickel only) is even more puzzling. At the present stage it seems reasonable to assume that the ferromagnetism is associated with T atoms (Fe,Co,Ni) residing on the Zr sites in the crystal lattice of $ZrCr_2$ similar to Co and

Table I. Magnetic data for the $ZrCr_2T_{0.8}$ (T=Fe,Co,Ni) alloys and their hydrides

Compound	a (Å)	c(Å)	χ_{ann} at 8 kOe 300 K (10^{-3} emu/mol)	σ_s (emu/mol)	θ_n (K)	C_H (emu/mol)	Mol. fraction of ferromagnetic phase (%)
$ZrCr_2$	5.104	8.292	0.33				
$ZrCr_2H_{3.44}$	5.388	8.835	0.82				
$ZrCr_2Fe_{0.8}$	5.037	8.258	1.35	6.20			0.06
$ZrCr_2Fe_{0.8}H_{3.25}$	5.404	8.822	6.09	37.0			0.38
$ZrCr_2Co_{0.8}$	5.012	8.223	0.52	4.64			0.06
$ZrCr_2Co_{0.8}H_{2.6}$	5.551	8.769	1.69	8.08			0.11
$ZrCr_2Ni_{0.8}$	5.020	8.216	6.67	18.6	-50.6	3.231	0.73
$ZrCr_2Ni_{0.8}H_{3.5}$	5.372	8.778	12.47	33.3	-55.8	4.689	1.30

Mn atoms residing on the Zr sites as observed in the nonstoichiometric $ZrCo_2$ and $ZrMn_2$, respectively [16,17]. Following the concept of electronegativity [18] an electron transfer from Zr to Cr, Fe, Co or Ni, as well as from Cr to Fe, Co or Ni is expected due to the increase in electronegativity. The result is a better 3d-band filling and consequently a decrease of 3d moments of Fe, Co and Ni. Hydrogen uptake increases the magnetic moments as a consequence of the decrease in concentration of delocalised electrons associated with longer interatomic distances (20 % larger unit cell volume). Alternatively, reduction in 3d band filling after hydrogen uptake and an increase in magnetic moments may also be caused by the change in T atom's surrounding from Zr (alloy) to H (hydride) where hydrogen is undoubtedly more electronegative than Zr. The Fe, Co and Ni atoms residing on the Cr sites in $ZrCr_2$ exhibit only a band like magnetism due to a strong 3d band overlap as a result of large spatial extent of the 3d wave function [19] and small interatomic distances.

Finally, it is worth mentioning that the most interesting magnetic feature of the systems investigated, i.e. addition of ferromagnetic metals to $ZrCr_2$ which results only in a small increase of the ferromagnetism of the prototype compound and is increased by hydrogenation is certainly not a result of segregation of the ferromagnetic metals after hydrogenation, because the magnetisation measurements were performed on alloys after dehydrogenation.

However, for a more general conclusion about the interesting magnetic behaviour of this type of Laves phases much more data accompanied with clear band structure calculations must be gathered.

LITERATURE

1) D.Shaltiel, I.Jacob and D.Davidov, J. Less-Common Met. 53 (1977) 83.

2) I.Jacob and D.Shaltiel, Solid State Commun. 27 (1978) 175.

3) R.M. van Essen and K.H.J.Buschow, Mater Res. Bull. 15 (1980) 1149.

4) F.Pourarian, H.Fuji, W.E.Wallace, V.K.Sinha and H.K.Smith, J. Phys. Chem. 85 (1981) 3105.

5) M.H.Mendelsohn and D.M.Gruen, J. Less-Common Met. 78 (1981) 275.

6) A.Pebler, E.A.Gulbransen, Electrochem. Technol. 4 (1966) 211.

7) A.Drasner and Z.Blazina, J. Less-Common Met. 163 (1990) 151.

8) A.Drasner and Z.Blazina, J. Less-Common Met. 168 (1991) 289.

9) A.Drasner and Z.Blazina, J. Less-Common Met. 175 (1991) 103.

10) D.G.Ivey and D.O.Northwood, Z. Phys. Chem. N.F. 147 (1986) 191.

11) S.Quian and D.O.Northwood, J. Less-Common Met. 147 (1989) 149.

12) I.Jacob, D.Davidov and D.Shaltiel, J. Magn. Magn. Mat. 20 (1980) 226.

13) S.Hirosava, F.Pourarian, V.K.Sinha and W.E.Wallace, J. Magn. Magn. Mat. 38 (1983) 159.

14) Z.Blazina and A.Drasner, J. Magn. Magn. Mat. 119 (1993) L15.

15) S.M.Westwood, Z.Blazina and A.Drasner, Submitted for publication in J. Mater. Sci.

16) F.Pourarian, H.Fuji, W.E.Wallace, V.K.Sinha and H.K.Smith, J. Phys. Chem. 85 (1981) 3105.

17) H.Fuji, F.Pourarian and W.E.Wallace, J. Magn. Magn. Mat. 24 (1981) 93.

18) K.H.J.Buschow and R.C.Sherwood, J. Appl. Phys. 49 (1978) 1480.

19) K.H.J. Buschow, Rep. Prog. Phys. 40 (1977) 1179.

MAGNETIC CHARACTERISATION OF THE $Zr(Cr_{1-x}Cu_x)_2$ ALLOYS AND THEIR HYDRIDES

S.M. Westwood, Z. Blazina*

Department of Physics, University of Durham, Durham DH1 3LE, U.K.

and

A. Drasner

Laboratory for Solid State Chemistry, Institute "Ruder Boskovic",

41001 Zagreb, Croatia.

ABSTRACT

Magnetisation measurements were carried out on the alloys $Zr(Cr_{1-x}Cu_x)_2$ (x = 0, 0.1, 0.3, 0.5) before and after hydrogenation. All, the binary and the ternary alloys, as well as their hydrides exhibit a temperature independent or nearly independent Pauli type of paramagnetism. Beside the Pauli paramagnetism a ferromagnetic contribution to the total magnetisation is observed for most alloys and their hydrides. This is particularly obvious for the $Zr(Cr_{0.9}Cu_{0.1})_2$ alloy and its hydride, where the corresponding saturation magnetic moments were found to be $3.83\ 10^{-2}$ emu/g and $4.32\ 10^{-2}$ emu/g, respectively. It is also observed that hydrogen absorption enhances the Pauli

* On leave from the Laboratory for Solid State Chemistry, "Ruder Boskovic" Institute, 41001 Zagreb, Croatia.

paramagnetism as well as the ferromagnetism of the alloys. The rather unusual magnetic behaviour of these systems is briefly discussed in terms of 3d band filling of the transition metal and compared with some related systems.

1. Introduction

Zirconium-based Laves phase intermetallics react reversibly and absorb large quantities of hydrogen and have therefore attracted a great deal of attention as possible hydrogen storage materials [1-5]. Apart from their possible practical application, these materials are also of interest due to the drastic electronic modifications which occur as a concomitant of
the hydriding process. For example in the system $Zr_{1-x}Ti_xMn_2$ which
exhibits Pauli paramagnetism, depending on the concentration of titaniun upon absorption of hydrogen paramagnetism is enhanced, ferromagnetism or spin-glass behaviour is induced [6].

It was found that partial substitution of chromium in $ZrCr_2$ by iron,cobalt, nickel or copper considerably affects the hydrogen capacity and dissociation equilibrium pressure of $ZrCr_2$ [7-10]. It was also found that the Pauli paramagnetism of $ZrCr_2$ is changed into ferromagnetism in the system $Zr(Cr_{1-x}Fe_x)_2$, strongly enhanced in the system $Zr(Cr_{1-x}Co_x)_2$ and only moderate enhanced in the system $Zr(Cr_{1-x}Ni_x)_2$. Hydrogen uptake acts in favour of these effects.

In this paper the results of the magnetisation measurements for the system $Zr(Cr_{1-x}Cu_x)_2$ and their hydrides are reported. The aim of this study was to obtain some further information on the magnetic behaviour of ternary systems based on $ZrCr_2$ and their hydrides which could help in obtaining a better understanding of their electronic makeup.

2. Experimental Procedure

The intermetallic compounds corresponding to the stoichiometry $Zr(Cr_{1-x}Cu_x)_2$ were prepared by arc melting . The purity of starting materials was Zr 99.9 wt.%, Cr 99.9 wt.% , and Cu 99.98 wt.% (all metals supplied by Ventron). One part of the samples was charged with hydrogen and the rest was used in the hydrogen-free form. The details on alloy preparation, the hydrogen absorption procedure, the hydrogen pressure-composition desorption measurements, as well as the apparatus used, have been described previously [9, 11].

X-ray powder diffraction patterns of alloys and their hydrides were obtained using a Philips PW 1050 diffractometer equipped with a pulse height analyser; nickel filtered Cu Kα radiation was employed.

Magnetisation measurements were performed on a vibrating sample magnetometer (VSM) in Physics Department, University of Durham, Durham, U.K. described in detail in references [12,13], this is fitted with a Oxford

Instruments CF 1200 helium gas flow cryostat. Measurements were made over the temperature range 4.2 - 330 K and in applied fields up to 12 kOe. $HgCo(CNS)_4$ was used as a calibrant.

No special procedure was undertaken in order to prevent the hydrogen release from alloys, because the hydrides were assumed to be relatively stable. This was concluded from desorption isotherms with equilibrium pressure values of only several kPa at room temperature. Furthermore, no changes were observed in the x-ray patterns even after the hydrides had been exposed to air for several months.

3. Results

It has been reported earlier [10] that chromium in $ZrCr_2$ can be replaced by copper up to the composition $Zr(Cr_{0.5}Cu_{0.5})_2$. The cubic Laves structure ($MgCu_2$ type) of the binary $ZrCr_2$ is preserved in the whole ternary region. It was also reported that all the alloys react readily with hydrogen to form hydrides having 2 - 3 hydrogen atoms per formula unit. Hydrogen absorption increases the unit cell volume of the alloys by 22-23 %. It should be noted that the magnetic properties before and after hydrogenation of the other, hexagonal polymorph of $ZrCr_2$, have been reported elsewhere [14] and this data are included here for comparison.

Magnetisation measurements were carried out for the alloys $Zr(Cr_{1-x}Cu_x)_2$ (x = 0, 0.1, 0.3, 0.5) and their corresponding hydrides in the temperature range

4.2 - 300 K and in applied fields up to 12 kOe. The dependence of the magnetisation on temperature (susceptibility) was extracted from the magnetisation measurement data for different field strengths. Figs. 1-3 illustrates the magnetisation versus field measurements and Fig.4 presents some characteristic susceptibility values at field strengths of 5.5 kOe.

All the systems investigated are paramagnetic. Most of the samples do not show a linear dependence of magnetisation versus field indicating there is a ferromagnetic component superimposed on Pauli paramagnetism. This is most pronounced for the alloy $Zr(_{0.9}Cu_{0.1})_2$ and its hydride. The possibility of ferromagnetic impurities in raw materials has been investigated using the same conditions for magnetisation measurements as used for the alloys and their hydrides. It was undoubtedly confirmed that all the materials used were of high magnetic purity, i.e. their magnetisation versus field dependence was found to be always linear (Fig.5.). Contamination of the alloys and their hydrides with ferromagnetic impurities during preparation and investigation was also rejected because the effect varies considerably and irregularly with the composition (see Table I) although all samples have been prepared from the same raw materials and treated in the same way.

It is assumed that the apparent susceptibility (χ_{app}) consists of two terms; a temperature independent term (χ_o) and a term which is the result of the ferromagnetic effect (σ_s /H). The saturation magnetisation (σ_s) was determined by extrapolation of the linear behaviour of magnetisation versus field (H) at high fields to zero field. The experimental values of susceptibility at fields above 5 kOe were fitted according to:

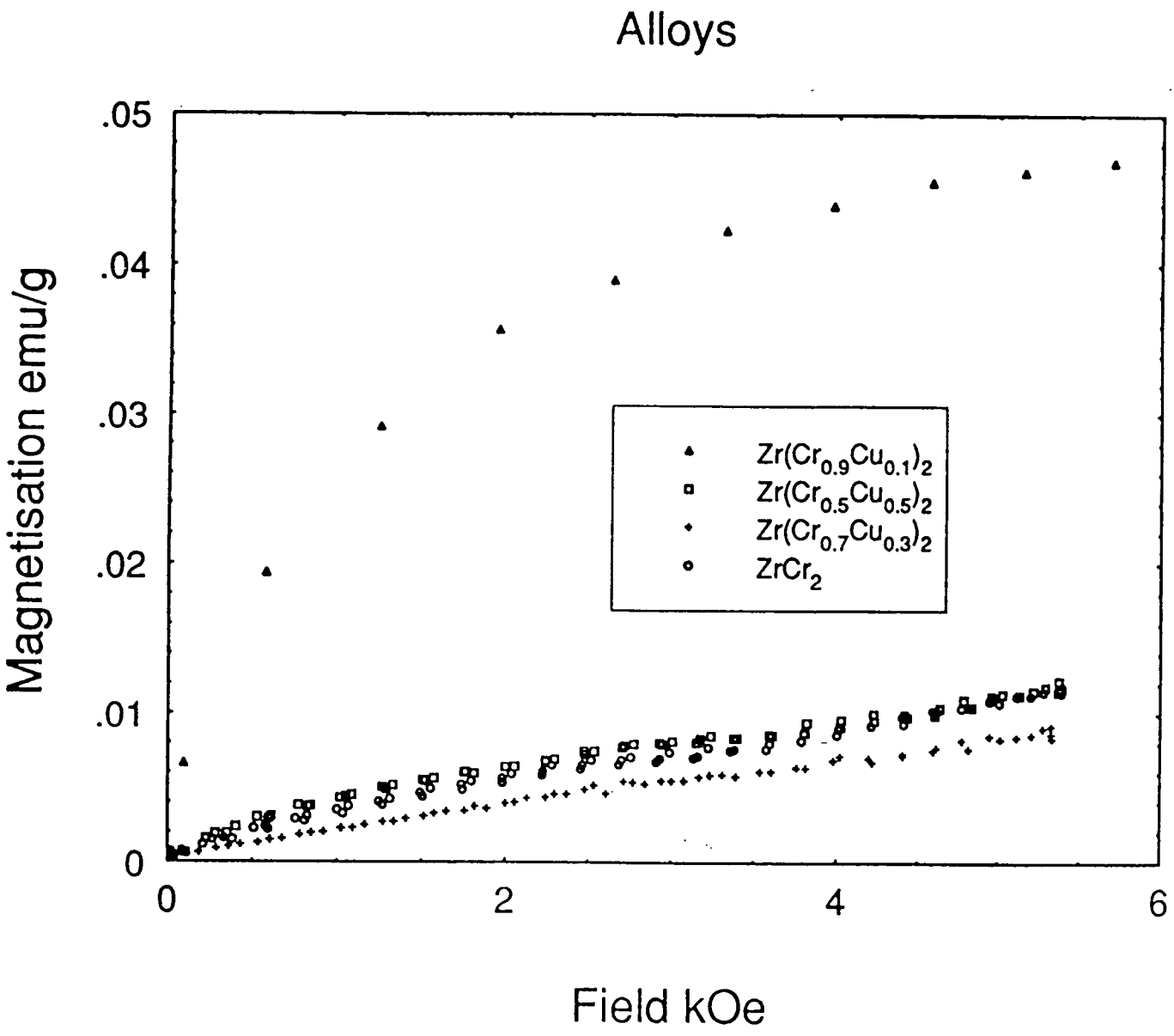

Fig.1. Magnetisation versus field for the alloys $Zr(Cr_{1-x}Cu_x)_2$, x=0,0.1,0.3 and 0.5 at 300 K.

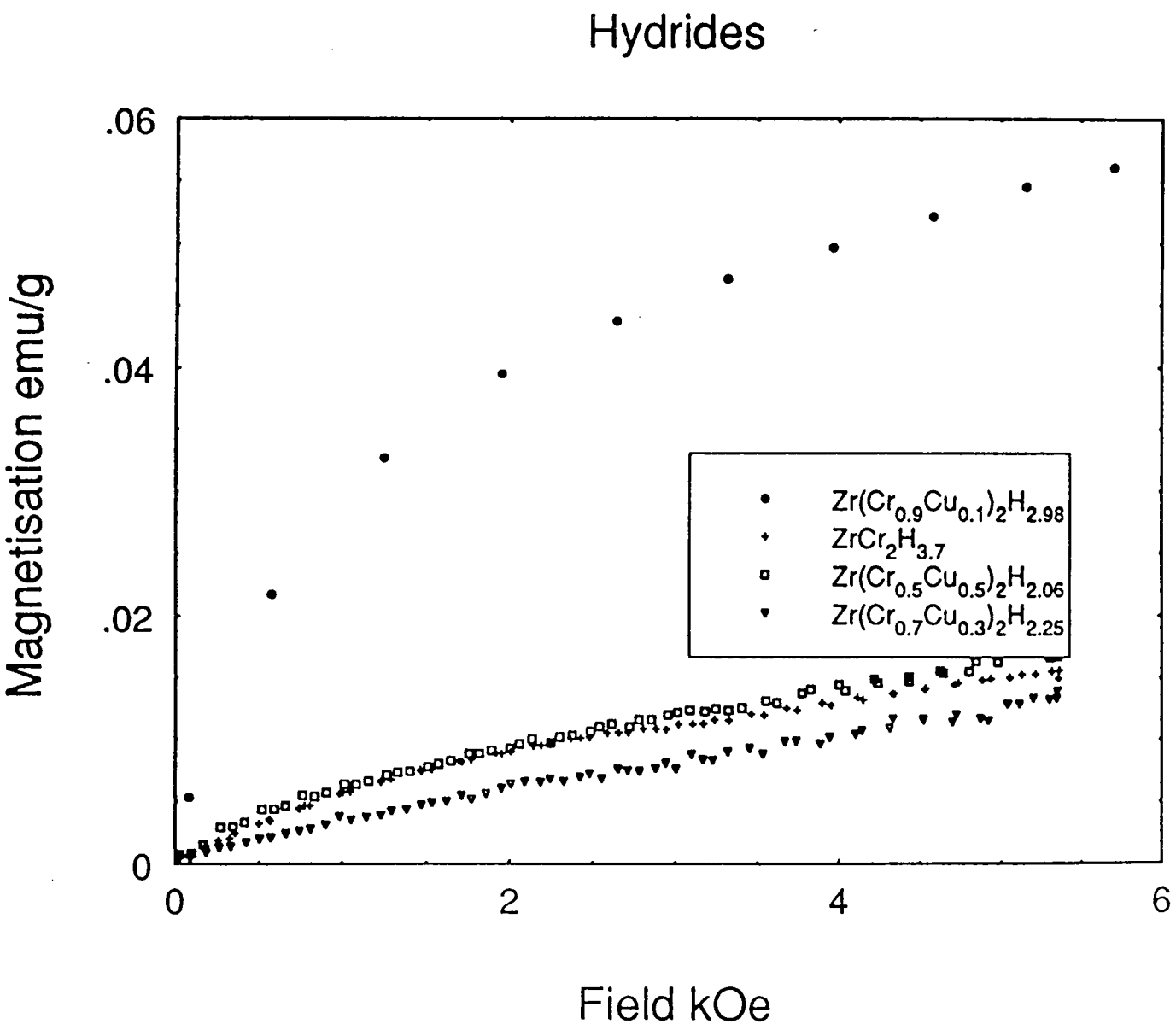

Fig.2. Magnetisation versus field for the hydrides $Zr(Cr_{1-x}Cu_x)_2$, x=0,0.1,0.3 and 0.5 at 300 K.

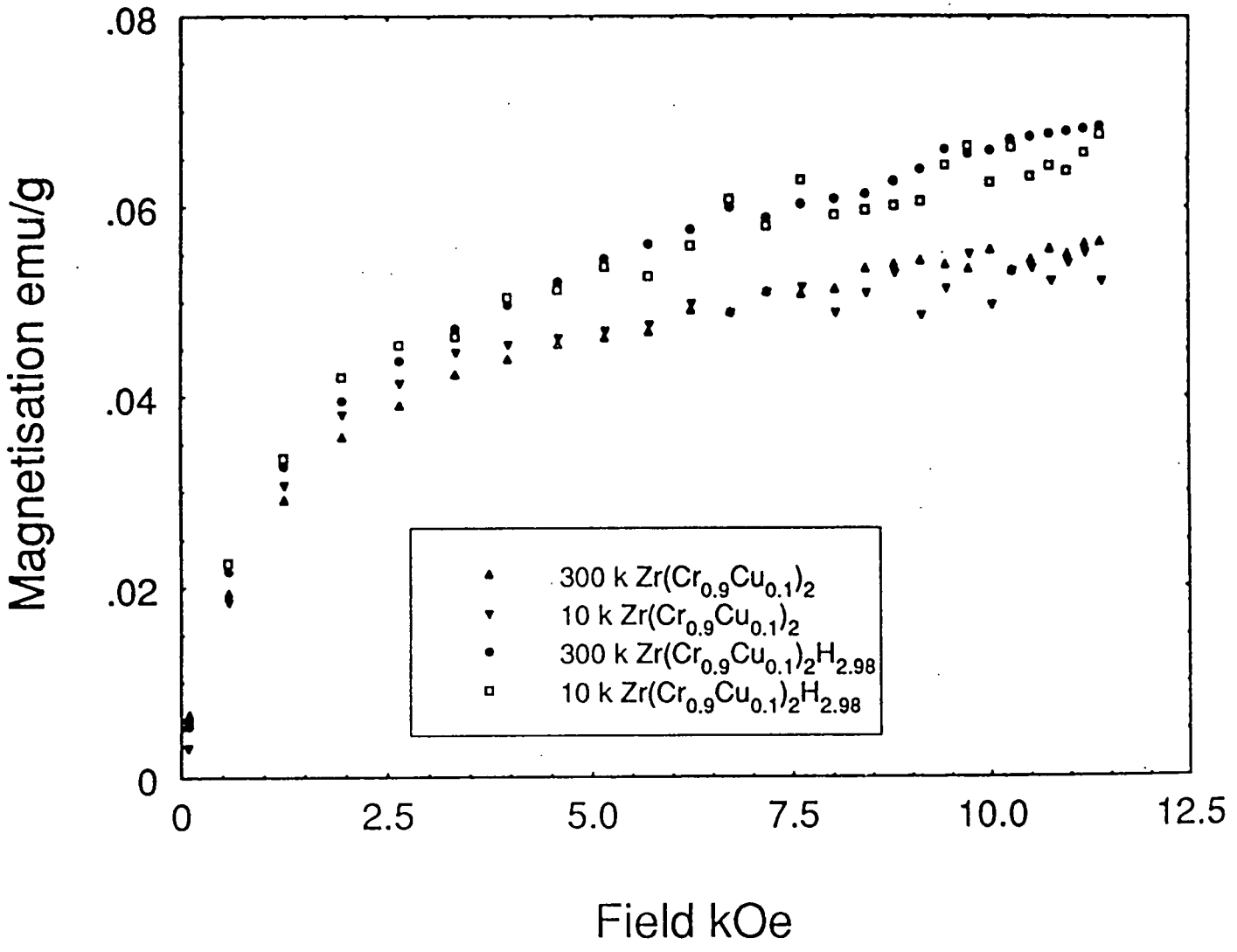

Fig.3. Magnetisation versus field for $Zr(Cr_{0.9}Cu_{0.1})_2$ and $Zr(Cr_{0.7}Cu_{0.3})H_{2.98}$ at 10 K and 300 K.

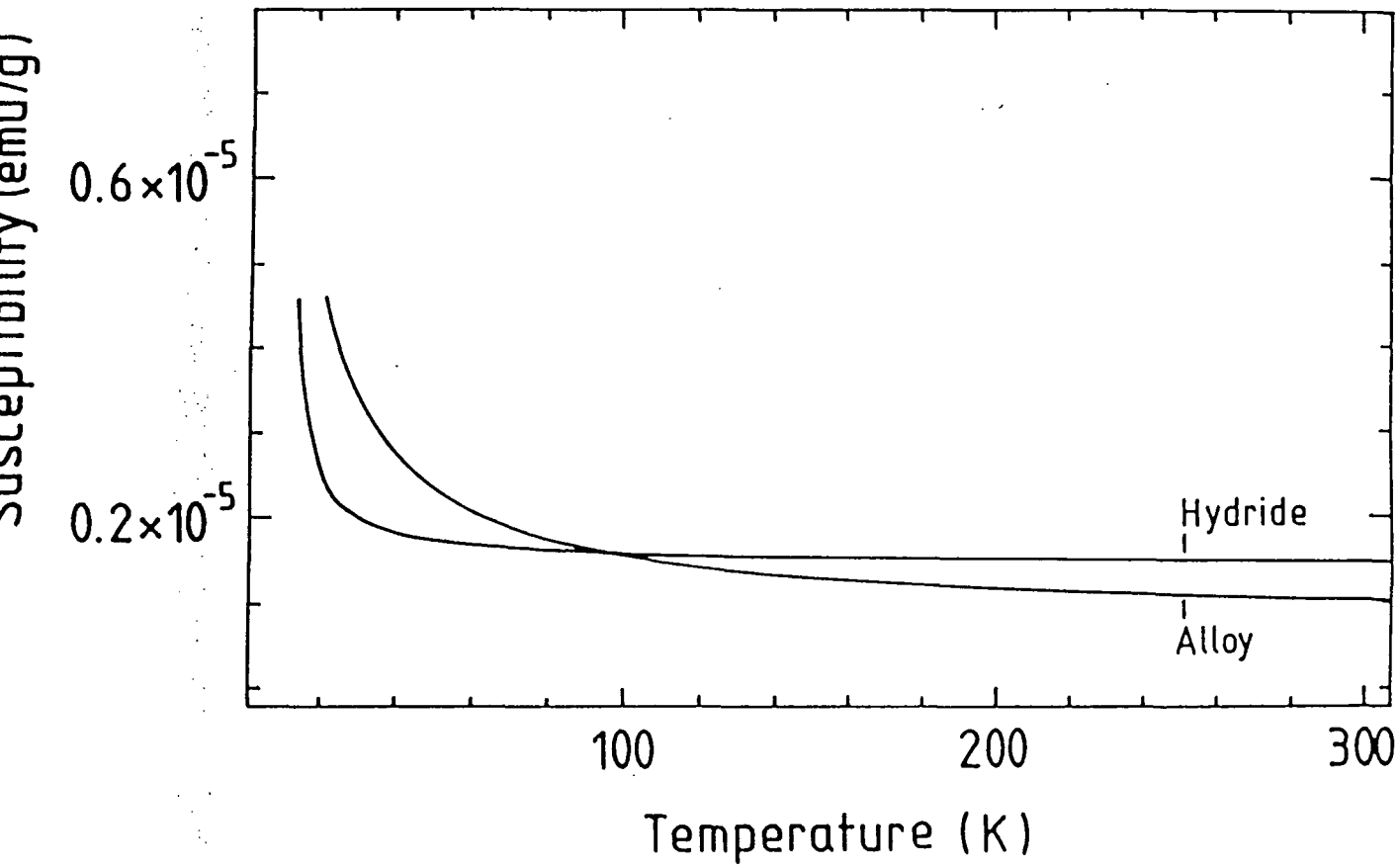

Fig.4. magnetic susceptibility versus temperature for $Zr(Cr_{0.7}Cu_{0.3})_2$ and $Zr(Cr_{0.7}Cu_{0.3})_2H_{2.25}$ at 5.5 kOe

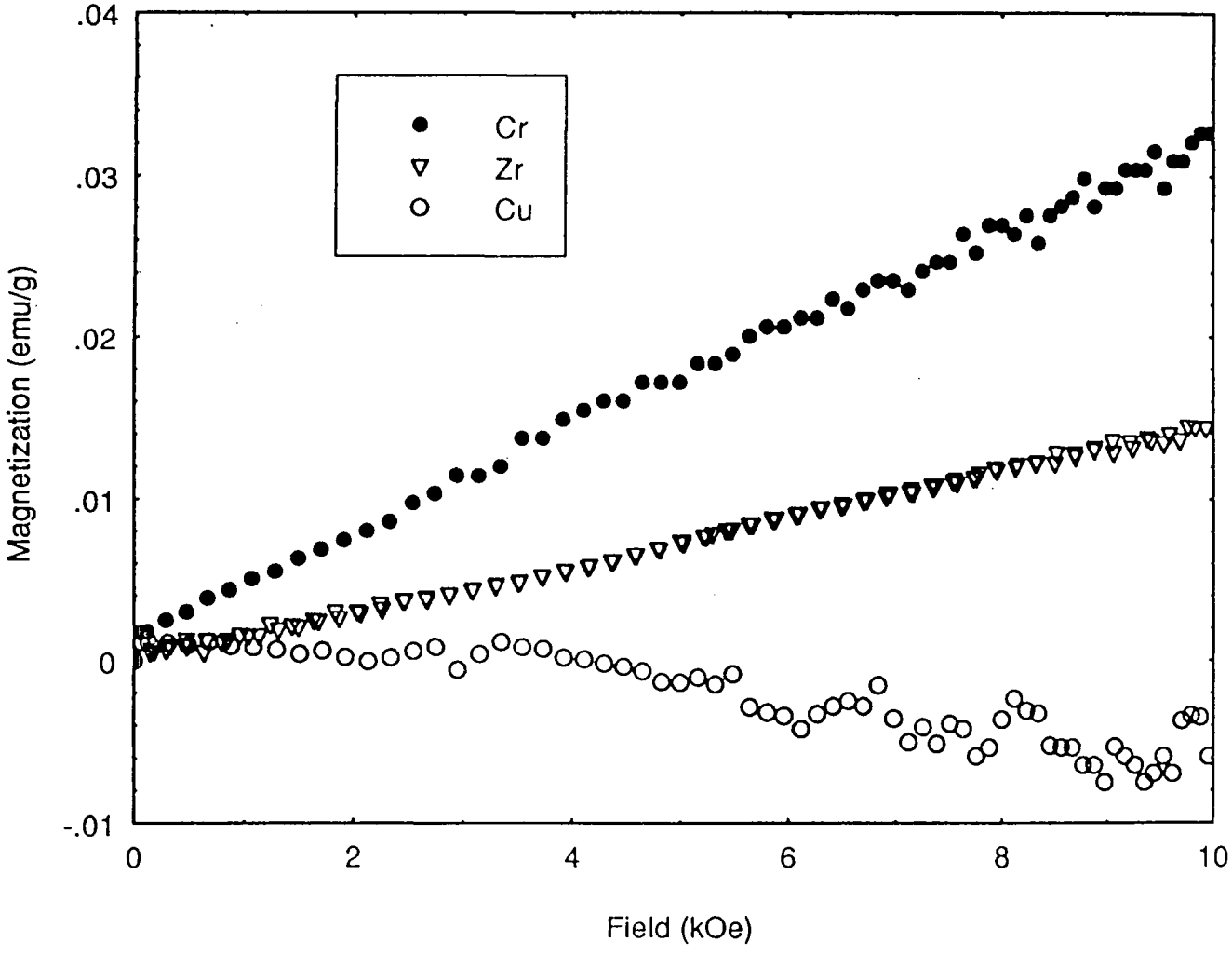

Fig.5 Magnetisation versus field for the raw materials

Table I Magnetic data for the $Zr(Cr_{1-x}Cu_x)_2$ alloys and hydrides

Compostion	Unit Cell Parameters (Å)	Susceptibility χ_0 (10^{-3} emu/mol)	Saturation Magnetisation σ_s (10^{-3} emu/g)	Literature
$ZrCr_2$	Hex a=? c=?	0.40	—	[15]
$ZrCr_2H_{3.8}$	Hex a=? c=?	1.16	—	[15]
$ZrCr_2$	a=5.104 c=8.292	0.41	—	[14]
$ZrCr_2H_{3.44}$	a=5.388 c=8.835	1.03	—	[14]
$ZrCr_2$	a=5.107 c=8.274	0.83	—	[8]
$ZrCr_2H_{4.2}$	a=5.470 c=8.944	1.23	—	[8]
$ZrCr_2$	a=7.200	0.88	—	[8]
$ZrCr_2$	a=7.755	0.97	—	[8]
$ZrCr_2$	a=7.213	0.31	1.34	P.W.
$ZrCr_2H_{3.7}$	a=7.732	0.35	5.94	P.W.
$Zr(Cr_{0.9}Cu_{0.1})_2$	a=7.194	0.32	38.30	P.W.
$Zr(Cr_{0.9}Cu_{0.1})_2H_{2.98}$	a=7.693	0.45	43.21	P.W.
$Zr(Cr_{0.7}Cu_{0.3})_2$	a=7.200	0.34	0.34	P.W.
$Zr(Cr_{0.7}Cu_{0.3})_2H_{2.25}$	a=7.690	0.52	0.44	P.W.
$Zr(Cr_{0.5}Cu_{0.5})_2$	a=7.203	0.32	3.60	P.W.
$Zr(Cr_{0.5}Cu_{0.5})_2H_{2.06}$	a=7.742	0.40	5.50	P.W.

P.W. - Present Work

$\chi_{app}=\chi_o+\sigma_s/H$

The relevant magnetic data are summarised in Table I.

4. Discussion

The results of this study indicate that all the samples, the host metals and the hydrides are paramagnetic. The magnetisation is temperature independent or nearly independent down to about 30 K. Below this temperature a graduate increase in magnetisation is observed. In this region neither of the systems studied reveal a Curie-Weiss behaviour. A possible source of the increase of magnetisation could be the presence of various oxygen contents retained with the sample which results in pronounced change in magnetisation as a consequence of l s transformation of oxygen. Taking all these into account it was concluded that the samples exhibit a Pauli paramagnetism. The samples also have a ferromagnetic component superimposed on the Pauli paramagnetism, which is most pronounced for the alloy $Zr(Cr_{0.9}Cu_{0.1})_2$. Hydrogen absorption increases the Pauli type of paramagnetism as well as the ferromagnetic component of the alloys.

Before we attempt to discuss the results summarised in Table I and in Figs. 1-4., it is well to compare the susceptibility values for both polymorphs of $ZrCr_2$ and their hydrides with the values obtained by other authors. Our results indicate that the hexagonal $ZrCr_2$ has a 33% larger susceptibility value than the cubic one. However, hydrogen uptake strongly enhances the paramagnetism of

the hexagonal phase, but moderately enhances the paramagnetism of the cubic phase. This difference in behaviour may either originate with slight differences in the electron structure of the cubic and hexagonal $ZrCr_2$ (c/a ratio differs from the ideal value 1.666) or with chromium atoms residing on the zirconium sites in the cubic $ZrCr_2$. This will be discussed later. The susceptibility values for the hexagonal $ZrCr_2$ are in excellent agreement with the values given by Jacob et all. [15] but not with the values found by Hirosawa et al. [8] which are larger by a factor of 2. After hydogenation our susceptibility values for the hexagonal phase are in good agreement with the values given by both authors. It is interesting to point out that hydrogen uptake increases the susceptibility of the cubic $ZrCr_2$ only moderately. This is in agreement with the available data in literature, i.e. with those given by Hirosawa, but he reported values which are again higher by a factor of 3.

The temperature independent Pauli paramagnetism most likely originates with the band like magnetism of 3d electrons. These values do not change significantly with substitution of chromium by copper. Probably two opposite effects take place, i.e. copper atoms increase the local electron density of state of chromium, but at the same time the concentration of chromium decreases because the concentration of copper is increased. After hydrogenation Pauli paramagnetism of $Zr(Cr_{1-x}Cu_x)_2$ alloys is increased as a consequence of an increase in the electron density of states.

The most interesting feature observed in these systems is the unexpected induction of weak ferromagnetism. This was observed in virtually all the alloys investigated and is increased after hydrogenation. The ferromagnetism is temperature independent what means that the temperature region investigated lies

well bellow the Curie temperature. Explanation of the presence of ferromagnetism seems not to be easy and just straightforward.

However, we believe that some semiqualitative discussion could be given:

a) The ferromagnetism may be associated with small amounts of chromium atoms residing on the zirconium sites in the crystal structure. These chromium atoms carry magnetic moments (becoming Mn-like, higher Tc) as a result of a better 3d band filling. This is the consequence of a larger electron transfer from zirconium to chromium (difference in electronegatity!) due to more surrounding zirconium atoms in comparison to other chromium atoms in the structure which are surrounded with fewer zirconium atoms. In the later case the electron transfer is less pronounced and chromium atoms exhibit a paramagnetism only. As a result there exist ferromagnetic clusters embedded in a paramagnetic matrix. The observed irregular variation in ferromagnetism with the composition could be explained by different amounts of chromium atoms residing on the zirconium sites.

Some of our results on nonstoichiometric $ZrCr_2$ [16] support this assumption as well as do the data published on the related systems based on $ZrMn_2$ [4].

The occurrence of ferromagnetism in cubic $ZrCr_2$ but not in hexagonal $ZrCr_2$ could also be explained this way, i.e. the much larger deviation from stoichiometry which is possible in the cubic structure [16] favour the chromium atoms to reside on zirconium sites.

b) Alternatively, in the alloy $Zr(Cr_{0.9}Cu_{0.1})_2$ showing the strongest ferromagnetism diluted copper atoms in chromium matrix release their electrons. This is caused by copper/chromium 3d band overlap. In this scheme copper atoms become Ni-like and carry magnetic moments.

It is worth comparing the results reported here with the results reported on related systems. In the system $Zr(Cr_{1-x}Fe_x)_2$ it was found that small quantities of iron induce Curie-Weiss behaviour besides the temperature independent Pauli susceptibility encountered for pure $ZrCr_2$, while higher iron quantities induce magnetic order [15]. In the system $Zr(Cr_{1-x}Co_x)_2$, the susceptibility of $ZrCr_2$ is enhanched by substitution, but much weaker than in systems containing iron. At higher cobalt contents (x=0.5) the total susceptibility is found to be a sum of Pauli and Curie-Weiss contributions [8,15]. Finally, in the system $Zr(Cr_{1-x}Ni_x)_2$ small quantities of nickel increase the temperature independent susceptibility of $ZrCr_2$, while higher quantities of nickel ($x \geq 0.375$) induce beside the temperature independent term of susceptibility a Curie-Weiss contribution to the total susceptibility , but is much weaker than in the system containing cobalt [14]. Hydrogen uptake always acts in favour of the observed effects .

The system $Zr(Cr_{1-x}Cu_x)_2$ does not strictly follow the observed trend in magnetic behaviour as the transition metal changes from iron to copper in the 3d transition metal period. It rather behaves as the system $Zr(Cr_{1-x}Co_x)_2$ where small quantities of cobalt and hydrogen uptake were found to induce ferromagnetism with very small saturation magnetic moment (0.01 μ_B/formula unit) [15], or as the systems based on $ZrMn_2$ where hydrogen absorption or

substitution of zirconium with titanium induces weak ferromagnetism which is not observed for binary $ZrMn_2$ [6, 15].

A more detailed investigation on the nonstoichiometric $ZrCr_2$, as well as on systems based on $ZrMn_2$ will probably shed more light on the interesting magnetic behaviour of the systems based on Laves phases containing zirconium.

Literature

1) D.Shaltiel, I.Jacob and D.Davidov, J. Less-Common Met. 53 (1977) 83.

2) I.Jacob and D.Shaltiel, Solid State Commun. 27 (1978) 175.

3) R.M. van Essen and K.H.J.Buschow, Mater Res. Bull. 15 (1980) 1149.

4) F.Pourarian, H.Fuji, W.E.Wallace, V.K.Sinha and H.K.Smith, J. Phys. Chem. 85 (1981) 3105.

5) M.H.Mendelsohn and D.M.Gruen, J. Less-Common Met. 78 (1981) 275.

6) H.Fuji, F.Pourarian, V.K.Sinha and W.E.Wallace, J. Phys. Chem. 85 (1981) 3112.

7) S.Quian and D.O.Northwood, J.Less-Common Met. 147 (1989) 149.

8) S.Hirosawa, F.Pourarian, V.K.Sinha and W.E.Wallace, J. Magn. Magn. Mat. 38 (1983) 159.

9) A.Drasner and Z.Blazina, J. Less-Common Met. 163 (1990) 151.

10) A.Drasner and Z.Blazina, J. Less-Common Met. 175 (1991) 103.

11) A.Drasner and Z.Blazina, Kem. Ind. 38 (1989) 149.

12) S.R.Hoon, Eur. J. Phys. 4 (1983) 61.

13) S.R.Hoon and S.N.M.Willoock, J. Phys. E. Sci. Instrum. 21 (1988) 772.

14) Z.Blazina and A.Drasner, J. Magn. Magn. Mat. 119 (1993) L15 .

15)I.Jacob, D.Davidov and D.Shaltiel, J. Magn. Magn. Mat. 20 (1980) 226.

16) A.Drasner and Z. Blazina, unpublished results.